

**THE DIRECT INFLUENCE OF AEROSOLS ON UV IRRADIANCE AND THE
DEVELOPMENT OF A SYNTHETIC CURRENT UV INDEX**

A DISSERTATION
Presented to
The Academic Faculty

by

Jeral G. Estupiñán

In Partial Fulfillment
of the Requirements for the Degree
Doctor of Philosophy in Earth and Atmospheric Sciences

GEORGIA INSTITUTE OF TECHNOLOGY
August 2006

**THE DIRECT INFLUENCE OF AEROSOLS ON UV IRRADIANCE AND THE
DEVELOPMENT OF A SYNTHETIC CURRENT UV INDEX**

Approved by:

Dr. Michael H. Bergin, Chairman
Civil and Environmental Engineering &
School of Earth and Atmospheric Sciences
Georgia Institute of Technology

Dr. Armistead G. Russell
Civil and Environmental Engineering
Georgia Institute of Technology

Dr. Derek M. Cunnold
School of Earth and Atmospheric Sciences
Georgia Institute of Technology

Dr. Irina N. Sokolik
School of Earth and Atmospheric Sciences
Georgia Institute of Technology

Dr. Judith A. Curry, School Chair
School of Earth and Atmospheric Sciences
Georgia Institute of Technology

Date Approved: July 6, 2006

This dissertation is dedicated to the following important people in my life:

The memory of Marcelino Estupiñán (my father) who was born September 11, 1927, and who died on December 10, 1996. “I know you are watching over us until the day we meet again.” In the meantime, we continue to progress and advance in all areas of our life.

My mother and brother who have provided me with their love and emotional support throughout my graduate studies and life.

The memory of my grandmother (Asunción) who is also watching over us and I know she is proud of us, and

Ariadne who came to my life in 2003 and who has expressed her unconditional love despite the physical distance that separates us right now and the long hours I have spent completing my degree in addition to my full time job at the Weather Channel.

ACKNOWLEDGEMENTS

There are many people who contributed to this dissertation in many ways. I would like to express my gratitude to the following people for their support. First, I would like to thank my advisor, Dr. Michael H. Bergin, for being so easy to work with. I want to thank him especially for the many thought-provoking conversations we have had throughout my degree at Georgia Tech, the detailed comments and suggestions on this work, and his support and advice in other areas of my professional career as well as for his forward-looking and sympathetic guidance during my comprehensive exam semester in spring 1999. He fostered a stress-free working relationship which was crucial to the completion of this work. I also would like to thank Kátia Fernandes for providing to me with electronic journals when I could not access them when I was off campus.

From the Weather Channel Patrick Rouse and Ken May from The GIS Department for their help with the GIS data used in this research, Joe Koval and Chris Peters from Weather Systems for their help with the retrieval of the ASOS and GOES data, and Dr. Bruce Rose (my manager) for the work flexibility that has been given to me to complete this work while working full time.

From the USDA UV network Gwen Scott and Dr. Jim Slusser for making available the UV data from the UV-MFRSR.

From the University of Georgia UV monitoring network Dr. John Rives, Dr. Richard Meltzer, Dr. Petra Udelhofen, Thomas Taylor, Dr. W. Mou for numerous helpful

discussions related to the operation and calibration of the Brewer spectrophotometer. Spatial thanks are given to Dr. John Rives and Dr. Richard Meltzer for providing Brewer 114 for the Atlanta Supersite experiment during the summer of 1999. The US EPA UV network was supported by the U.S. EPA contract number (CR 821589-01-1).

From the National Center for Atmospheric Research I would like to thank Siri Flocke and Sasha Madronich for their help with the radiative transfer model.

Finally, I would like to thank my parents, Mr. and Mrs. Estupiñán for their support and care over the years.

This dissertation would not have been accomplished without the Weather Channel computer/facilities support.

TABLE OF CONTENTS

	Page
DEDICATION	iii
ACKNOWLEDGEMENTS	iv
LIST OF TABLES	ix
LIST OF FIGURES	x
SUMMARY.....	xv
CHAPTER	
I MEASUREMENT OF AEROSOL OPTICAL DEPTH IN THE UV-A: A COMPARISON BETWEEN UV-MULTIFILTER ROTATING SHADOWBAND RADIOMETER AND A BREWER SPECTROPHOTOMETER	
1.1 Summary	1
1.2 Introduction	2
1.3 Retrieval of Aerosol Optical Depths in the UV	4
1.3.1 Overview	4
1.3.2 Retrieval of Aerosol Optical Depths	8
1.3.2.1 Brewer Spectrophotometer	8
1.3.2.2 UV-MFRSR	11
1.4 Results and Discussion	12
1.4.1 Comparison of Brewer and UV-MFRSR Aerosol Optical Depths	12

	1.4.2 Wavelength Dependence of the Aerosol Optical Depths	19
	1.4.3 Interpretation of the Wavelength Dependence of the Aerosol Optical Depth	24
	1.5 Conclusions	31
II	RETRIEVAL OF AEROSOL OPTICAL DEPTHS, ANGSTRÖM EXPONENT, AND SINGLE SCATTERING ALBEDO IN THE UV DURING THE 1999 ATLANTA SUPERSITE EXPERIMENT	
	2.1 Summary	33
	2.2 Introduction	35
	2.3 Instrumentation and Technique for Measurement	37
	2.4 Analysis and Results	44
	2.4.1 Aerosol optical depth (τ_a) and Angström exponent (α)	44
	2.4.2 Single scattering albedo (ω_o)	52
	2.4.3 Effects of Aerosol Optical Depth (τ_a) and single scattering albedo (ω_o) on the surface UV radiation	60
	2.5 Conclusions	66
III	A NEW SYNTHETIC CURRENT UV INDEX IS DEVELOPED TO PROVIDE UV INDEX VALUES AT LOCATIONS WITHOUT UV MEASUREMENTS	
	3.1 Summary	68
	3.2 Introduction	69
	3.3 Quantification of the Effects of Clouds on the UV Index	71
	3.4 Results	82
	3.4.1 Verification of the Synthetic Current UV Index	82

	3.4.2 Comparison of the Synthetic Current UV Index with Actual Sky Conditions	96
	3.4.2.1 Comparison at METAR Points	97
	3.4.2.2 Comparison of the UV Index Derived Using METAR-derived Clouds with the UV Index Derived Using GOES-augmented METAR Clouds	112
	3.5 Conclusions	128
IV	SUMMARY OF FINDINGS	131
V	RECOMMENDATIONS FOR FUTURE WORK	136
	APPENDIX A: ALL AEROSOL OPTICAL DEPTH AND ÅNGSTRÖM EXPONENT MEASUREMENTS.....	141
	Atlanta, GA	142
	Griffin, GA	150
	REFERENCES	158
	VITA	166

LIST OF TABLES

	Page
Table 1-1: Daily mean, standard deviation, maximum, and minimum $\tau_{a,\lambda}$ for each of the measurement days.....	13
Table 1-2: Mean, standard deviation, maximum, and minimum Ångström exponents for each of the measurement days.....	22
Table 1-3: Effect of absorbing aerosols on the 320-360 nm Ångström exponent for aerosol size distributions with geometric mass mean particle sizes of 0.1, 0.3, 0.5, and 0.6 μm , and geometric standard deviation of 2.0...	30
Table 3-1: Geographic Details about the METAR Stations and UV Observation Sites considered in this study.....	75
Table 3-2: Estimated cloud optical depth in the UV for an overcast cloud layer having transmission properties corresponding to cloud amounts of 10, 20, 30, 40, 50, 60, 70, 80, 90, and 100%.....	81

LIST OF FIGURES

	Page
Figure 1-1: Daily temporal variation of $\tau_{a,\lambda}$ (aerosol optical depth) as a function of time and wavelength for the UV-MFRSR and the Brewer spectrophotometer.....	16
Figure 1-2: Aerosol optical depth for the Brewer and the UV-MFRSR for the seven measurement days.....	17
Figure 1-3: Regression plots of the hourly averages of the $\tau_{a,\lambda}$ for each of the instruments. The wavelength pairs used for the comparison of the $\tau_{a,\lambda}$ are 317 and 320 nm, 332 and 340 nm, and, 368 and 360 nm.....	18
Figure 1-4: Correlation coefficient between the UV-MFRSR and Brewer Ångström exponent calculated from the hourly values of τ_a . The Ångström exponent (α) is calculated using the 320-360 wavelength range for the Brewer and the 317-368 wavelength range for the UV-MFRSR.....	21
Figure 1-5: Hourly averages of the Ångström exponents for each of the seven measurement days.....	23
Figure 1-6: Aerosol extinction (β_{ext}) calculated using the Mie model of Bohren and Huffman for an aerosol size distribution with geometric mass mean diameters of 0.1, 0.3, 0.5, and 0.6 μm , a geometric standard deviation of 2.0, a refractive index of 1.53 – 0.0 i, and a total number of particles equals to 1000.....	26
Figure 1-7: Comparison of the calculated Ångström exponents shown in Figure 6 to the measured Ångström exponents. The measured Ångström exponents are indicated by the two symbols (Brewer, open square and UV-MFRSR, filled circle) which depict the average mean and standard deviations for each of the instruments.....	27
Figure 2-1: Location of Jefferson, Street (plus sign) and Griffin, GA (circle) measurement site.....	38
Figure 2-2: Frequency distribution of aerosol optical depth (τ_a) for Atlanta at 340 nm and for Griffin at 332 nm for all the measurements for the 16 measurement days of the month of August, 1999. The average and standard deviation for τ_a are shown on the graph.....	45
Figure 2-3: Overview of the main weather conditions that affected τ_a during the month of August for Atlanta and Griffin. The values of τ_a shown are for	

340 nm.....	46
Figure 2-4: Shows all aerosol optical depth measurements taken by the Brewer in Atlanta (red) and by the UV-MFRSR in Griffin (black).....	47
Figure 2-5: Frequency distribution of the Angström exponent (α) for Griffin (left y-axis) and Atlanta (right y-axis) for all measurements taken during the month of August, 1999.....	49
Figure 2-6: Shows all measurements of the Ångström exponent (α) taken by the Brewer in Atlanta (red) and by the UV-MFRSR at Griffin (black).....	50
Figure 2-7: Daily averages of the Ångström exponent (α) for Atlanta (red) and Griffin (black). A dashed line joins the values of α for Griffin to better illustrate the day-to-day variation of α . The error bars depict the daily average measurement uncertainty for each of the 16 days.....	51
Figure 2-8: Schematic showing the iteration process used to derive ω_0	53
Figure 2-9: The effect of g on ω_0 was investigated using TUV. g was changed from 0.6 to 0.8 and the resulting irradiance (0.65 W m^{-2}) is compared to the irradiance that results from changing ω_0 from 0.70 to 0.99. In this calculation the spectral range 286-363 nm is used to match that of the Brewer.....	55
Figure 2-10: Frequency distribution of ω_0 derived from the Atlanta Brewer measurements for the 16 days used in this study. The average ω_0 is 0.87 with a standard deviation of 0.08.....	56
Figure 2-11: Average daily single scattering albedo (ω_0) for each of the measurement days.....	58
Figure 2-12: Relationship between τ_a and ω_0 for the 16 days considered in this study.....	59
Figure 2-13: UV Index calculated from the erythemally-weighted UV irradiance measured with the Brewer spectroradiometer (solid line). The hypothetical calculated UV index for the continental aerosols measured by Elterman (1968) corresponding to the highest sun, or lowest solar zenith angle (SZA), is shown by the red symbols. The blue symbols correspond to the UV Index for an atmosphere with no aerosols. Note that UV index values are given as integer numbers.....	61
Figure 2-14: Daily changes in total column ozone (O_3) for the month of August 1999 measured by the Brewer spectroradiometer.....	62

Figure 2-15: Effect of ω_0 on the UV Index (a-e) and on the total UV radiation (286-363 nm) (f). The measurements correspond to August 7 th with an average τ_a of 1.1 and a total column O ₃ of 339.6 DU. ω_0 for this day was estimated to be 0.90 represented by the line with triangles in (f).....	64
Figure 2-16: Effect of τ_a on the UV Index (a-e) and on the total UV radiation (286-363 nm) (f). The measurements correspond to August 7 th with an average τ_a of 1.1 and a total column O ₃ of 339.6 DU. The line with the triangles shows the ratio of the calculated to measured UV irradiance.....	65
Figure 3-1: Geographical distribution of UV locations Selected in this Study.....	76
Figure 3-2: Representation of the distance of the UV observation station to its closest METAR station.....	77
Figure 3-3: Comparison of the cloud UV transmission obtained in this study the ones obtained by Illyas (1987), Bais (1993), Cutchis (1980) and Joseffson (1986). The error bars represent the standard deviations of the average UV transmission obtained from our study.....	79
Figure 3-4: Schematic of the calculation and verification of the current UV Index.....	85
Figure 3-5: Histogram for all 13 locations. The total number of records verified is 6566. The graph displays the percentage of points for each of the following categories: (a) with synthetic current UV Index identical to the observed UV Index; (b) with synthetic current UV Indices showing a difference of +/- 1 UV Index unit from the measured UV Index; (c) with synthetic current UV Indices within +/- 2 UV Index units of the measured index.....	86
Figure 3-6: Histograms for each of the 13 locations. Each graph displays: -The four digit code of the METAR station. -The number of points verified. -The percentage of points for each of the following categories: (a) with synthetic current UV Index identical to the observed UV Index; (b) with synthetic current UV Indices showing a difference of +/- 1 UV Index unit from the measured UV Index; (c) with synthetic current UV Indices within +/- 2 UV Index units of the measured index.....	87
Figure 3-7: Comparison of UV Index errors (+/-0, +/-1, and +/-2) for all thirteen locations.....	92
Figure 3-8: Correlation between monthly average cloud cover and the	

correlation between the measured UV radiation and cloud cover for each site.	93
Figure 3-9: Simulation of the synthetic UV Index for September 27, 2004 (1950Z-1958Z). The calculation corresponds to the maximum clear sky UV Index that would have been measured without the presence of clouds.....	99
Figure 3-10: Simulation of the synthetic UV Index for September 27, 2004 (1950Z-1958Z). The calculation corresponds to synthetic UV Index that would have been measured considering the effects of clouds.....	100
Figure 3-11: UV Index reduction due to clouds (Clear sky UV Index – UV Index considering clouds) for September 27, 2004 from 1950Z to 1958Z.....	101
Figure 3-12: Observed percentage cloud cover as reported from the surface METAR stations from 1272 locations across the United States for September 27, 2004 (1950Z-1958Z).....	102
Figure 3-13: Satellite image taken on September 27, 2004 at 2015Z. In the southeastern United States the remnants of hurricane Jeanne move toward the northeast. Over western Texas an upper level low pressure is responsible for abundant cloudiness in the center of the United States. From Colorado to the Great lakes a cold front separates cooler drier air from the Canadian prairies from warmer air to the south. Fog and stratus clouds are observed off the west coast.....	103
Figure 3-14: Surface map for 00z September 28, 2004.....	105
Figure 3-15: Simulation of the synthetic UV Index for April 21, 2005 (1950Z-1958Z). The calculation corresponds to the maximum clear sky UV Index that would have been measured without the presence of clouds.....	106
Figure 3-16: Simulation of the synthetic UV Index for April, 21, 2005 (1950Z-1958Z). The calculation corresponds to synthetic UV Index that would have been measured considering the effects of clouds.....	107
Figure 3-17: UV Index reduction due to clouds (Clear sky UV Index – UV Index considering clouds) for April, 21, 2005 from 1950Z to 1958Z.....	108
Figure 3-18: Observed percentage cloud cover as reported from the surface METAR stations from 1272 locations across the United States for April, 21, 2005 (1950Z-1958Z).....	109
Figure 3-19: Satellite image taken April 21, 2005 at 2004Z. A low pressure area over eastern Kansas with an associated cold front stretching south into Texas and occluded front extending to coastal Virginia dominate the weather features this day.....	110

Figure 3-20: Surface map corresponding to 00z April 22, 2005 (4 hours after 20z).....	111
Figure 3-21: Observed percentage cloud cover as reported from the surface METAR stations from 1272 locations across the United States for April, 28, 2005 (1950Z-1958Z).....	116
Figure 3-22: Observed percentage cloud cover from GOES augmented METAR stations expanded to nearly 10,000 locations across the United States for April, 28, 2005 (1950Z-1958Z).....	117
Figure 3-23: GOES east satellite image corresponding to April 28, 2005 (2015Z).....	118
Figure 3-24: GOES west satellite image corresponding to April 28, 2005 (2000Z).....	119
Figure 3-25: GOES east satellite image corresponding to April 28, 2005 (2015Z).....	120
Figure 3-26: Simulation of the synthetic UV Index for April, 28, 2005 (1950Z-1958Z). The calculation corresponds to synthetic UV Index that would have been measured considering the effects of clouds.....	122
Figure 3-27: Simulation of the synthetic UV Index for April, 28, 2005 (1950Z-1958Z). The calculation corresponds to synthetic UV Index that would have been measured considering the effects of clouds. The calculation is expanded to all 9,500 points.....	123
Figure 3-28: Simulation of the synthetic UV Index for April 28, 2005 (1950Z-1958Z). The calculation corresponds to the maximum clear sky UV Index that would have been measured without the presence of clouds.....	124
Figure 3-29: Simulation of the synthetic UV Index for April 28, 2005 (1950Z-1958Z). The calculation corresponds to the maximum clear sky UV Index that would have been measured without the presence of clouds. The calculation is expanded to all 9,500 points.....	125
Figure 3-30: UV Index reduction due to clouds (Clear sky UV Index – UV Index considering clouds) for April, 28, 2005 from 1950Z to 1958Z.....	126
Figure 3-31: UV Index reduction due to clouds (Clear sky UV Index – UV Index considering clouds) for April, 28, 2005 from 1950Z to 1958Z. The calculation is expanded to all 9,500 points.....	127

SUMMARY

This dissertation covers two main topics. The first two chapters include the first topic, which investigates the effects of aerosols on UV radiation through the use of direct sun measurements. The second topic, in the third chapter, expands previous knowledge about the UV Index and presents a new synthetic current UV Index or “near real time UV Index” capable of providing current UV Index values at locations without UV instruments. Although many studies report comprehensive measurements of aerosol optical depths for visible wavelengths, (Dutton et al., 1994; Harrison and Michalsky, 1994; Adayefa and Holmgren, 1996; Jun et al., 1996; Bokoye et al., 1997; Hastenrath, 1997) by contrast the wavelength dependence of the aerosol optical depth at UV wavelengths is not well understood (Bais, 1997; Marenco et al., 1997; Kerr, 1997; Kylling et al., 1998; Borghesi et al., 1982; Jaroslowski and Krzyscin, 2000). The motivation driving this research are: (1) advance our knowledge of the effects of aerosols in the UV providing the medical and scientific community with more details about the effects of aerosols on UV radiation; and (2) provide information to the general public about the most recent values of the observed UV Index. Chapter IV presents an overall summary of the results presented in each of the three chapters and Chapter V discusses recommendations for future work.

The health effects of UV exposure are well documented (Brash et al. 1991; Duthie et al. 1999; Elwood, 1992, Gilmour et al., 1993, Kraus et al., 1998; Longstreth and Wiseman, 1989, Ohnaka, 1993; Taylor et al., 1988). These health effects include immune suppression, skin cancer, infectious disease, and cataract development. There is strong evidence that exposure to solar radiation is a major factor for the production of basal cell

carcinoma (BCC), squamous cell carcinoma (SCC) and malignant melanoma (MM). BCC and SCC are commonly referred as non melanoma skin cancers (NMSC). Furthermore, more recent research indicates that the effects of UV-A radiation on skin cancer and ocular disease can be equally harmful as the effects of UV-B radiation, mainly for SCC and MM (Longstreth et al. 1998). Exposure to UV radiation is also associated with the formation of cataracts (de Gruijl, 1997; Taylor et al. 1998). Studies indicate that there is a direct association between cataract incidence and UV levels. However, it is not clear which part of the solar spectrum (UV-A or UV-B) is producing the cataract (de Gruijl, 1997).

In the first two chapters the total aerosol optical depth, spectral dependence of the aerosol optical depth, and single scattering albedo are determined using measurements from a Brewer spectrophotometer and a UV Multifilter Shadowband Radiometer (UV-MFRSR) from the US Department of Agriculture (USDA). The first chapter presents an instrument intercomparison between a Brewer spectrophotometer from the US Environmental Protection Agency and a UV-MFRSR from the USDA co-located at Boulder, Colorado. Boulder was chosen as the measurement site for the instrument intercomparison since it has good visibility and relatively low aerosol optical depths in comparison to other locations in the country due to its geographic location. The purpose of this intercomparison is to assess the feasibility of the use of the Brewer spectrophotometer using a new routine, referred as the “ps” direct sun measurement, to determine aerosol optical depths in the UV. It has not been until very recently that the Brewer spectrophotometer has been utilized by scientists in Europe to determine aerosol optical depth in the UV using the quartz window (Marenco et al. 1997; Marenco et al.

2002; Kazadzis et al, 2005). Two methods have been employed to retrieve aerosol optical depths using the Brewer's quartz window. The first method utilizes the wavelengths that are used for the retrieval of total column ozone (303.2, 306.3, 310.1, 313.5, 316.8, and 320.1 nm) known as the "ds" routine. The second method consists in programming the photomultiplier tube at certain wavelengths utilizing the Brewer filters which are positioned into the beam path to protect the photomultiplier from overexposure to sunlight. Each one of these two techniques has advantages and disadvantages when measuring aerosol optical depths in the UV. The first method, which makes use of the total column ozone wavelengths, is limited by the uncertainties encountered when measuring aerosol optical depths in the UV-B due to the strong absorbing effects of the ozone in the UV-B wavelength range. The only wavelength that provides less uncertainty is 320.1 nm. Thus, the spectral dependence of the aerosol optical depth cannot be derived with confidence in the UV-B using this method. However, the advantages of this method are two: (1) it provides an opportunity to retrieve aerosol optical depth from previous observational records taken by the Brewer network; and (2) this technique employs the Langley method and thus, does not require an absolute calibration of the Brewer direct sun window. The second method provides the opportunity to derive the spectral dependence of the aerosol optical depth in the UV through the use of the UG-11 filter and a neutral density filter. This technique provides a lot of flexibility and once the routine is created and put into operation it runs automatically not requiring the absolute calibration of the instrument since the Langley method can be used. In addition, different wavelengths in the UV can be used to retrieve aerosol optical depths which allows for the determination of the wavelength dependence of the aerosol optical depth.

Once it is determined that the Brewer spectrophotometer can be used to retrieve aerosol optical depths in the UV using the “ps” routine, in chapter two we utilize a Brewer spectrophotometer located in Atlanta, GA to determine the aerosol optical depth, the spectral dependence of the aerosol optical depth, and the single scattering albedo during typical summer time conditions in Atlanta, GA. The results are also compared to the ones obtained from a USDA UV-MFRSR located 46 miles south of Atlanta.

The measurements of aerosol optical depth provided in this research extend over the UV-A region of the spectrum where the effects of aerosols can be investigated with less uncertainty than in the UV-B where ozone absorption is capable of providing uncertainties that sometimes exceed the actual measurement uncertainty.

The third chapter presents the development of a current synthetic UV Index or “real time UV Index” capable of providing current UV Index values at locations without UV instruments. The term “real time” refers to the most recent UV Index that can be issued to the public according to the required input parameters (usually less than one hour). The results of the current UV Index are then verified against ground UV Index measurements from the USDA network. The results are presented and interpreted in context of the observed meteorological conditions at 10000 points across the United States.

CHAPTER I

MEASUREMENT OF AEROSOL OPTICAL DEPTH IN THE UV-A: A COMPARISON BETWEEN UV-MULTIFILTER ROTATING SHADOWBAND RADIOMETER AND A BREWER SPECTROPHOTOMETER

1.1 Summary

The extinction of solar radiation by atmospheric aerosols influences the Ultraviolet (UV) flux at the surface, which in turn has implications on both human and environmental health. In this study we present measurements of aerosol optical depth ($\tau_{a,\lambda}$) spectral dependence in the (UV) (317-368 nm) from a USDA UV-Multi-Filter Rotating Shadow band Radiometer (UV-MFRSR) and an EPA Brewer spectrophotometer (320-360 nm) collocated at Boulder, Colorado. The purpose of this study is to measure the spectral attenuation of radiation in the UV by comparing measurements of different wavelengths from two spectral UV instruments. The instruments are in close agreement with the square of the correlation coefficients between the two instruments of 0.92 for the 317-320 nm wavelength pair, 0.86 for the 332-340 nm wavelength pair, and 0.94 for the 368-360 nm wavelength pair (first wavelength of each pair represents the UV-MFRSR, while the second represents the Brewer). The ratio of the UV-MFRSR to Brewer τ_a for all wavelengths is $1.0242 \pm (0.17 \text{ standard deviation})$. The hourly-averaged τ_a , range from 0.07 to 0.51 at 317 nm for the UV-MFRSR and from 0.07 to 0.47 at 320 nm for the Brewer; from 0.09 to 0.52 at 332 nm for the UV-MFRSR and from 0.09 to 0.45 at 340 nm for the Brewer; and from 0.08 to 0.48 at 368 nm for the UV-MFRSR and from 0.07 to 0.45 at 360 nm for the Brewer. Hourly mean Ångström exponents were calculated to be

$0.82 \pm (0.11 \text{ measurement uncertainty})$ for the UV-MFRSR and $0.84 \pm (0.165 \text{ measurement uncertainty})$ for the Brewer. The Ångström exponents ranged from -0.49 to 2.36 for the UV-MFRSR and from 0.15 to 2.24 for the Brewer. The observed wavelength dependence of $\tau_{a,\lambda}$ is explained based on reasonable assumptions for the size distribution and optical properties of the aerosol particles using Mie theory. The measurements presented in this study are for seven days and thus not meaningful statistically in a monthly, seasonal or yearly climatological sense.

1.2 Introduction

The potential effects of overexposure to UV radiation on human health include immune suppression (Gilmour et al., 1993), skin cancer (Elwood, 1992), infectious disease (Longstreth and Wiseman, 1989), and cataract development (Taylor et al., 1988). Recent investigations involving medical studies suggest that the adverse effects of cumulative doses of UV-A radiation on humans have been underestimated (Lavker et al. 1995; Lavker and Kaidbey, 1997). Most of the UV flux is concentrated in the UV-A region of the spectrum (320 nm to 400 nm). Due to the lack of continuous measurements of the spectral dependence of aerosols at UV wavelengths, it is not currently possible to assess the extent to which aerosols impact UV surface irradiance. Furthermore, using $\tau_{a,\lambda}$ measurements at visible wavelengths to approximate the amount of aerosol UV attenuation (Wenny et al., 1998) may not be sufficient to accurately determine the UV attenuation since the wavelength dependence of τ_a is not well known, specifically within the UV wavelengths. In order to characterize the atmospheric transmission of ultraviolet

(UV) radiation it is necessary to know the spectral dependence of the aerosol optical depth ($\tau_{a,\lambda}$).

The first long-term effort to derive $\tau_{a,\lambda}$ in the United States was established by the U.S. Environmental Protection Agency (EPA) and the National Oceanic and Atmospheric Administration (NOAA) (Flowers et al., 1969). This program provided τ_a at 500 nm for the period 1961-1966. Peterson et al. (1981) also measured τ_a at 500 nm in Central North Carolina from 1969 to 1975. Although many studies have reported comprehensive measurements of $\tau_{a,\lambda}$ for visible wavelengths, (Dutton et al., 1994; Harrison and Michalsky, 1994; Adayefa and Holmgren, 1996; Jun et al., 1996; Bokoye et al., 1997; Hastenrath, 1997) the wavelength dependence of $\tau_{a,\lambda}$ at UV wavelengths has not been investigated until more recently (Bais, 1997; Marengo et al., 1997; Kerr, 1997; Kylling et al., 1998; Borghesi et al., 1982; Jaroslowski and Krzyscin, 2000). Variations in the spectral dependence of $\tau_{a,\lambda}$ affect surface UV irradiance and introduce uncertainties in the retrievals of total column ozone (O_3). Long et al (1996) point out that the UV absorption and scattering of radiation by tropospheric aerosols can decrease the surface irradiance in the UV by 15%, especially in the eastern United States, resulting in lower measured UV fluxes than the ones predicted by the National Ultraviolet Index forecasts. Changes in atmospheric turbidity have been responsible for reducing surface UV irradiance in the eastern US by more than 20% (Estupiñán et al., 1996). Attenuation of UV radiation by aerosols is also believed to influence gas phase chemistry associated with O_3 formation (Dickerson et al. 1997; Jacobson, 1999).

Several measurement networks have begun to measure $\tau_{a,\lambda}$ at wavelengths located at the long end of the UV spectrum. Currently the largest worldwide optical

ground-based aerosol monitoring network is AERONET (AErosol RObotic NETwork) supported by the National Atmospheric and Space Administration's (NASA) Earth Observing System and expanded with cooperation from many non-NASA institutions worldwide (Holben, 1998). This network measures $\tau_{a,\lambda}$ at two wavelengths in the UV (340 and 380 nm) using Cimel sun photometers. In the United States, the Department of Agriculture Ultraviolet Monitoring Program possesses a total of 30 sites capable of measuring $\tau_{a,\lambda}$ at 300, 305, 317, 325, 332, and 368 nm using Yankee Multi-Filter Rotating Shadow band Radiometers (Bigelow et al., 1998).

In this study we present measurements of $\tau_{a,\lambda}$ in the UV-A (317-368 nm) from a USDA UV-Multi-Filter Rotating Shadow band Radiometer (UV-MFRSR) and an EPA Brewer spectrophotometer collocated at Boulder, Colorado. Measurements were conducted in 1999 and 2000. Five days were chosen from 1999 (Julian days 225, 230, 234, 235, and 236) and two days from 2000 (Julian days 172 and 182). The purpose of this study is to compare and assess the spectral dependence of $\tau_{a,\lambda}$ in the UV-A by comparing measurements of $\tau_{a,\lambda}$ from two different collocated instruments.

1.3 Retrieval of Aerosol Optical Depth in the UV

1.3.1 Overview

Retrievals of $\tau_{a,\lambda}$ from ground-based sensors generally employ two methods: (1) the standard Langley method and (2) measurements of absolute spectrally-resolved solar flux with a calibrated Sun photometer. The standard Langley method is a technique based on Sun photometry introduced for the first time on 23 November, 1725, by Pierre

Bouguer (Middleton, 1961). This relative measure does not require an absolute calibration of the direct input of the sensor. Retrievals of optical depths with the Langley method do not provide instantaneous information about the atmospheric optical depth since it requires measurements over a period of time, usually a morning or an afternoon. As a result, it assumes that both total atmospheric optical depth and the sensitivity of a sensor remain constant during the measurement period. Langley analysis is a linear regression of the natural logarithm (\ln) of the signal that is measured versus airmass (m). The signal can be measured as a voltage or photon counts depending on the instrument used. A graph of the natural logarithm of the signal versus airmass falls along a straight line assuming that the aerosol loading does not change with time. Extending the straight line to where it crosses the y-axis at $m = 0$, (zero airmass) yields an estimate of the signal that would be measured at the top of the atmosphere ($m = 0$). Measurements of absolute spectrally-resolved solar flux with a calibrated Sun photometer differ from the standard Langley method in that the characterized y-intercept is used to directly calculate the total atmospheric optical depth providing instantaneous information about changes in the total atmospheric optical depth and therefore $\tau_{a, \lambda}$.

In this study, the y-intercept was characterized by averaging the results of a series of Langley regressions for both the UV-MFRSR (as a voltage signal) and Brewer (as photon counts) at specific wavelengths in order to directly calculate the total atmospheric optical depth (τ_{λ}). The averaged extraterrestrial constant is referred to as the characterized Langley intercept. Once τ_{λ} has been established, $\tau_{a, \lambda}$ at specific UV wavelengths is obtained by subtracting the sum of the Rayleigh and O_3 optical depths. NO_2 and SO_2 also contribute to the optical depth in the UV, although their contribution

was not considered in this study. Cede et al. (2006) indicate that the absorbing effects of NO₂ could lead to overestimation of the aerosol absorption mainly in the range between 360 and 450 nm. The Rayleigh optical depth is well known and comparisons of different techniques to compute scattering by air molecules are within 1% (Teillet, 1990).

To minimize the errors associated retrieving aerosol optical depths at higher solar zenith angles we only used solar zenith angles between 34 and 63 degrees corresponding to air masses between 1.2 and 2.2 for all Langley plots performed in this study. The changes in sensitivity of the Brewer spectrophotometer as a function of the solar zenith angle are negligible for solar zenith angles less than 50 degrees as indicated by Cede et al. (2006). At a solar zenith angle of 60 degrees Cede et al. (2006) show that the sensitivity of the Brewer is only reduced by 1% yielding a marginal effect on the Langley method. For solar zenith angles greater than 50 degrees these changes in sensitivity are independent of wavelength and therefore do not have an effect on the Ångström exponent and the retrieval of total column ozone. The following conditions were established to characterize the y-intercept with the Brewer spectroradiometer. (1) 21 half-days were chosen during May and June 1999 which satisfied the following criteria: (2) More than 8 direct measurements yielding a correlation in the Langley plots of better than 0.99; (3) At least 7 measurements corresponding to air masses between 1.2 and 2.2. No measurements above $m = 3.5$. (4) Standard deviation of ozone and τ_a columns of less than 2.5 DU and 0.04 respectively, during the Langley characterization day. Changes in the y-intercept photon counts did not exceed 3% between the characterization period and the time of the measurements. This 3% change in the y-intercept yields an uncertainty of 0.0176 on τ_a for an airmass of 1.7 (average for our measurements). For the UV-MFRSR the voltage

intercept is automatically characterized using the previous 5-20 successful half-day plots where a successful half-day plot meets the following requirements: (a) At least 1/3 of all points within the air mass range 1.2 – 2.2. No measurements above $m = 3.5$; (b) 1.5 standard deviations allowed in each least square test. (c) 12 or more points in the final regression.

Since the measurement frequency and time it takes to measure the direct irradiance is different for each instrument (every 20 seconds and integrated into 3-minute averages for the UV-MFRSR and 3 minutes 3-4 times an hour for the Brewer) we calculated hourly averages of $\tau_{a,\lambda}$ to be able to compare $\tau_{a,\lambda}$ from the two instruments. The data were carefully scrutinized to ensure that no passing clouds were present at the time of the direct sky measurements. This was accomplished by checking if there were any fluctuations in the global UV radiation (287-363 nm) during the times at which the direct UV scans were taken. Any change in smoothness in the global radiation curve indicates the presence of clouds. Any data suspected to be contaminated by clouds were removed manually. A second check was established comparing the measured and modeled global UV radiation. The total column O_3 measurements from the Brewer were used as input for the modeling of the global UV radiation. The Brewer raw files were also inspected to look for clear days that did not report total column O_3 . This inconsistency in the measurements of total column O_3 usually occurs when the Brewer quartz window does not accurately follow the sun path. In order to select the seven days used in this study, 2-3 months of data were carefully inspected.

1.3.2 Retrieval of Aerosol Optical Depths

1.3.2.1 Brewer Spectroradiometer

Instantaneous measurements of $\tau_{a,\lambda}$ were obtained from the Brewer spectrophotometer after characterizing the Langley photon count intercept using the criteria described in the last section. A description of the methodology used to calculate $\tau_{a,\lambda}$ using this technique is described as follows. The Langley plots are constructed by plotting the logarithm of the measured direct normal photon counts by the Brewer as a function of the air mass (m). This yields a straight line whose slope is the total atmospheric optical depth. This method is based on the Beer-Lambert law

$$\frac{I_{B,\lambda}}{I_{o,\lambda}} = e^{-\tau_{\lambda}m} \quad (1)$$

where $I_{B,\lambda}$ represents the photon counts measured by the Brewer at a specific wavelength λ , $I_{o,\lambda}$ corresponds to the photon counts that would be measured at the top of the Earth's atmosphere, and τ_{λ} is the sum of aerosol and gas extinction by air molecules and O_3 ($\tau_{\lambda} = \tau_{a,\lambda} + (\tau_{r,\lambda} + \tau_{O_3,\lambda})$). Once the $I_{o,\lambda}$ has been characterized, the aerosol optical depth ($\tau_{a,\lambda}$) at a specific wavelength is calculated at any instant using expression (2).

$$\tau_{a,\lambda} = \left(\frac{1}{m}\right) \ln\left(\frac{I_{o,\lambda}}{I_{B,\lambda}}\right) - \tau_{r,\lambda} - \tau_{O_3,\lambda} \quad (2)$$

where $\tau_{r,\lambda}$ is the pressure-scaled Rayleigh optical depth, $\tau_{O_3,\lambda}$ is the O_3 optical depth, and $I_{B,\lambda}$ the photon counts measured at any instant by the Brewer. The sea level Rayleigh optical depth ($\tau_{r,\lambda}$) was taken from the expression of Hansen and Travis (1974).

The Brewer direct photon counts were measured using a routine that points the Brewer's quartz window at the Sun in order to measure direct normal photon counts. The positioning of the UV filter (UG-11), mounted on a filter wheel, in order to reduce background scattered light from other wavelengths in the Brewer, allows the accurate measurement of photon counts at 320, 340, and 360 nm. In addition to the UV filter, a neutral density filter is used at all times to avoid saturation of the photomultiplier tube. Five measurements are performed at each of the three wavelengths and the sum of the photon and dark counts (or dark leakage current of the diode) are recorded at each wavelength and solar zenith angle. The Brewer takes 2-3 minutes to collect the photon counts for the five passes. Approximately 2 to 3 direct photon count measurements are performed every hour.

Several factors affect the accuracy of the τ_a measurements using sun photometers. This section discusses the sensitivity of the Brewer to measurement error.

1. Fluctuations of the photon count intercept (I_0) remained between 1-3% before and during the period of the measurements for all three wavelengths (320, 340, and 360 nm). A 3% fluctuation on I_0 yields on average a 0.0176 uncertainty in τ_a .
2. Changes in total column O_3 have an effect on the retrieved values of τ_a . Total column O_3 is the major absorber of UV radiation for wavelengths shorter than 340 nm. Therefore, measurements of $\tau_{a,\lambda}$ obtained from measurements of direct irradiance are directly affected by the total column of O_3 in the atmosphere. The Brewer's uncertainty for a measurement of total column O_3 is roughly $\pm 2.5\%$ (Kerr and McElroy, 1995). A 3% fluctuation in total column O_3 from the average values of total column O_3 observed during the study was estimated to be ~ 12 DU. The uncertainties

introduced to $\tau_{a, \lambda}$ due to this variation in total column O_3 are ($\tau_{a,320} \pm 0.009$) at 320 nm, ($\tau_{a,340} \pm 0.00054$) at 340 nm, and $< 0.01\%$ at 360 nm.

3. Changes in the vertical structure of temperature and pressure of the atmosphere also have an effect in the retrieved $\tau_{a,\lambda}$. This effect is small but non-negligible in the retrieved $\tau_{a, \lambda}$ for the UV-B ($\lambda < 320$ nm) due to Rayleigh scattering. These effects were assessed by simulating $\tau_{a,\lambda}$ with the Tropospheric Ultraviolet-Visible (TUV) model developed at the National Center for Atmospheric Research (NCAR) for three different atmospheric profiles: a mid-latitude summer (*mls*), a mid-latitude winter (*mlw*), and an Arctic winter (*aw*) profile. Since changes in the vertical distribution of O_3 have a smaller effect on the surface UV irradiance than changes in the total column of O_3 (Schwander et al., 1997), the vertical distribution of the O_3 was left constant corresponding to that of the US standard atmosphere for all three profiles in this calculation (NOAA, 1976). The aerosol optical depth is calculated for each layer of the model ($\tau_{a(i),\lambda}$) using equation 2. The total atmospheric $\tau_{a,\lambda}$ is then calculated by summing all the ($\tau_{a(i),\lambda}$) from each individual layer. The vertical distribution of the aerosol extinction coefficients obtained by Elterman (1968) was used for this calculation. The radiation model was run using the eight-stream discrete ordinates scheme radiation solver. A full description of the model is given by Madronich and Flocke (1999). The range of wavelengths investigated corresponds to the spectral range of the Brewer spectrophotometer (287-363 nm). It was found that significant changes will occur to the calculated $\tau_{a,\lambda}$ as a function of the atmospheric profile for wavelengths shorter than 320 nm. For example, at 287 nm, the percentage increase in the retrieved $\tau_{a, \lambda}$ due to a change in the atmospheric profile from a mid-latitude

summer to an Arctic winter profile is about 20%. At 305 nm, the percentage difference is 3.5% and at 320 nm the percentage difference is only 0.4%. Changes in $\tau_{a,\lambda}$ above 325 nm are for the most part around 0.3%. Therefore, variability in atmospheric pressure have a small effect on $\tau_{a,\lambda}$ retrieved in this study.

4. The uncertainty of these effects on τ_a were investigated propagating the errors produced by the individual uncertainties. Propagation of errors at 320 nm yields a 0.0198 change in τ_a . At 340 nm the propagation of errors yields a 0.0177 change in τ_a . At 360 nm the effect on τ_a is 0.0176.

1.3.2.2 UV-MFRSR

Harrison et al. (1994) describes how the multifilter rotating shadow-band radiometer uses independent interference-filter photodiode detectors and the automated rotating shadow-band technique to make spectrally resolved measurements of direct-normal, total horizontal, and diffuse horizontal irradiances at 300, 305, 317, 325, 332, and 368 nominal center wavelengths. These measurements are well-suited to retrieve τ_a . An advantage of the UV-MFRSR is that the diffuse- and total-horizontal irradiance measurements have the same passband and sensitivity as the direct normal irradiances. Since both the passband and transmission of interference filters are sensitive to temperature, the temperature of the internal detector assembly is stabilized at 35° C or 45° C depending on the geographical location of the instrument. The direct irradiance is calculated subtracting the diffuse component of the irradiance from the total-horizontal component. Division by cosine of the solar zenith angle then produces the direct-beam flux on a normal surface. The UV-MFRSR measurements are stored as 3-min averages

from measurements made every 20-s intervals. The flat diffusing receivers do not employ glass domes and therefore provide the MFRSR with the advantages of the Lambertian-like diffusers. Before $\tau_{a,\lambda}$ can be calculated, the total column ozone values measured by the collocated Brewer spectrophotometer are used to calculate the filter weighted O₃ optical depths. Propagation of errors at 317 nm yields a 0.02 change in τ_a . At 332 nm the propagation of errors yields a 0.0181 change in τ_a . At 368 nm the effect on τ_a is 0.012.

1.4 Results and Discussion

1.4.1 Comparison of Brewer and UV-MFRSR Aerosol Optical Depths

Before $\tau_{a,\lambda}$ can be compared between the two instruments the measurements of $\tau_{a,\lambda}$ from each instrument were averaged over the same period of time. This was achieved by calculating hourly averages from the measurements collected by each instrument. Table 1-1 summarizes overall differences in $\tau_{a,\lambda}$ for each of the seven days considered in this study. Three quantities: daily mean $\tau_{a,\lambda}$, standard deviation of $\tau_{a,\lambda}$, and maximum and minimum $\tau_{a,\lambda}$ are shown in Table 1-1.

Table 1-1: Daily mean, standard deviation, maximum, and minimum $\tau_{a,\lambda}$ for each of the measurement days.

Day, Year	<i>BREWER SPECTROPHOTOMETER</i>					<i>UV-MFRSR</i>				
	(λ)	Mean	Std. Dev	Max.	Min.	(λ)	Mean	Std. Dev.	Max	Min
225, 99 Aug. 13	320	0.195	0.089	0.303	0.098	317	0.239	0.087	0.346	0.142
	340	0.203	0.089	0.312	0.104	332	0.248	0.081	0.346	0.155
	360	0.172	0.080	0.269	0.086	368	0.200	0.068	0.280	0.121
230, 99 Aug. 18	320	0.111	0.026	0.137	0.073	317	0.114	0.026	0.139	0.073
	340	0.133	0.031	0.176	0.087	332	0.138	0.021	0.157	0.100
	360	0.103	0.023	0.128	0.070	368	0.104	0.017	0.125	0.078
234, 99 Aug. 22	320	0.267	0.152	0.466	0.117	317	0.271	0.176	0.505	0.110
	340	0.269	0.130	0.450	0.141	332	0.292	0.170	0.521	0.136
	360	0.257	0.148	0.450	0.113	368	0.259	0.162	0.481	0.113
235, 99 Aug. 23	320	0.182	0.044	0.256	0.131	317	0.175	0.037	0.236	0.133
	340	0.237	0.037	0.282	0.184	332	0.201	0.031	0.250	0.161
	360	0.174	0.042	0.247	0.129	368	0.167	0.030	0.213	0.131
236, 99 Aug. 24	320	0.235	0.090	0.333	0.150	317	0.230	0.085	0.364	0.169
	340	0.306	0.070	0.388	0.234	332	0.262	0.082	0.389	0.203
	360	0.225	0.089	0.321	0.141	368	0.220	0.075	0.341	0.170
172, 00 June 21	320	0.213	0.114	0.420	0.129	317	0.189	0.088	0.356	0.108
	340	0.195	0.110	0.412	0.119	332	0.164	0.090	0.333	0.086
	360	0.179	0.107	0.375	0.103	368	0.154	0.092	0.328	0.076
182/00 July 1 st	320	0.330	0.090	0.466	0.261	317	0.375	0.088	0.490	0.301
	340	0.318	0.071	0.432	0.261	332	0.337	0.079	0.438	0.270
	360	0.281	0.074	0.392	0.224	368	0.297	0.070	0.385	0.238

The daily quantities presented in this table were derived from the hourly averages. The lowest $\tau_{a,\lambda}$ was measured on day 230 (August 18th, 1999) with a daily mean τ_a of 0.114 and 0.111 at 317/320 nm for the UV-MFRSR and Brewer, respectively. The maximum τ_a was measured on day 182 (July 1st, 2000) with daily mean τ_a of 0.375 and 0.330 at 317/320 nm for the UV-MFRSR and Brewer, respectively. The meteorological conditions are directly related to the maximum and minimum reported τ_a , with the highest values of τ_a associated with stagnant conditions observed under the influence of an upper level high pressure.

The daily variation and the spectral dependence of the retrieved $\tau_{a,\lambda}$ are shown as 3-D plots of the hourly averages of the aerosol optical depth as a function of wavelength, $\tau_{a,\lambda}$ (Figure 1-1). In general, a diurnal variability is observed in $\tau_{a,\lambda}$ measured by both instruments. For the measurements presented in this study there is a clear increase in $\tau_{a,\lambda}$ from the mornings to the evenings (hours are displayed in GMT). This diurnal variation is also seen in the global UV radiation measured by the Brewer spectrophotometer which uses independent optics to the quartz window. For instance, day 225 shows a 20% decrease in the measured UV irradiance (287-363 nm) when morning and afternoon measurements are compared for the same solar zenith angle. This change in global radiation corresponds to a three-fold increase in $\tau_{a,\lambda}$ from sunrise to sunset for all wavelengths for day 225. Figure 1-2 shows the diurnal variation in τ_a for all seven days considered in this study. This increase in the aerosol optical depth is probably associated with the observed changes in wind direction that are present at the front range of the Rocky Mountains associated with differences in heating between the mountains and the lower elevations. The wind climatology of the region indicates that the winds shift from

southerly or westerly to easterly or northeasterly during the course of the day at the base of the mountains. This produces an area of convergence of low level boundary layer air against the mountains. Day 225 experienced a pronounced wind shift from southerly to northeasterly during the course of the day.

Figure 1-3 compares hourly-averaged $\tau_{a,\lambda}$ estimated by the Brewer and UV-MFRSR for the nearest measured wavelength pairs. The square of the correlation coefficient between the two instruments is 0.92 for the 317-320 nm wavelength pair, 0.86 for the 332-340 nm wavelength pair, and 0.94 for the 368-360 nm wavelength pair. The ratio of the $\tau_{a,\lambda}$ measured by the Brewer to that measured by the UV-MFRSR is within $1.0243 \pm (0.17 \text{ standard deviation})$ when averaged over the three wavelength pairs.

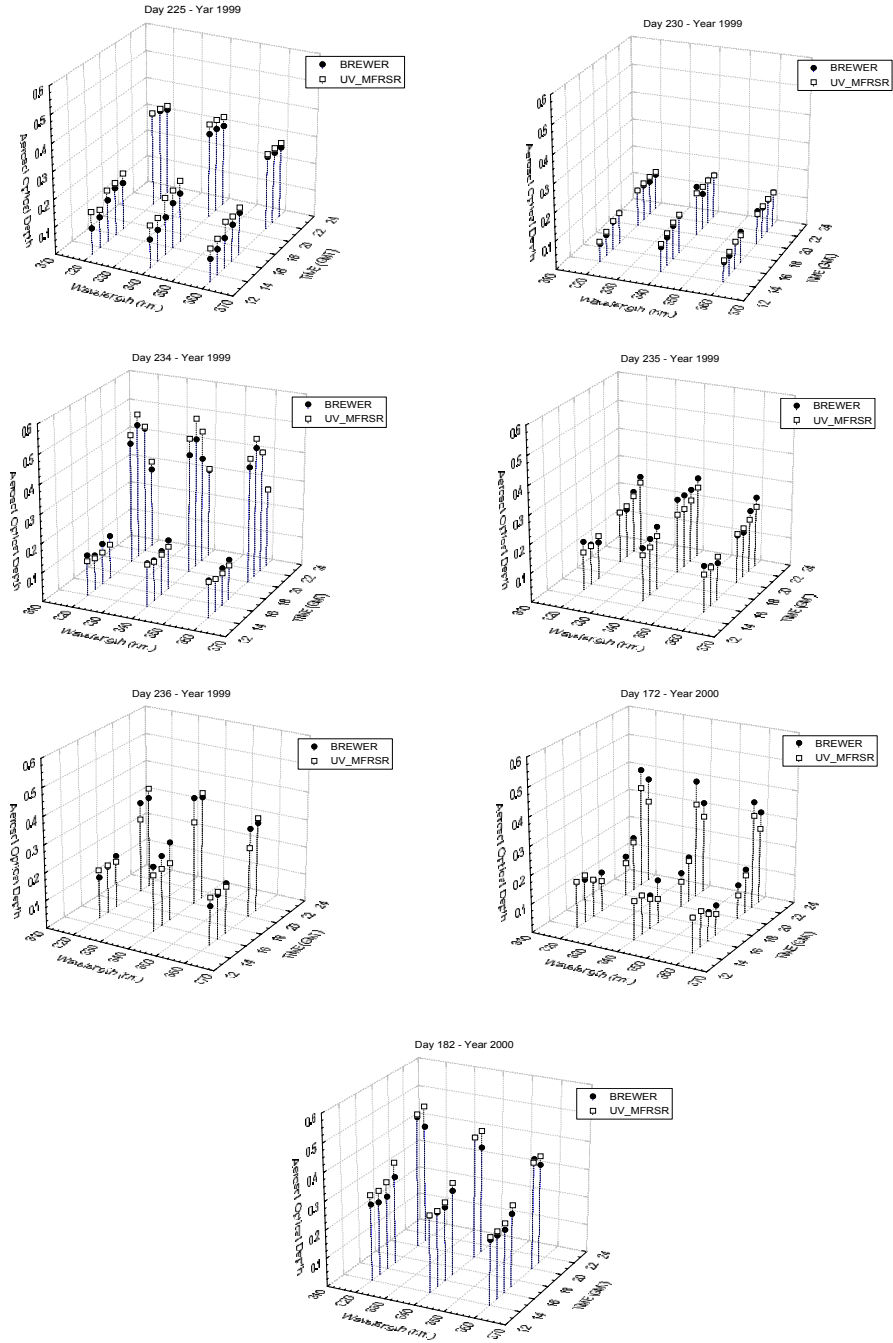


Figure 1-1: Daily temporal variation of $\tau_{a,\lambda}$ (aerosol optical depth) as a function of time and wavelength for the UV-MFRSR and the Brewer spectrophotometer.

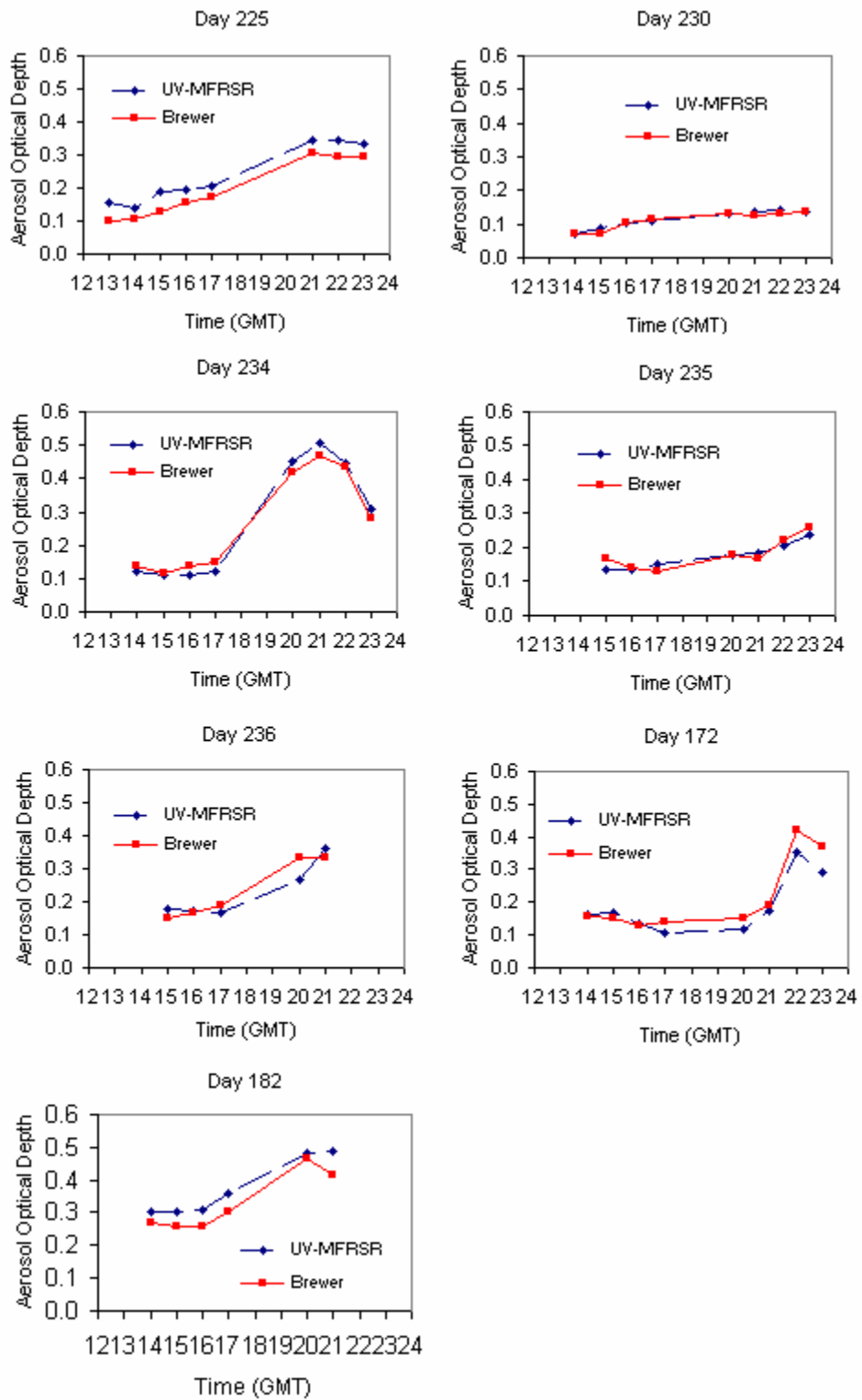


Figure 1-2: Aerosol optical depth for the Brewer and the UV-MFRSR for the seven measurement days.

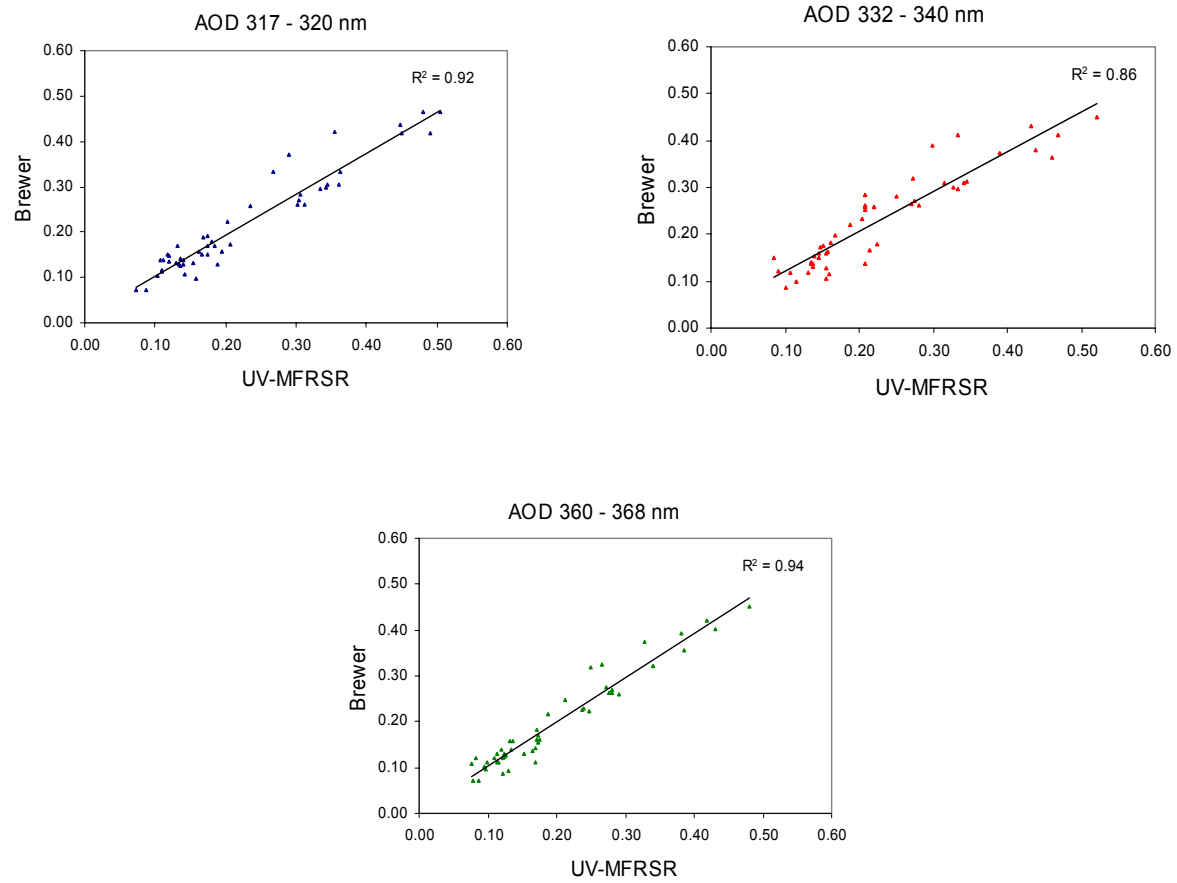


Figure 1-3: Regression plots of the hourly averages of the $\tau_{a,\lambda}$ for each of the instruments. The wavelength pairs used for the comparison of the $\tau_{a,\lambda}$ are 317 and 320 nm, 332 and 340 nm, and, 368 and 360 nm.

1.4.2 Wavelength Dependence of the Aerosol Optical Depths

The Ångström exponent yields qualitative information on the aerosol size distribution with higher values typically corresponding to smaller particles. The day-to-day variability in the Ångström exponent very likely reflects shifts in air mass types resulting in different aerosol properties. The Ångström exponent (α) is calculated using the 320-360 wavelength range for the Brewer and the 317-368 wavelength range for the UV-MFRSR where:

$$\alpha = -\frac{\ln(\tau_{a,\lambda_2} / \tau_{a,\lambda_1})}{\ln(\lambda_2 / \lambda_1)} \quad (3)$$

Propagating the errors through the Ångström equation yields an overall average uncertainty of 0.16 for the Brewer, ranging between 0.06 and 0.37 for high and low values of τ_a respectively. For the UV-MFRSR the propagation of the errors through the Ångström equation yields an overall average uncertainty of 0.11, ranging between 0.04 and 0.23 for high and low values of τ_a respectively. Arola and Koskela (2004) have studied the different factors that could induce systematic error when deriving Ångström exponents with the Brewer Spectrophotometer. These factors are: (1) diffuse irradiance in the Field of view (which is 2.5 degrees for the Brewer), diurnal ozone changes, NO₂ influence, and stray light influence. In their analysis they found that the Brewer Spectrophotometer underestimates the Ångström exponent due to the combination of these factors. Arola and Koskela (2004) estimated a bias in τ_a of -0.0794 (negative bias) between 306.3 and 320.1 nm. They compared this negative bias with the expected difference in τ_a between these two wavelengths using an Angstrom exponent of 1.0. The expected difference using the Ångström exponent of 1.0 yielded a positive bias in τ_a of

+0.0224 between 306.3 and 320.1 nm. Arola and Koskela (2004) concluded that the systematic errors can mask the real differences in τ_a and result at times in a negative Ångström exponent. In order to consider the uncertainties produced by these effects in our measurements we use of a bias in τ_a of -0.0794 between 320 and 360 nm to estimate the Ångström exponent uncertainty for our measurements. This yields an additional uncertainty of ± 0.04 making the overall estimated uncertainty to be ± 0.165 for the Brewer retrieved Ångström exponents. A bias in τ_a of -0.0794 is probably a large estimate of the bias that we could expect from our measurements since Arola and Koskela (2004) found lesser biases -0.0347 in τ_a between 310.1 and 320.1 nm in comparison to shorter wavelength ranging between 306.3 and 320.1 nm. For the UV-MFRSR propagation of the errors through the Ångström equation yields an overall average uncertainty of 0.11. The uncertainty in α range between 0.04 and 0.23 for high and low values of τ_a respectively.

The correlation coefficient between the Brewer and UV-MFRSR Ångström exponents is 0.77 (Figure 1-4). Table 2-1 shows the mean, standard deviation, maximum and minimum Ångström exponents for each day. There is no clear relationship between $\tau_{a,\lambda}$ and Ångström exponent for these measurements. The overall lack of correlation implies that the intensive aerosol properties (size distribution and optical characteristics) do not seem to vary with the amount of aerosol present in the atmosphere. Figure 1-5 shows the hourly averages of the Ångström exponents for each of the seven measurement days for both instruments.

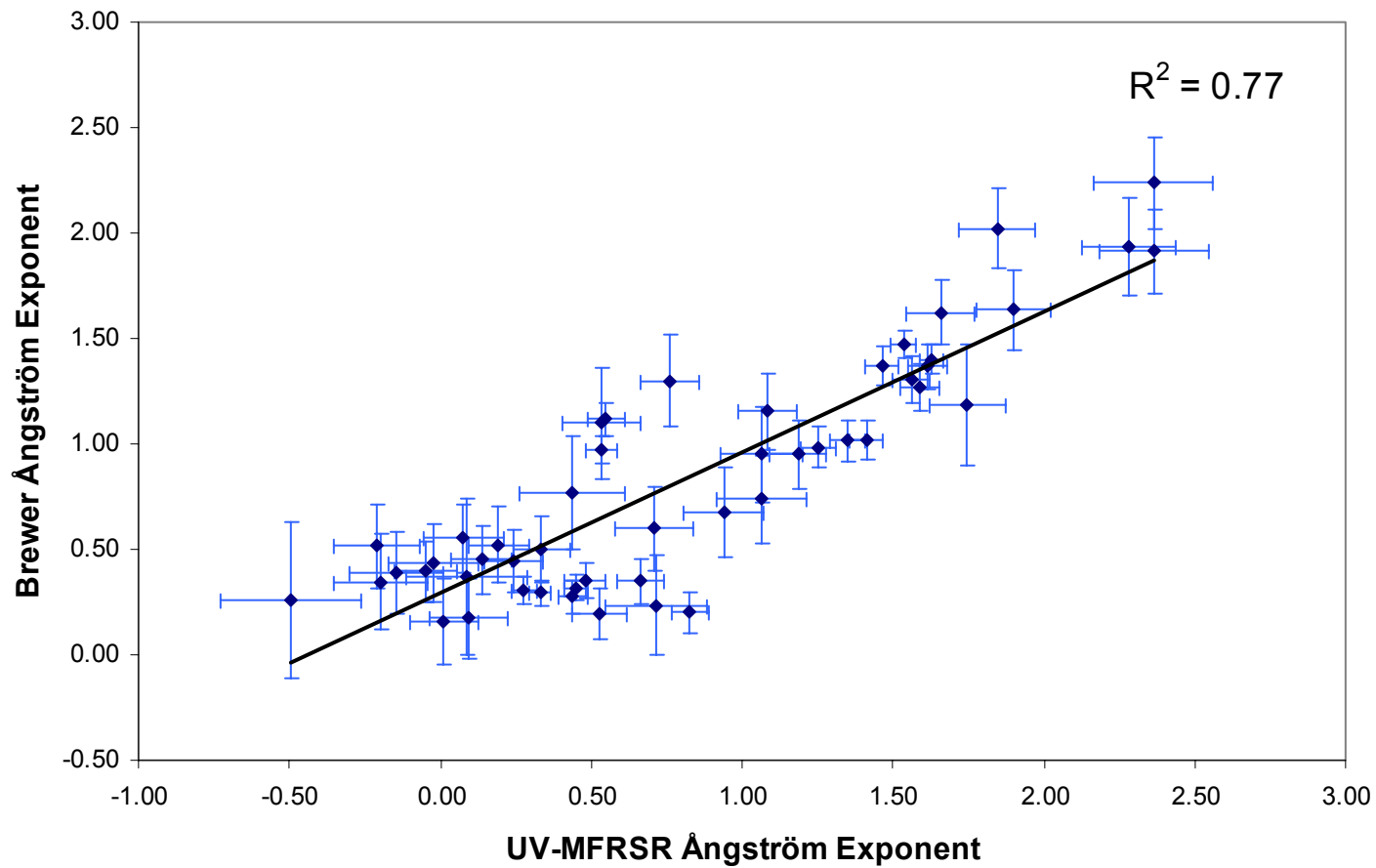


Figure 1-4: Correlation coefficient between the UV-MFRSR and Brewer Ångström exponent calculated from the hourly values of τ_a . The Ångström exponent (α) is calculated using the 320-360 wavelength range for the Brewer and the 317-368 wavelength range for the UV-MFRSR.

Table 1-2: Mean, standard deviation, maximum, and minimum Ångström exponents for each of the measurement days.

<i>Day, Year</i>	<i>Brewer Spectrophotometer</i>				<i>UV-MFRSR</i>			
	Mean	Std. Dev.	Max.	Min.	Mean	Std. Dev.	Max.	Min.
225, 99	1.09	0.12	1.30	0.95	1.17	0.38	1.75	0.53
230, 99	0.57	0.26	0.95	0.23	0.57	0.54	1.06	-0.49
234, 99	0.35	0.10	0.52	0.20	0.16	0.37	0.83	-0.21
235, 99	0.34	0.17	0.55	0.16	0.28	0.25	0.66	0.01
236, 99	0.40	0.09	0.52	0.27	0.27	0.26	0.66	-0.05
172, 00	1.68	0.44	2.24	0.97	1.68	0.75	2.36	0.54
182, 00	1.36	0.07	1.47	1.27	1.42	0.39	1.63	0.53

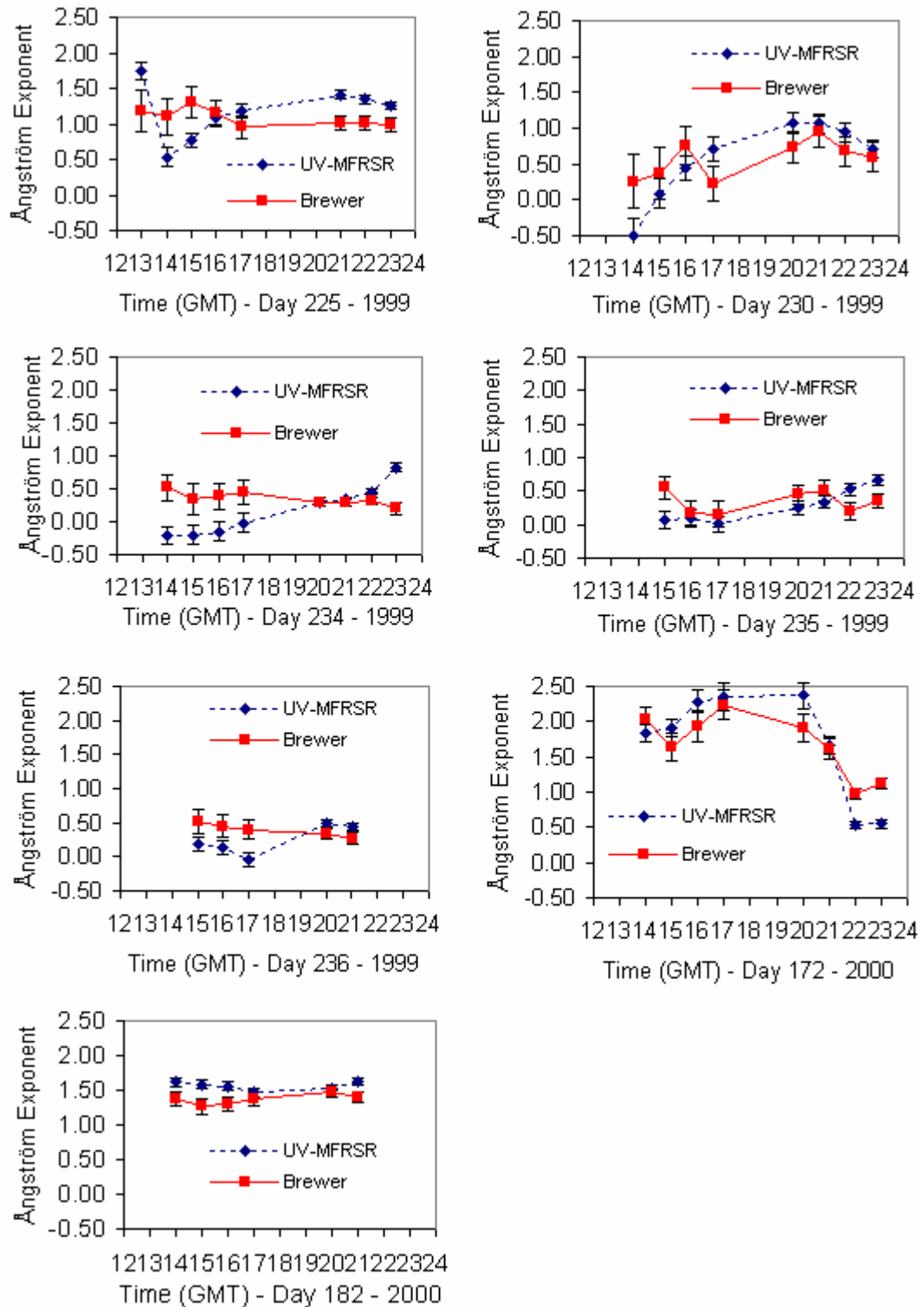


Figure 1-5: Hourly averages of the Ångström exponents for each of the seven measurement days

The daily standard deviations in the Ångström exponent ranged from 0.07 to 0.44 for the Brewer and from 0.25 to 0.75 for the UV-MFRSR. Large variability of the Ångström exponent are presented in the literature. For instance, Marengo et al. (1997) measured Ångström exponents in the UV as high as 4.0. Kylling et al. (1998) found values between 0.1 and 2.3 at Athens, Greece during June 1996. In addition to these studies, Borghesi et al. (1982) obtained wavelength exponents in the UV between 0.3 and 4.0 at the Mediterranean Sea at the same time of the year. Wenny et al. (2001) report mean wavelength exponents of 1.86 with a standard deviation of 1.05 in North Carolina, USA. The hourly mean Ångström exponents are $0.82 \pm (0.11 \text{ measurement uncertainty})$ for the UV-MFRSR and $0.84 \pm (0.165 \text{ measurement uncertainty})$ for the Brewer. In general, the day-to-day variability in the Ångström exponent is seen by both instruments.

1.4.3 Interpretation of the Wavelength Dependence of the Aerosol Optical Depth

In order to understand the observed day-to-day variability in the wavelength dependence of the aerosol optical depth, measurements are compared with model estimates. The wavelength dependence of $\tau_{a,\lambda}$ is modeled using the Mie code of Bohren and Huffman (1983), as described by Bergin et al. (1997), for typical aerosol size distributions found in the continental areas of the mid-latitudes and the results are compared with the measurements presented in this study. Four aerosol size distributions with geometric mass mean diameters of 0.1, 0.3, 0.5, and 0.6 μm , a geometric standard deviation of 2.0, with a refractive index of $1.53 - 0.0i$ were used in the Mie calculations in order to represent a broad range of aerosol size distributions. Figure 1-6 shows the calculated aerosol extinction coefficients as a function of wavelength corresponding to

the four aerosol size distributions described above. This figure shows how the curves flatten at shorter wavelengths. The wavelength where the curves flatten increases as the particle size increases. This explains why aerosol size distributions with larger geometric mass mean diameters present a smaller Ångström exponent than aerosol size distributions with smaller geometric mass mean diameters for the same wavelength. Figure 1-7 compares the calculated Ångström exponents corresponding to the aerosol extinction coefficients of Figure 1-6 to the Ångström exponents measured in this study. The measured Ångström exponents are depicted by two symbols, representing the mean and the standard deviations for each of the instruments.

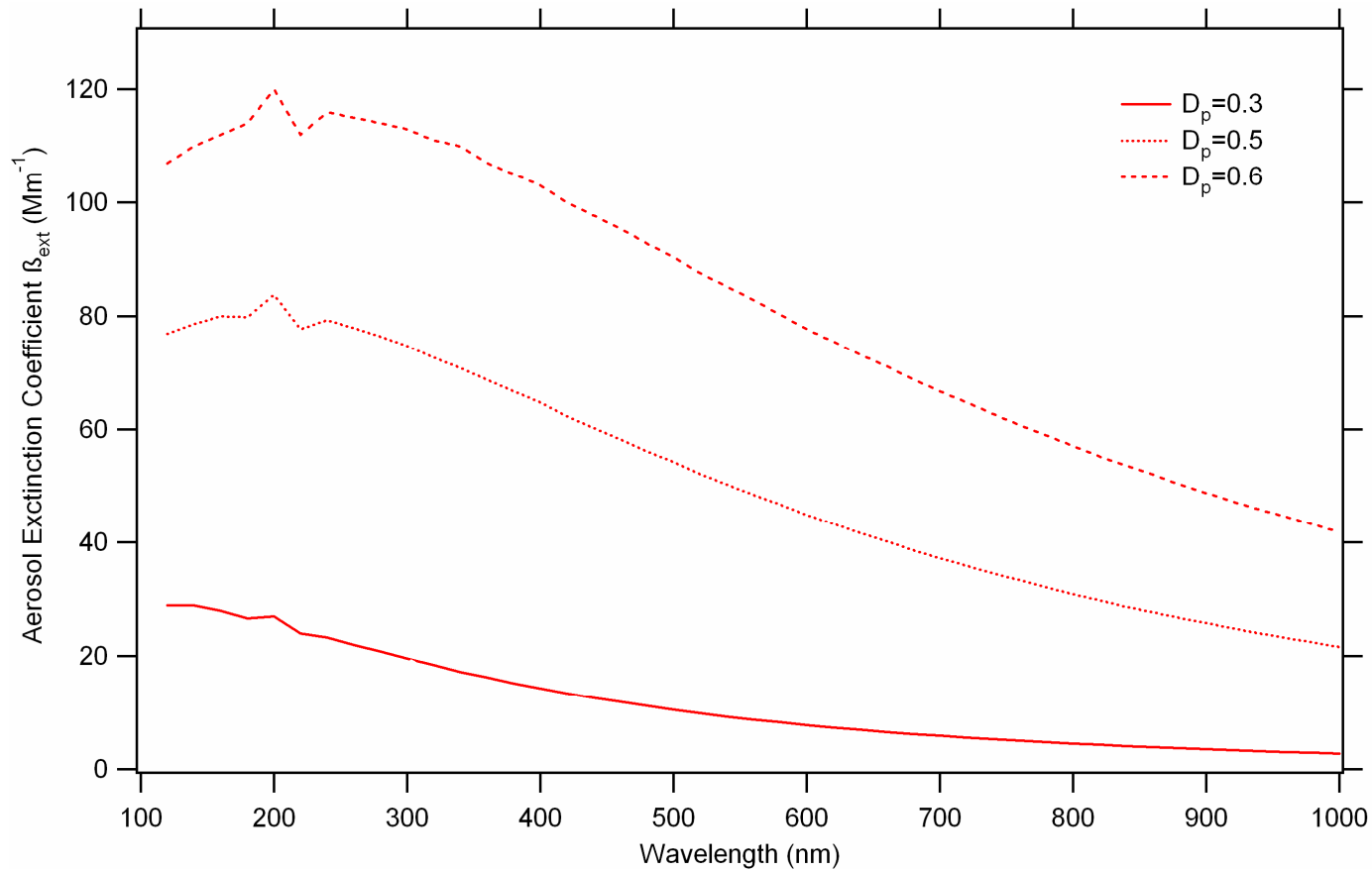


Figure 1-6: Aerosol extinction (β_{ext}) calculated using the Mie model of Bohren and Huffman for an aerosol size distribution with geometric mass mean diameters of 0.1, 0.3, 0.5, and 0.6 μm , a geometric standard deviation of 2.0, a refractive index of $1.53 - 0.0 i$, and a total number of particles equals to 1000.

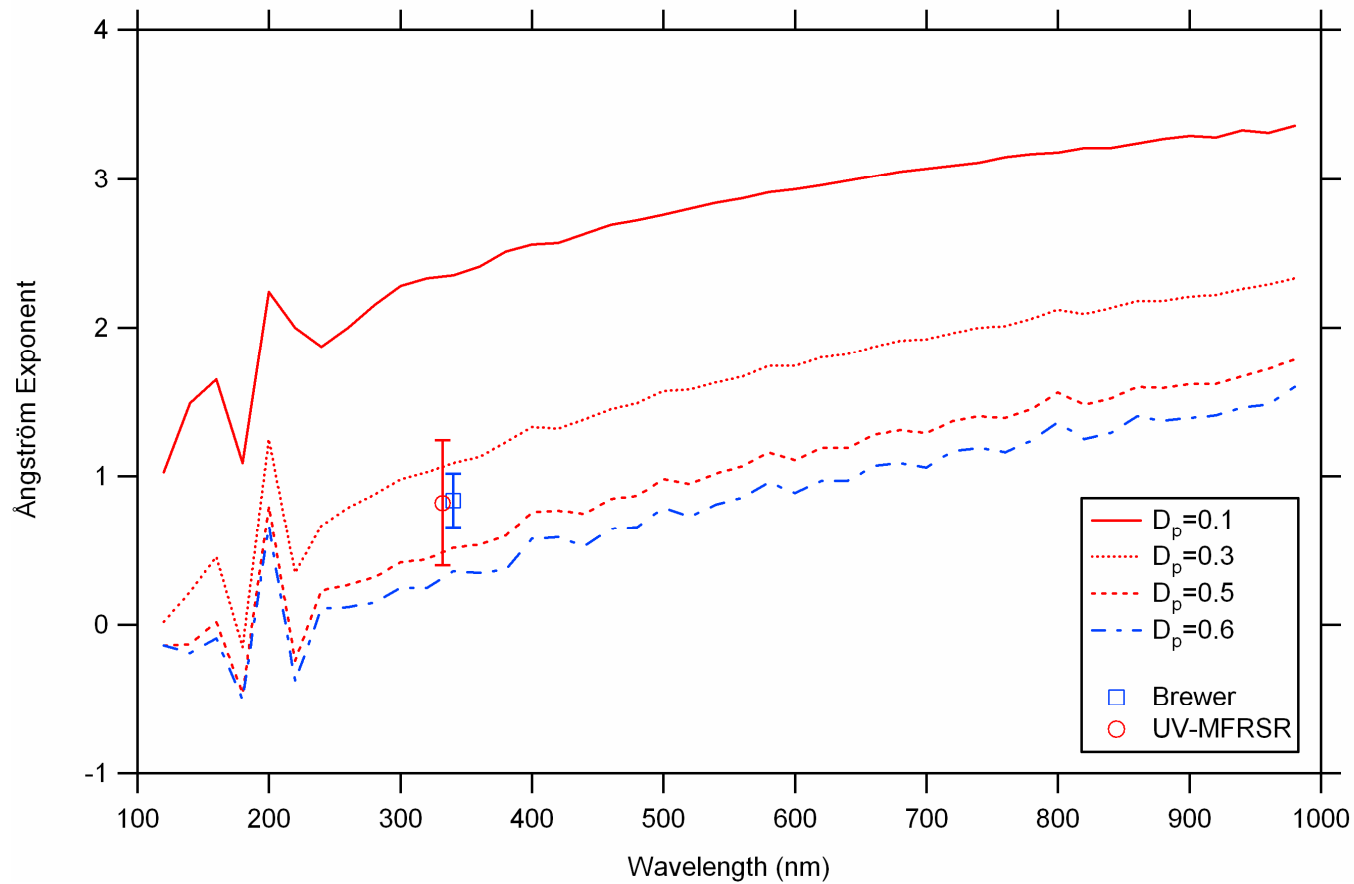


Figure 1-7: Comparison of the calculated Ångström exponents shown in Figure 1-6 to the measured Ångström exponents. The measured Ångström exponents are indicated by the two symbols (Brewer, open square and UV-MFRSR, filled circle) which depict the average mean and standard deviations for each of the instruments.

The calculated Ångström exponents range from about 0.25 to 2.50. Considering that the hourly mean Ångström exponents are $0.82 \pm (0.42$ average standard deviation of the measurements) for the UV-MFRSR and $0.84 \pm (0.18$ average standard deviation of the measurements) for the Brewer, the calculated Ångström exponents are within the range of the values estimated by the field measurements. This suggests that the average wavelength dependence of $\tau_{a,\lambda}$ can be explained based on reasonable assumptions for the size distribution and optical properties of the aerosol particles using Mie theory. Considering the full range of the standard deviations from both instruments the estimated geometric mass mean diameters of the aerosols is estimated to range between 0.25 and 0.5 μm at the time of the measurements.

The model calculations presented in the previous paragraph do not consider the effect of absorption. In order to illustrate the effect of absorbing aerosols on the Ångström exponent, the index of refraction was changed in the model for aerosol size distributions with geometric mass mean diameters of 0.1, 0.3, 0.5, and 0.6 μm and a geometric standard deviation of 2.0 (Table 3-1). The results in Table 1 show the decrease in the Ångström exponent with the increase in the geometric mass mean diameter. The Ångström exponent decreases with an increase in the imaginary part of the index of refraction when the real part of the index of refraction is kept constant. The results shown in Table 3-1 assume that the aerosol refractive index is constant with wavelength. Increased absorption into the UV as mentioned by Jacobson (1999) is also possible, and it could lead to an increase of the Ångström exponents in the UV. Jacobson (1999) suggests that nitrated and aromatic aerosols and nitrated aromatic gases were the major cause of stronger attenuation in the UV than at visible wavelengths at Claremont and

Riverside, California. In one of their measurement studies, the imaginary index of refraction of liquid nitrobenzene was found to increase from 0.1 at 400 nm to 0.4 at 300 nm (Jacobson, 1999). In order to simulate this effect, a small aerosol absorption (1.53, 0.02 i) is introduced up to 320 nm with no absorption at 360 nm (1.53, 0 i). For these absorption characteristics we yield Ångström exponents of 4.00, 1.97, and 0.97 for aerosol size distributions with geometric mass mean diameters of 0.1, 0.2, and 0.3 μm respectively. If finer aerosol distributions, with a geometric mass mean diameter of 0.05 μm are considered, the calculated Ångström exponent increases to 9.0. These results show that preferential absorption as a function of wavelength could be the culprit of some of the higher Ångström exponents measured in our study. On the other hand, the small negative Ångström exponents could be explained by an increase in the particle size and/or the decrease in the Ångström exponents associated with the larger particle sizes in the presence of absorbing materials.

The calculations presented in this section suggest that the measured variations in the Ångström exponent are probably related to changes in the aerosol size distribution and/or changes in the absorbing properties of the aerosols. The range of the Ångström exponents measured in this study generally agree when compared with the modeled Ångström exponents for typical continental aerosols with little or no absorption.

Table 1-3: Effect of absorbing aerosols on the 320-360 nm Ångström exponent for aerosol size distributions with geometric mass mean particle sizes of 0.1, 0.3, 0.5, and 0.6 μm , and geometric standard deviation of 2.0.

<i>Index of Refraction</i>	<i>$D_p=0.1$</i>	<i>$D_p=0.3$</i>	<i>$D_p=0.5$</i>	<i>$D_p=0.6$</i>
1.4, 0 i	2.36	1.28	0.74	0.55
1.4, 0.02 i	2.05	1.21	0.71	0.53
1.4, 0.06 i	1.69	1.07	0.65	0.49
1.4, 0.66 i	0.81	0.34	0.15	0.09
1.53, 0 i	2.25	1.05	0.50	0.33
1.53, 0.02 i	2.06	1.01	0.49	0.34
1.53, 0.06 i	1.80	0.94	0.47	0.31
1.53, 0.66 i	0.87	0.34	0.14	0.07

1.5 Conclusions

Measurements of aerosol optical depths (τ_a) in the UV-A are compared between an EPA Brewer spectrophotometer and an USDA UV MultiFilter Rotating Shadow-band Radiometer (UV-MFRSR) collocated at Boulder Colorado for seven days during the summer of 1999 and 2000. The square of the correlation coefficients between the two instruments is 0.92 for the 317-320 nm wavelength pair, 0.86 for the 332-340 nm wavelength pair, and 0.94 for the 368-360 nm wavelength pair (first wavelength represents the UV-MFRSR, while the second represents the Brewer). The ratio of the $\tau_{a,\lambda}$ measured by the Brewer to that measured by the UV-MFRSR is within $1.0243 \pm (0.17$ standard deviation) when averaged over the three wavelength pairs. A general increase in $\tau_{a,\lambda}$ from morning to late afternoon is observed for all measurement days presented in this study. This increase in the aerosol optical depth is probably associated with the observed changes in wind direction that are present at the front range of the Rocky Mountains associated with differences in heating between the mountains and the lower elevations. The correlation coefficient between the Brewer and UV-MFRSR Ångström exponents is 0.77. The hourly mean Ångström exponents are 0.82 ± 0.11 for the UV-MFRSR and 0.84 ± 0.165 for the Brewer. The Ångström exponents ranged from 0.16 to 2.24 for the Brewer and -0.49 to 2.36 for the UV-MFRSR. There is no correlation between the Ångström exponent and the aerosol load for a given wavelength, which indicates that the intensive aerosol properties (size distribution and optical characteristics) do not seem to change with changes in the aerosol loading. However, the Ångström exponents show hour-to-hour and day-to-day variability suggesting changes in the aerosol optical properties and/or size distribution. The measured spectral dependence of the $\tau_{a,\lambda}$ is in

qualitative agreement with the spectral dependence obtained from Mie theory using aerosol size distributions having geometric mean mass diameters ranging between 0.25 and 0.5 μm for the measurement days presented in this study.

CHAPTER II

RETRIEVAL OF AEROSOL OPTICAL DEPTHS, ANGSTRÖM EXPONENT, AND SINGLE SCATTERING ALBEDO IN THE UV DURING THE 1999 ATLANTA SUPERSITE EXPERIMENT

2.1 Summary

Investigation of the effects of aerosols on the surface UV irradiance were conducted as part of the Atlanta Supersite experiment during August, 1999. The aerosol optical depth at UV wavelengths, and the single scattering albedo, which provides information about the relative absorbing properties of the aerosols, are both important factors in determining surface UV irradiance. In order to estimate these parameters measurements of direct and global (direct + diffuse) UV radiation and total column ozone (O_3) were made using a Brewer spectroradiometer under cloud-free conditions. Aerosol optical depths (τ_a) in the UV were retrieved at 320, 340, and 360 nm. Daily averages of $\tau(340 \text{ nm})$ range from 0.23 and 2.09 with a mean and standard deviation of 0.93 ± 0.51 . The daily average spectral dependence of the aerosol optical depth, calculated via the Angström exponent (α), ranges from 0.80 and 1.92 with a mean and standard deviation of 1.44 ± 0.32 . No apparent relationship was found between τ_a and α . The retrieved values of τ_a and α were used in the Tropospheric Ultraviolet and Visible (TUV) radiation model to estimate the surface UV irradiance. Estimates of aerosol single scattering albedo (ω_o) were made by matching the measured irradiance values to model computed irradiances. The results suggest an increasing trend in ω_o with increases in τ_a . The estimated ω_o ranges from 0.80 and 0.99 with a mean and standard deviation of 0.87 ± 0.08 . Variability in τ_a and ω_o during the measurement period are capable of changing the UV Index up to 2 UV

Index units when all other effects are kept constant. The values of τ_a and α are compared with the ones obtained at a nearby rural location in Griffin, GA located 47 miles south of Atlanta using a UV-MFRSR from the US Department of Agriculture. At Griffin, daily averages of $\tau(332 \text{ nm})$ range between 0.43 and 1.53 with a mean and standard deviation of 0.94 ± 0.34 . For α the daily averages range between 0.88 and 1.97 with a mean and standard deviation of 1.33 ± 0.33 . These results indicate that on average the values of τ_a and α are similar between Griffin and Atlanta. Differences in the day-to-day estimates of τ_a and α between Atlanta and Griffin indicate that there is some regional influence of aerosols on UV irradiance, and hence UV index in the South Eastern United States during the period of the measurements.

2.2 Introduction

The health effects of UV exposure are well documented (Brash et al. 1991; Duthie et al. 1999; Kraus et al., 1998; Ohnaka, 1993). There is strong evidence that exposure to solar radiation is a major factor for the production of basal cell carcinoma (BCC), squamous cell carcinoma (SCC) and malignant melanoma (MM). BCC and SCC are commonly referred as non melanoma skin cancers (NMSC). Furthermore, more recent research indicates that the effects of UV-A radiation on skin cancer and ocular disease can be equally harmful as the effects of UV-B radiation, mainly for SCC and MM (Longstreth et al. 1998). Exposure to UV radiation is also associated with the formation of cataracts (de Gruijl, 1997; Taylor et al. 1998). Studies indicate that there is a direct association between cataract incidence and UV levels. However, it is not clear which part of the solar spectrum (UV-A or UV-B) is producing the cataract (de Gruijl, 1997).

In recent years there has been a substantial interest regarding the influence of aerosols on climate, through both direct and indirect effects (Charlson et al, 1992; Andreae 1995). Aerosols alter the magnitude of solar radiation through both scattering and absorption (direct effect). They also enhance the cloud albedo by acting as cloud condensation nuclei and therefore producing an indirect effect on radiation. Aerosols are highly variable over space and time, making it very difficult to quantify their radiative properties and climatological influences.

The majority of aerosol studies related to aerosol forcing have been conducted over the visible spectrum. However, substantial progress has been made in recent years to expand our understanding of the effects of aerosols on ultraviolet UV radiation (UV). Without accurate knowledge of the effects of aerosols on the surface UV irradiance it is

problematic to quantify the differences between modeled and measured UV irradiances (Krotkov et al. 2005) or the observed differences between UV irradiances measured by satellites and ground UV sensors (McKenzie et al., 2001a; Fioletov et al., 2002). The aerosol optical depth (τ_a) and the single scattering albedo (ω_o), which is the ratio of scattering to extinction, are two important atmospheric factors which affect the amount of UV radiation reaching the earth surface under cloud-free conditions. The spectral dependence of τ_a is typically represented by the Angström exponent (α).

Several studies have shown that the value of α in the UV is close to 1.0 and that ω_o at UV wavelengths ranges between 0.84 and 0.98. (Marenco et al., 1997; Kazantzidis et al., 2000; Kylling et al., 1998; Wenny et al. (2001). Petters et al. (2003) found that ω_o at 325 nm varied between 0.76 and 0.96 at Black Mountain, North Carolina. Krotkov et al. (2005) found that ω_o decreased with decreasing wavelength. ω_o (440 nm) = 0.96, ω_o (368 nm) = 0.94, and ω_o (325 nm) = 0.92 in Greenbelt, Maryland which is attributed to the presence of selectively UV absorbing aerosols. Kouvarakis et al. (2002) found that τ_a and ω_o measurements in Greece and Italy correlated well with surface measurements of ammonium sulfate and calcium originating from the Sahara and Schnaiter et al. (2000) found that the organic coating of the soot aerosol led to a strong increase of ω_o .

The goal of this study is to determine the values of τ_a , α , and ω_o in the UV-A during typical summertime meteorological conditions in Atlanta, GA. The measurements were conducted as part of the Atlanta Supersite experiment during August, 1999. τ_a , α , and ω_o are retrieved in the UV-A where column O_3 has a smaller effect on surface radiation than in the UV-B and the effects of aerosol on surface radiation can be investigated with less uncertainties than in the UV-B. In addition, the values of τ_a and α

are compared with the values obtained at Griffin, GA (located 47 miles to the south of Atlanta – Figure 2-1) using a UV Multifilter Shadowband Radiometer (UV-MFRSR).

The Supersite experiment was coordinated through the Southern Oxidants Study and the Georgia Institute of Technology and funded by the US EPA along with other sponsors. The Atlanta Supersite Project was located on Jefferson St. in NW Atlanta, GA. The site was located in a mixed commercial-residential neighborhood within approximately 200 meters of a bus maintenance yard and several warehouse facilities, and approximately 200 meters from the two closest streets. The primary objective of the Atlanta Supersite Project was to evaluate and compare advanced measurement methods for particular matter mass and its components. The meteorological regimes manifested during the study allowed for the stagnation of pollutants for the majority of the study.

2.3 Instrumentation and Technique for Measurement

Direct sun aerosol optical thickness measurements were made with a Brewer spectroradiometer. Instantaneous measurements of $\tau_{a,\lambda}$ were obtained from the Brewer spectroradiometer after characterizing the Langley photon count intercept. A description of the methodology used to calculate $\tau_{a,\lambda}$ using this technique is described below.

The Langley plots are constructed plotting the logarithm of the measured direct normal photon counts by the Brewer as a function of the air mass (m). This yields a straight line whose slope is the total atmospheric optical depth. This method is based on the Beer-Lambert law

$$\frac{I_{B,\lambda}}{I_{o,\lambda}} = e^{-\tau_{\lambda}m} \quad (1)$$

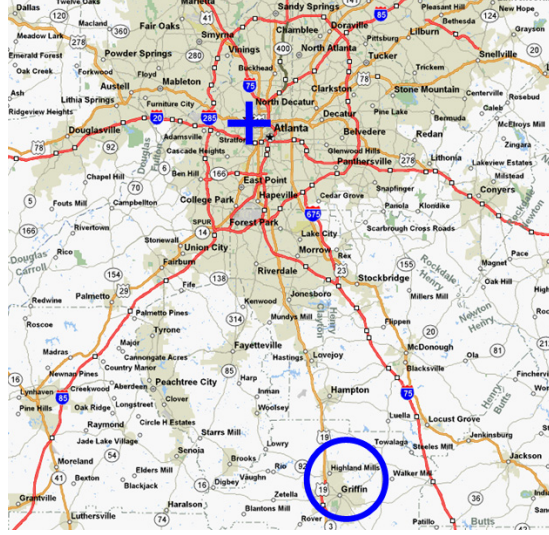


Figure 2-1: Location of Jefferson, Street (plus sign) and Griffin, GA (circle) measurement site.

where $I_{B,\lambda}$ represents the photon counts measured by the Brewer at a specific wavelength λ , $I_{o,\lambda}$ corresponds to the photon counts that would be measured at the top of the Earth's atmosphere (characterized Langley photon count intercept), and τ_λ is the sum of aerosol and gas extinction by air molecules and O_3 [$\tau_\lambda = \tau_{a,\lambda} + (\tau_{r,\lambda} + \tau_{O_3,\lambda})$]. The O_3 is obtained from the Brewer spectroradiometer. Once the $I_{o,\lambda}$ has been characterized, the aerosol optical depth ($\tau_{a,\lambda}$) at a specific wavelength is calculated at any instant using expression (2).

$$\tau_{a,\lambda} = \left(\frac{1}{m}\right) \ln\left(\frac{I_{o,\lambda}}{I_{B,\lambda}}\right) - \tau_{r,\lambda} - \tau_{O_3,\lambda} \quad (2)$$

where $\tau_{r,\lambda}$ is the pressure-scaled Rayleigh optical depth, $\tau_{O_3,\lambda}$ is the O_3 optical depth, and $I_{B,\lambda}$ the photon counts measured at any instant by the Brewer. The sea level Rayleigh optical depth ($\tau_{r,\lambda}$) was taken from the expression of Hansen and Travis (1974).

The Brewer direct photon counts were measured using a routine that points the Brewer's quartz window at the Sun in order to measure direct normal photon counts. The positioning of the UV filter (UG-11), mounted on a filter wheel, in order to reduce background scattered light from other wavelengths in the Brewer, allows the accurate measurement of photon counts at 320, 340, and 360 nm. In addition to the UV filter, a neutral density filter is used at all times to avoid saturation of the photomultiplier tube. Five measurements are performed at each of the three wavelengths and the sum of the photon and dark counts are recorded at each wavelength and solar zenith angle. The routine saves this information directly to the Brewer computer for further data processing. The Brewer takes 2-3 minutes to collect the photon counts for the five passes. Approximately 2 to 3 direct photon count measurements are performed every hour.

In addition to the quartz window the Brewer spectroradiometer is equipped with a Teflon diffuser under a quartz dome. Though the Teflon diffuser the Brewer records UV scans covering the spectral region 286.5 to 363.0 nm in steps of 0.5 nm. These scans were performed daily, both in the morning and evening. On average, a total of 25-30 scans were performed daily. The proper wavelength calibration of the spectroradiometer is ensured before each scan using an internal mercury lamp. The absolute calibration of this lamp is achieved by comparison to 50-W secondary lamps, traceable to the standards of the National Institute of Standards and Technology (NIST). The overall stability of the Brewer spectroradiometer is checked several times daily by recording the results from an internal standard lamp, and it was found to be within 1%.

The Brewer performs direct sun O₃ measurements on a regular basis (a few times per hour). The total O₃ value is computed from the extinction of ultraviolet sunlight.

During the measuring period and previous calibrations only small $\sim 1.1\%$ systematic errors were found. Stability checks with an internal standard lamp gave no indication of a deterioration of the instrument since the beginning of the calibration period. Typical errors of the Brewer O₃ measurement are on the order of 2% (Waben and Kuik, 1998). In general, errors increase with the solar zenith angle.

Several factors affect the accuracy of the τ_a measurements using sun photometers. This section discusses the sensitivity of the Brewer to measurement error.

1. Fluctuations of the photon count intercept (I_0) remained between 1-3% before and during the period of the measurements for all three wavelengths (320, 340, and 360 nm). A 3% fluctuation on I_0 yields on average a 0.018 uncertainty in τ_a .
2. Changes in total column O₃ have an effect on the retrieved values of τ_a . Total column O₃ is the major absorber of UV radiation for wavelengths shorter than 340 nm. Therefore, measurements of $\tau_{a,\lambda}$ obtained from measurements of direct irradiance are directly affected by the total column of O₃ in the atmosphere. The Brewer's uncertainty for a measurement of total column O₃ is roughly $\pm 2.5\%$ (Kerr and McElroy, 1995). A 3% fluctuation in total column O₃ from the average values of total column O₃ observed during the study was estimated to be ~ 12 DU. The uncertainties introduced to $\tau_{a,\lambda}$ due to this variation in total column O₃ are ($\tau_{a,320} \pm 0.0090$) at 320 nm, ($\tau_{a,340} \pm 0.00054$) at 340 nm, and $< 0.01\%$ at 360 nm.
3. Changes in the vertical structure of temperature and pressure of the atmosphere also have an effect in the retrieved $\tau_{a,\lambda}$. This effect is small but non-negligible in the retrieved $\tau_{a,\lambda}$ for the UV-B ($\lambda < 320$ nm) due to Rayleigh scattering. These

effects were assessed by simulating $\tau_{a,\lambda}$ with the Tropospheric Ultraviolet-Visible (TUV) model developed at the National Center for Atmospheric Research (NCAR) for three different atmospheric profiles: a mid-latitude summer (*mls*), a mid-latitude winter (*mlw*), and an Arctic winter (*aw*) profile. Since changes in the vertical distribution of O₃ have a smaller effect on the surface UV irradiance than changes in the total column of O₃ (Schwander et al., 1997), the vertical distribution of the O₃ was left constant corresponding to that of the US standard atmosphere for all three profiles in this calculation (NOAA, 1976). The aerosol optical depth is calculated for each layer of the model ($\tau_{a(i),\lambda}$) using equation 2. The total atmospheric $\tau_{a,\lambda}$ is then calculated by summing all the ($\tau_{a(i),\lambda}$) from each individual layer. The vertical distribution of the aerosol extinction coefficients obtained by Elterman (1968) was used for this calculation. The radiation model was run using the eight-stream discrete ordinates scheme radiation solver. A full description of the model is given by Madronich and Flocke (1999). The range of wavelengths investigated corresponds to the spectral range of the Brewer spectroradiometer (286.5-363 nm). It was found that significant changes will occur to the calculated $\tau_{a,\lambda}$ as a function of the atmospheric profile for wavelengths shorter than 320 nm. For example, at 287 nm, the percentage increase in the retrieved $\tau_{a,\lambda}$ due to a change in the atmospheric profile from a mid-latitude summer to an Arctic winter profile is about 20%. At 305 nm, the percentage difference is 3.5% and at 320 nm the percentage difference is only 0.4%. Changes in $\tau_{a,\lambda}$ above 325 nm are for the most part around 0.3%.

Therefore, variability in atmospheric pressure have a small effect on $\tau_{a,\lambda}$ retrieved in this study.

4. The uncertainty of these effects on τ_a were investigated propagating the errors produced by the individual uncertainties. Propagation of errors at 320 nm yields a 0.020 change in τ_a . At 340 nm the propagation of errors yields a 0.018 change in τ_a . At 360 nm the effect on τ_a is 0.018.

To minimize the errors associated retrieving aerosol optical depths at higher solar zenith angles we only used solar zenith angles (SZA) between 34 and 63 degrees corresponding to air masses between 1.2 and 2.2 for all Langley plots performed in this study. The changes in sensitivity of the Brewer spectroradiometer as a function of the solar zenith angle are negligible for solar zenith angles less than 50 degrees as indicated by Cede et al. (2006). At a solar zenith angle of 60 degrees Cede et al. (2006) show that the sensitivity of the Brewer is only reduced by 1% yielding a marginal effect on the Langley method. For solar zenith angles greater than 50 degrees these changes in sensitivity are independent of wavelength and therefore do not have an effect on the Ångström exponent and the retrieval of total column O_3 . The following conditions were established to characterize the y-intercept with the Brewer spectroradiometer. (1) 21 half-days were chosen during May and June 1999 which satisfied the following criteria: (2) More than 8 direct measurements yielding a correlation in the Langley plots of better than 0.99; (3) At least 7 measurements corresponding to air masses between 1.2 and 2.2. No measurements above $m = 3.5$. (4) Standard deviation of O_3 and τ_a columns of less than 2.5 DU and 0.04 respectively, during the Langley characterization day. Changes in the y-intercept photon counts did not exceed 3% between the characterization period and the

time of the measurements. This 3% change in the y-intercept yields an uncertainty of 0.018 on τ_a for an airmass of 1.7 (average for our measurements).

The Yankee Environmental Systems UV Multifilter Rotating Shadowband Radiometer (UV-MFRSR) uses 7 independent interference filter photodiode detector combinations to make total horizontal solar irradiance measurements at 300, 305.5, 311.4, 317.6, 325.4, 332.4 and 368 nm (nominal 2 nm FWHM bandwidth) through a single Lambertian detector. A computer-controlled, automatic rotating shadow band permits the near simultaneous determination of total horizontal, direct normal and diffuse radiation at each filtered passband. Measurements are made sequentially at each wavelength every 20 seconds and integrated into 3-minute averages by an on-board computer. The computer also serves as the data logger for the UV-MFRSR. The UV-MFRSR is polled daily via a dedicated telephone line. As with other multifilter rotating shadowband radiometers the choice of wavelengths permits a Langley analysis for the direct determination of optical depth. The 332.4nm wavelength serves as a reference to Dobson instruments and the 311.5 is designed to be a reference point to a relatively unstructured (flat) portion of the UV spectra.

For the UV-MFRSR the voltage intercept was automatically characterized using the previous 5-20 successful half-day plots where a successful half-day plot meets the following requirements: (a) At least 1/3 of all points within the air mass range 1.2 – 2.2. No measurements above $m = 3.5$; (b) 1.5 standard deviations allowed in each least square test. (c) 12 or more points in the final regression. Krotkov et al. (2005) describes the instrument uncertainty of the UV-MFRSR for the retrieval of τ_a and ω_o .

2.4 Analysis and Results

2.4.1 Aerosol Optical Depth (τ_a) and Angström Exponent (α)

Figure 2-2 shows the frequency distribution of τ_a for Atlanta (red) and Griffin (black). The values of τ_a displayed on the graph are for 340 nm (Atlanta) and 332 nm (Griffin). The mean value of τ_a for all measurements between the two sites is almost identical (0.90 for Atlanta and 0.91 for Griffin), suggesting that fine particulate matter is relatively uniformly distributed over the Atlanta region. The standard deviation is smaller for Griffin (0.37) than for Atlanta (0.48). Daily averages of τ_a (340 nm) for Atlanta range between 0.23 and 2.09 with a mean and standard deviation of 0.93 ± 0.51 and between 0.43 and 1.53 at τ_a (332 nm) for Griffin with a mean and standard deviation of 0.94 ± 0.34 . These results show that the hourly means are similar between the two sites while some day-to-day variability is observed due to local effects. A total of 16 days are included in the results presented here. For the remainder of the month clouds obstructed the Brewer measurements which did not allow for the accurate measurement of total O_3 and τ_a . Figure 2-3 shows the daily variation of τ_a at the two sites. The text boxes describe the main meteorological conditions that occurred during the month of August. The beginning of the month was dominated by stagnant weather conditions. During the most stagnant events τ_a is on average 37% higher in Atlanta than in Griffin from August 1 to August 5. This is probably due to a larger contribution of local pollution sources in Atlanta than in Griffin with little transport. Figure 2-4 shows all measurements that were taken for the month of August for each day both in Atlanta (red) and Griffin (black).

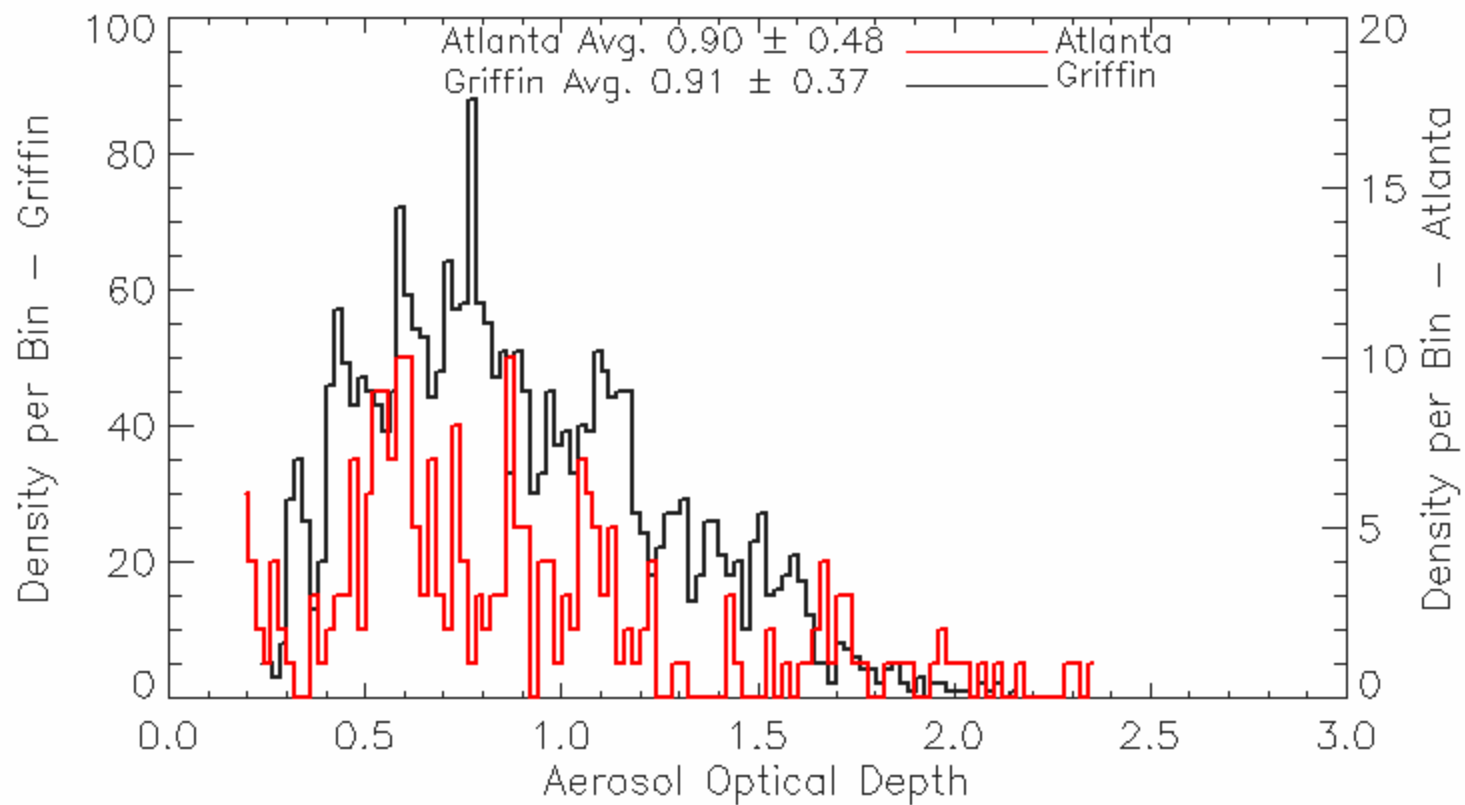


Figure 2-2: Frequency distribution of aerosol optical depth (τ_a) for Atlanta at 340 nm and for Griffin at 332 nm for all the measurements for the 16 measurement days of the month of August, 1999. The average and standard deviation for τ_a are shown on the graph.

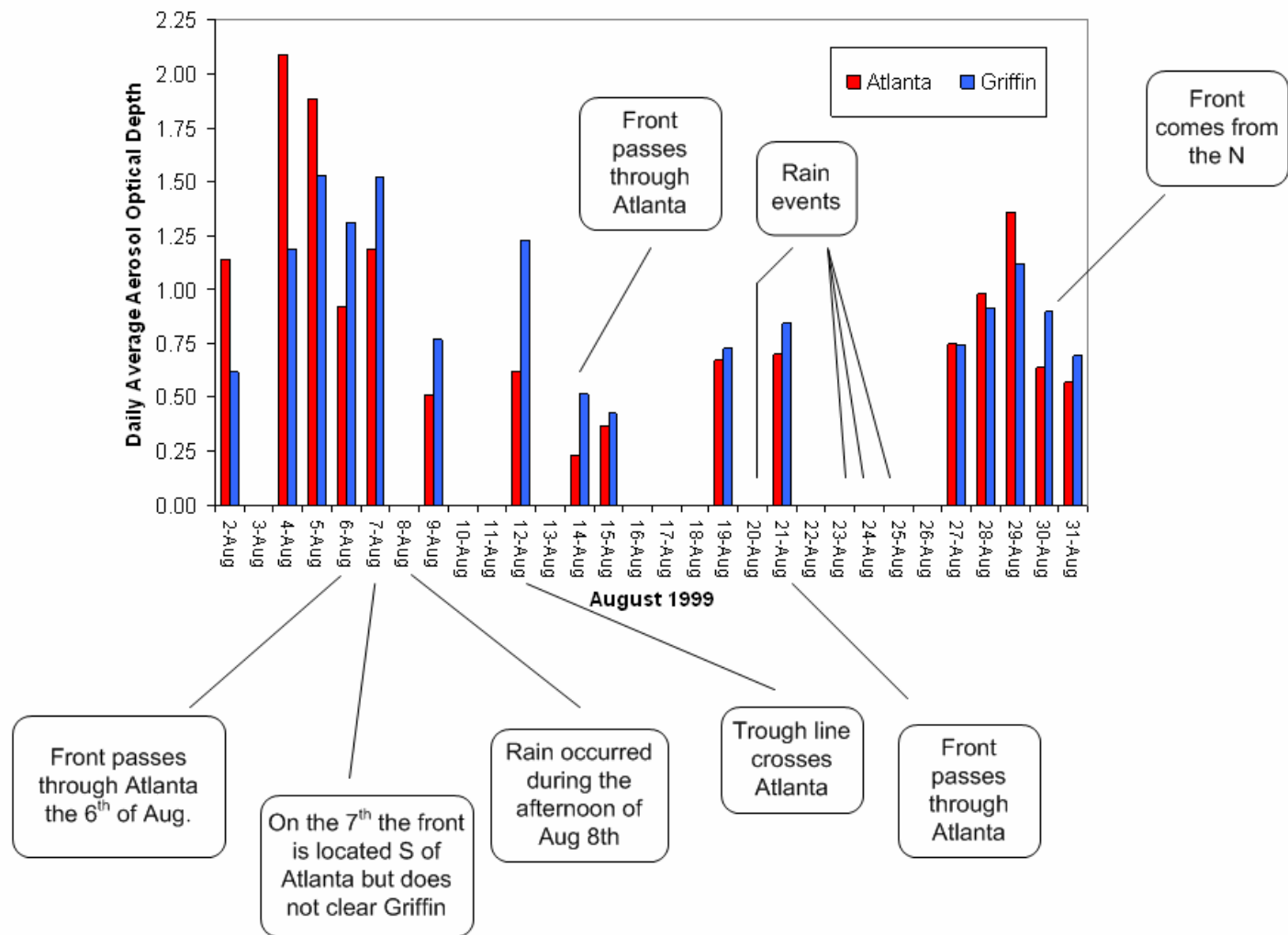


Figure 2-3: Overview of the main weather conditions that affected τ_a during the month of August for Atlanta and Griffin. The values of τ_a shown are for 340 nm.

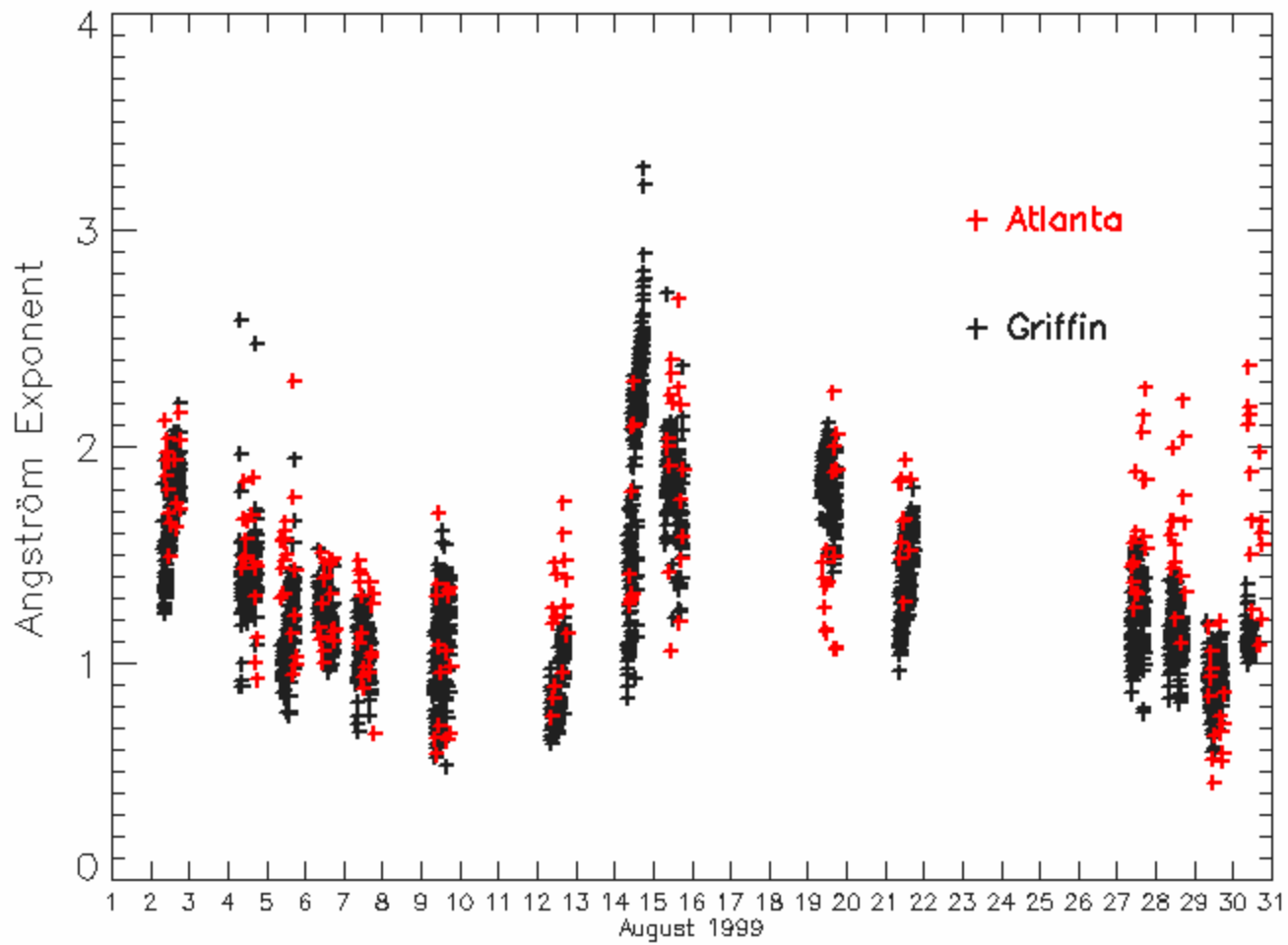


Figure 2-4: Shows all aerosol optical depth measurements taken by the Brewer in Atlanta (red) and by the UV-MFRSR in Griffin (black).

During the measurement period several fronts traveled through Atlanta but did not completely pass through the Griffin area. During these events τ_a is on average 47% lower in Atlanta than in Griffin. These events occurred on August 6th, 7th, 9th, 12th, 14th, 15th, 21st, and 30th.

The Angström exponent (α) was calculated from τ_a for the Atlanta and Griffin data. For the Atlanta data α was calculated between 320 and 360 nm for Griffin it was calculated between 325 and 368 nm. Figure 2-5 shows the frequency distribution of α for the 16 measurement days. Averaging all measurements the Angström exponent is $\alpha = 1.43 (\pm 0.44 \text{ standard deviation})$ for Atlanta and $\alpha = 1.37 (\pm 0.40 \text{ standard deviation})$ for Griffin. The daily averages range between 0.80 and 1.92 with a mean and standard deviation of 1.44 ± 0.32 for Atlanta and from 0.88 and 1.97 with a mean and standard deviation of 1.33 ± 0.33 for Griffin. Figure 2-6 shows all measurements of α as a function of day of the month for both Atlanta and Griffin. In general, there is very little difference in α between Atlanta and Griffin. August 5th, 12th, 27th, 28th, and 30th show higher values in α for Atlanta in comparison to Griffin with no overlap in the measurement uncertainty. Figure 2-7 shows the daily average values of α for Atlanta and Griffin including the average measurement uncertainty for each day. For the Atlanta measurements the α measurement uncertainty ranges between 0.10 and 0.28 corresponding to August 4th and August 14th respectively. For Griffin the α measurement uncertainty ranges between 0.09 and 0.17 corresponding to August 5th and August 15th respectively. The highest uncertainties occur during days of lower values of τ_a since the uncertainty of α is inversely proportional to the square of τ_a .

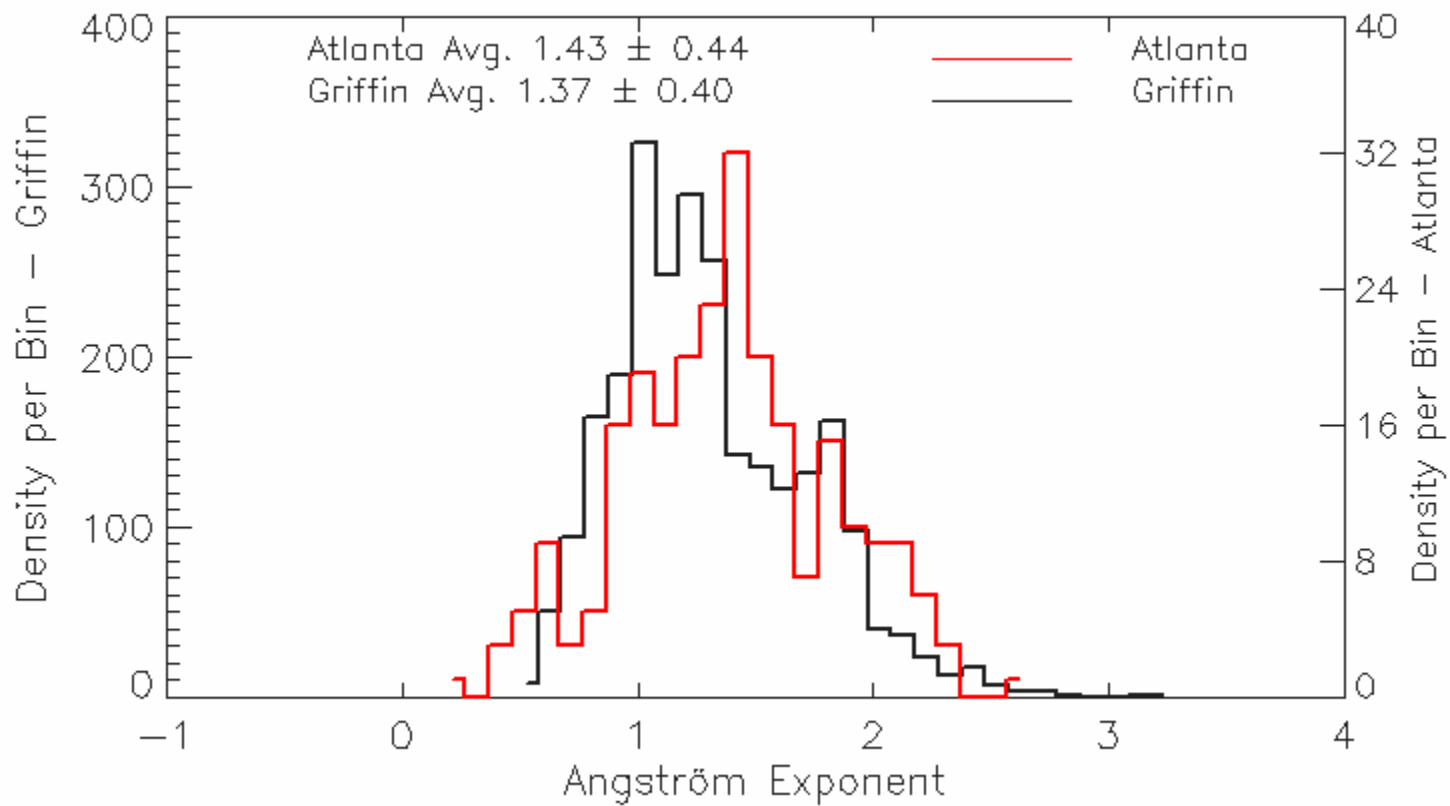


Figure 2-5: Frequency distribution of the Angström exponent (α) for Griffin (left y-axis) and Atlanta (right y-axis) for all measurements taken during the month of August, 1999.

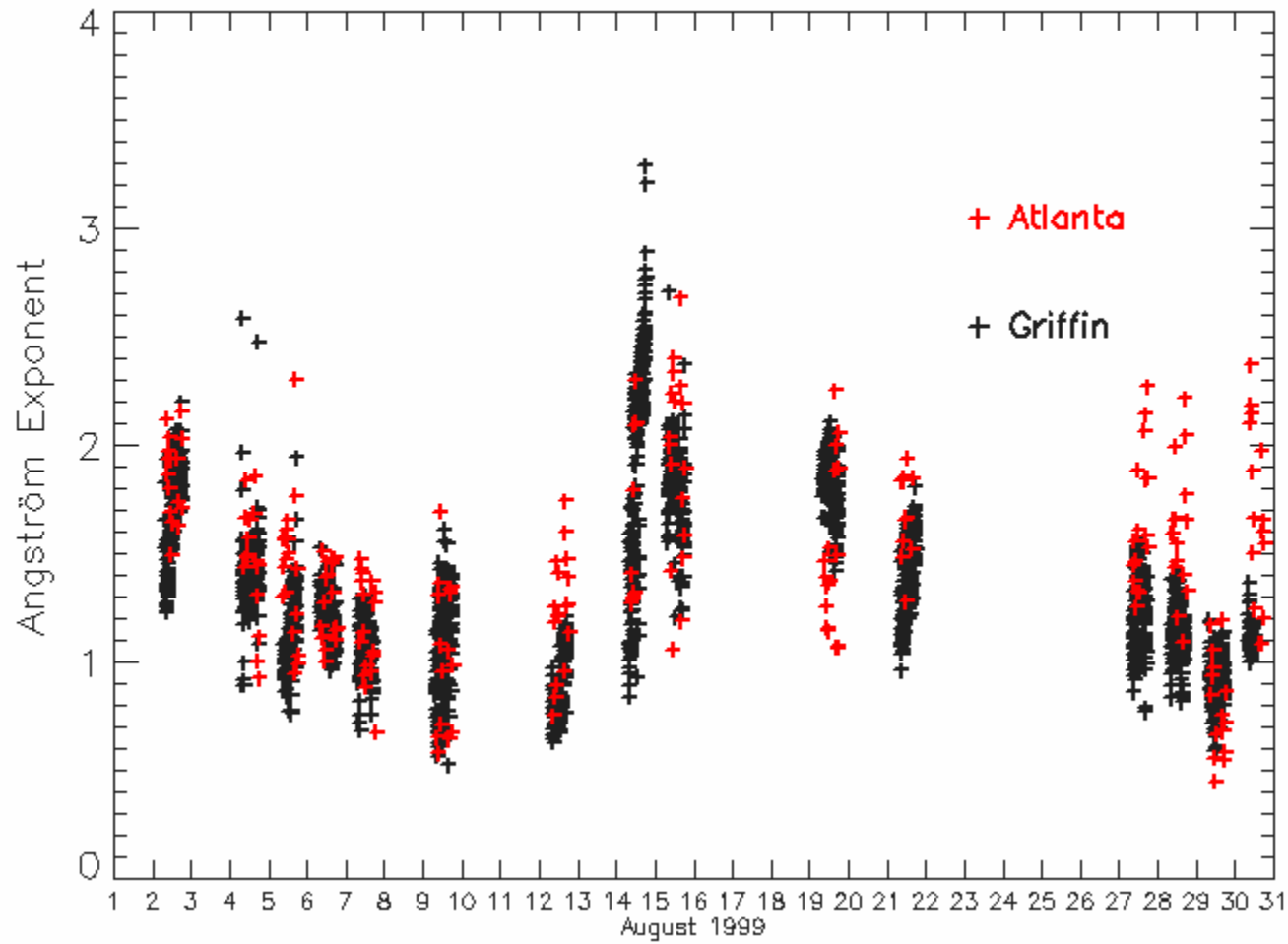


Figure 2-6: Shows all measurements of the Ångström exponent (α) taken by the Brewer in Atlanta (red) and by the UV-MFRSR at Griffin (black).

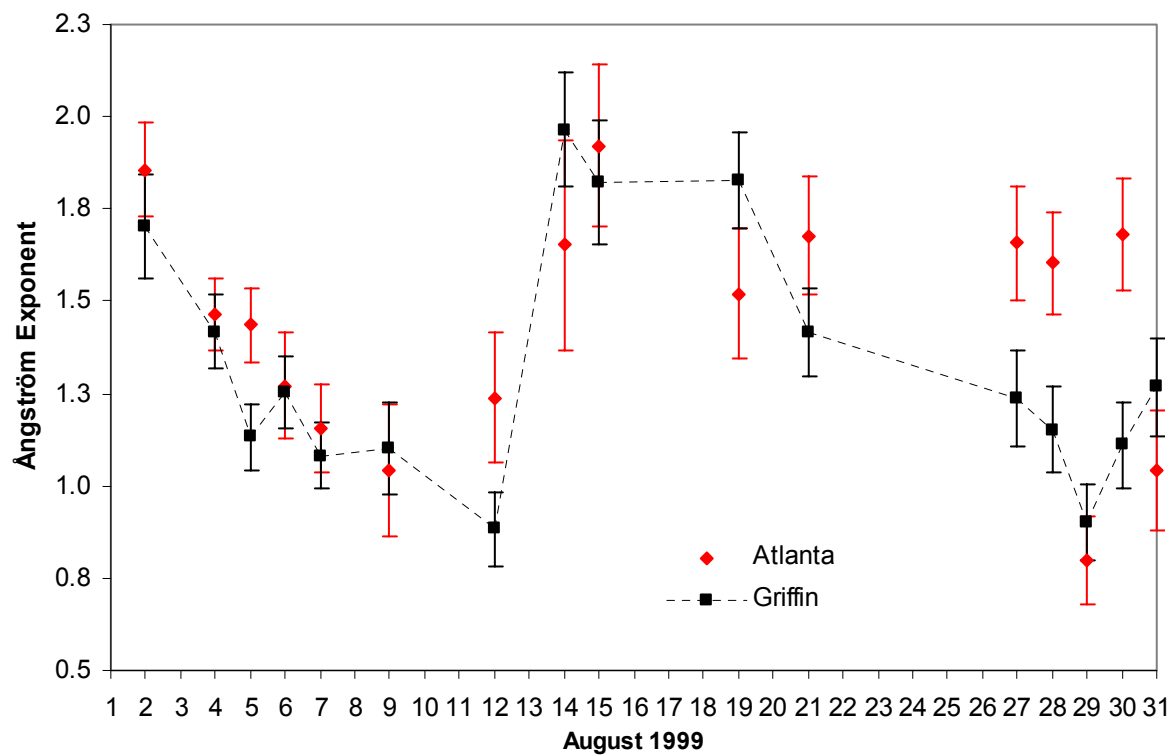


Figure 2-7: Daily averages of the Ångström exponent (α) for Atlanta (red) and Griffin (black). A dashed line joins the values of α for Griffin to better illustrate the day-to-day variation of α . The error bars depict the daily average measurement uncertainty for each of the 16 days.

2.4.2 Single Scattering Albedo (ω_0)

The single scattering albedo, ω_0 , was estimated using the UV radiation measurements taken by the Brewer spectroradiometer, the retrieved values of τ_a shown in section 4.1, and the Tropospheric Ultraviolet and Visible (TUV) radiative transfer model. TUV uses a discrete ordinate transfer method of determining radiative transfer through the atmosphere, and was ran using 8-streams. TUV was iterated by varying ω_0 until the model irradiance output matched that measured by the Brewer spectroradiometer for the same spectral range (286-363 nm). Figure 2-8 shows a schematic representing the inversion process of ω_0 . The asymmetry parameter (g) was assumed to be 0.7 for all wavelengths and the ground albedo was assumed to be 0.1.

Madronich (1993) indicates that g typically varies between 0.6 and 0.8 for the UV. Bais et al. (2005) used Mie calculations to generate $P(\theta)$ that corresponds to urban aerosol type. They found that g for the urban aerosol is 0.7 at 340 nm. D'Almeida et al (1991) also report g values between 0.66 and 0.77 for maritime clean and polluted aerosols and only for maritime mineral aerosols the asymmetry parameter is larger than 0.84. The phase function $P(\theta)$ was determined in our study for coastal and marine, continental, and high altitude stratospheric aerosols. The popular modified gamma distribution analytic size distribution model for atmospheric particles, or Deirmendjian distribution (Deirmendjian, 1969), was used in the Mie code to calculate $P(\theta)$. An index of refraction of 1.53, -0.02 i was used for the calculations.

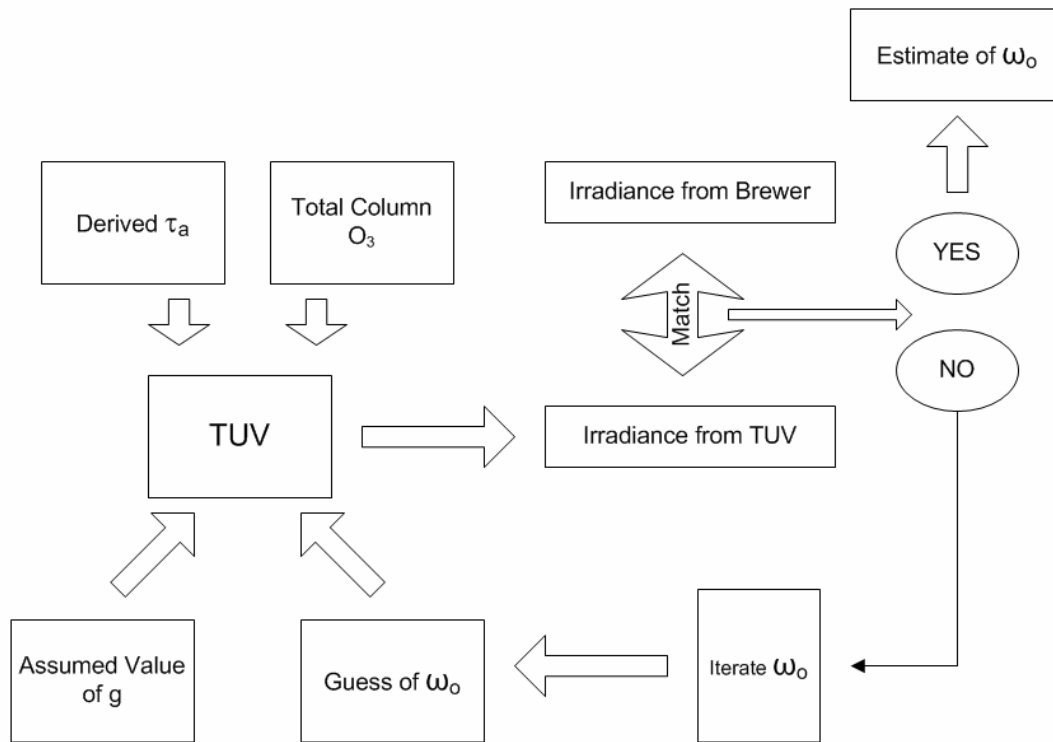


Figure 2-8: Schematic showing the iteration process used to derive ω_0 .

The asymmetry parameter g was calculated to be 0.77 for the marine aerosols, 0.74 for the continental aerosols, and 0.71 for the high altitude stratospheric aerosols. The effect of g on ω_0 was investigated using TUV by changing g and comparing the change in irradiance to that produced by changing ω_0 . A change in g from 0.6 to 0.8 yields an uncertainty of ± 0.06 in ω_0 (Figure 2-9).

Overall, sensitivity studies indicate that the uncertainty in global irradiance calculations due to a change in g from 0.6 to 0.8 yield an uncertainty of 0.06 in ω_0 . Errors of lesser magnitude are expected from the assumptions made for the aerosol vertical profile, uncertainties in the instrument measurement of total column O_3 , and estimate of the surface albedo. These errors were estimated and considered in the overall uncertainty of ω_0 . The overall (or average) uncertainty is estimated to be ± 0.08 for ω_0 units and it ranges between ± 0.05 and ± 0.12 for the highest and lowest τ_a respectively. Similar uncertainties in the retrieval of ω_0 were obtained by Bais et al. (2005) at Thessaloniki using measurements of direct and diffuse radiation with a Brewer spectroradiometer. Their uncertainties ranged between ± 0.04 at 340 nm for $\tau_a = 0.4$ and about ± 0.06 units for $\tau_a = 0.2$. Figure 2-10 shows the frequency distribution of ω_0 for the 16 days.

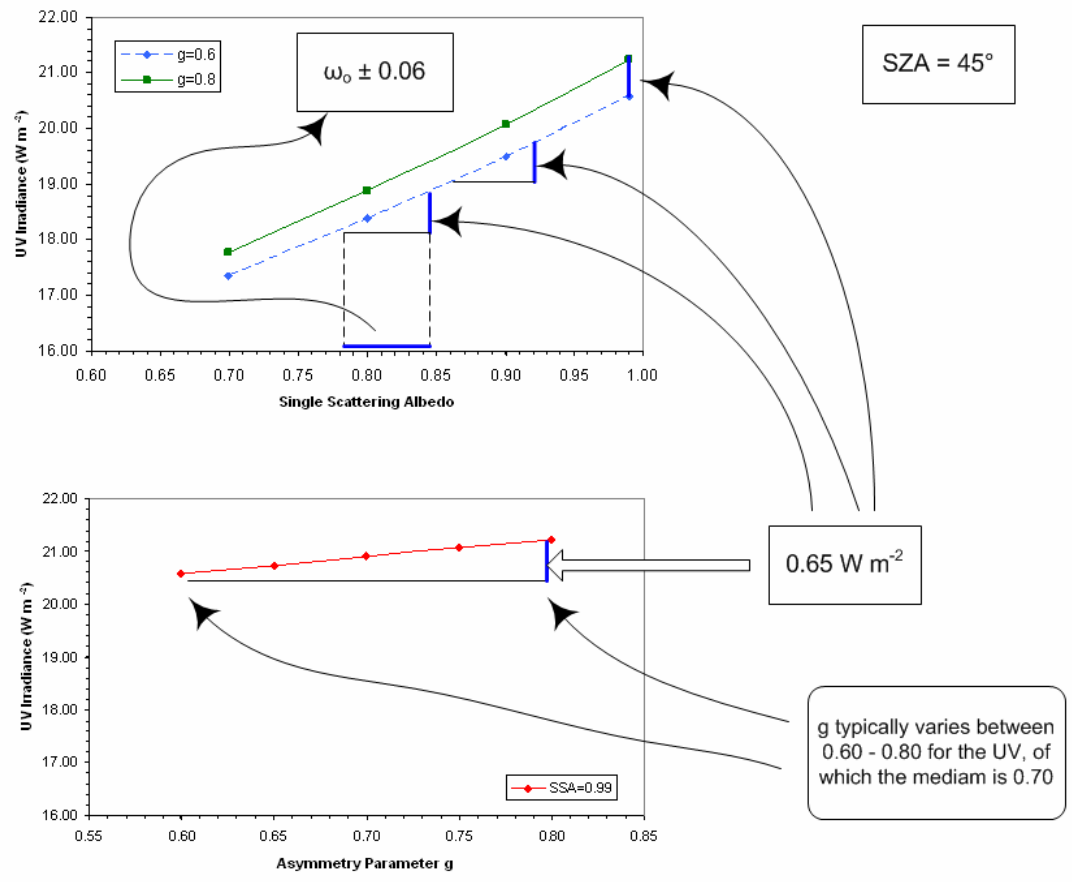


Figure 2-9: The effect of g on ω_0 was investigated using TUV. g was changed from 0.6 to 0.8 and the resulting irradiance ($0.65 W m^{-2}$) is compared to the irradiance that results from changing ω_0 from 0.70 to 0.99. In this calculation the spectral range 286-363 nm is used to match that of the Brewer.

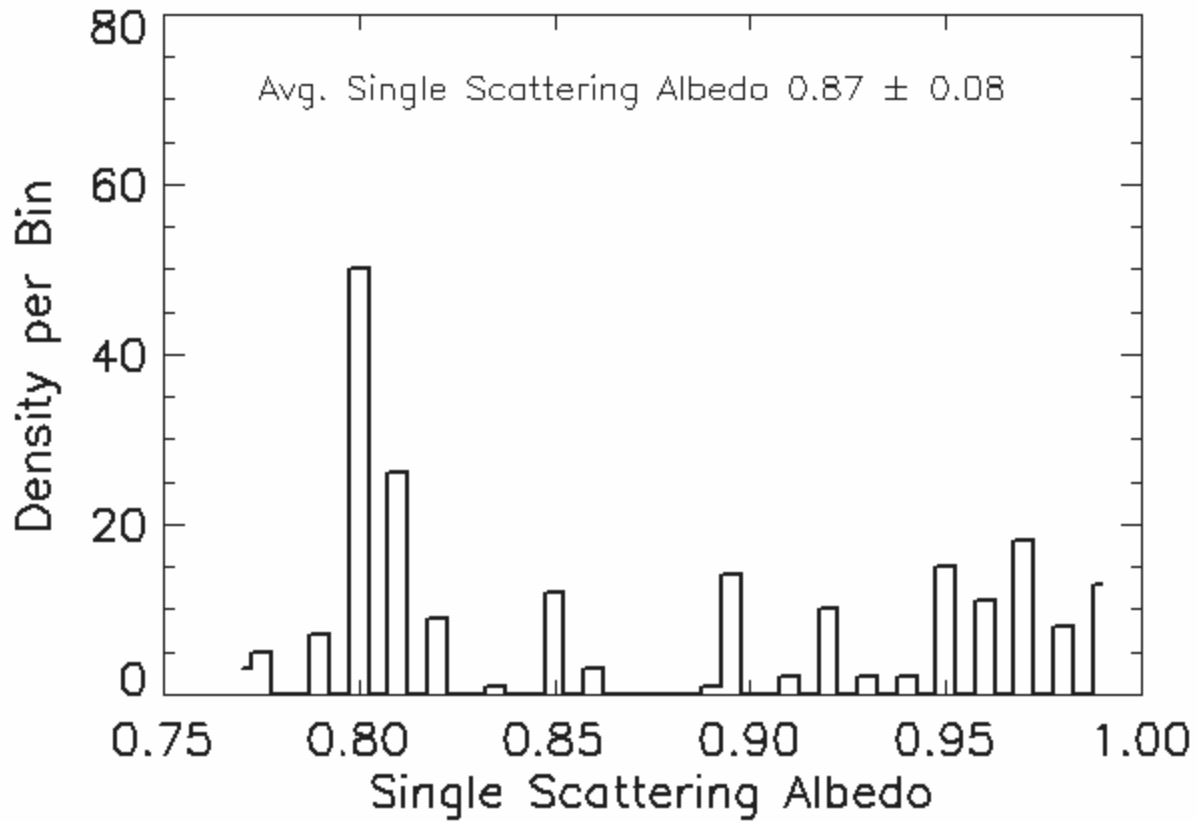


Figure 2-10: Frequency distribution of ω_0 derived from the Atlanta Brewer measurements for the 16 days used in this study. The average ω_0 is 0.87 with a standard deviation of 0.08

The average ω_0 is 0.87 with a standard deviation of 0.08. Figure 2-11 shows the daily average ω_0 for the different measurement days. The highest values of ω_0 were reported at the beginning of the month when τ_a is highest. The first precipitation event during the measurement period occurred August 8 (12 mm). The average ω_0 for August 2nd, August 4th, and August 5th (which report the highest values of τ_a – with an average of 1.7 for the three days) is 0.97. The second precipitation event occurred August 20th with 3 mm and the third and more substantial precipitation event occurred between August 23rd and August 25th with a total of 42 mm. Values of ω_0 of around 0.80 were obtained during the rainy period. Figure 2-12 shows the ω_0 as a function of $\tau_{a, 340}$. In general, as depicted by Figure 2-13, the lowest values of τ_a correspond to the lowest values of ω_0 . This is probably due to a more absorbing nature of the aerosols after precipitation events as suggested by Carrico et al. (2003). Carrico et al. (2003) measured ω_0 in the visible (530 nm) at the surface and at dry relative humidity measuring absorption and scattering coefficients at the Atlanta Supersite. They found that the scavenging of particles by fog and precipitation droplets is the likely predominant removal mechanism responsible for the decrease in the scattering coefficient during rain events. During the precipitation event on 23-25 August they estimated a decrease in ω_0 from 0.95 to 0.4 over the course of 9 h. Carrico et al. (2003) determined an average value of ω_0 during the month of August of 0.87 ± 0.08 which are identical to the average values we obtained at 340 nm using the Brewer spectroradiometer. Krotkov et al. (2005) also found in Greenbelt, Maryland the highest values of ω_0 were all obtained in summer, when τ_a was larger than 0.40 at 440 nm.

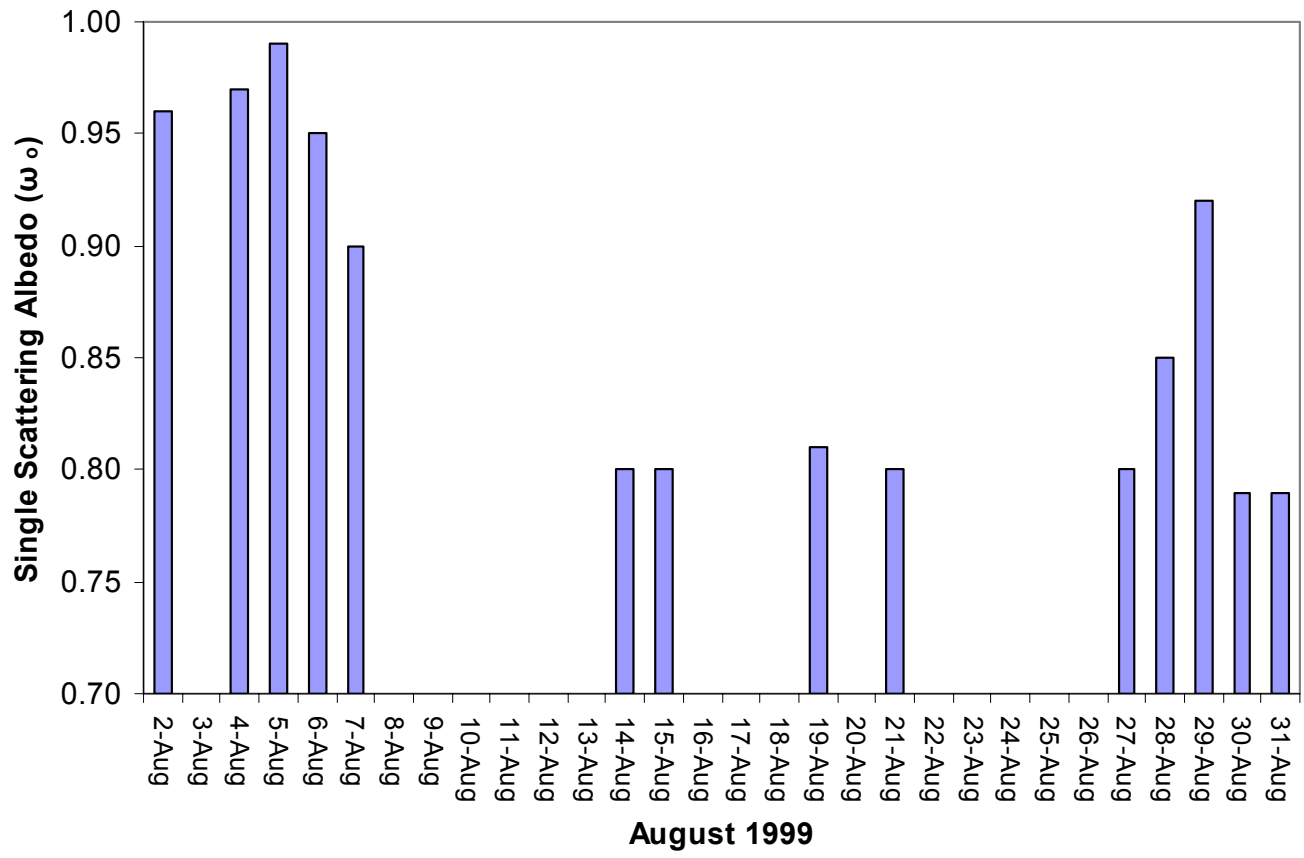


Figure 2-11: Average daily single scattering albedo (ω_0) for each of the measurement days.

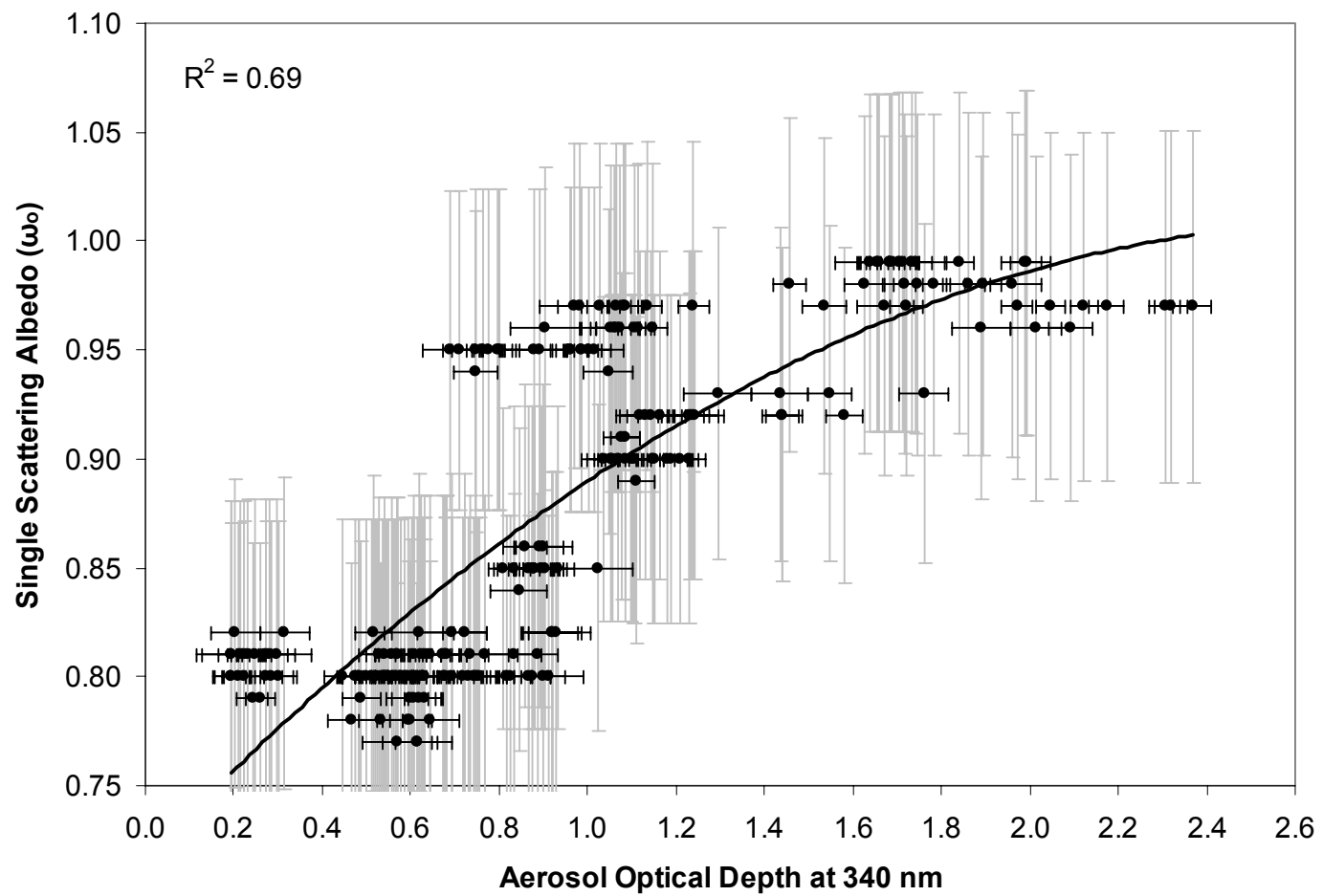


Figure 2-12: Relationship between τ_a and ω_0 for the 16 days considered in this study.

2.4.3 Effects of Aerosol Optical Depth (τ_a) and Single Scattering Albedo (ω_0) on the Surface UV Radiation and UV Index for the Atlanta Area

The UV index was measured for the 16 measurement days using the Brewer spectroradiometer. The standard way to calculate the UV index is to measure the spectral intensity of solar UV radiation up to 400 nanometers. Multiply these UV intensities by the weighting factors at the corresponding wavelengths in the erythemal action spectrum to reflect the human skin's response to each wavelength. Sum up the products above to obtain the total erythemally weighted UV intensity in milliWatt/square meter. Multiply the total erythemally weighted UV intensity by 0.04 to obtain the UV index. The result is expressed as a rounded integer number.

Figure 2-13 shows the measured UV Index for the whole month of August. In addition to the measured UV index, Figure 2-13 shows the calculated UV index for the continental aerosols measured by Elterman (1968) corresponding to the highest sun measurement for each day (red symbols). The Elterman aerosol profile corresponds to a value of τ_a of 0.33. The hypothetical UV Index for an atmosphere with no aerosols is also shown in Figure 2-13 by the blue symbols. The total column O_3 from the Brewer spectroradiometer was used for these hypothetical calculations. August 4th reported the highest values of τ_a (daily average > 2.0), and also measured two UV Index units lower than August 2nd (from 8 to 6 at solar noon). Note that August 2nd measured a higher total column O_3 than August 4th (Figure 2-14). The lower UV Index values reported on August 4th are due to the high values of τ_a measured on August 4th. Other differences of 1-2 UV Index units are observed between the different measurement days.

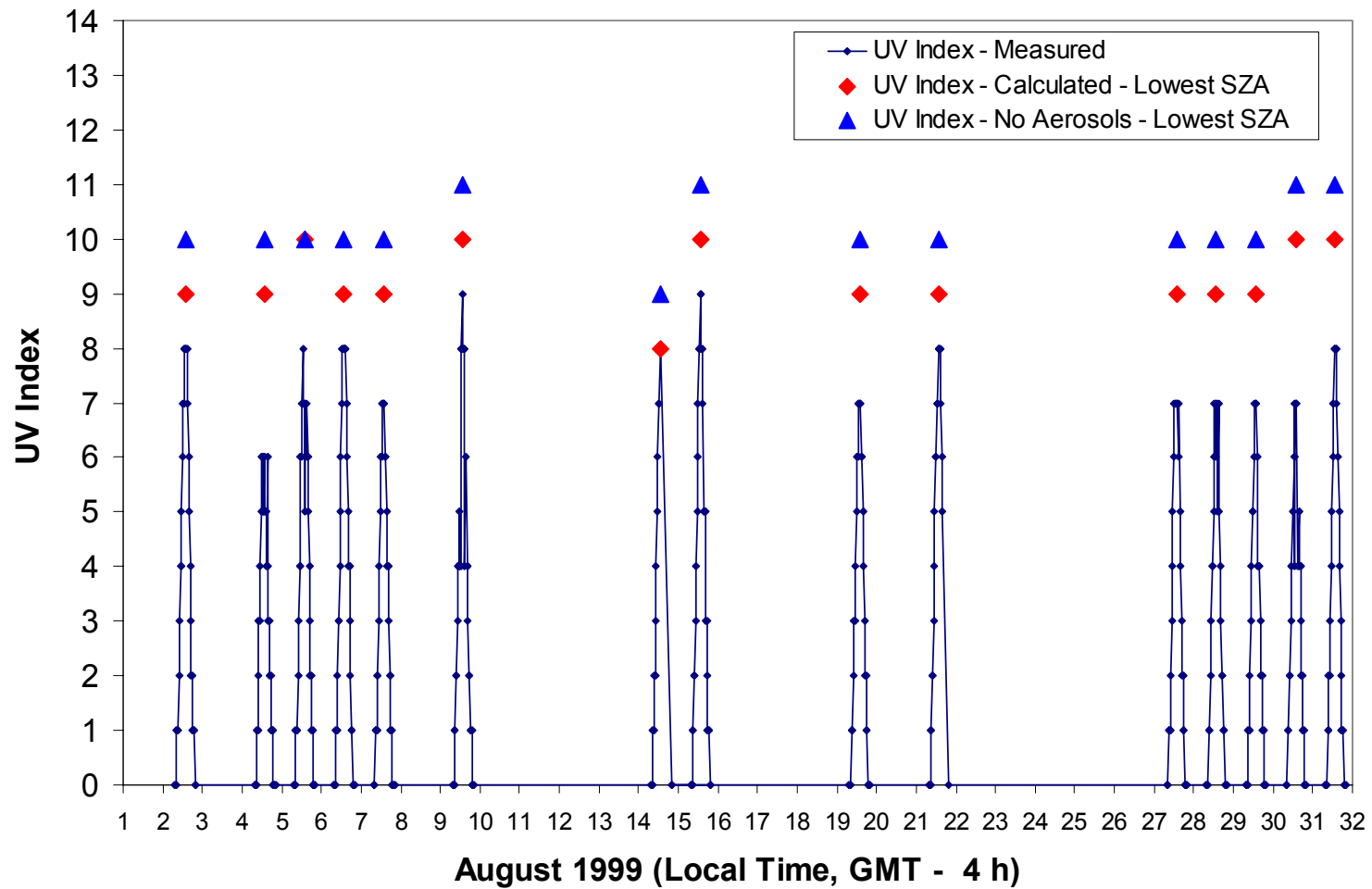


Figure 2-13: UV Index calculated from the erythemally-weighted UV irradiance measured with the Brewer spectroradiometer (solid line). The hypothetical calculated UV index for the continental aerosols measured by Elterman (1968) corresponding to the highest sun, or lowest solar zenith angle (SZA), is shown by the red symbols. The blue symbols correspond to the UV Index for an atmosphere with no aerosols. Note that UV index values are given as integer numbers.

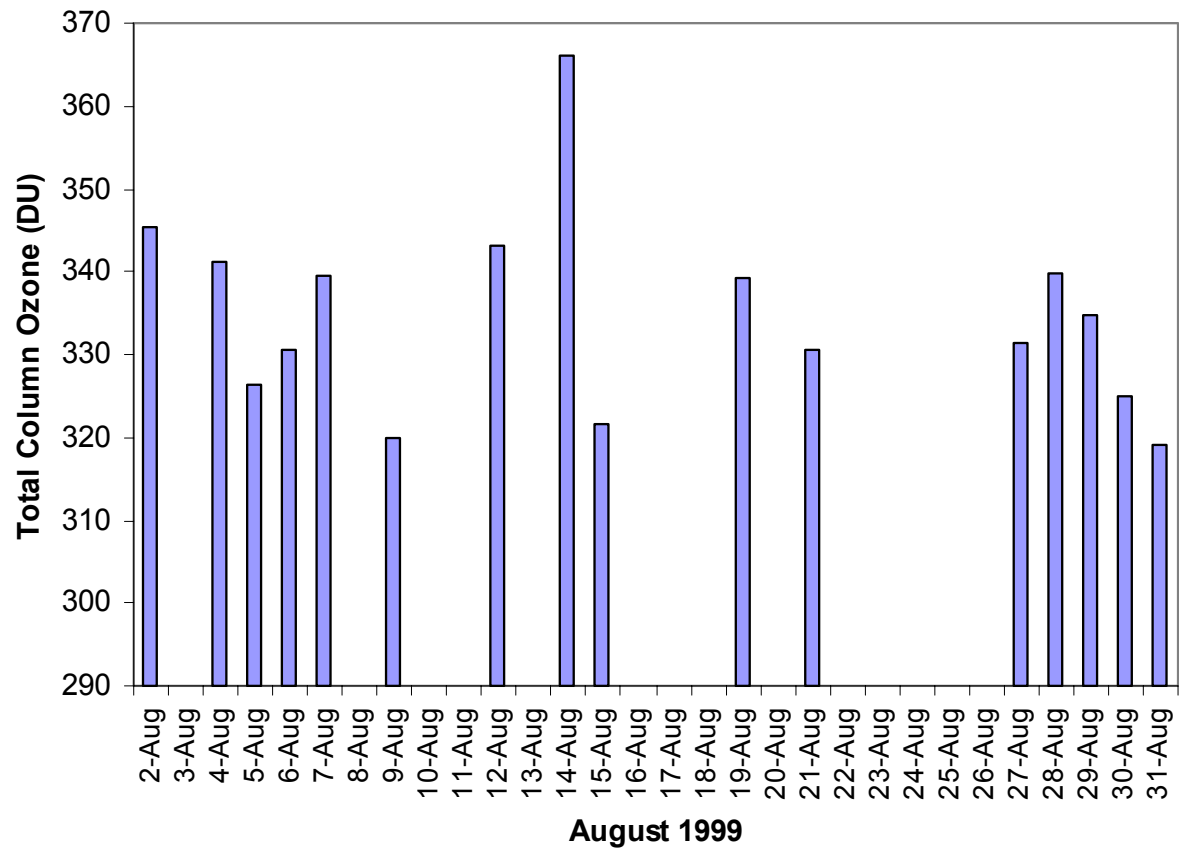


Figure 2-14: Daily changes in total column ozone (O_3) for the month of August 1999 measured by the Brewer spectroradiometer.

The difference in UV index between 6 (measured August 4th) and 9 (for the Elterman continental aerosols for the same day) corresponds to a 33% decrease in the UV index. Estupiñán et al. (1996) reported changes in UV radiation of 20% for cloudless skies during a six month study in North Carolina that were attributed to changes in turbidity of the atmosphere after normalizing the measurements to a constant total column O₃.

In order to illustrate more thoroughly the effects of the aerosols on the UV Index, global UV Irradiance measurements from the Brewer spectroradiometer (286.5-363 nm) were used in conjunction with the TUV radiative transfer model to determine the effects of τ_a and ω_o on the measured UV irradiances. August 7th (day 219) was arbitrarily chosen to investigate the sensitivity of τ_a and ω_o to the measured UV irradiances and the UV Index. The measured UV irradiance for this day was compared with the calculated irradiance for different values of ω_o and τ_a (Figures 2-15 and 2-16 respectively). A change in ω_o from 0.9 (average ω_o for August 7th) to 0.99 produces a 20% increase in UV radiation at solar noon. A decrease in ω_o from 0.9 to 0.8 produces a decrease in UV radiation of 10% at solar noon (Figure 2-15f). A maximum of 2 UV Index units can be obtained for each of these changes in ω_o (Figure 2-15a-e). Note that the UV Index is defined as an integer number leading to some stepping of the results presented here. A change in $\tau_{a,340}$ from the average value of 1.1 measured for August 7th to 0.2 produces an increase in UV radiation of 30% at solar noon. An increase in $\tau_{a,340}$ from 1.1 to 2 produces a decrease in UV radiation of 30% (Figure 2-16f). A maximum change of 2 UV Index units can be obtained due to each of these changes in τ_a (Figure 2-16a-e) which agrees with the observed values reported at the beginning of the measurement period under stagnant conditions.

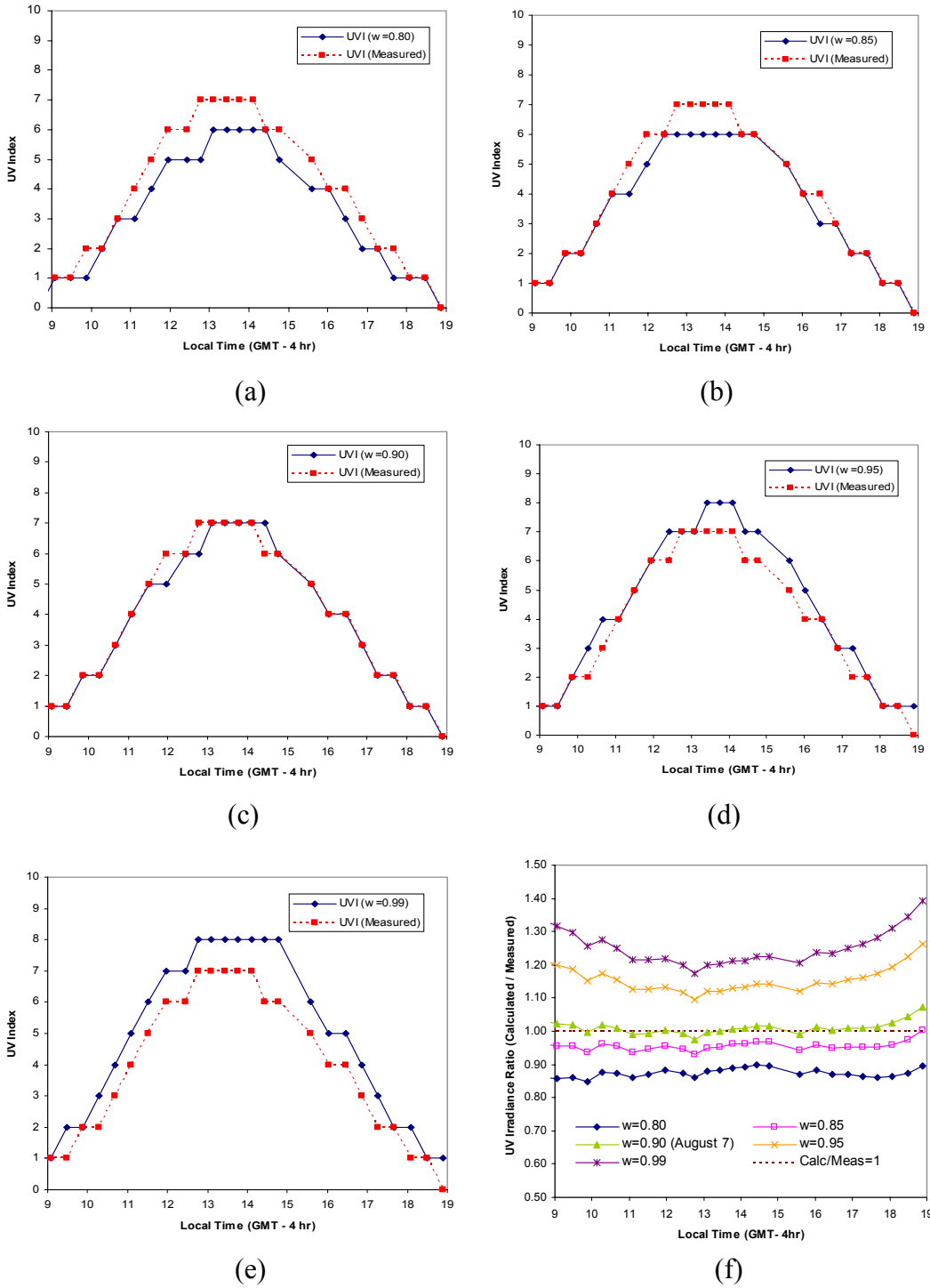


Figure 2-15: Effect of ω_0 on the UV Index (a-e) and on the total UV radiation (286-363 nm) (f). The measurements correspond to August 7th with an average τ_a of 1.1 and a total column O_3 of 339.6 DU. ω_0 for this day was estimated to be 0.90 represented by the line with triangles in (f).

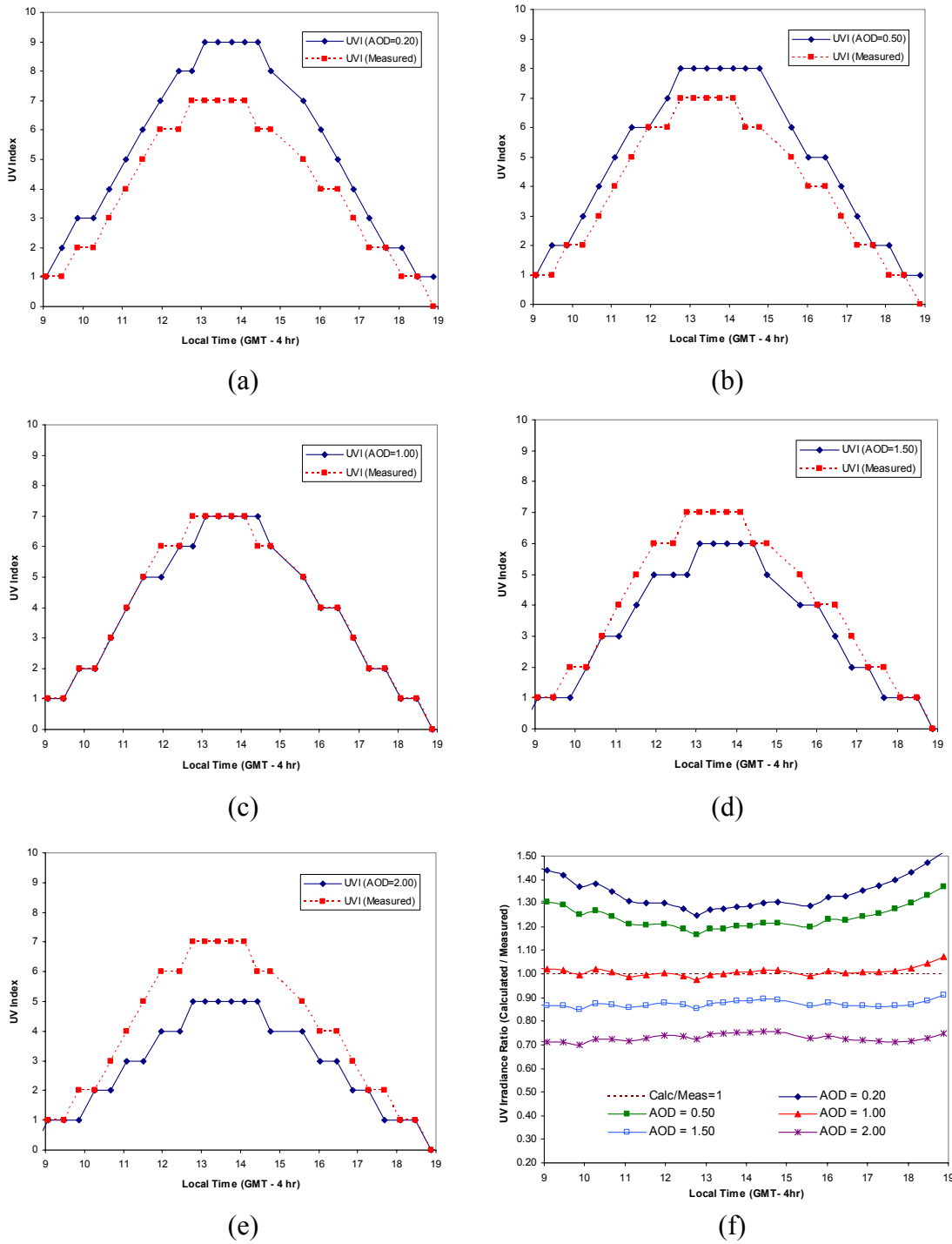


Figure 2-16: Effect of τ_a on the UV Index (a-e) and on the total UV radiation (286-363 nm) (f). The measurements correspond to August 7th with an average τ_a of 1.1 and a total column O_3 of 339.6 DU. The line with the triangles shows the ratio of the calculated to measured UV irradiance (f).

2.5 Conclusions

This study presents the first measurements of aerosol optical depths (τ_a), Angström exponent (α), and single scattering albedo (ω_o) measured from surface measurements of solar irradiance in the UV in the Atlanta area (an urban metropolitan area with a population of 4 million people in 1999 in the South Eastern United States). The study was conducted as part of the Atlanta Supersite experiment in August, 1999. The main results are the following:

Aerosol optical depths (τ_a) in the UV were retrieved at 320, 340, and 360 nm. Daily averages of $\tau(340 \text{ nm})$ range from 0.23 and 2.09 with a mean and standard deviation of 0.93 ± 0.51 . The daily average spectral dependence of the aerosol optical depth, calculated via the Angström exponent (α), ranges from 0.80 and 1.92 with a mean and standard deviation of 1.44 ± 0.32 . No apparent relationship was found between τ_a and α . The retrieved values of τ_a and α were used in the Tropospheric Ultraviolet and Visible (TUV) radiation model to estimate the surface UV irradiance. Estimates of aerosol single scattering albedo (ω_o) were made by matching the measured irradiance values to model computed irradiances. The results suggest an increasing trend in ω_o with increases in τ_a . The estimated ω_o ranges from 0.80 and 0.99 with a mean and standard deviation of 0.87 ± 0.08 . Changes in τ_a and ω_o during the measurement period are capable of changing the UV Index up to 2 UV Index units when all other effects are kept constant.

The values of τ_a and α are compared with the ones obtained at a nearby rural location in Griffin, GA located 47 miles south of Atlanta using a UV-MFRSR from the

US Department of Agriculture. At Griffin, daily averages of $\tau(332 \text{ nm})$ range between 0.43 and 1.53 with a mean and standard deviation of 0.94 ± 0.34 . For α the daily averages range between 0.88 and 1.97 with a mean and standard deviation of 1.33 ± 0.33 .

The results presented in this study indicate that the effects of aerosols (quantified through τ_a and ω_o) have a significant effect on the solar UV radiation, and hence the UV Index. Changes in τ_a and ω_o can yield maximum changes of approximately 4 UV Index units. Day-to-day changes of 2 UV Index units were measured during the month of August of 1999. Changes in UV Index of 2 to 4 units correspond to changes in UV radiation of 50-100 milliWatts/square meter, which can change the amount of time needed to obtain the "Minimal Erythemal Dose" (MED) or erythemal potential of UV radiation. 1 MED is defined as the effective UV dose that causes a perceptible reddening of previously unexposed human skin UV dose.

CHAPTER III

A NEW SYNTHETIC CURRENT UV INDEX IS DEVELOPED TO PROVIDE UV INDEX VALUES AT LOCATIONS WITHOUT UV MEASUREMENTS

3.1 Summary

A new synthetic current UV Index is developed and successfully verified against direct surface measurements of UV index values. Surface and satellite cloud cover information as well as total column ozone values are used to calculate the synthetic current UV index for 10,000 cities across the United States. This synthetic current UV index value can be used to expand by more than a factor of 200 the number of possible UV Index observations in the United States and other countries. The goal is to provide instantaneous current UV Index values to any city in the United States. Based on this research you can now see a synthetic current UV Index across the United States at the Weather Channel web site. The results of the synthetic current UV Index were verified against the UV index values measured by the US Department of Agriculture (USDA) measured UV index values for a total of 6566 data points (at 13 different locations across the US) over a period of a month. In 50% of these cases, the synthetic UV index is identical to the observations. In 67% of these cases the synthetic UV index shows a difference of +/- 1 UV index unit from the measured values. In 83% of the cases the synthetic UV index is within +/- 2 UV index units of the observed index. This synthetic UV index can be used to better inform the public of the diurnal variations in the UV index that are caused by changes in cloud cover, total column ozone, time of the day, and geographical location at many more locations than the ones equipped with UV sensors.

Presently, current or measured UV indices are strictly limited in coverage to locations where surface values of UV radiation are measured by broadband or spectral UV sensors. This synthetic index has the advantage that it can be derived at any point where surface cloud observations are available. The synthesized UV index can be published in many different forms such as national maps and daily line graphs for a given location with the purpose of raising the public's awareness of the harmful effects of the sun's ultraviolet rays.

3.2 Introduction

Ultraviolet radiation (UV) can be harmful to both human and environmental health. One of the most common effects of UV radiation is erythema (or sunburn). Sunburn occurs when skin cells are damaged by the absorption of UV radiation. To compensate for this damage the skin drives extra blood to the damaged area in an attempt to heal it, which accounts for skin redness and sunburn (Setlow, 1974; Peak et al., 1984; Sullivan, 1992). Long term exposure to UV radiation is linked to many varieties of skin cancer, some of them fatal (Kripke, 1992). The UV Index has been created as a means to warn the public of the damaging effects of UV radiation. The UV Index is given in terms of a dimensionless UV radiation unit equal to 25 milliwatts m^{-2} of erythemally weighted UV radiation (WMO, 1994).

Efforts to make the public aware of UV radiation began with previous day UV radiation report during the Australian sun protection campaign in the 1980's (Lemus et al., 1997). Then, in 1992 Environment Canada began issuing a next day forecast of clear sky UV levels called UV Index (Wilson, 1993). Since then, many other countries

including the United States (Long et al., 1996) have issued UV Index forecasts in order to increase the public's awareness of the damaging solar UV levels.

There is not currently a mechanism to inform the general public of the amount of UV radiation (or UV Index) being received *right now* at a given town or city. Surface UV instruments are difficult to maintain and their coverage is limited to a few dozen instruments for a given country (Bigelow et al., 1998; Sabburg et al., 2002). This has motivated us to create a synthetic UV Index to provide current UV Index values for locations that do not have UV measurements available. This expands significantly the number of locations for which we can generate *current UV Index* values.

With the exception of clouds, the primary input factors used for the calculation of the UV Index are geographical location, altitude, time and date, and total column ozone (O_3) which can be integrated as input parameters to the current UV Index without surface measurements of these parameters. Cloud cover reports from ground observations are available several times an hour during active weather and at least once an hour during fair weather by the Meteorological Aeronautical Report (METAR). Total column O_3 values from satellites are in general available a day after the data is processed. This means that in the worse case scenario the current UV Index will be calculated using cloud cover data that is one hour old and total column O_3 values that are a day old. The impacts of these delays on the overall accuracy and value of the current UV Index are small and should not hold us back from distributing to the public current UV Index values as the verification results confirm later on in this paper. For example, Vignola (2003) showed that the comparison of global radiation data taken five and fifteen minutes apart yields a maximum error of 5% in spring and almost no error in January. Additionally, the largest

day-to-day changes in total column O_3 occur during the winter season and at high latitudes when the amount of solar UV radiation is smaller associated with changes in the polar jet and the mid latitude storm systems. The effects of aerosols on the synthetic current UV index are not included in this initial development of the index. As shown in the previous chapter the effects of aerosols can reduce the UV Index by two UV Index units within the summer season and by more than that if we compare UV Index values between turbid summer days and pristine winter days. However, a high frequency of bad visibility reports found in the METAR reports prohibited to use of the visibility as an input parameter during routine operations.

This study demonstrates that it is viable to use the current UV Index as an operational tool capable of providing near-real time synthetic UV Index values to nearly 10,000 cities across the United States. GOES-augmented METAR cloud cover information in conjunction with interpolated values of cloud cover are used to provide current UV Index results for all important population centers in the United States.

3.3 Quantification of the Effects of Clouds on the UV Index

Clouds are the most important contributors to the variability in surface UV irradiance due to their dynamic, spatial, and temporal variability as well as wide ranging physical properties. Although radiative transfer calculations through clouds are theoretically possible, the input parameters needed by the radiative transfer models are not generally available. The lack of standard information about cloud type, altitude, cloud optical properties (e.g. optical depth) prevent cloud radiative transfer calculations in routine operations.

Surface observations of cloud cover are operationally limited to fractional cloud cover and height. This has allowed for direct comparisons between cloud fraction and UV transmission (Bais et al., 1993; Cutchis, 1980; Ilyas, 1987; Josefsson, 1986). For instance, the National Atmospheric and Oceanic Administration (NOAA) currently compares (Model Output Statistics) MOS cloud fractions with measured UV transmission to determine the average UV attenuation of clouds when calculating the forecast UV Index (Long et al., 1996).

In this study we follow a similar approach except that instead of using forecast values of fractional cloud cover we compare instantaneous measured values of fractional cloud cover with UV transmission to derive an empirical relationship accounting for the effects of clouds on UV radiation. The comparison of the cloud cover reports to measured UV values in order to derive the empirical relationship is limited to US Department of Agriculture (USDA) USDA UV measuring sites that are within 24 km (15 miles) of the METAR reporting stations. Thirteen METAR reporting locations met the 24 km distance criteria. Small distances between the UV observing sites and the METAR locations will ensure that no additional uncertainties are introduced due to cloud cover differences.

The USDA data offers a high frequency network of UV measurements (UV data taken every three minutes) with the Eppley UV pyranometer for all of their measurement sites. The Model UVB-1 has a relative spectral response similar to the erythemal action spectrum and is well suited to measuring erythemally effective solar irradiance. The overlap between the erythemally effective solar irradiance and the effective spectrum measured by the UVB-1 (280-330 nm) does not vary appreciably with zenith angle up to

about 60° and, therefore, the output signal of the UVB-1 can be used to accurately determine the erythemally effective radiant exposure (dose).

The majority of cloud cover observations at METAR stations are produced automatically. Only one of the 13 METAR locations used in this study was a manual augmented station (Washington DC / Reagan National Airport). The automated METAR stations are only capable of reporting clouds below 3658 m (12,000 feet). This means that clouds above 3658 m are not detected by the automatic stations. When higher altitude clouds are present they can attenuate a portion of the UV radiation if the cloud thickness is significant. In general, only 22% of all METAR stations that report sky conditions in the US are manual, where an observer is present at least for part of the day. In order to minimize any uncertainties introduced by the cloud detection of the METAR stations only data corresponding to the summer months (July 31 to August 30, 2003 with more convective clouds and less large scale fronts containing altostratus, altocumulus, and cirrus clouds) are used in the derivation of the cloud empirical relationship.

Table 1-3 shows the details of the USDA UV measuring sites and the co-located METAR locations. The locations of these 13 sites are shown in Figure 3-1. Figure 3-2 displays the distance between the UV observing sites and the METAR locations for each site. The average distance between the METAR sites and UV instruments is 11.9 km. Cloud cover from METAR reports are available once an hour during fair weather and several times an hour when special reports are issued during active weather. The METAR cloud reports are converted to percentage cloud cover before they are compared to the closest three minute measured UV radiation from the USDA UV network. Only data for solar zenith angles (SZA) between 37° and 39° are used in the derivation of the cloud

relationship. This range of solar angles provided the largest number of observations for the data collected in this study. The two degree range is small enough not to introduce uncertainties related to changes in solar elevation.

Table 3-1. Geographic Details about the METAR Stations and UV Observation Sites considered in this study.

NAME OF UV LOCATION	LAT OF UV LOC.	LONG. OF UV LOC.	ALTITUDE (M) OF UV LOC.	METAR	NAME OF METAR LOCATION	LAT. OF METAR LOC.	LON. OF METAR LOC.	STATE	ALTITUDE (M) OF METAR LOC.	DISTANCE OF UV TO METAR (MILES)
North Central Research and Outreach Center(Grand Rapids)	-93.53	47.18	394	KGPZ	Grand Rapids Automatic Weather Observing	47.22	-93.52	MN	399	2.3
Albion Field Station(Pullman)	-117.18	46.75	804	KPUW	Pullman / Moscow / Pullman / Moscow Region	46.74	-117.11	WA	778	3.9
Agronomy Research Center(West Lafayette)	-86.99	40.47	216	KLAF	Lafayette / Purdue University Airport	40.41	-86.95	IN	185	4
Bondville Road Station(Bondville)	-88.36	40.04	213	KCMI	Champaign / Urbana / University Of Illinois	40.03	-88.27	IL	230	5
Lake Dubay(Dancy)	-89.76	44.7	381	KCWA	Mosinee / Central Wisconsin	44.78	-89.67	WI	388	6.7
Abyss Site at Grand Canyon National Park(Flagstaff)	-112.18	36.05	2073	KGCN	Grand Canyon National Park	35.93	-112.15	AZ	2034	6.9
Utah Climate Center(Logan)	-111.9	41.66	1368	KLGU	Logan / Logan-Cache Airport	41.78	-111.85	UT	1357	7.2
University of Michigan Biological Station at Douglas Lake(Pellsto	-84.66	45.55	238	KPLN	Pellston / Pellston Regional Airport of Em	45.57	-84.8	MI	220	7.9
Desert Research and Extension Center(Holtville)	-115.44	32.8	-18	KIPL	Imperial / Imperial County Airport	32.83	-115.58	CA	-17	8
USDA Phytonutrients Lab(Beltsville)	-76.95	39.01	64	KDCA	Washington DC / Reagan National Airport	38.85	-77.03	VA	5	9.9
LSU Central Research Station(Baton Rouge)	-91.16	30.35	7	KBTR	Baton Rouge Metropolitan	30.54	-91.15	LA	21	10.6
Mississippi Agricultural and Forestry Experiment Station(Starkvil	-88.78	33.46	85	KGTR	Golden Tri AWS	33.45	-88.58	MS	79	11.1
Proctor Maple Research Center(Burlington)	-72.85	44.53	408	KMVL	Morrisville / Morrisville-Stowe State Airp	44.54	-72.62	VT	223	12.8

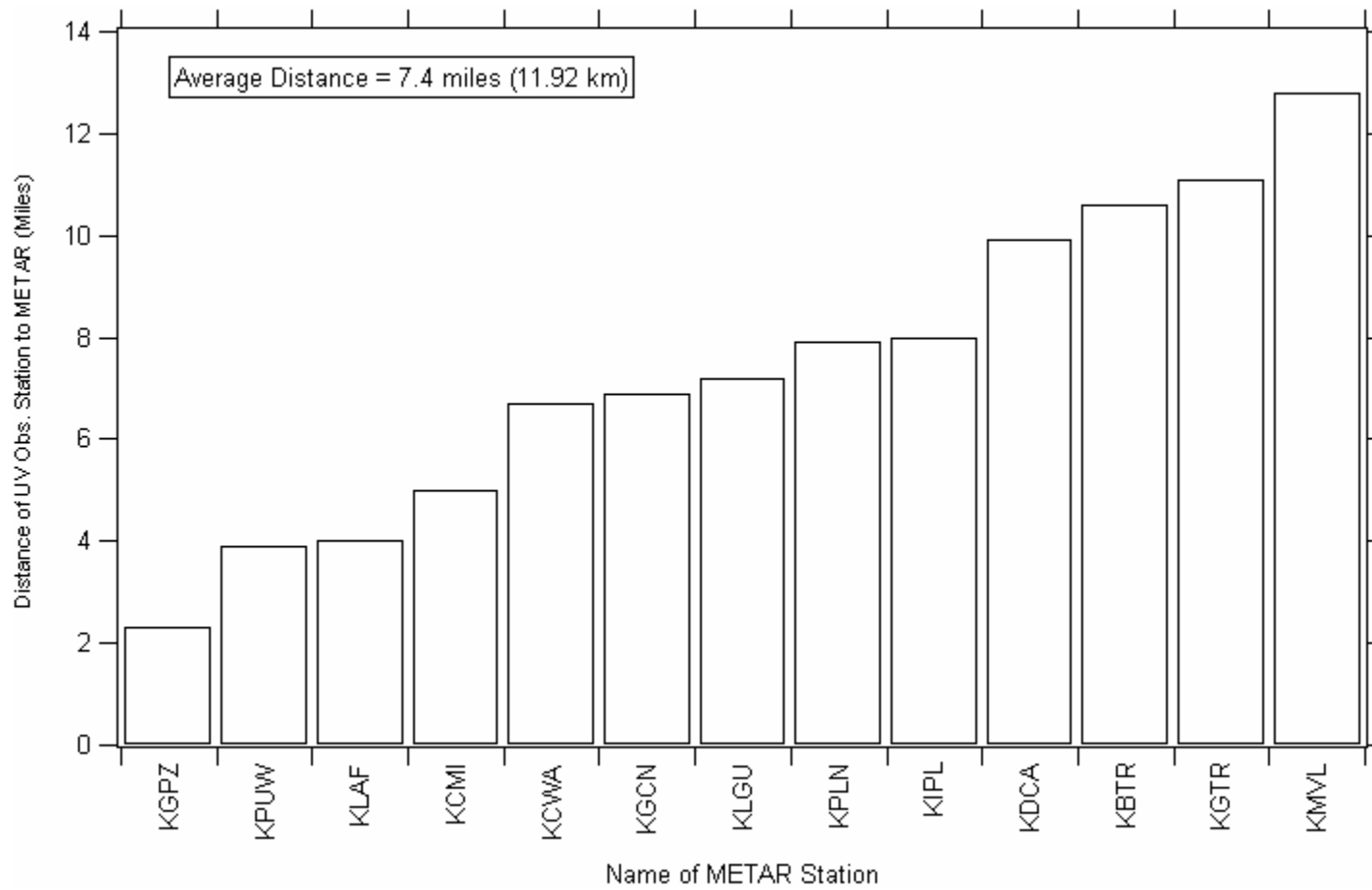


Figure 3-2: Representation of the distance of the UV observation station to its closest METAR station.

The comparison of the cloud cover reports from the METAR locations to the measured UV values from the USDA UV network yields the relationship in equation 1. The UV radiation is expressed in reference to the clear sky UV radiation that would have been measured without the presence of clouds or cloud transmission factor (T_{clouds}).

$$T_{clouds} = 1 - 0.62 * cld \quad (1)$$

Cld is the fraction of the sky covered by clouds (0 to 1).

Figure 3-3 compares the UV transmission calculated using equation 1 with the results obtained by Ilyas (1987), Cutchis (1980), Josefsson (1986), and Bais et al. (1993). Ilyas (1987) and Cutchis (1980) obtained a linear relationship between cloud cover and UV transmission. Equation 1 yields slightly less transmission than the one obtained by Ilyas (1987) and Cutchis (1980) for all cloud amounts. Bais et al. (1993) and Josefsson (1986) found that the effects of cloud cover were better explained by a second order polynomial relationship. Both studies found that the effects of clouds were small when less than half of the sky is covered by clouds. However, when more than half of the sky is covered by clouds they found that clouds attenuated more UV radiation than in the other three studies, including our study. The difference in the results can be explained by differences in sky conditions between the different locations, different instruments used, and different measurement periods. It is possible that the actual position of the clouds in the sky due to orographic effects have contributed to different results between the four studies. Ilyas (1987) also used an Eppley UV radiometer with a spectral response over wavelengths 295-390 nm very similar to the erythemal action spectrum.

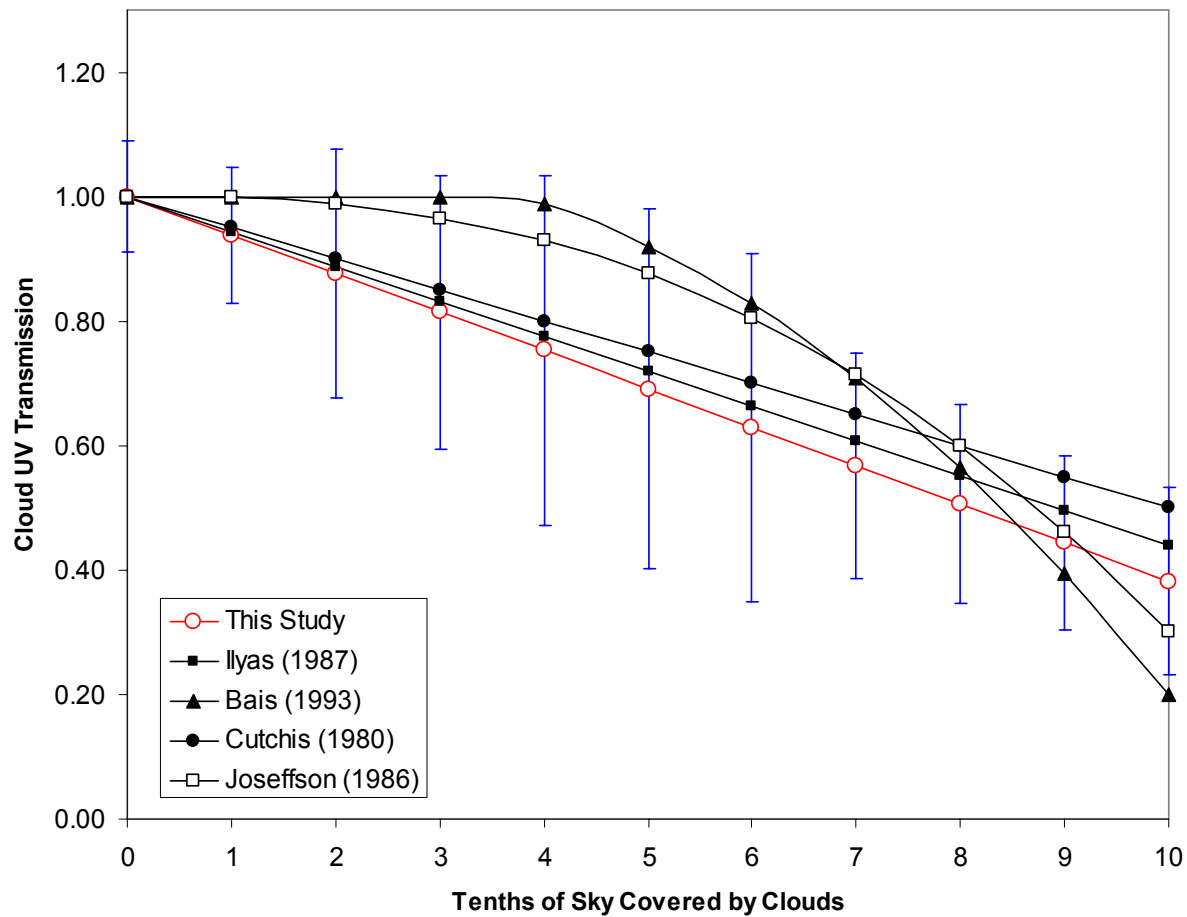


Figure 3-3: Comparison of the cloud UV transmission obtained in this study the ones obtained by Ilyas (1987), Bais (1993), Cutchis (1980) and Joseffson (1986). The error bars represent the standard deviations of the average UV transmission obtained from our study.

However, instead of using a fixed SZA he used daily total dosages to obtain monthly averages and yearly averages for 4 years. It is encouraging to see that the different data analysis methodology employed by Ilyas (1987) arrived to very similar results obtained in this study.

The cloud optical depth is an important optical property that can be used to estimate the cloud attenuation of UV radiation. Yet, retrievals of cloud optical depth are difficult to conduct given the non uniform nature of cloud coverage. The results from equation 1 represent the average attenuation of UV radiation over a period of time and not for specific conditions. However, these results can be used to estimate average cloud optical depths in the UV for different sky conditions. In order to estimate the cloud optical depths that would correspond to the different transmissions obtained with equation 1 we use the radiative transfer model from Madronich (1992). A uniform cloud layer with a thickness of 1.5 km at 2 km above the ground is used in the model to calculate the erythemal UV radiation. The same calculation is performed for clear skies. The ratio of these two yields the cloud transmission. The cloud optical depth in the UV that matches the cloud transmission corresponding to percentage cloud cover amounts of 10-100% from equation 1 is then calculated. Table 2-3 shows the estimated cloud optical depths that represent sky transmissions for these cloud amounts. These results are valid for erythemally integrated UV radiation. The corresponding cloud optical depths range between 1.2 (1/10 of the sky covered by clouds) to 26 for overcast conditions. On two individual cases large cumulonimbus clouds were observed to reduce more than 99% of the UV radiation, which corresponds to cloud optical depths of several hundreds.

Table 3-2. Estimated cloud optical depth in the UV for an overcast cloud layer having transmission properties corresponding to cloud amounts of 10, 20, 30, 40, 50, 60, 70, 80, 90, and 100%.

<i>CLOUD TRANSMISSION (T_{CLOUDS})</i>	<i>CLOUD OPTICAL DEPTH IN THE UV (FOR ERYTHEMAL UV RADIATION)</i>
0.94	1.2
0.88	2.5
0.81	4.0
0.75	5.5
0.69	7.5
0.63	10
0.57	13
0.51	16
0.44	20
0.38	26

3.4 Results

3.4.1 Verification of the Synthetic Current UV Index

The calculated UV Index is verified against UV measurements taken by the USDA UV network. The measured UV Index is calculated deriving the measured erythemal UV radiation in milliwatts m^{-2} by 25. The verification is done at the same 13 UV measuring sites that were found within 24 km of a METAR station. However, the time period for the verification corresponds to July 25 to August 25, 2004, which is a year later of the period used in the derivation of the cloud-UV empirical relationship. The synthetic UV Index is calculated at each one of these locations using the following input parameters: total column ozone values measured by the USDA UV Multifilter Shadow Band Radiometers (UV-MFRSR), total cloud cover from the empirical relationship (equation 1), an aerosol optical depth of 0.2, and solar elevation angles corresponding to the location and time of each of the measurements. A uniform aerosol optical depth of 0.2 was chosen to account for some of the effects of aerosols on UV radiation. The UV Index is calculated using the clear sky two-stream radiative transfer model from Madronich (1982). This UV model runs very quickly on modern computers and does not limit the concurrent calculation of large numbers of synthetic current UV Index values. Data for SZA greater than 75° were excluded from the dataset. The calculation is attained in two steps. First, the clear sky erythemal UV radiation (from 280 to 400 nm) is calculated for all METAR reports at the 13 locations listed in Table 1-3 using the total column ozone that was measured by the UV-MFRSR at the time of the measurements (July 25 to August 25, 2004). The altitude above sea level for each site is considered in the calculation. Then the cloud cover transmission factor (T_{clouds}) from equation 1 is applied to correct the clear sky UV

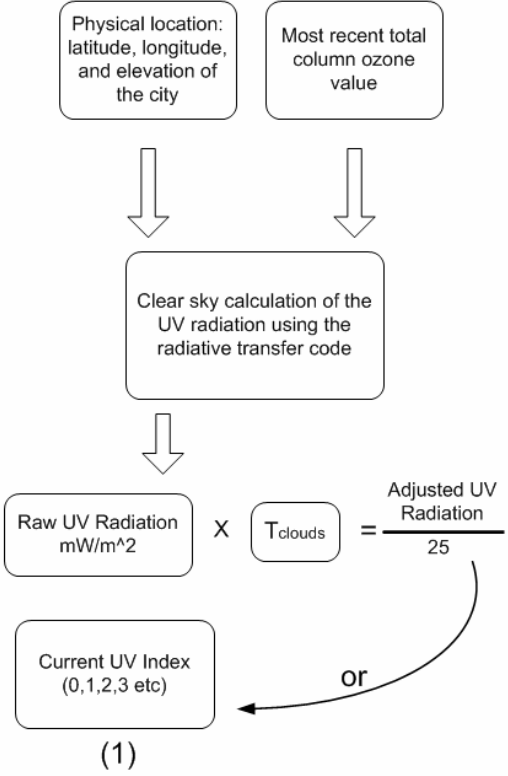
radiation. The last step consists in calculating the difference between the calculated or synthetic UV Index and the measured UV Index for all records between July 25, 2004 and August, 25 2004. Figure 3-4 shows a schematic of the calculation and verification of the current UV Index.

A total of 6566 points are verified. In 50% of these cases, the synthetic current UV Index is identical to the observed UV Index. In 67% of the cases the synthetic current UV Index shows a difference of +/- 1 UV Index unit from the measured UV Index. In 83% of the cases the synthetic current UV Index is within +/- 2 UV Index units of the measured index. The cloud cover data used in the verification comes from the METAR stations. Only sky reporting METAR stations were used in the comparison. These overall results are presented in Figure 3-5 in the form of a histogram. Figure 3-6 shows individual histograms for each of the 13 locations. These results are compared against the verification results corresponding to tomorrow's UV forecast provided by NOAA (Long et al, 1996). The forecast UV Index verification shows that in 32% of the cases the synthetic current UV Index is identical to the observed UV Index. In 76% of the cases the synthetic current UV Index shows a difference of +/- 1 UV Index unit from the measured UV Index. In 92% of the cases the synthetic current UV Index is within +/- 2 UV Index units of the measured index. The differences are probably explained by more uncertainty in the cloud forecasts compared with cloud observations. Uncertainties in the total column ozone forecasts can also account for a smaller portion of the differences.

The places having the highest average cloud cover for the entire measuring period have the lowest correlation coefficient between the synthetic and observed UV Index.

The highest correlation between the synthetic and observed UV Index is 0.98 found at KIPL (Imperial County Airport in desert California).

Calculation of the Current UV Index



Verification of the Current UV Index

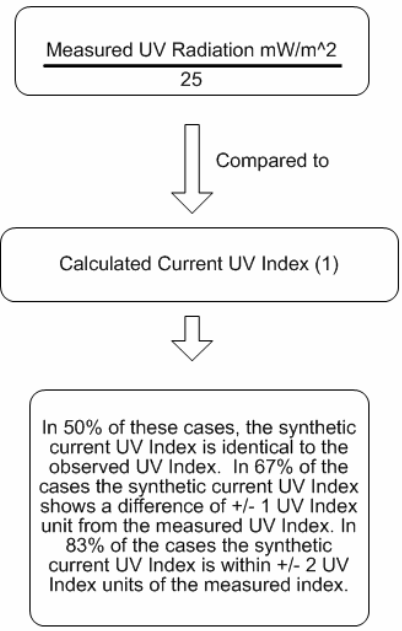


Figure 3-4: Schematic of the calculation and verification of the current UV Index.

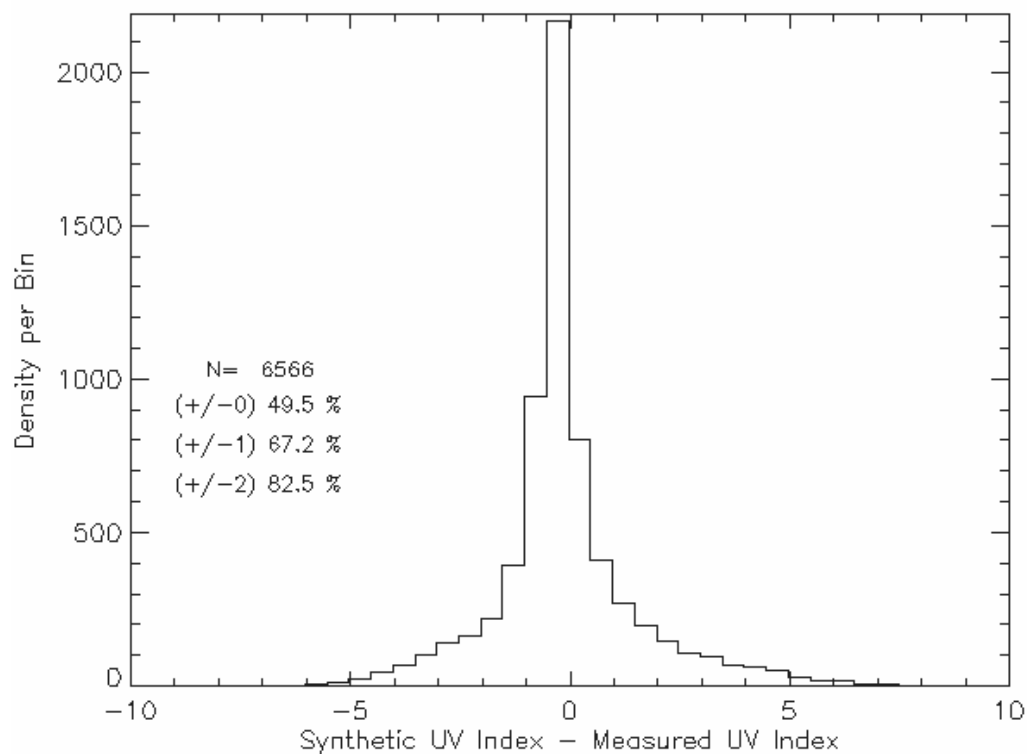


Figure 3-5: Histogram for all 13 locations. The total number of records verified is 6566. The graph displays the percentage of points for each of the following categories: (a) with synthetic current UV Index identical to the observed UV Index; (b) with synthetic current UV Indices showing a difference of +/- 1 UV Index unit from the measured UV Index; (c) with synthetic current UV Indices within +/- 2 UV Index units of the measured index.

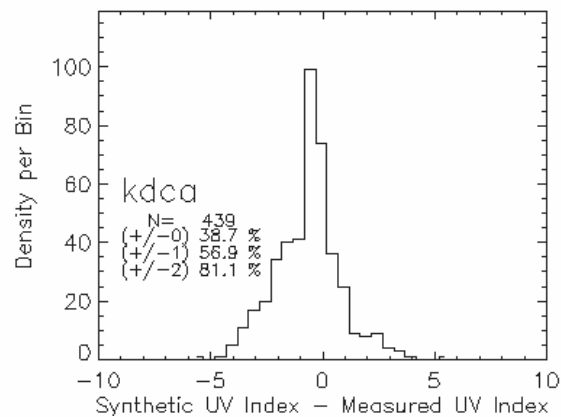
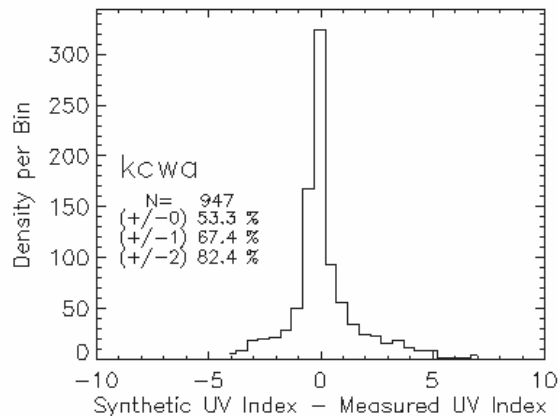
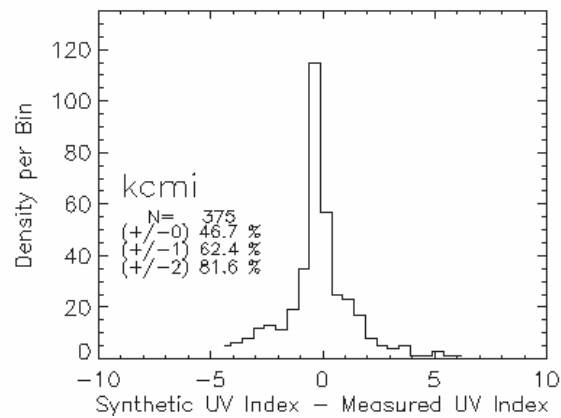
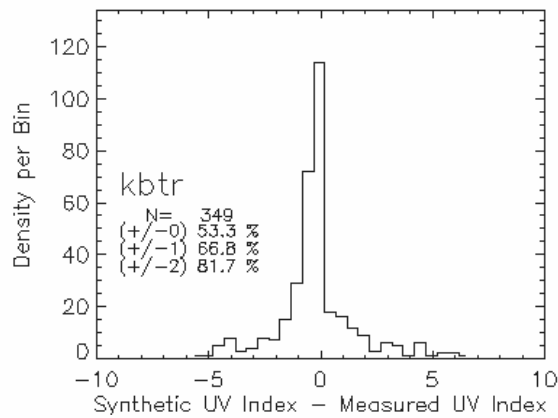


Figure 3-6: Histograms for each of the 13 locations. Each graph displays:

- The four digit code of the METAR station.
- The number of points verified.
- The percentage of points for each of the following categories: (a) with synthetic current UV Index identical to the observed UV Index; (b) with synthetic current UV Indices showing a difference of +/- 1 UV Index unit from the measured UV Index; (c) with synthetic current UV Indices within +/- 2 UV Index units of the measured index.

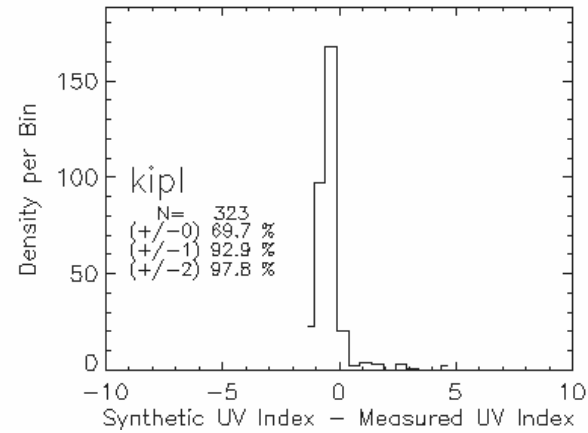
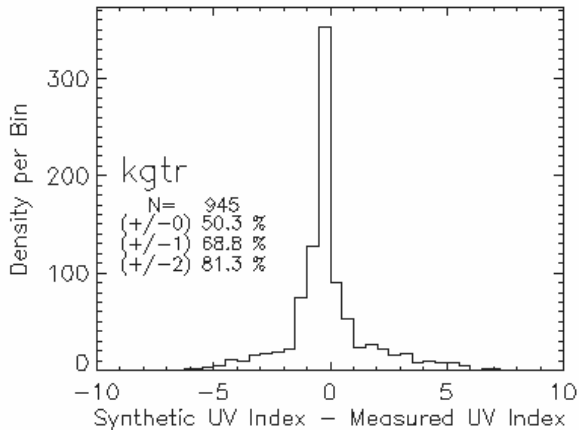
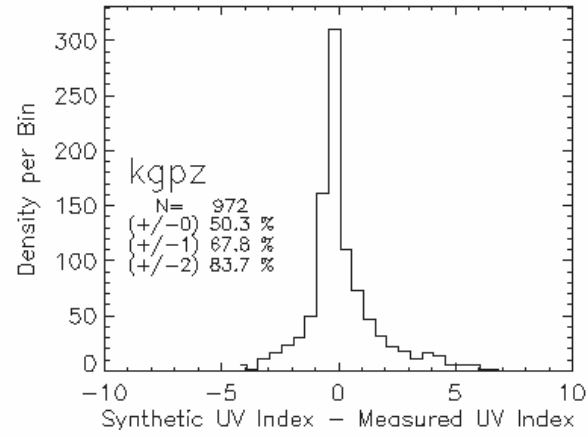
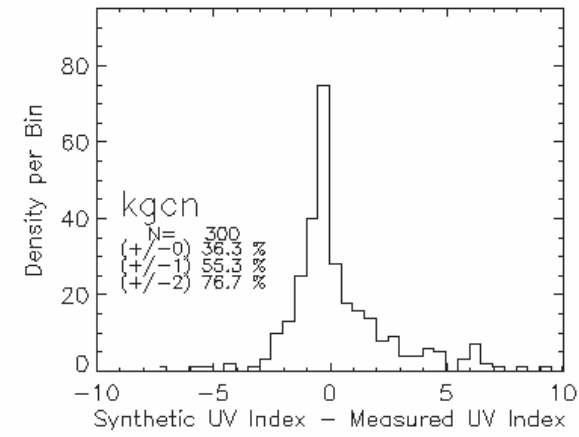


Figure 3-6: (Cont'd)

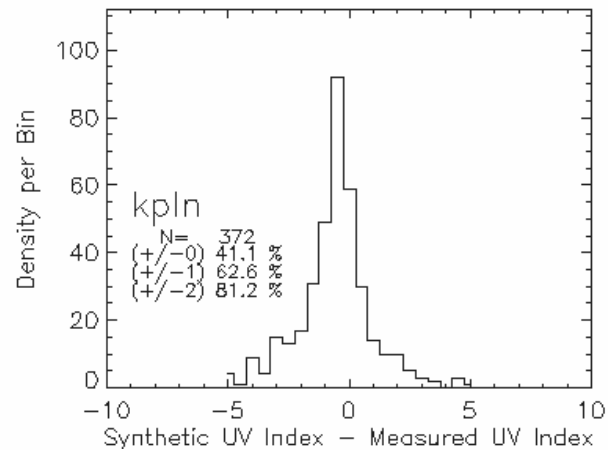
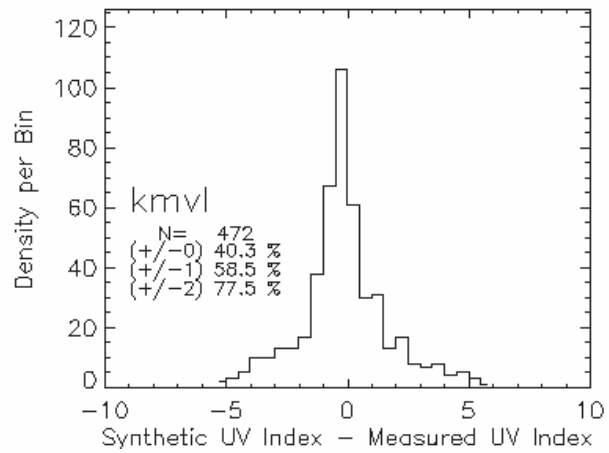
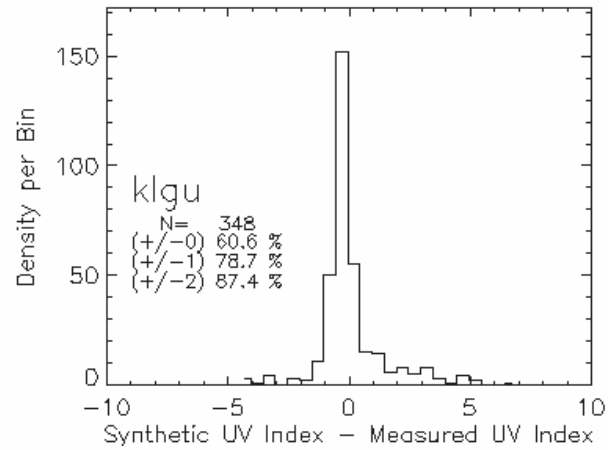
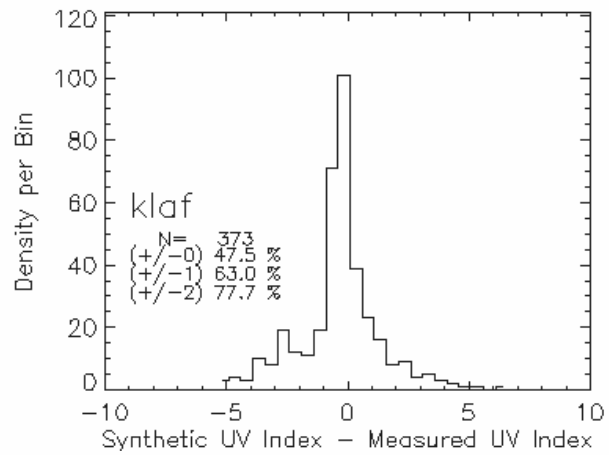


Figure 3-6: (Cont'd)

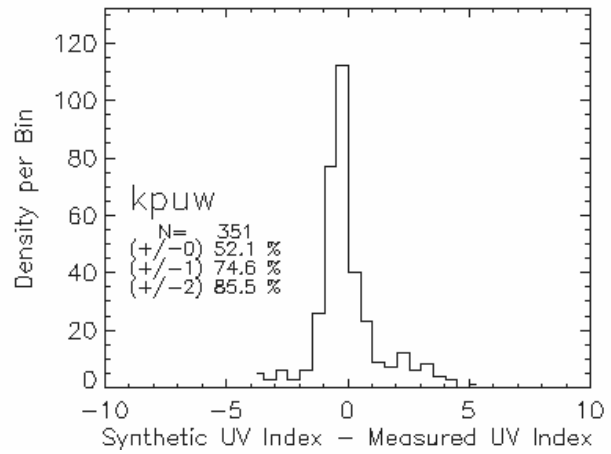


Figure 3-6: (Cont'd)

The average cloud cover for this location was 21%. The number of identical cases at KIPL is 59.4% which corresponds to the second highest in this study. The highest number of identical cases corresponds to KLGU (Logan-Cache Airport in Utah) with 66.1%, 47% average cloud cover, and a correlation of 0.88 between the synthetic and the observed UV Index. The lowest correlation coefficient (0.60) is found at KMVL (Morrisville-Stowe State Airport in Vermont). This location presents the highest average cloud cover (60%) of all locations considered in this study. The number of identical cases at KMVL is 40.3%, which corresponds to the fourth lowest. The lowest number of identical cases (35.7%) is found at KGCN (Grand Canyon National Park at an elevation of 2073 m) with 38% average cloud cover, and a correlation of 0.79 between the synthetic and the observed UV Index. Figure 3-7 compares the percentage of UV Index errors for each of the three categories (+/-0, +/-1, and +/-2 UV Index units) for all 13 locations.

In the event that clouds are not detected below 3658 m, but are present above 3658 m, the synthetic current UV Index will lead to a small overestimate of the UV radiation. When clouds are not present at all, the synthetic current UV Index will, in most cases, be calculated with no bias.

These data provide some insight into the range of agreement that one could expect between the synthetic and observed UV Index at different locations depending on the cloud cover climatology that a specific location may have. The correlation of the 13 regression coefficients with the average cloud cover for the whole month for each location yields a small correlation ($R^2=0.38$) (Figure 3-8). This indicates that for locations with a higher cloud cover there is a smaller correlation between clouds and UV radiation.

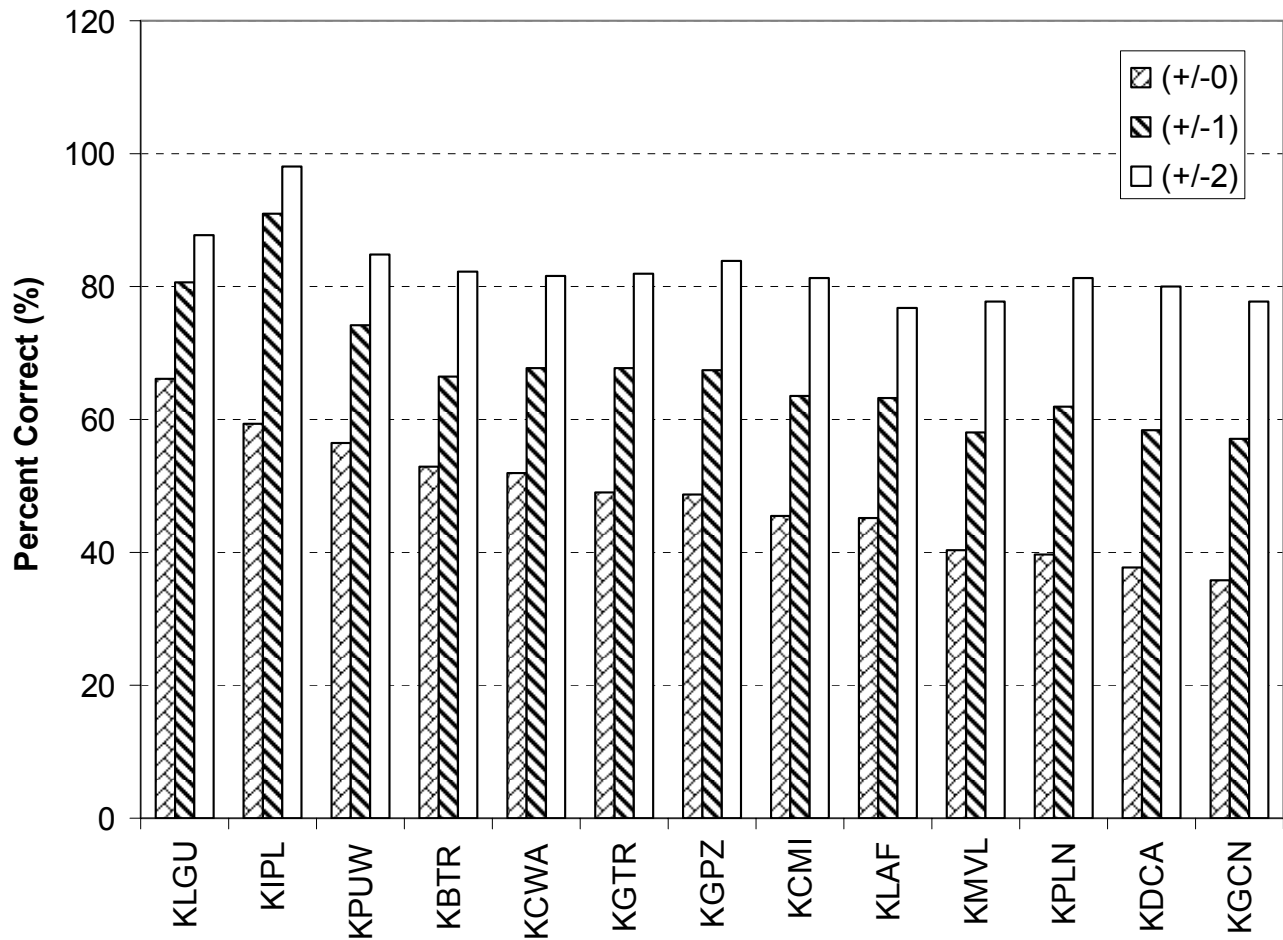


Figure 3-7: Comparison of UV Index errors (+/-0, +/-1, and +/-2) for all thirteen locations.

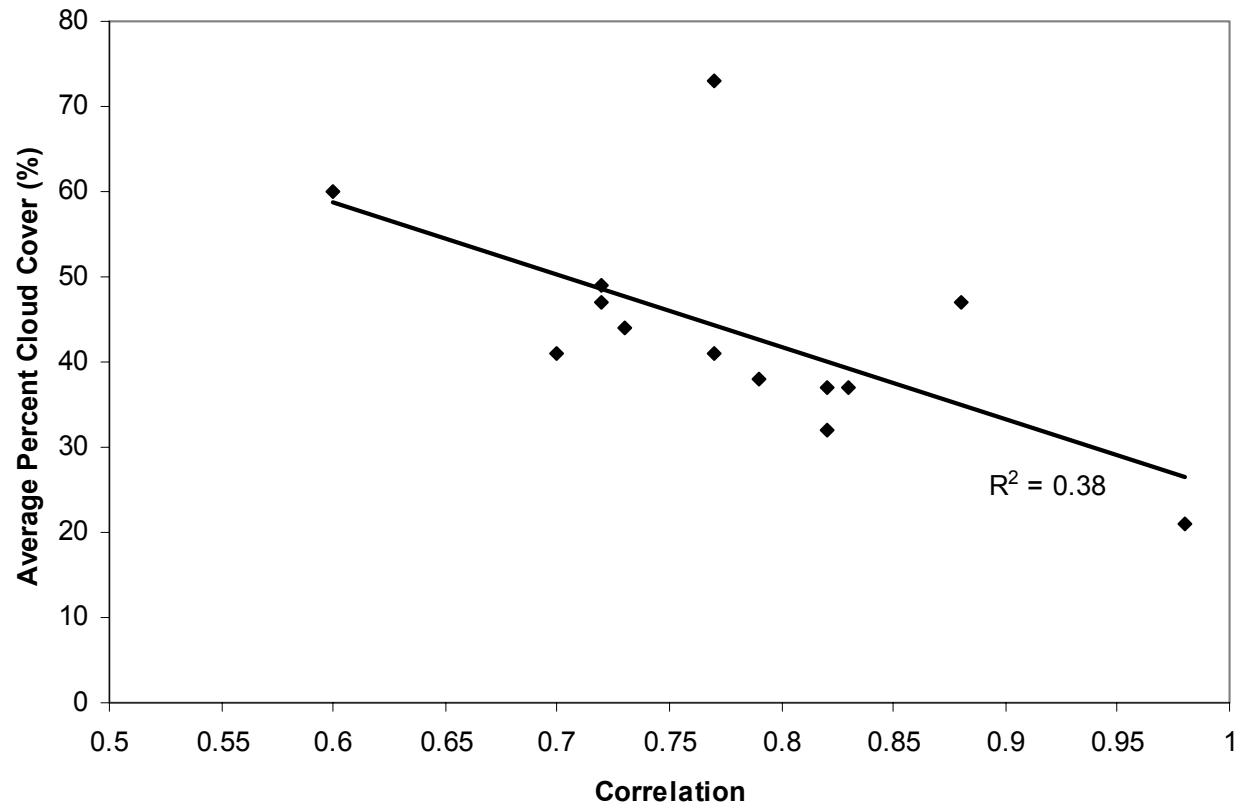


Figure 3-8: Correlation between monthly average cloud cover and the correlation between the measured UV radiation and cloud cover for each site.

However, there is no apparent correlation between the percentage of cases in each of the three accuracy categories (± 0 , ± 1 , and ± 2 UV Index units) and the monthly average cloud cover.

The measured UV Index from the 13 USDA locations was also verified against the calculated UV Index values using the cloud-UV relationships obtained by Ilyas (1987), Cutchis (1980), Josefsson (1986), and Bais et al. (1993). The results are the following. Using the equation derived by Ilyas (1987), in 51% of these cases, the synthetic current UV Index is identical to the observed UV Index. In 67% of the cases the synthetic current UV Index shows a difference of ± 1 UV Index unit from the measured UV Index. In 83% of the cases the synthetic current UV Index is within ± 2 UV Index units of the measured index. Using the equation derived by Cutchis (1980) we find that in 52% of these cases, the synthetic current UV Index is identical to the observed UV Index. In 68% of the cases the synthetic current UV Index shows a difference of ± 1 UV Index unit from the measured UV Index. In 83% of the cases the synthetic current UV Index is within ± 2 UV Index units of the measured index. Using the relationship derived by Bais (1993) yields the following results: in 32% of these cases, the synthetic current UV Index is identical to the observed UV Index. In 55% of the cases the synthetic current UV Index shows a difference of ± 1 UV Index unit from the measured UV Index. In 77% of the cases the synthetic current UV Index is within ± 2 UV Index units of the measured index. Using the relationship obtained by Josefsson (1986) we find the following results: in 41% of these cases, the synthetic current UV Index is identical to the observed UV Index. In 62% of the cases the synthetic current UV Index shows a

difference of +/- 1 UV Index unit from the measured UV Index. In 80% of the cases the synthetic current UV Index is within +/- 2 UV Index units of the measured index.

The fact that there is very little difference between the results of the verification of the UV Index values calculated using equation 1 and the results obtained using the cloud-UV relationships obtained by Ilyas (1987) and Cutchis (1980), confirms that the UV measurements used in this study are representative of the general effects of clouds on UV radiation.

Uncertainties in the measurements of total column ozone have a direct effect on the calculation of the current UV Index (e.g. use of yesterday's total column ozone to represent last hour's total column ozone). In order to estimate the uncertainty introduced by using yesterday's ozone amount, the UV Index was calculated using total column ozone values corresponding to the daily climatology values provided from the Total Ozone Mapping Spectrometer (TOMS) for the time period used in this study. The results of this calculation were compared against the current UV Index values obtained using the actual measured ozone values by the USDA network. The difference in results is very small for the data considered in this study. In 48% (versus 50%) of these cases, the synthetic current UV Index is identical to the observed UV Index. In 66% (versus 67%) of the cases the synthetic current UV Index shows a difference of +/- 1 UV Index unit from the measured UV Index. In 82% (versus 83%) of the cases the synthetic current UV Index is within +/- 2 UV Index units of the measured index. Larger differences are expected in the winter months when changes of 10-30 DU are possible with the passage of synoptic disturbances. However, the effect of these changes in total column ozone approach in order of magnitude the instruments' uncertainty of the measurement of the

total column ozone and the uncertainties due to the varying path lengths of the ozone optical depth inside clouds.

The results presented in this section show that the effects of clouds on UV radiation can be represented well using the linear relationship derived in this study. Clouds, due to their natural variability, affect UV radiation in different ways depending on cloud type, amount, position of the clouds in the sky, or number of cloud layers.

3.4.2 Comparison of the Synthetic Current UV Index with Actual Sky Conditions

This section shows the results of calculating the current UV Index for three given days. The results are presented graphically and compared against cloud cover from satellite images. The first two days (September 27, 2004 and April 21, 2005) show the calculation of the synthetic current UV Index at METAR locations. The third day (April 28, 2005) expands the calculation of the synthetic current UV Index to nearly 10,000 cities across the United States which allows for the distribution of the current UV Index to a greater number of people across the country. The calculation of the UV Index for April 28, 2005 also takes into account GOES-augmented METAR clouds and compares the results to those obtained only using METAR-derived clouds.

3.4.2.1 Comparison at METAR Points

September 27, 2004

The UV Index is calculated for September, 27, 2004 when the remnants of hurricane Jeanne moved over the southeastern United States. Figure 3-9 shows the clear sky (no clouds) synthetic current UV Index for the most recent observation issued between 1950Z and 1958Z for each of the 1272 METAR observations that reported sky conditions for September 27, 2004. Figure 3-10 shows the calculated synthetic current UV Index for the actual sky conditions that were reported by the METAR observations. Total column ozone values from the TOMS satellite are used to account for the effects of ozone on UV radiation. Note that most of the METAR observations, with the exception of specials (additional observations reported during times of active weather), come in around 53 minutes after each hour. However, AWOS stations come in at different times and are not used in this study to calculate the current UV Index. The time window between 50 and 58 minutes after the hour was used to ensure that we capture most of the observations, even if they are reported at slightly different times at different stations. Figure 3-11 shows the UV Index reduction from the clear sky UV Index shown in Figure 3-9. The largest reductions, 4 UV Index units, correspond to a difference of 100 W m^{-2} of erythemal UV radiation in western Texas, Alabama and Georgia associated with the remnants of hurricane Jeanne. The derived percentage cloud cover from the METAR reports is shown in Figure 3-12. The warm colors correspond to higher amounts of cloud cover. The largest amounts of cloud cover are found along a cold front that extended from southern Colorado to the Great Lakes and associated with the remnants of Jeanne in the eastern United States. Other less widespread areas of cloud cover are found in the

Cascade Mountains near the Canadian border, coastal central California, associated with the intrusion of the marine layer over the coastal areas, and Wyoming and Montana associated with the cold front and mountain convection. Figure 3-13 shows the satellite image that corresponds to 2015Z, only fifteen minutes later than the simulation time. Rain was reported by radar during the course of the day in the southeastern United States

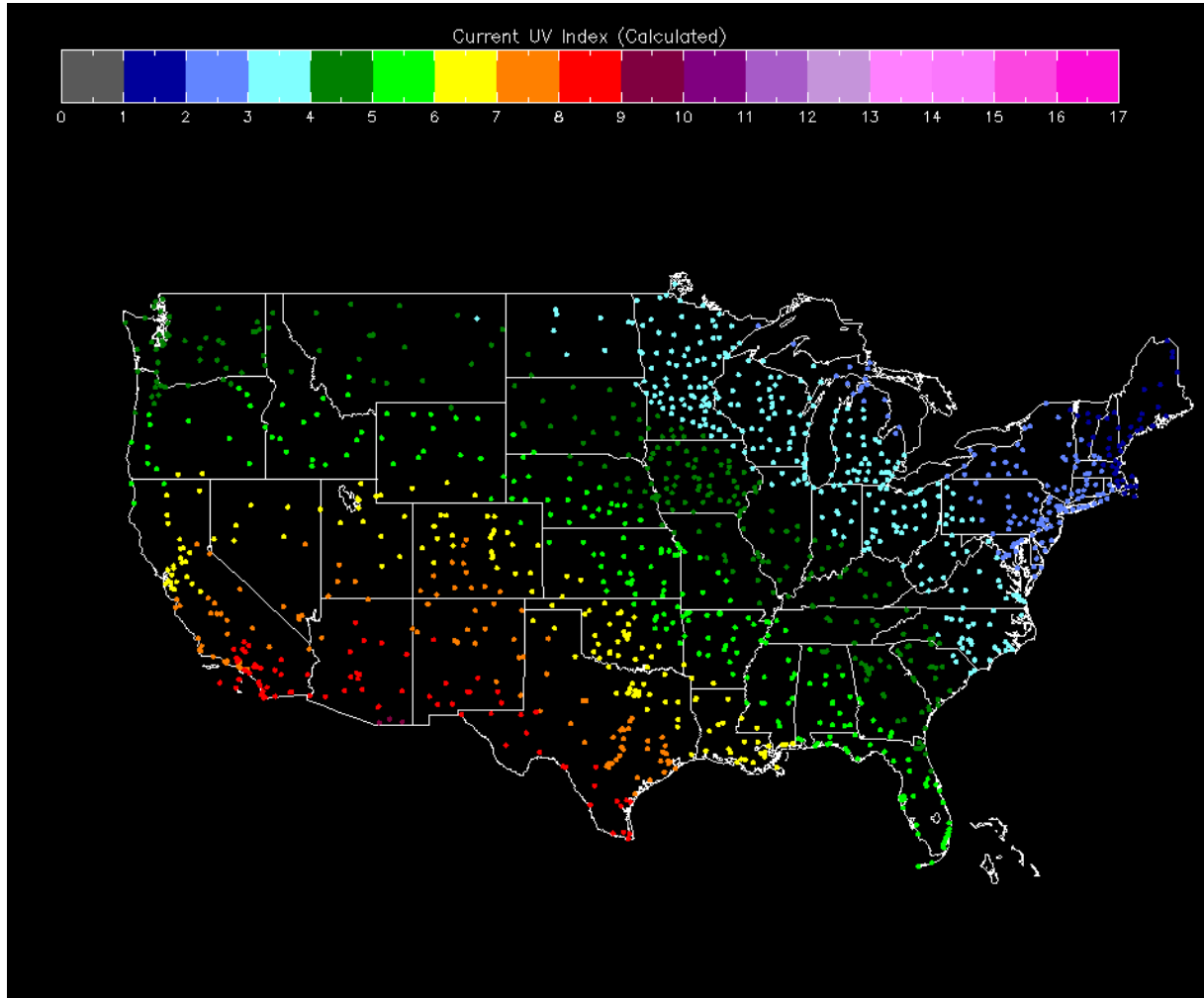


Figure 3-9: Simulation of the synthetic UV Index for September 27, 2004 (1950Z-1958Z). The calculation corresponds to the maximum clear sky UV Index that would have been measured without the presence of clouds.

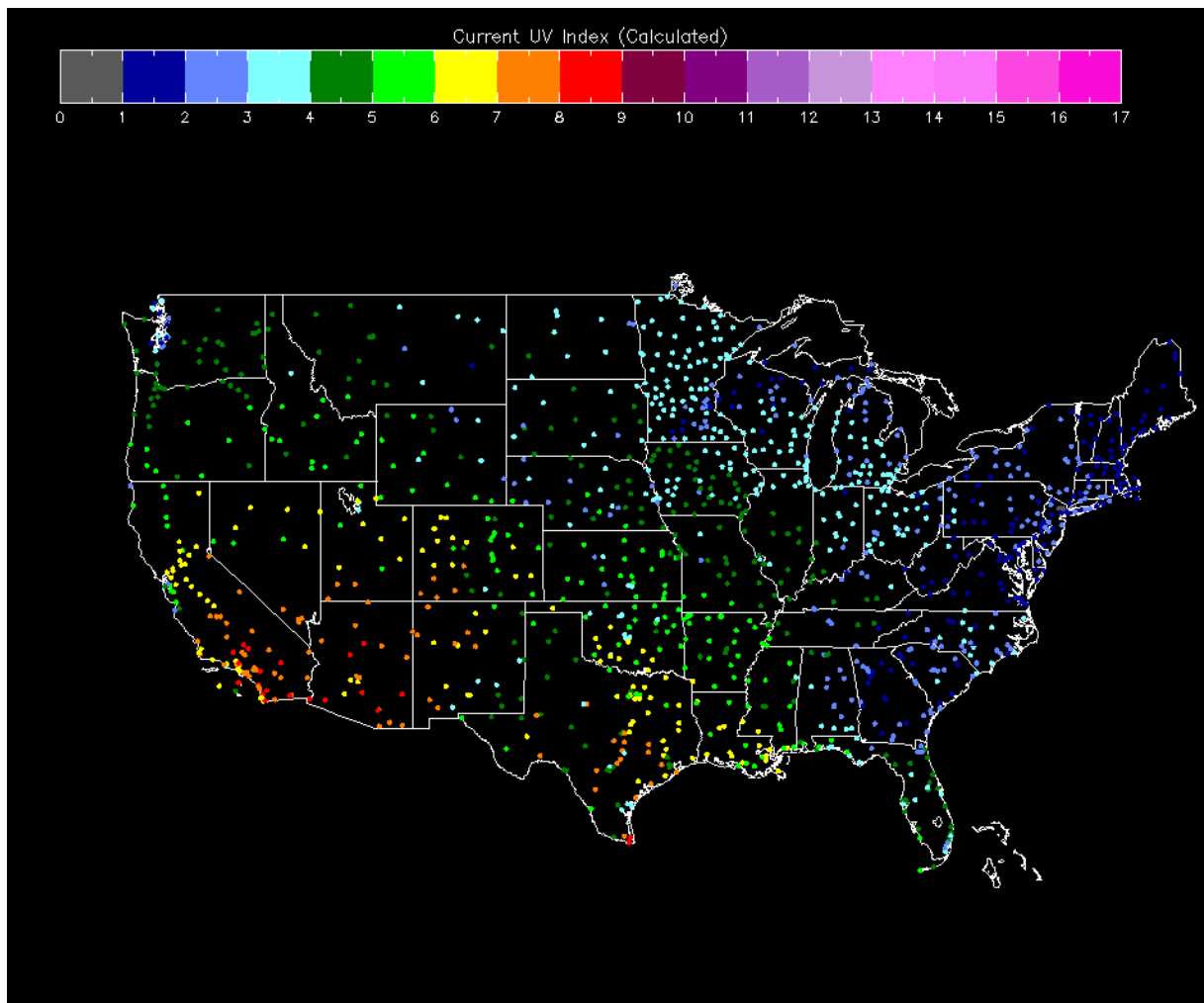


Figure 3-10: Simulation of the synthetic UV Index for September 27, 2004 (1950Z-1958Z). The calculation corresponds to synthetic UV Index that would have been measured considering the effects of clouds.

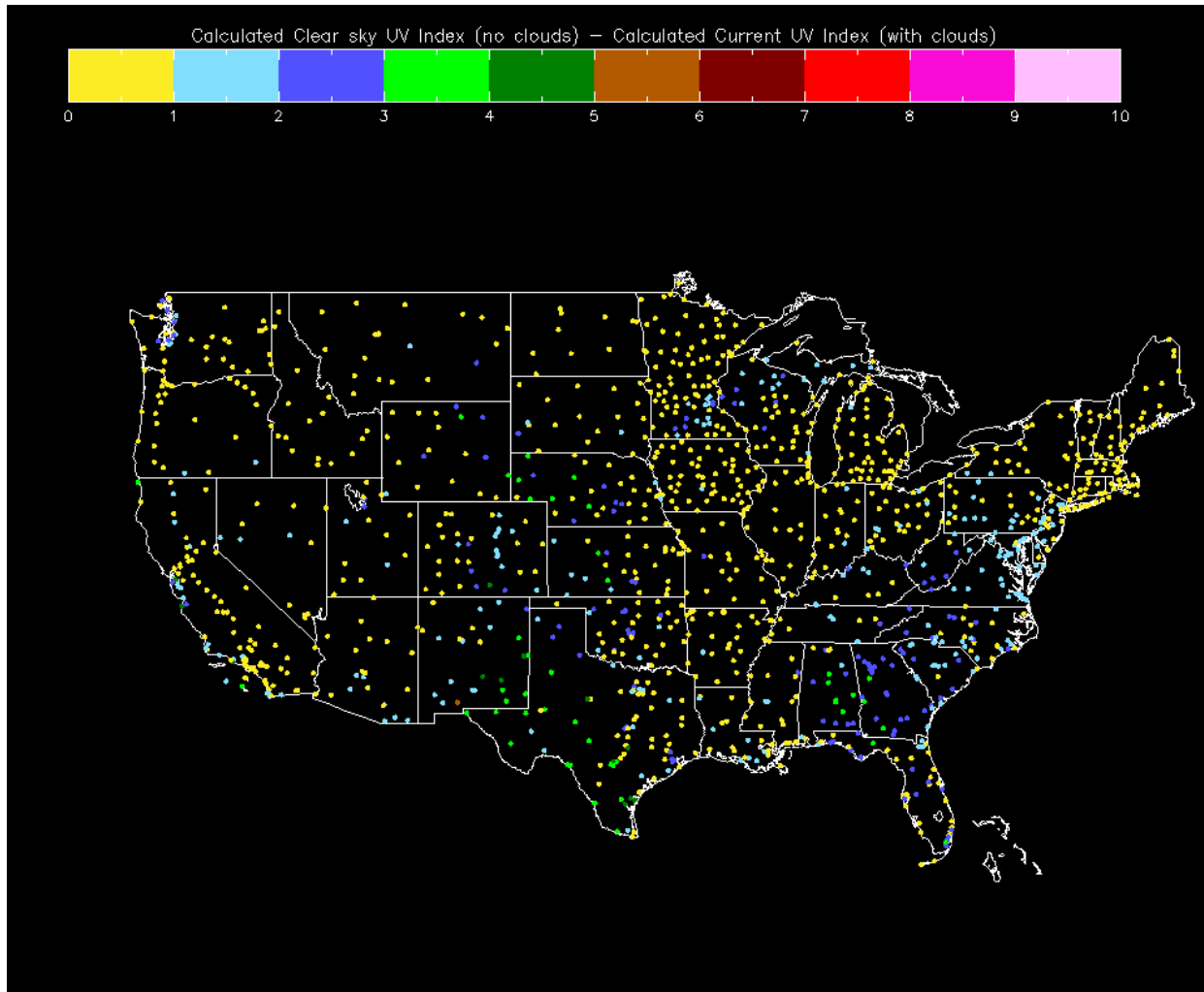


Figure 3-11: UV Index reduction due to clouds (Clear sky UV Index – UV Index considering clouds) for September 27, 2004 from 1950Z to 1958Z.

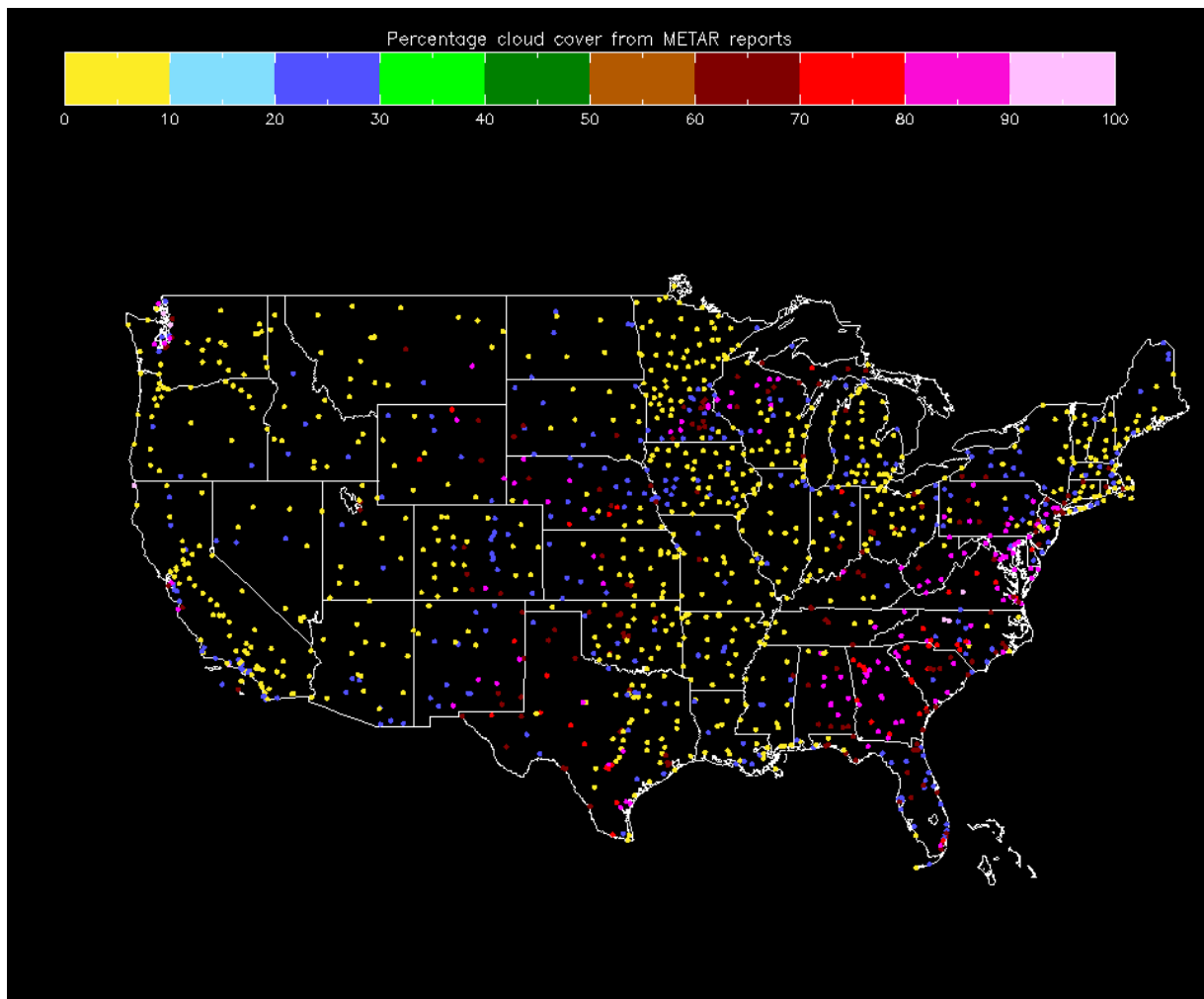


Figure 3-12: Observed percentage cloud cover as reported from the surface METAR stations from 1272 locations across the United States for September 27, 2004 (1950Z-1958Z).

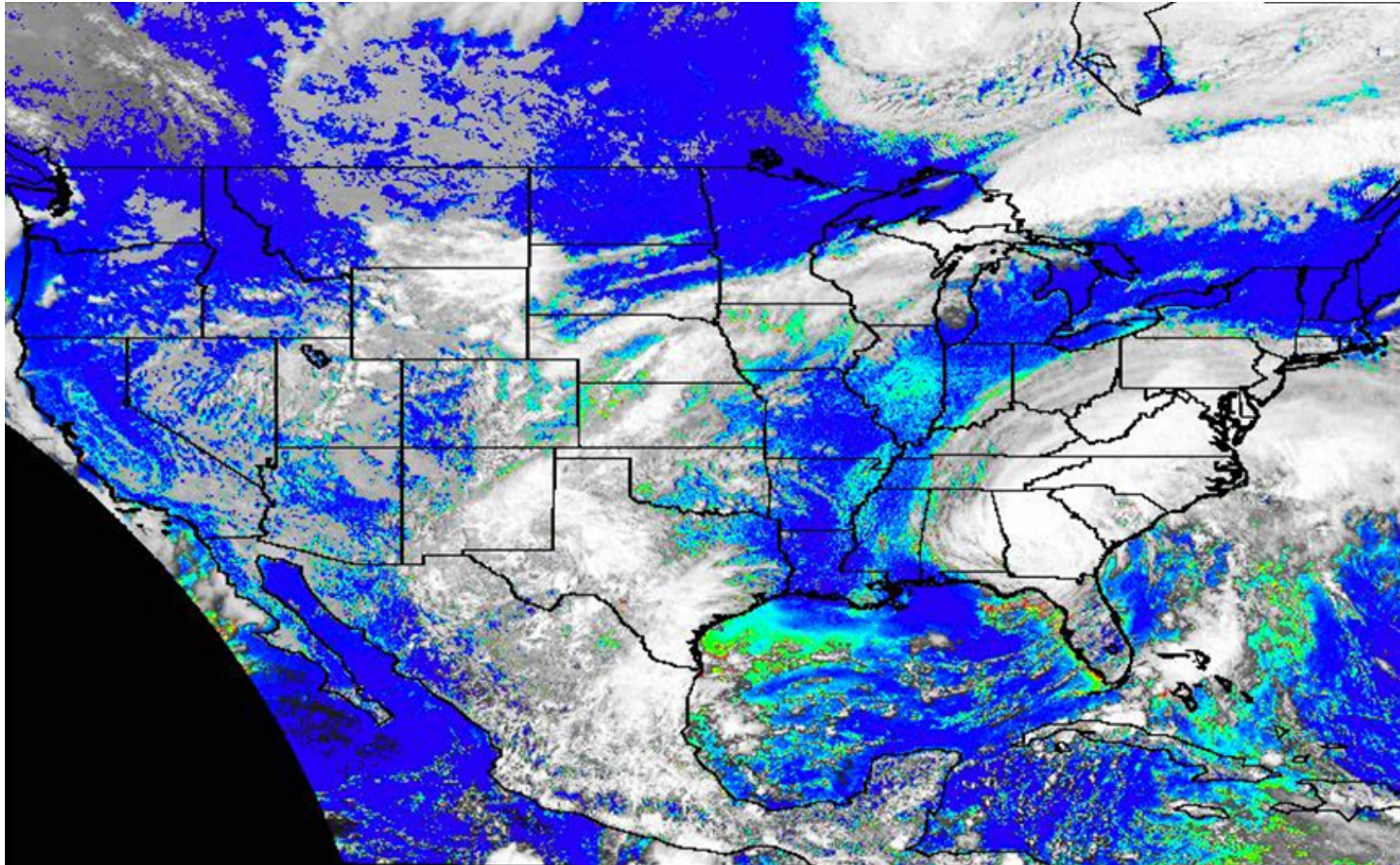


Figure 3-13: Satellite image taken on September 27, 2004 at 2015Z. In the southeastern United States the remnants of hurricane Jeanne move toward the northeast. Over western Texas an upper level low pressure is responsible for abundant cloudiness in the center of the United States. From Colorado to the Great lakes a cold front separates cooler drier air from the Canadian prairies from warmer air to the south. Fog and stratus clouds are observed off the west coast.

from Alabama as far north as northern Virginia and eastern Pennsylvania, in central Wisconsin, in western Texas, Kansas, southern Nebraska, in the mountain west, and in central coastal California. The surface meteorological features and sky conditions for selected METAR locations are shown in Figure 3-14.

April 21, 2005

April 21, 2005 shows a low pressure system located over east Kansas with associated cloud masses extending over a large portion of the United States. Figure 3-15 shows the synthetic clear sky UV Index (no clouds) for April 21, 2005 at 1953Z. The most recent METAR cloud cover report for each point collected from 1950Z to 1958Z is used in the simulation. Higher elevations of the Rocky Mountains increase the UV Index by one unit compared to nearby points. Figure 3-16 shows the calculated synthetic current UV Index including clouds. Figure 3-17 shows the UV Index reduction from clear skies due to the effect of clouds. Figure 3-18 shows the percentage cloud cover reported by the METAR stations used as input for the results shown in Figure 3-19. Clouds in southern Texas reduced the clear sky UV Index by a maximum 5-6 UV Index units (brownish color). Reductions of 2-5 UV Index units are common in the mass of clouds that extends from Oregon to Maryland. The UV Index reduction ranges between 2-5 UV Index units from Oregon to Nebraska and 1-3 UV Index units eastward toward Maryland. Figure 3-20 shows the satellite image for April 21, 2005 at 2004Z. Figure 3-21 shows the surface meteorological features at 00Z (April 22, 2005).

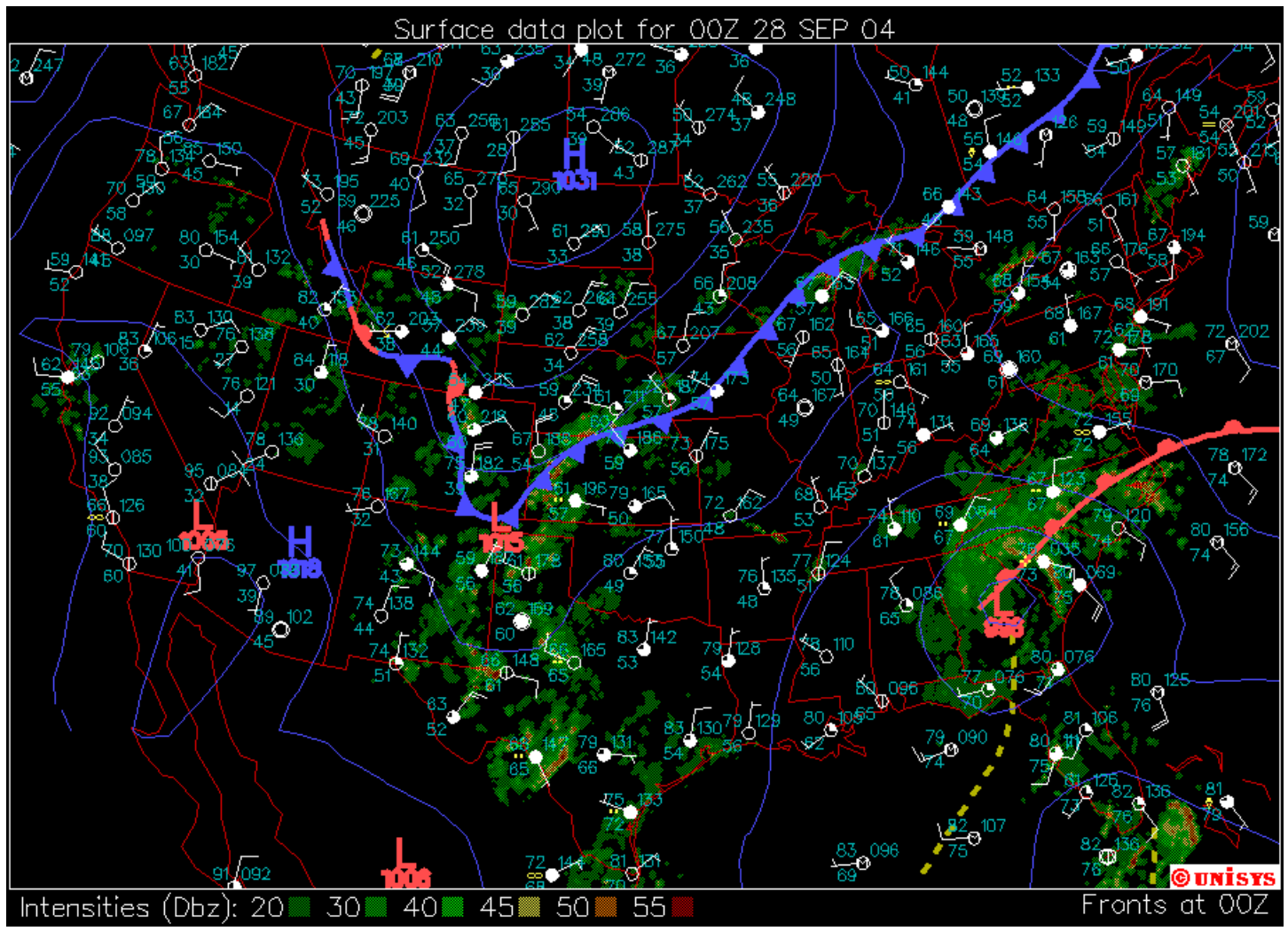


Figure 3-14: Surface map for 00z September 28, 2004.

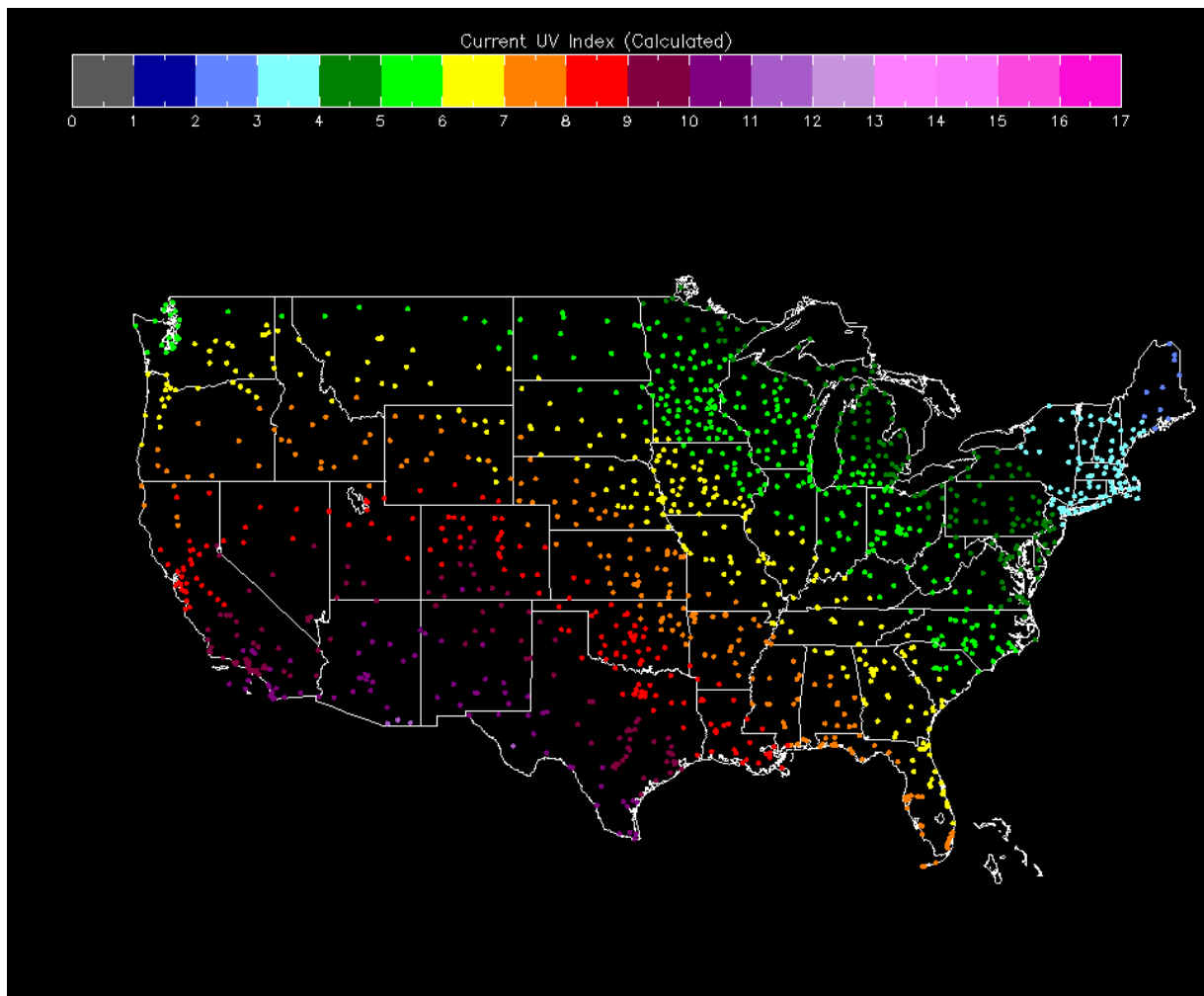


Figure 3-15: Simulation of the synthetic UV Index for April 21, 2005 (1950Z-1958Z). The calculation corresponds to the maximum clear sky UV Index that would have been measured without the presence of clouds.

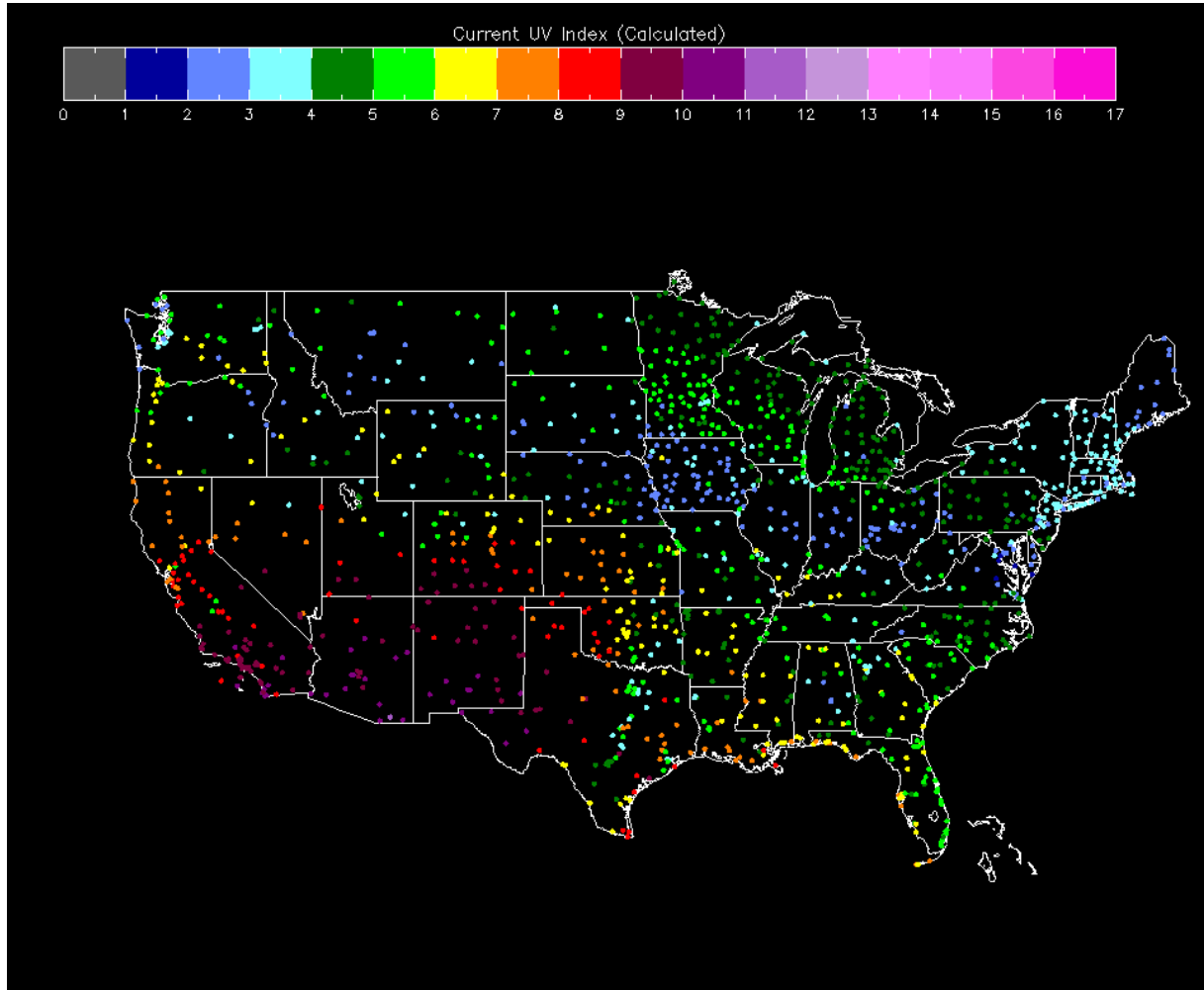


Figure 3-16: Simulation of the synthetic UV Index for April, 21, 2005 (1950Z-1958Z). The calculation corresponds to synthetic UV Index that would have been measured considering the effects of clouds.

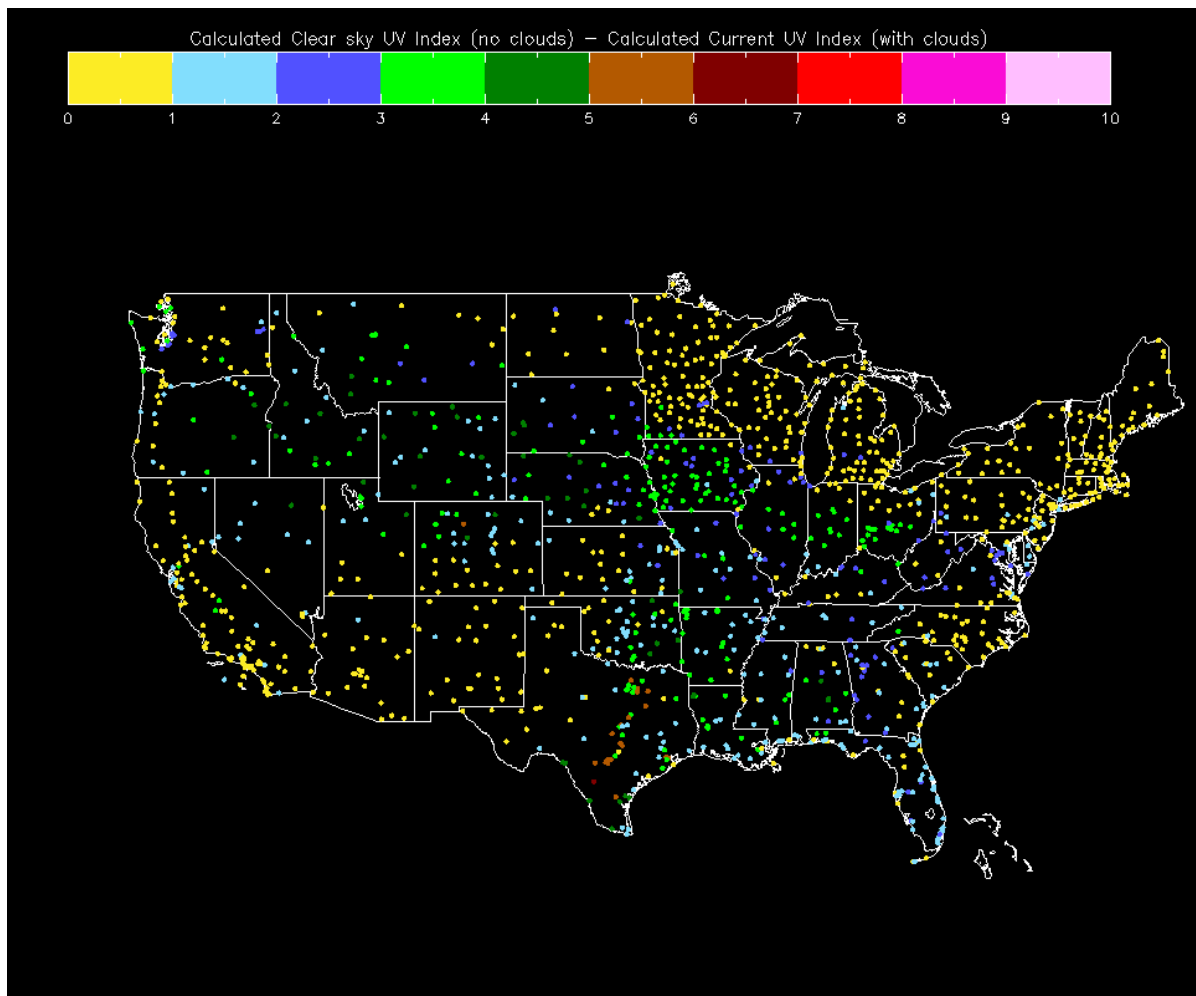


Figure 3-17: UV Index reduction due to clouds (Clear sky UV Index – UV Index considering clouds) for April, 21, 2005 from 1950Z to 1958Z.

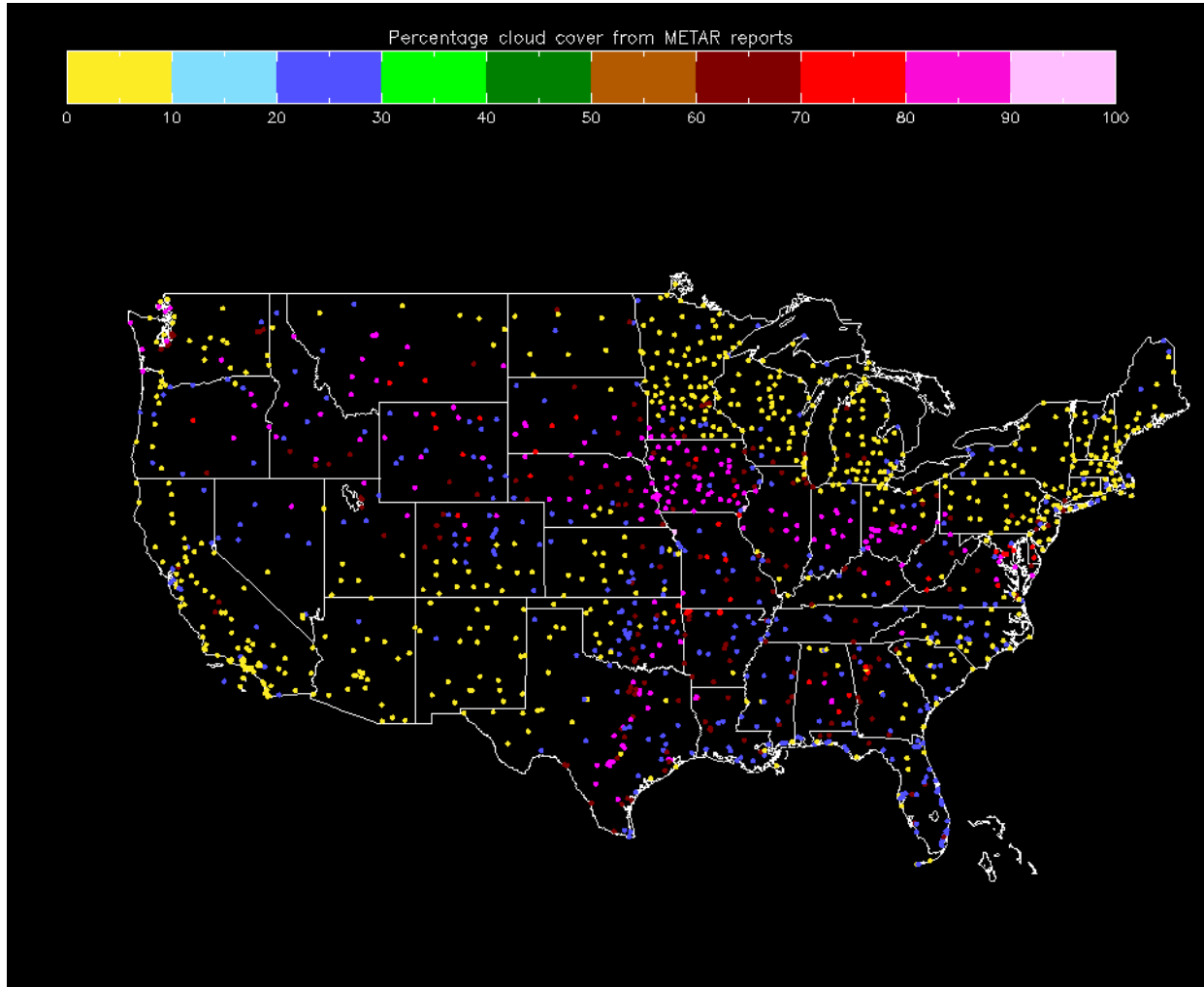


Figure 3-18: Observed percentage cloud cover as reported from the surface METAR stations from 1272 locations across the United States for April, 21, 2005 (1950Z-1958Z).

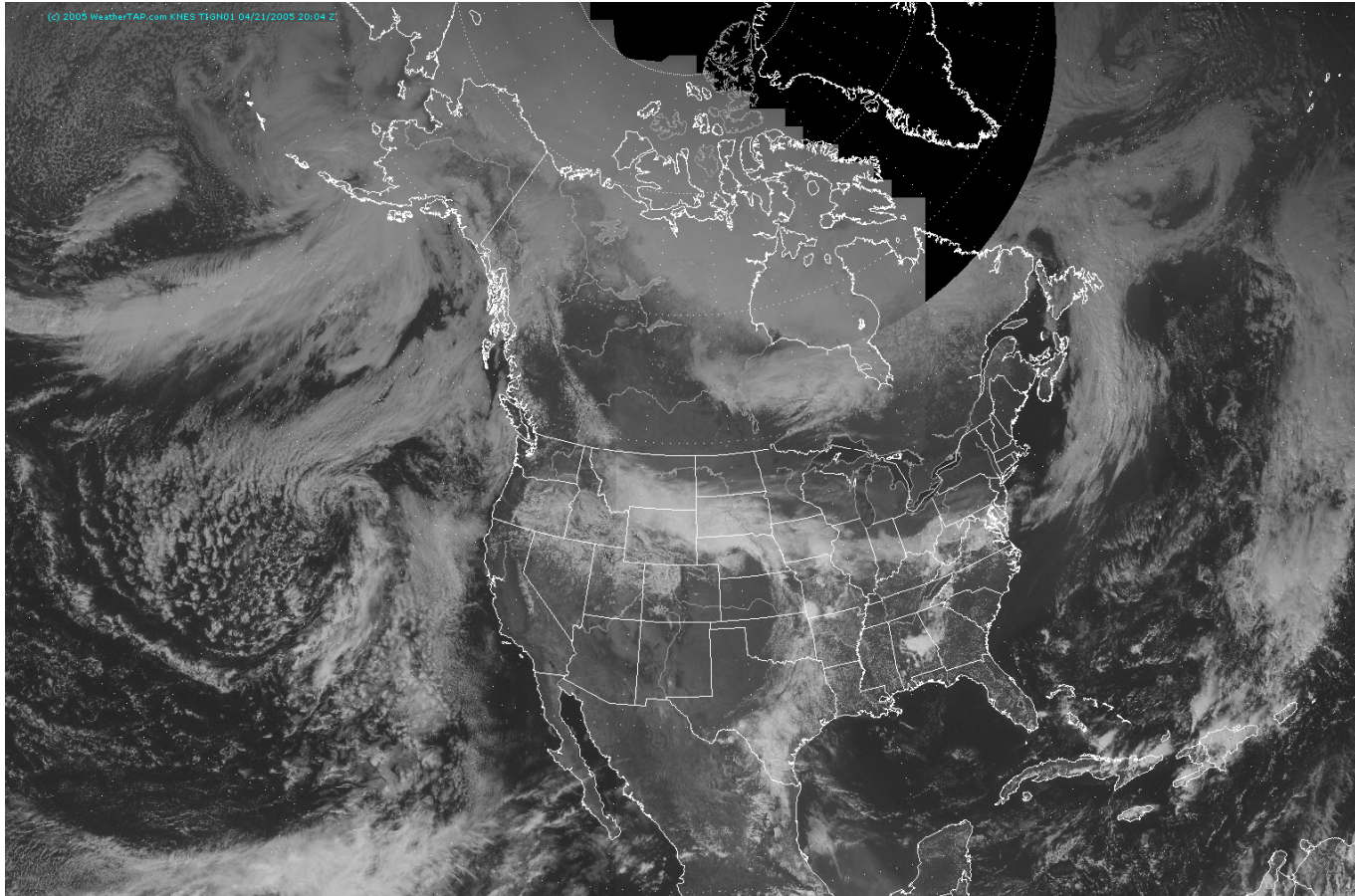


Figure 3-19: Satellite image taken April 21, 2005 at 2004Z. A low pressure area over eastern Kansas with an associated cold front stretching south into Texas and occluded front extending to coastal Virginia dominate the weather features this day.

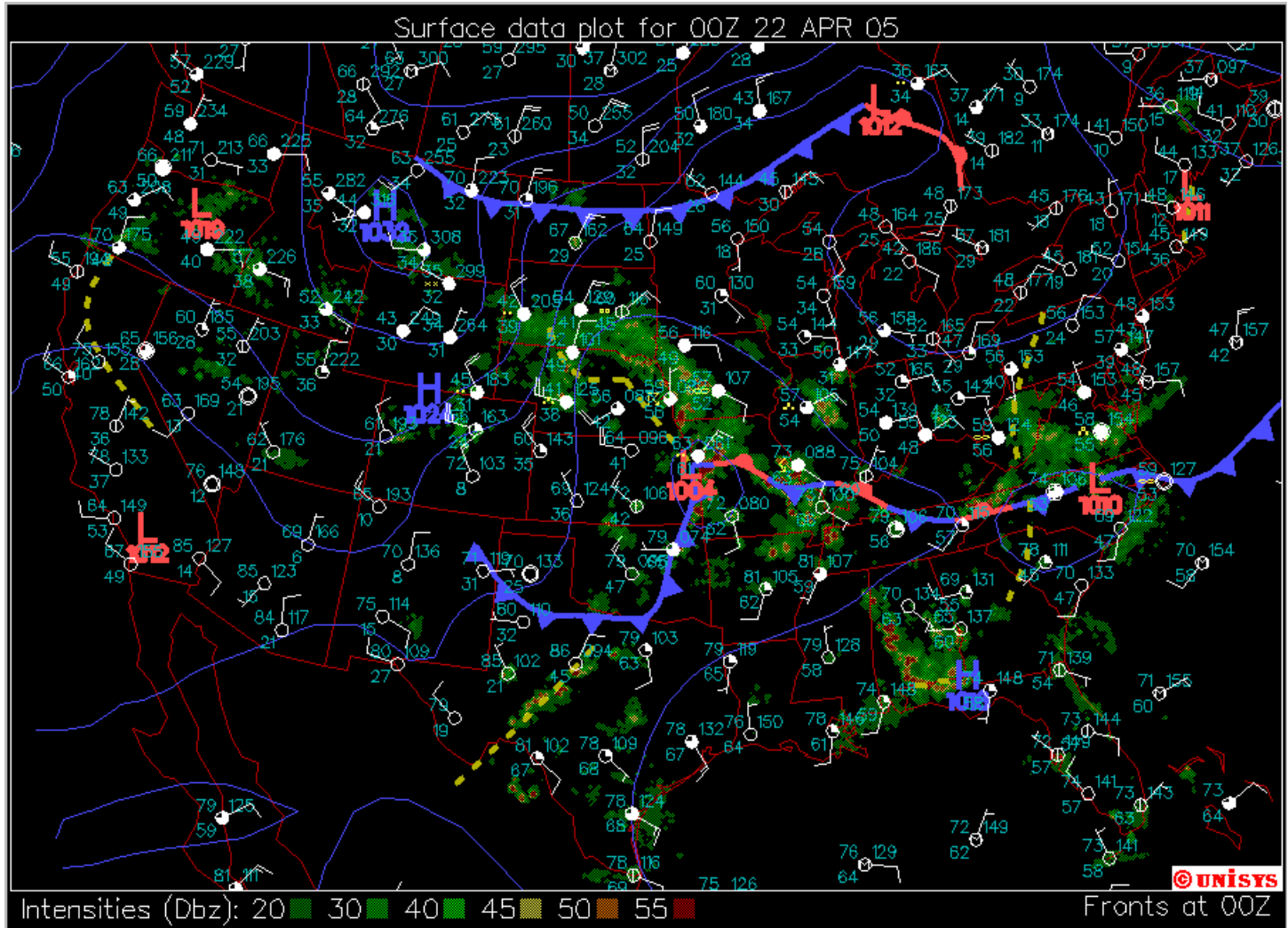


Figure 3-20: Surface map corresponding to 00z April 22, 2005 (4 hours after 20z).

The results presented here show that the current synthetic current UV Index represents well the reduction in UV radiation associated with the different areas of clouds in the country. Even the small area of clouds in the Cascade Mountains is captured by the current synthetic current UV Index. Obviously, the best results will be found in those regions where there is a high density of METAR stations.

3.4.2.2 Comparison of the UV Index Derived Using METAR-derived Clouds with the UV Index Derived Using GOES-augmented METAR Clouds

In the previous section we calculated the current UV Index using METAR cloud cover data solely from METAR stations. In this section we expand this approach to include both GOES and METAR derived cloud cover data in the calculation of the current UV Index. The GOES data comes from the GOES satellite, which provides effective cloud amount information in support of the Automated Surface Observing System (ASOS). These data is valid at the top of every hour and it is available 15 minutes after the top of the hour. Wylie and Menzel (1999) describe the technique used to derive effective cloud amount from the GOES imager which uses the CO₂ absorption technique.

It is important to keep in mind the distinction between using the GOES data set to augment sky cover reported in a METAR and using it to fill in sky cover information where none exists. The latter scenario will occur when a station fails to report any sky cover, either due to instrument failure or lack of any ceiling/visibility instrument. It is also important to keep in mind that the GOES data set and the METAR reported sky

cover do not measure the same quantity. The GOES data set is valid for middle and high levels (above 630 hPa layer) while the automated METAR sky cover is usually valid below 3658 m (12,000 feet). There are times when they overlap, such as when a METAR reports sky cover in the midlevel or above 3658 m. These overlap cases represent the biggest challenge. There are also temporal inconsistencies. Therefore, the best strategy for dealing with temporal inconsistencies between METAR and GOES may be to use a conservative approach – only incorporate GOES when it is certain that it will enhance an automated METAR and will not "overrule" a legitimate METAR-reported sky cover.

Two separate algorithms are developed and used to augment the METAR cloud cover depending on whether a station reports clouds or if it is manned or automatic. Stations in the “no sky cover” list are modified according to the following algorithm: (1) determine the exact time of the METAR observation; (2) determine whether a GOES satellite observation exists for the station within a fixed time (temporal consistency check); (3) if a GOES observation exists, and it reports high or mid level cloud coverage at BKN or higher, then populate the sky cover field for that station and that hour. Automated stations that report sky cover and do not fall into either the “24 hour manned” list or the “no sky cover” list are modified in the following manner: (1) determine the exact time of the METAR observation; (2) determine whether a GOES satellite observation exists for the station within a fixed time (temporal consistency check); (3) if a GOES observation exists check the sky cover of the METAR observation; (4) if METAR = (SKC || CAVOK || CLR || MISSING) then replace the METAR-based sky cover with the GOES sky cover only if the GOES reports at least SCT coverage at some

level; (5) otherwise, if the METAR reports some cloud layers, augment the report by adding additional GOES high or mid level cloud information, where available. Essentially this means that we never drop valid METAR cloud layers, only add to them where the GOES provides extra information. Once the augmentation process is complete at all METAR locations the cloud cover data is expanded to nearly 10,000 cities across the United States using a proprietary system of the Weather Channel similar to the Real Time and Retrospective Mesoscale Objective Analysis which originated in the National Weather Service to develop a process to produce real-time, National Digital Forecast Database (NDFD) matching resolution analyses, which has begun to be referred to as an "Analysis Of Record" (AOR). In this paper we use the initial conditions ($t=0$) of our system to derive current cloud cover reports at 10,000 locations across the United States. The details of this system and its performance are described by Neilley and Rose (2006) and Koval et al (2006).

The GOES augmented cloud cover is able to detect clouds that the ASOS network cannot detect. Figures 3-21 and 3-22 show the METAR and GOES-augmented METAR clouds, respectively, for the continental United States for 2000z April 28, 2005. Figures 3-23 and 3-24 show the satellite images from the GOES east and west satellites at 2015 and 2000z, respectively. For example, areas of western and central North Carolina and northwestern South Carolina are covered by cirrus and altostratus clouds (Figure 3-25) that are depicted as partly cloudy or clear by the automated METAR reports. ASOS stations report anywhere between 0-30% cloud cover in these areas. However, manned METAR stations report cloud cover amounts greater than 60% in the same areas. KFBG (Fort Bragg) in central-eastern North Carolina or KATL (Atlanta, Georgia) show as dark

red dots surrounded by yellow or blue dots in Figure 3-21 to 3-22. The same effect can be seen in other areas where manned METAR stations are surrounded by ASOS stations. KLBB (Lubbock), KSAT (San Antonio) and KIAH (Houston) in Texas are manned METAR stations capable of reporting cloud cover above 3658 m. The high cirrus clouds that stretch over

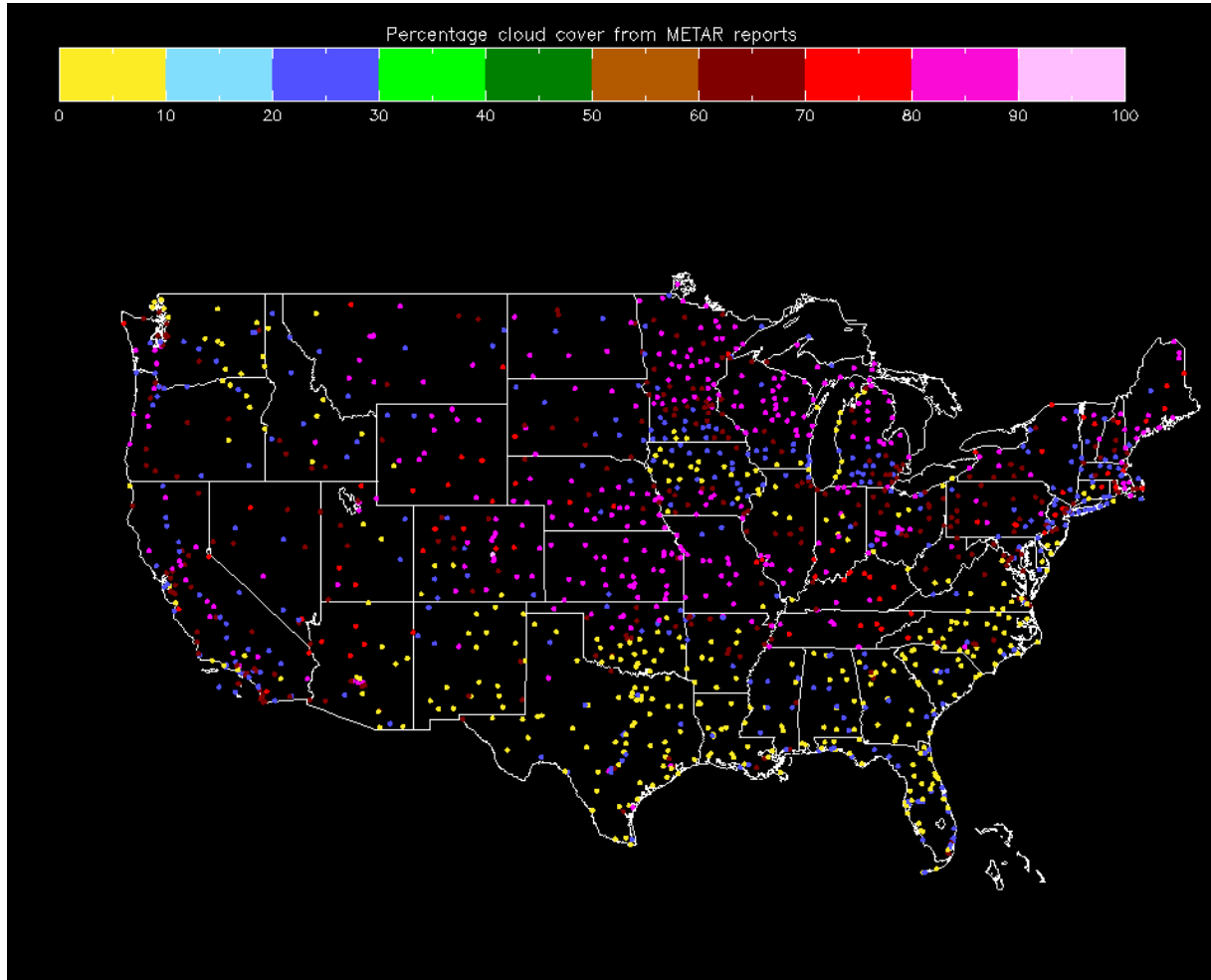


Figure 3-21: Observed percentage cloud cover as reported from the surface METAR stations from 1272 locations across the United States for April, 28, 2005 (1950Z-1958Z).

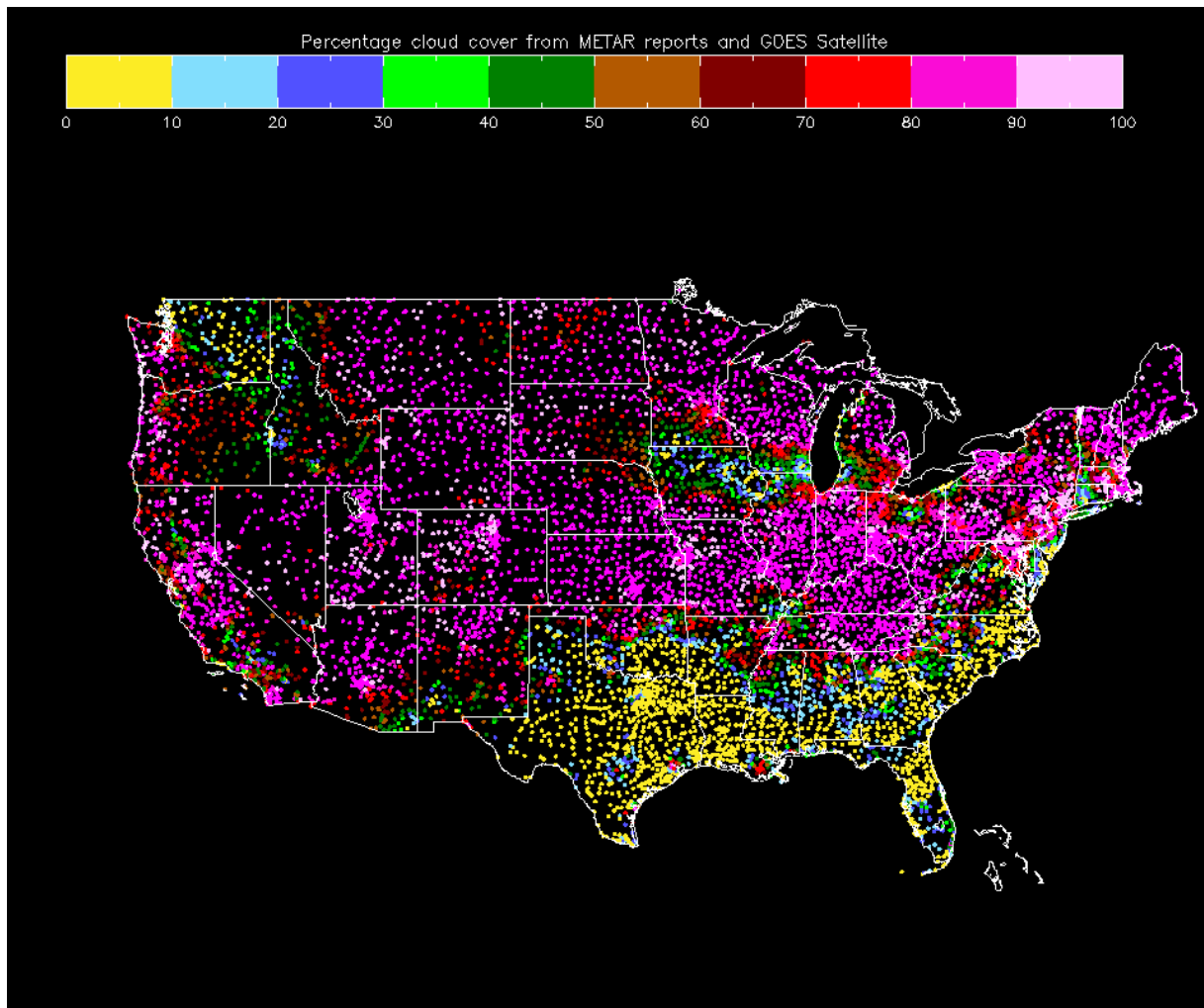


Figure 3-22: Observed percentage cloud cover from GOES augmented METAR stations expanded to nearly 10,000 locations across the United States for April, 28, 2005 (1950Z-1958Z).

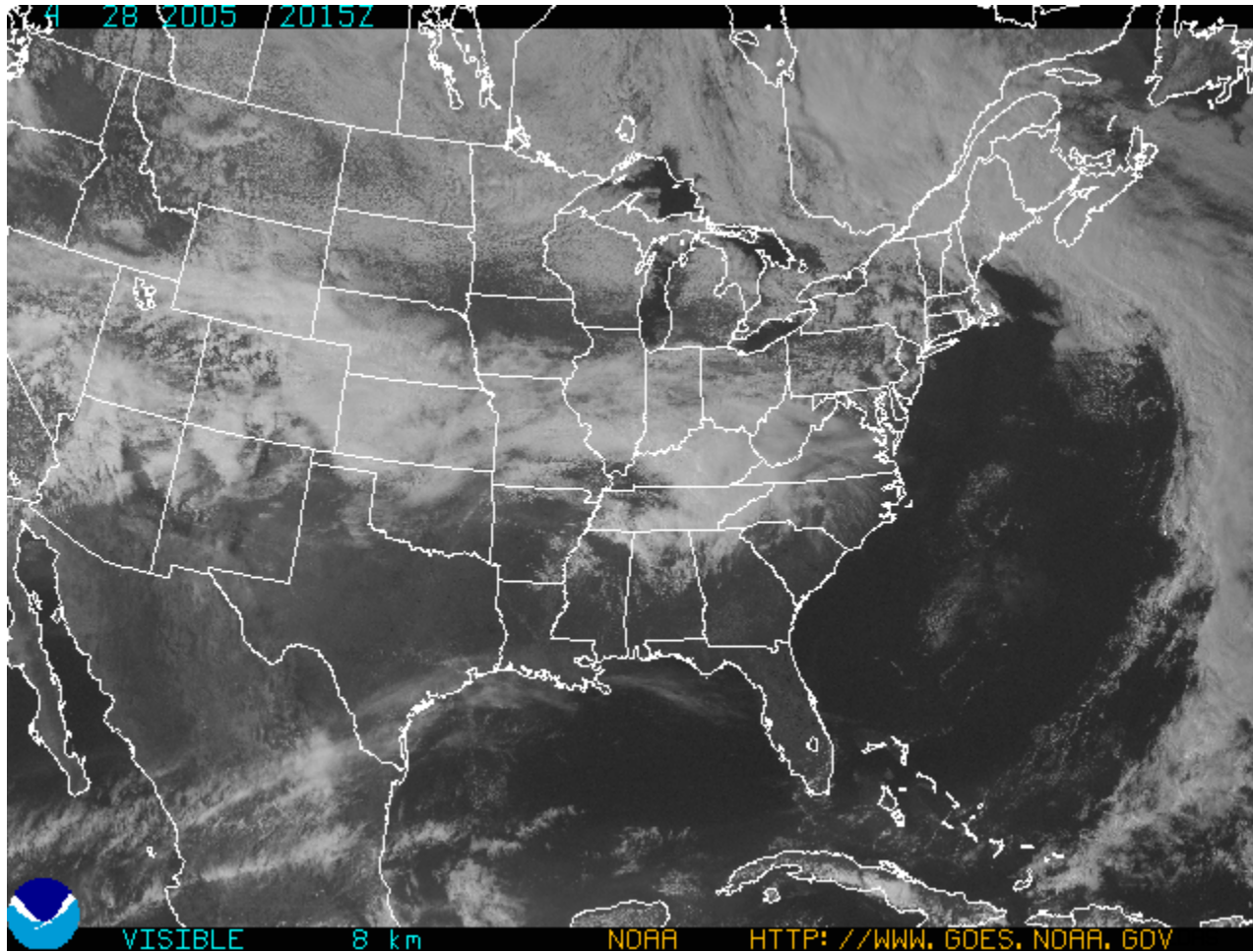


Figure 3-23: GOES east satellite image corresponding to April 28, 2005 (2015Z).

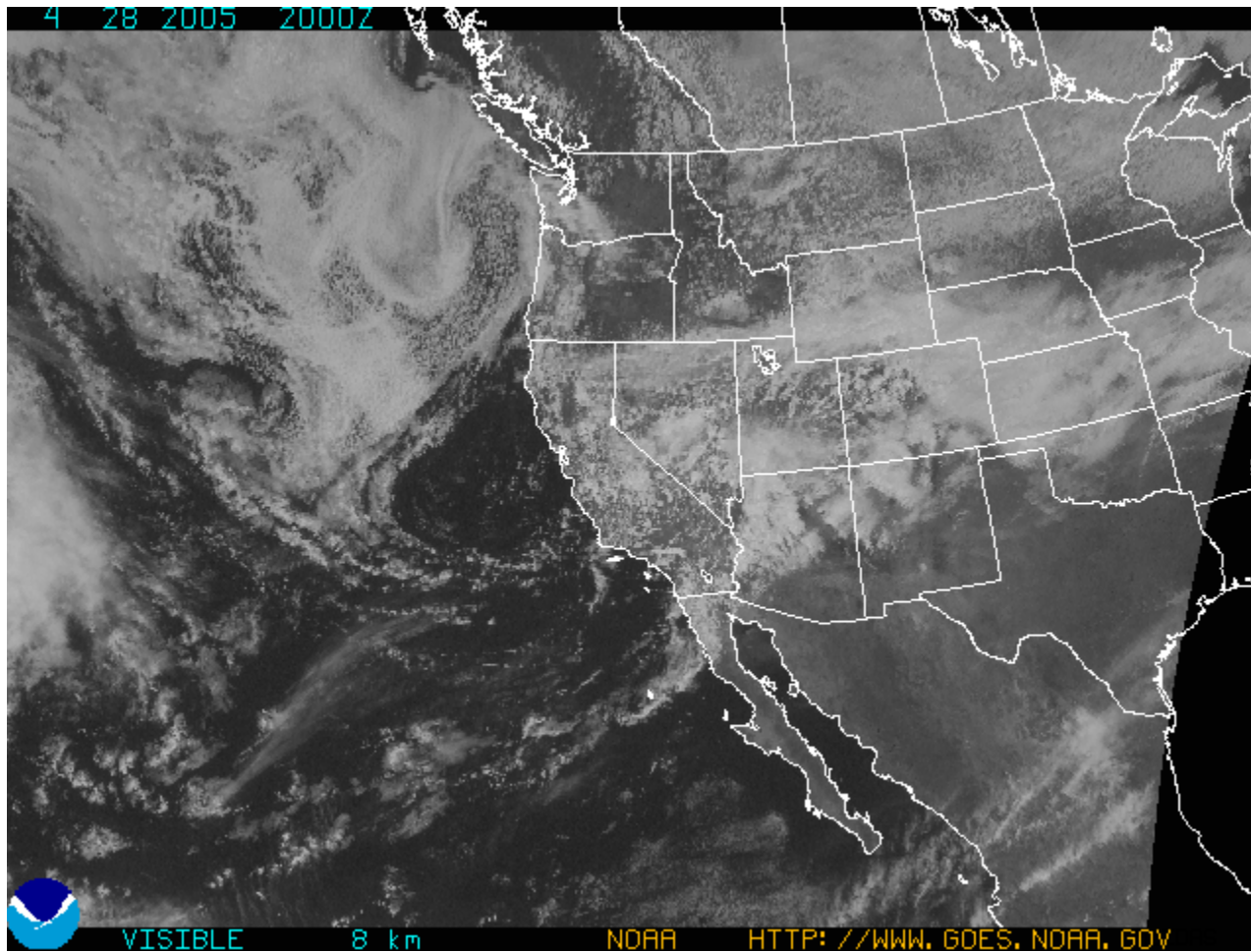


Figure 3-24: GOES west satellite image corresponding to April 28, 2005 (2000Z).

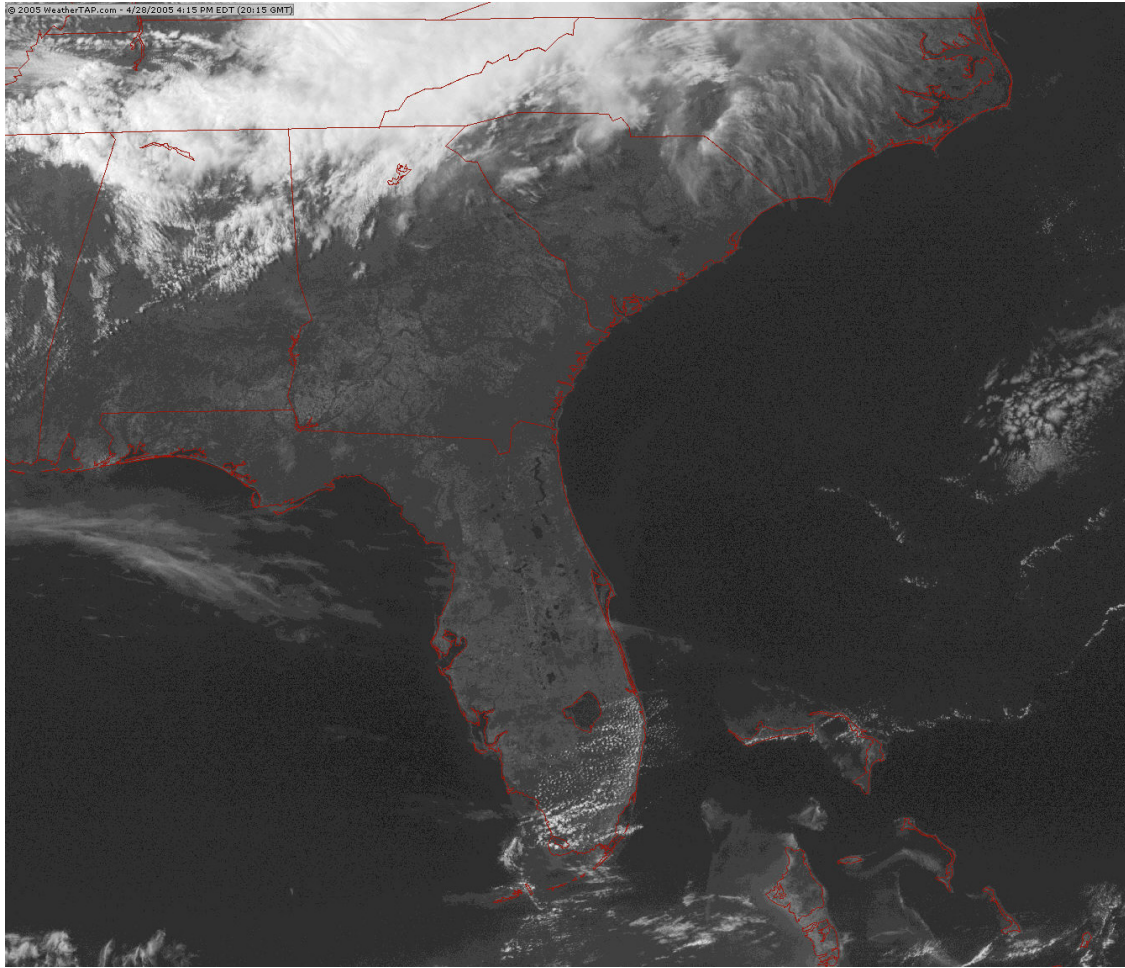


Figure 3-25: GOES east satellite image corresponding to April 28, 2005 (2015Z).

south Texas (Figure 3-23) cannot be detected by the surrounding ASOS stations. The GOES augmented cloud cover captures well the high clouds in central North Carolina and northwestern South Carolina as well as other surrounding regions. The gap in clouds that extends over northern Illinois and Indiana (Figure 3-23) is well captured by the METAR and the GOES augmented data.

Figures 3-26 (METAR only) and 3-27 (GOES augmented) show the calculated current UV Index for 20z for the sky conditions reported at the same hour. The clear sky UV Index (calculated with no clouds) is shown in Figures 3-28 (METAR site list only) and 3-29 (GOES augmented site list). The largest differences (6-7 UV Index units) between the clear sky UV Index and the one calculated for the reported sky conditions are found over northern New Mexico, the northern two thirds of Arizona and from eastern Kansas to California associated with an area of low pressure and precipitation in these states (Figures 3-30 to 3-31). The differences are largest for the GOES augmented data, especially over Arizona where more convective clouds triggered thunderstorms. The breaks in clouds over Massachusetts, northern Illinois, or southeastern Minnesota (Figure 3-23) or in eastern Washington (Figure 3-24) are well captured as yellow or light blue dots in the UV difference map (Figure 3-31).

In general, the GOES augmented cloud cover provides more accurate cloud observations in areas where high clouds cannot be detected by ASOS stations. This yields more representative UV Index values, especially in areas where opaque altostratus or altocumulus clouds are present. Thin cirrus clouds have a small effect in the

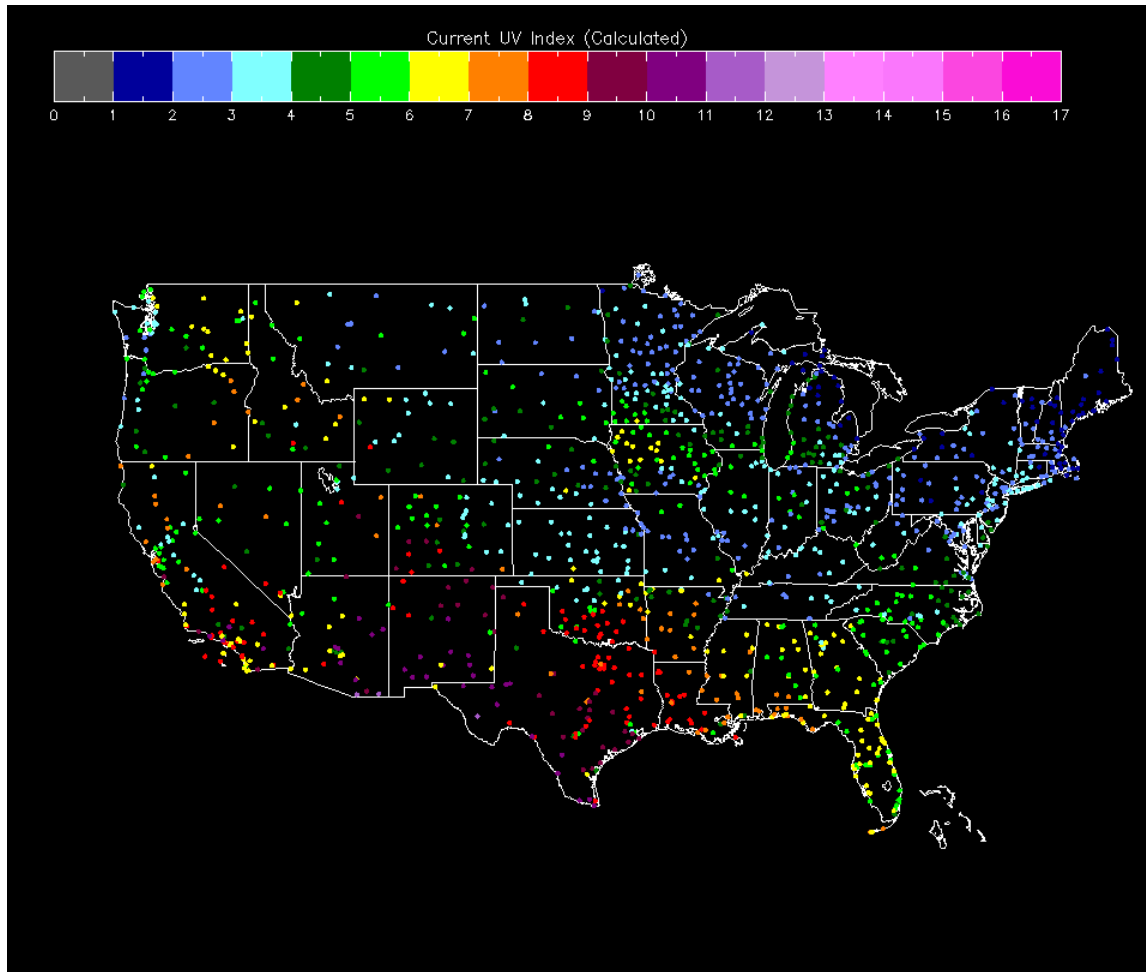


Figure 3-26: Simulation of the synthetic UV Index for April, 28, 2005 (1950Z-1958Z). The calculation corresponds to synthetic UV Index that would have been measured considering the effects of clouds.

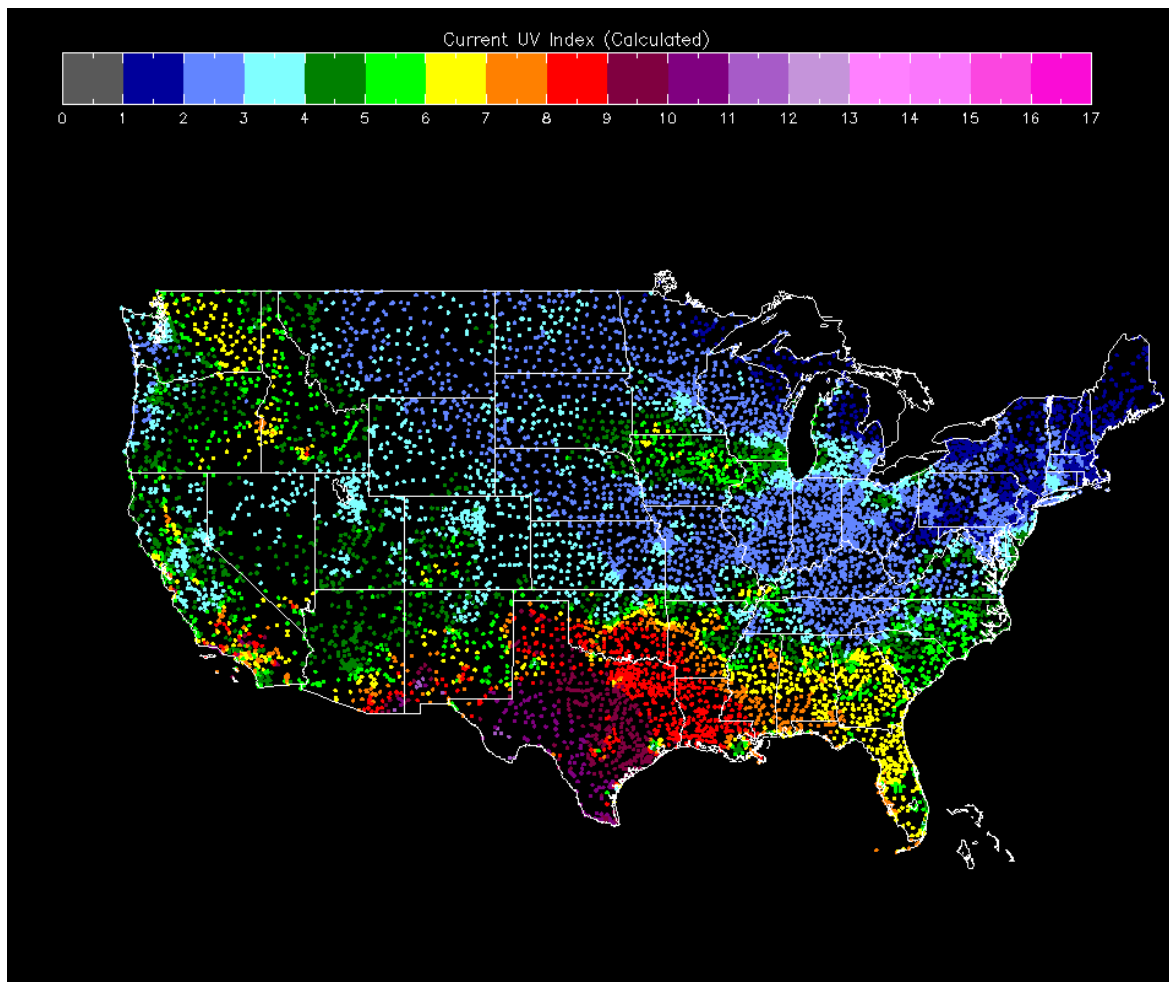


Figure 3-27: Simulation of the synthetic UV Index for April, 28, 2005 (1950Z-1958Z). The calculation corresponds to synthetic UV Index that would have been measured considering the effects of clouds. The calculation is expanded to all 9,500 points.

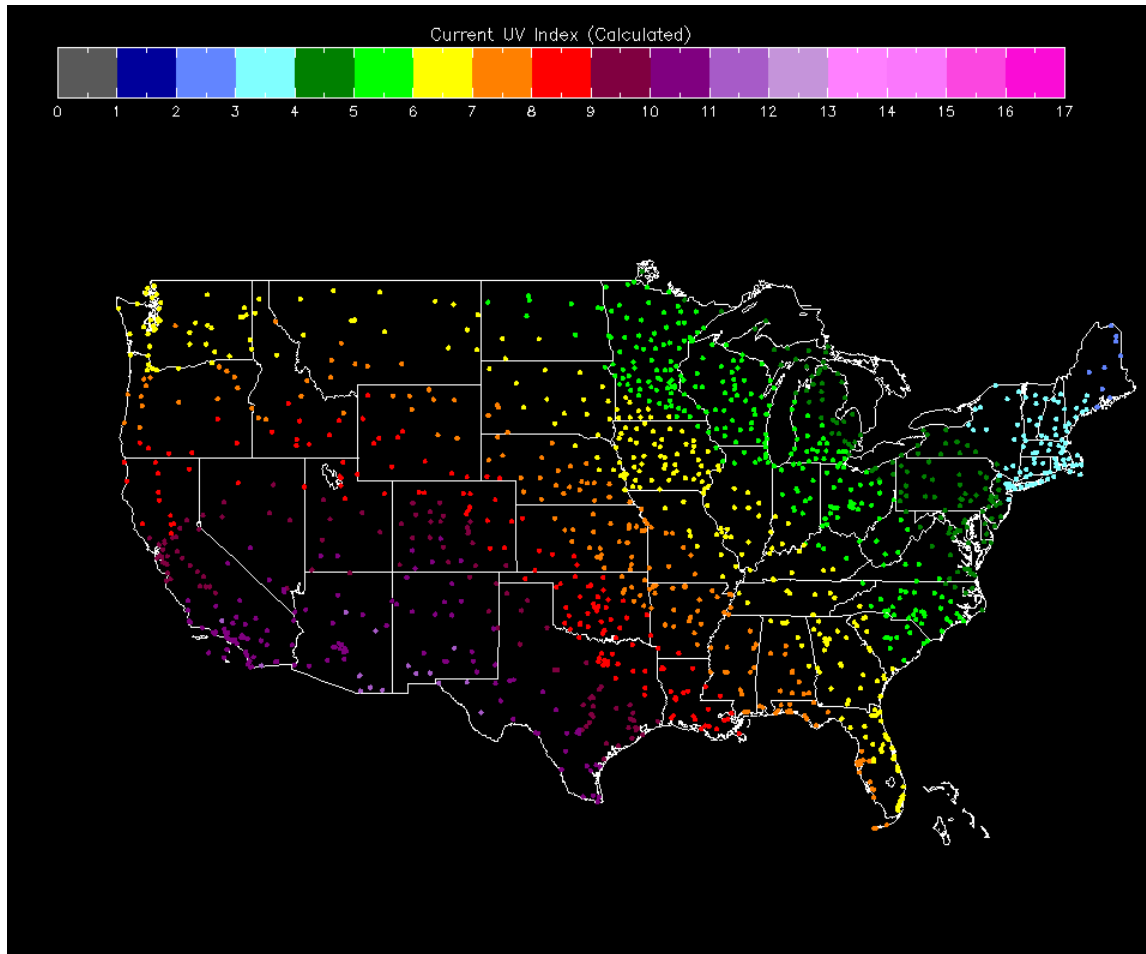


Figure 3-28: Simulation of the synthetic UV Index for April 28, 2005 (1950Z-1958Z). The calculation corresponds to the maximum clear sky UV Index that would have been measured without the presence of clouds.

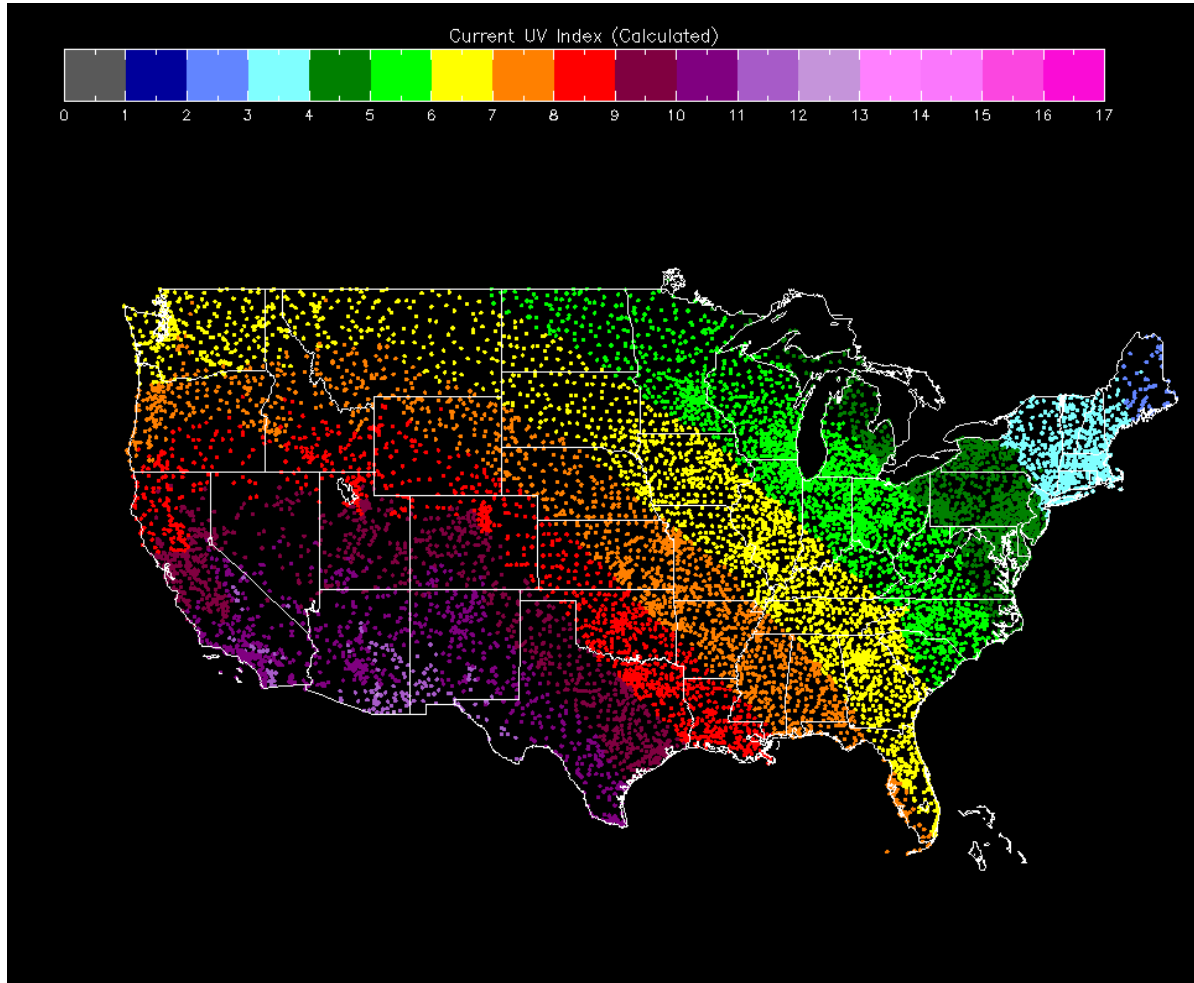


Figure 3-29: Simulation of the synthetic UV Index for April 28, 2005 (1950Z-1958Z). The calculation corresponds to the maximum clear sky UV Index that would have been measured without the presence of clouds. The calculation is expanded to all 9,500 points.

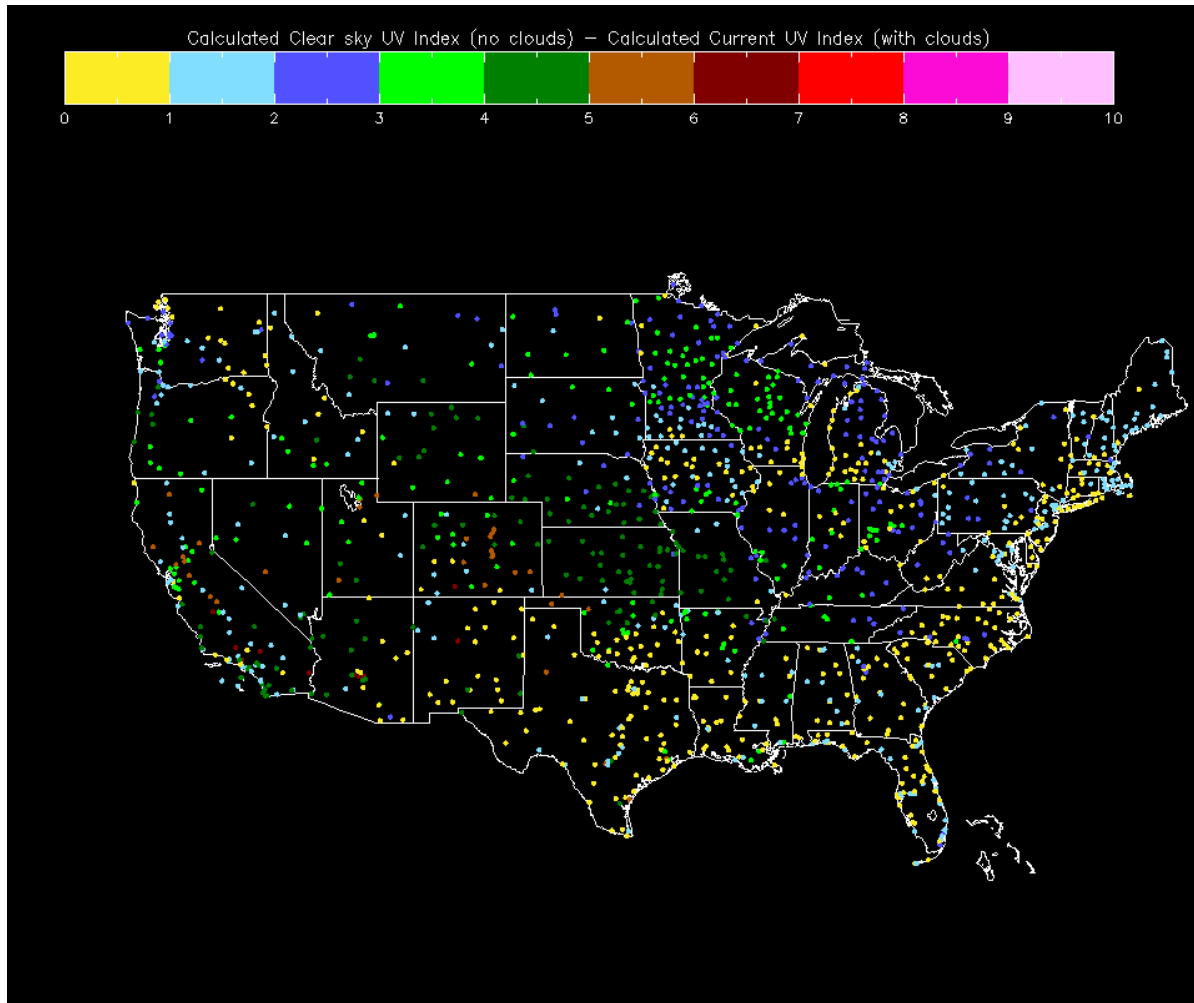


Figure 3-30: UV Index reduction due to clouds (Clear sky UV Index – UV Index considering clouds) for April, 28, 2005 from 1950Z to 1958Z

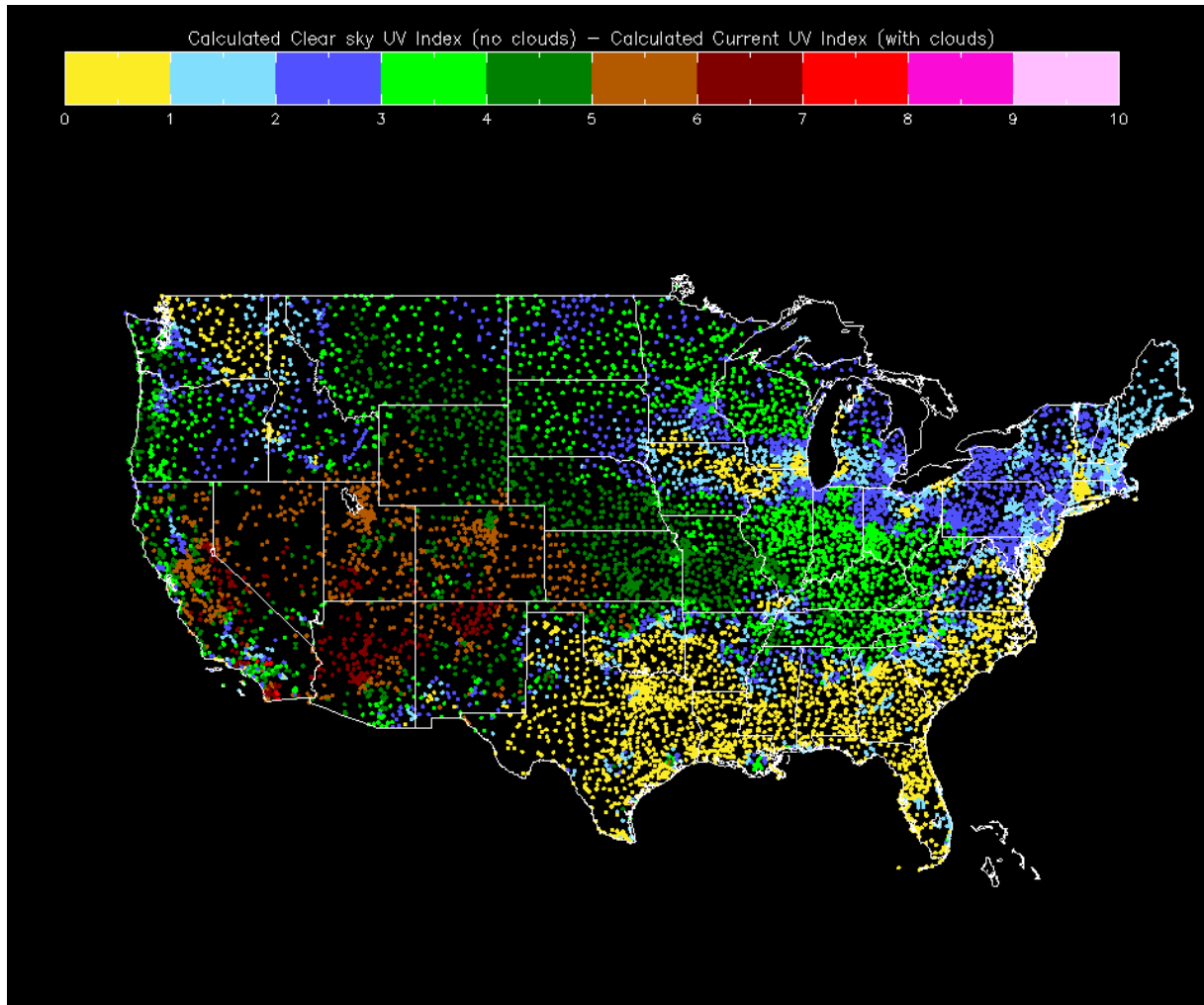


Figure 3-31: UV Index reduction due to clouds (Clear sky UV Index – UV Index considering clouds) for April, 28, 2005 from 1950Z to 1958Z. The calculation is expanded to all 9,500 points.

attenuation of surface UV radiation and if the sky is not fully covered by these clouds their effects are minimal and transient. The verification results presented in section 4.1 were recalculated to include the effects of GOES enhanced METAR cloud cover for the 13 stations verified between July 25, 2004 and August 25, 2004. The results are almost identical probably due to the fact that a small amount of cases correspond to situations where high level cloud attenuated a considerable portion of the UV radiation during this time period.

3.5 Conclusions

A new synthetic current UV Index is calculated which expands by a factor greater than 200 the number of current UV Index reports that can be distributed to the public in the United States. Right now, current UV Index values are limited to specific UV measuring sites, constrained by the difficulties of maintaining accurate calibration within the network of UV instruments. Reports of cloud cover from surface METAR stations and/or GOES augmented METAR data are used as an input variable in the calculation of the current UV Index. The following are the main conclusions.

A verification of this synthetic current UV Index is done at 13 USDA UV measuring sites using cloud cover reports from collocated METAR stations. In 50% of these cases, the synthetic current UV Index is identical to the observed UV Index. In 67% of the cases the synthetic current UV Index shows a difference of +/- 1 UV Index unit from the measured UV Index. In 83% of the cases the synthetic current UV Index is within +/- 2 UV Index units of the measured index. These results are compared against the verification results corresponding to tomorrow's UV forecast provided by NOAA

(Long et al, 1996). The forecast UV Index verification shows that in 32% of the cases the synthetic current UV Index is identical to the observed UV Index. In 76% of the cases the synthetic current UV Index shows a difference of +/- 1 UV Index unit from the measured UV Index. In 92% of the cases the synthetic current UV Index is within +/- 2 UV Index units of the measured index. The differences are probably explained by more errors in the cloud forecasts compared with cloud observations. Uncertainties in the total column ozone forecasts can also account for a smaller portion of the differences.

An empirical relationship is derived which accounts for the effects of clouds on UV transmission based on surface METAR observations from 13 different locations for a full month. The results of this empirical relationship compare well with other linear empirical relationships derived in other studies (e.g. Ilyas, 1987 and Cutchis, 1980). The measured UV Index from the 13 USDA locations is also verified against the calculated UV Index values using the cloud-UV relationships obtained by Ilyas (1987), Cutchis (1980), Josefsson (1986), and Bais et al. (1993). The fact that there is very little difference between the results of the verification of the UV Index values calculated using equation 1 and the results obtained using the cloud-UV relationships obtained by Ilyas (1987) and Cutchis (1980) confirms that the average effects of clouds on UV radiation can be represented well using the linear relationship derived in this study.

The synthetic current UV Index is calculated for actual sky conditions for 1200+ METAR locations in the continental United States. The results of the current UV Index capture well the cloud features that were reported at the time of the simulations. The synthetic current UV Index is also calculated using GOES augmented METAR data and compared with the results obtained using METAR-only cloud data. The GOES

augmented cloud cover provides a better representation of the current UV Index ahead of large scale weather systems with opaque high and mid level clouds as indicated by comparison with satellite images during a case study.

In addition, the synthetic current UV Index is calculated using an algorithm capable of interpolating/spreading cloud cover information from the GOES augmented METAR cloud data to almost 10,000 locations (or cities) across the United States. The resulting current UV Index depicts very well the effect of clouds at a very high resolution. This allows us to distribute Current UV Index values for about 10,000 cities in the country.

CHAPTER IV

SUMMARY OF FINDINGS

Chapter I

The extinction of solar radiation by atmospheric aerosols influences the Ultraviolet (UV) flux at the surface, which in turn has implications on both human and environmental health. In this study we present measurements of aerosol optical depth ($\tau_{a,\lambda}$) spectral dependence in the (UV) (317-368 nm) from a USDA UV-Multi-Filter Rotating Shadow band Radiometer (UV-MFRSR) and an EPA Brewer spectrophotometer (320-360 nm) collocated at Boulder, Colorado. The purpose of this study is to measure the spectral attenuation of radiation in the UV by comparing measurements of different wavelengths from two spectral UV instruments. The instruments are in close agreement with the square of the correlation coefficients between the two instruments of 0.92 for the 317-320 nm wavelength pair, 0.86 for the 332-340 nm wavelength pair, and 0.94 for the 368-360 nm wavelength pair (first wavelength of each pair represents the UV-MFRSR, while the second represents the Brewer). The ratio of the UV-MFRSR to Brewer τ_a for all wavelengths is $1.0242 \pm (0.17 \text{ standard deviation})$. The hourly-averaged τ_a , range from 0.07 to 0.51 at 317 nm for the UV-MFRSR and from 0.07 to 0.47 at 320 nm for the Brewer; from 0.09 to 0.52 at 332 nm for the UV-MFRSR and from 0.09 to 0.45 at 340 nm for the Brewer; and from 0.08 to 0.48 at 368 nm for the UV-MFRSR and from 0.07 to 0.45 at 360 nm for the Brewer. Hourly mean Ångström exponents were calculated to be $0.82 \pm (0.11 \text{ measurement uncertainty})$ for the UV-MFRSR and $0.84 \pm (0.165 \text{ measurement uncertainty})$ for the Brewer. The Ångström exponents ranged from -0.49 to 2.36 for the UV-MFRSR and from 0.15 to 2.24 for the Brewer. The observed

wavelength dependence of $\tau_{a,\lambda}$ is explained based on reasonable assumptions for the size distribution and optical properties of the aerosol particles using Mie theory. The measurements presented in this study are for seven days and thus not meaningful statistically in a monthly, seasonal or yearly climatological sense.

Chapter II

Investigation of the effects of aerosols on the surface UV irradiance were conducted as part of the Atlanta Supersite experiment during August, 1999. The aerosol optical depth at UV wavelengths, and the single scattering albedo, which provides information about the relative absorbing properties of the aerosols, are both important factors in determining surface UV irradiance. In order to estimate these parameters measurements of direct and global (direct + diffuse) UV radiation and total column ozone (O_3) were made using a Brewer spectroradiometer under cloud-free conditions. Aerosol optical depths (τ_a) in the UV were retrieved at 320, 340, and 360 nm. Daily averages of $\tau(340 \text{ nm})$ range from 0.23 and 2.09 with a mean and standard deviation of 0.93 ± 0.51 . The daily average spectral dependence of the aerosol optical depth, calculated via the Angström exponent (α), ranges from 0.80 and 1.92 with a mean and standard deviation of 1.44 ± 0.32 . No apparent relationship was found between τ_a and α . The retrieved values of τ_a and α were used in the Tropospheric Ultraviolet and Visible (TUV) radiation model to estimate the surface UV irradiance. Estimates of aerosol single scattering albedo (ω_o) were made by matching the measured irradiance values to model computed irradiances. The results suggest an increasing trend in ω_o with increases in τ_a . The estimated ω_o ranges from 0.80 and 0.99 with a mean and standard deviation of 0.87 ± 0.08 . Variability in τ_a

and ω_0 during the measurement period are capable of changing the UV Index up to 2 UV Index units when all other effects are kept constant. The values of τ_a and α are compared with the ones obtained at a nearby rural location in Griffin, GA located 47 miles south of Atlanta using a UV-MFRSR from the US Department of Agriculture. At Griffin, daily averages of $\tau(332 \text{ nm})$ range between 0.43 and 1.53 with a mean and standard deviation of 0.94 ± 0.34 . For α the daily averages range between 0.88 and 1.97 with a mean and standard deviation of 1.33 ± 0.33 . These results indicate that on average the values of τ_a and α are similar between Griffin and Atlanta. Differences in the day-to-day estimates of τ_a and α between Atlanta and Griffin indicate that there is some regional influence of aerosols on UV irradiance, and hence UV index in the South Eastern United States during the period of the measurements.

Chapter III

A new synthetic current UV Index is calculated which expands by a factor greater than 30 the number of current UV Index reports that can be distributed to the public in the United States. Right now, current UV Index values are limited to specific UV measuring sites, constrained by the difficulties of maintaining accurate calibration within the network of UV instruments. Reports of cloud cover from surface METAR stations and/or GOES augmented METAR data are used as an input variable in the calculation of the current UV Index.

A verification of this synthetic current UV Index is done at 13 USDA UV measuring sites using cloud cover reports from collocated METAR stations. In 50% of these cases, the synthetic current UV Index is identical to the observed UV Index. In

67% of the cases the synthetic current UV Index shows a difference of +/- 1 UV Index unit from the measured UV Index. In 83% of the cases the synthetic current UV Index is within +/- 2 UV Index units of the measured index. These results are compared against the verification results corresponding to tomorrow's UV forecast provided by NOAA (Long et al, 1996). The forecast UV Index verification shows that in 32% of the cases the synthetic current UV Index is identical to the observed UV Index. In 76% of the cases the synthetic current UV Index shows a difference of +/- 1 UV Index unit from the measured UV Index. In 92% of the cases the synthetic current UV Index is within +/- 2 UV Index units of the measured index. The differences are probably explained by more errors in the cloud forecasts compared with cloud observations. Uncertainties in the total column ozone forecasts can also account for a smaller portion of the differences.

An empirical relationship is derived which accounts for the effects of clouds on UV transmission based on surface METAR observations from 13 different locations for a full month. The results of this empirical relationship compare well with other linear empirical relationships derived in other studies (e.g. Ilyas, 1987 and Cutchis, 1980). The measured UV Index from the 13 USDA locations is also verified against the calculated UV Index values using the cloud-UV relationships obtained by Ilyas (1987), Cutchis (1980), Josefsson (1986), and Bais et al. (1993). The fact that there is very little difference between the results of the verification of the UV Index values calculated using equation 1 and the results obtained using the cloud-UV relationships obtained by Ilyas (1987) and Cutchis (1980) confirms that the average effects of clouds on UV radiation can be represented well using the linear relationship derived in this study.

The synthetic current UV Index is calculated for actual sky conditions for 1200+ METAR locations in the continental United States. The results of the current UV Index capture well the cloud features that were reported at the time of the simulations. The synthetic current UV Index is also calculated using GOES augmented METAR data and compared with the results obtained using METAR-only cloud data. The GOES augmented cloud cover provides a better representation of the current UV Index ahead of large scale weather systems with opaque high and mid level clouds as indicated by comparison with satellite images during a case study.

In addition, the synthetic current UV Index is calculated using an algorithm capable of interpolating/spreading cloud cover information from the GOES augmented METAR cloud data to almost 10,000 points across the United States. The resulting current UV Index depicts very well the effect of clouds at a very high resolution. This allows us to distribute Current UV Index values for about 10,000 cities in the country.

CHAPTER V

RECOMMENDATIONS FOR FUTURE WORK

Aerosols are highly variable over space and time. Aerosols attenuate UV radiation due to scattering and absorption of radiation. The aerosol optical depth and the average column value of the single scattering albedo are the two most important parameters responsible for the attenuation of UV radiation by aerosols. However, these two parameters vary considerably in space and time making their effects different from place to place. Following the results obtained from our study and the results found in the literature more research is needed in the following areas:

Aerosol Optical Depth in the UV

Different studies have shown that long-term UV changes are not driven by ozone alone, but also by changes in cloudiness, aerosols, and surface albedo (Dickerson et al, 1997; Kylling et al. 1998; Krzyścin et al., 1998; Sabziparvar et al., 1998; Zerefos et al., 1998; Gröbner et al., 2001). This implies that long-term UV-aerosol experiments are needed to gain a better understanding of the variability of the effects of aerosols on UV radiation. In addition, comparisons of satellite estimates of surface UV radiation with ground-based measurements show better agreement at the cleaner sites (Mckenzie et al. 2001a; Fioletov et al., 2002), which suggests that the differences are due to aerosols and pollution near the ground. The total reduction of UV radiation due to atmospheric aerosols also varies considerably from study to study. Large reductions in UV-B radiation has been reported under biomass burning aerosols. Jacobson (2001) reported that

anthropogenic aerosols that absorb in the UV region may play a more important role in attenuating UV irradiances than has been thought previously. In this context it is necessary to conduct more localized UV-aerosol experiments since local conditions play an important role in the amount of UV radiation that gets to the earth's surface.

Wavelength Dependence of the Aerosol Optical Depth (Angström exponent) and Single Scattering Albedo in the UV

The UV literature and the results presented in this study report a range of values for the spectral dependence of the aerosol optical depth (Borghesi et al. 1982; Marengo et al. 1997; Kylling et al. 1998, Wenny et al. 2001) and the single scattering albedo (Kouvarakis et al. 2002; Krotkov et al. 2005). The standard deviation of the spectral dependence of the aerosol optical depth (Angström exponent) also shows significant variations from experiment to experiment. Most studies agree that the aerosol optical depth in the UV is shown to be approximately inversely proportional to wavelength (i.e. $\alpha = 1.0$); however, more measurements are needed to determine which are the conditions that yield to the observed deviations from the average measured value of $\alpha = 1.0$.

The relationship between the single scattering albedo and the aerosol optical depth seems to be positive based from the UV measurements taken in August 1999 in Atlanta, GA. In addition to the results presented in this study Carrico et al. (2003) also found that the single scattering albedo at 550 nm decreased during rain events in Atlanta during August 1999. However, it is not clear if this phenomenon is observed at all locations. Eck et al. (2003) report no correlation between the aerosol optical depth at and the single scattering albedo from 440 to 1020 nm in the southern African region during

August and September 2000. In another southern African site Eck et al. (2003) found a small correlation between the single scattering albedo and the aerosol optical depth at 500 nm. More research is needed in order to determine the factors responsible for the relationship between the single scattering albedo and the aerosol load in the atmosphere in the UV.

The relationship between the spectral dependence of the aerosol optical depth and the aerosol optical depth has been more widely investigated in the visible region of the spectrum. Some studies report an inverse relationship between the spectral dependence of the aerosol optical depth and the aerosol optical depth which suggests that aerosol growth tends to be a dominant factor attenuating the radiation (Holben et al. 1991a). Other studies report no correlation between the aerosol optical depth and the spectral dependence of the aerosol optical depth (Holben et al., 1991b; Sung-Nam OH, 2004). However, the geographical and seasonal distribution of the relationship between these two parameters in the UV is not known. The results presented in this study show strong day-to-day variability between the spectral dependence of the aerosol optical depth and the aerosol optical depth. The variation in the spectral dependence of the aerosol optical depth is due to changing aerosol properties caused by changes in aerosol composition and size distribution. More co-located experiments are needed to develop a climatology of the spectral dependence of the aerosol optical depth in the UV at different locations.

In summary, more localized experiments need to be conducted measuring aerosol optical depths in the UV at different wavelengths, preferably using co-located instruments, in order to gain a better understanding of the geographical and seasonal

variations of the spectral dependence and single scattering albedo of the atmospheric aerosols.

UV Index

Since the early 90's scientists have been able to increase worldwide the public's awareness about the harmful effects of the solar UV rays (WMO, 1995). We can now take precautions to protect ourselves from harmful UV radiation using the forecast UV Index. Simple activities, such as standing in the shade, wearing protective clothing, applying sunscreen and visiting a doctor if we suspect skin cancer, are positive steps that the general public can now follow to protect from the harmful effects of the sun.

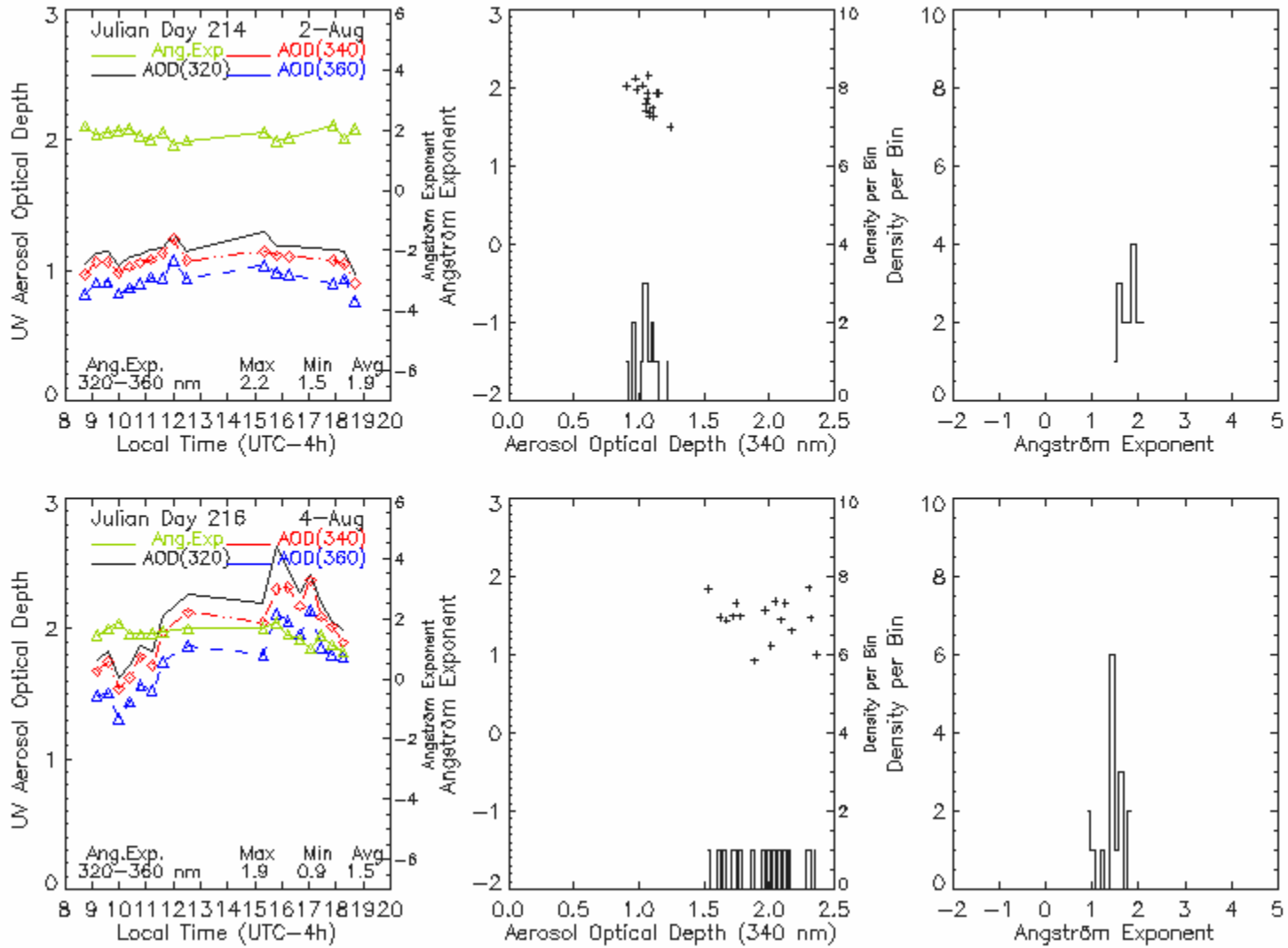
Future work related to the UV Index should focus on the operational aspects of the problem, distributing UV Index forecasts and current conditions to many more points across the world. The distribution of UV Index values to more cities will increase the public's awareness of the harmful effects of the sun. Being aware of the forecast or current UV Index values at your own city or town will provide the media with the opportunity to distribute these values locally which will increase the public's awareness of the harmful effects of the sun in your local area. The work presented in chapter III of this dissertation provides a groundbreaking advance in the synthesis of current UV Index information, providing current UV Index values at a very high resolution for the continental United States. Future advances of this research should focus on increasing the accuracy of the current UV Index using total column ozone values which are more recent to the latest synthesized UV Index values. In addition, more analysis should be conducted to be able to consider the most recent aerosol conditions at each distribution point. This

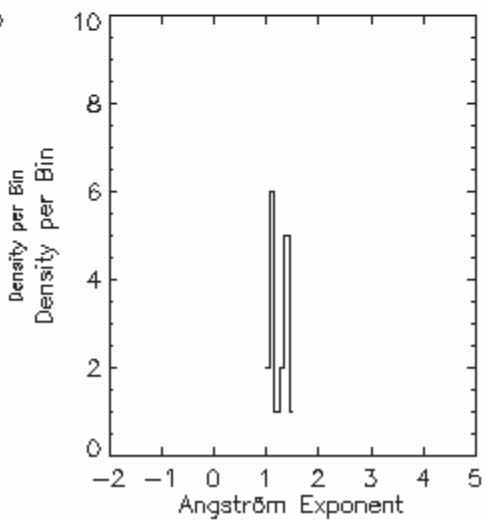
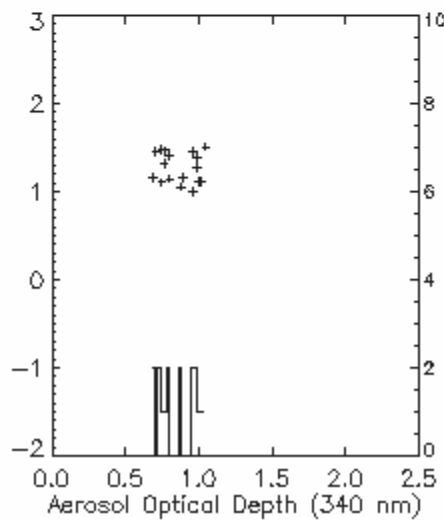
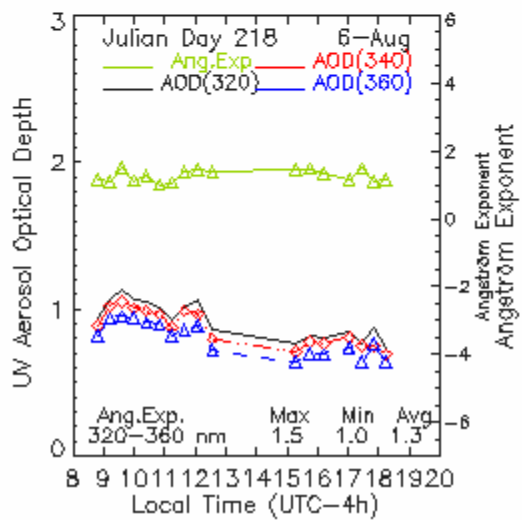
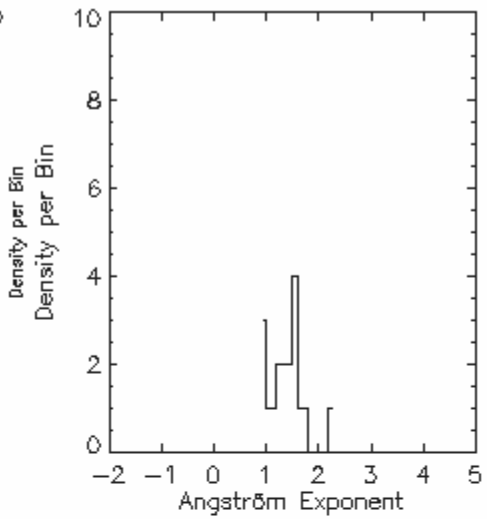
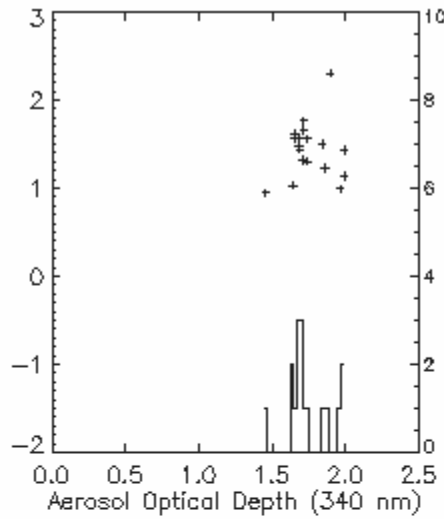
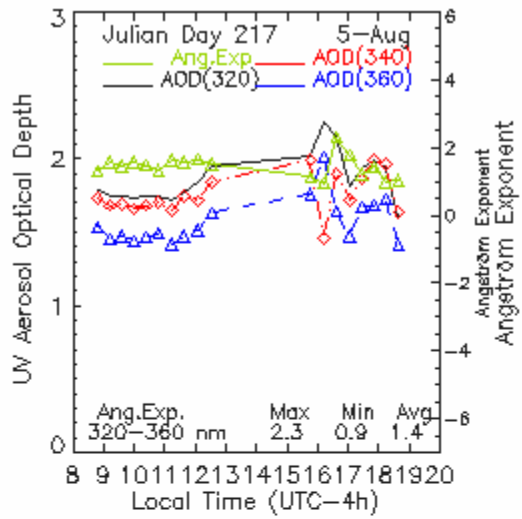
can be done creating more robust algorithms that utilize ground truth measurements from the METAR report or aerosol optical depth climatological studies in the UV and spread these results to nearby points to account for the regional effects of aerosols on UV radiation.

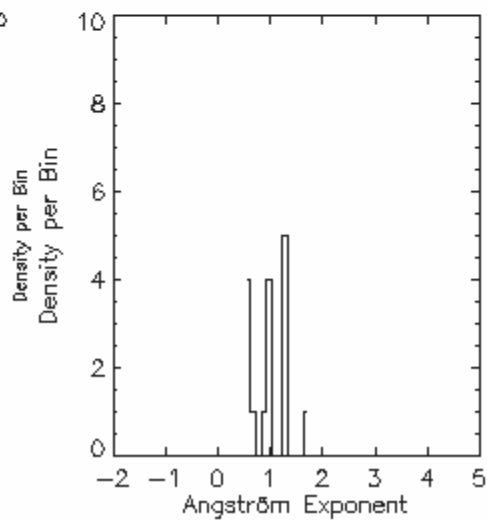
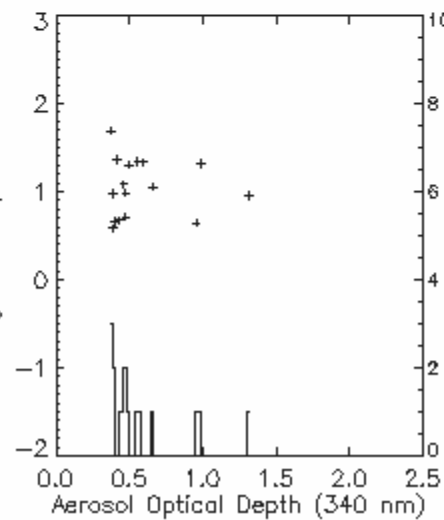
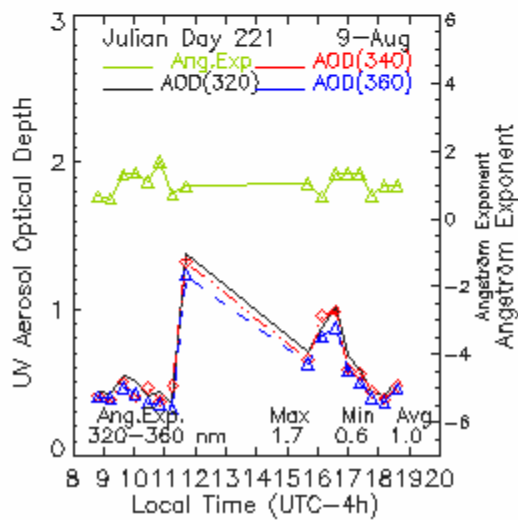
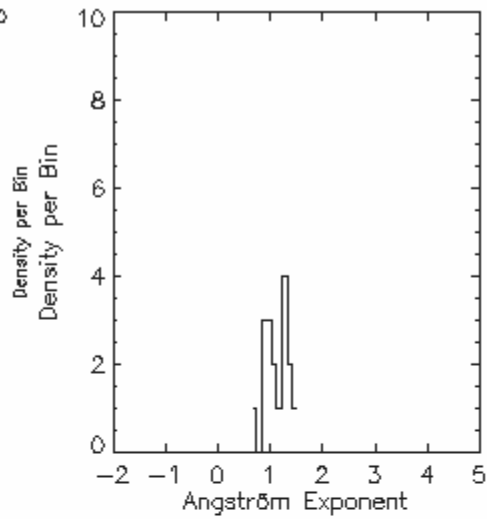
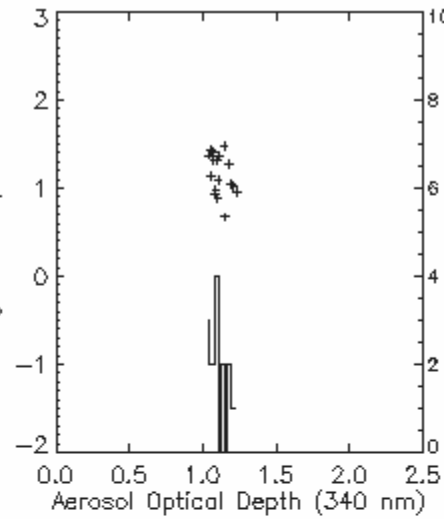
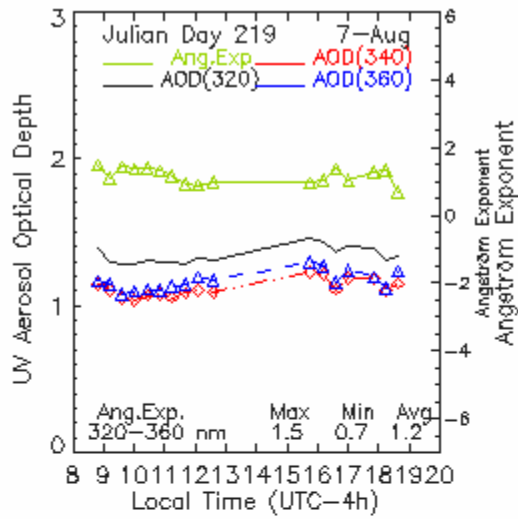
APPENDIX A: ALL AEROSOL OPTICAL DEPTH AND ÅNGSTRÖM EXPONENT MEASUREMENTS

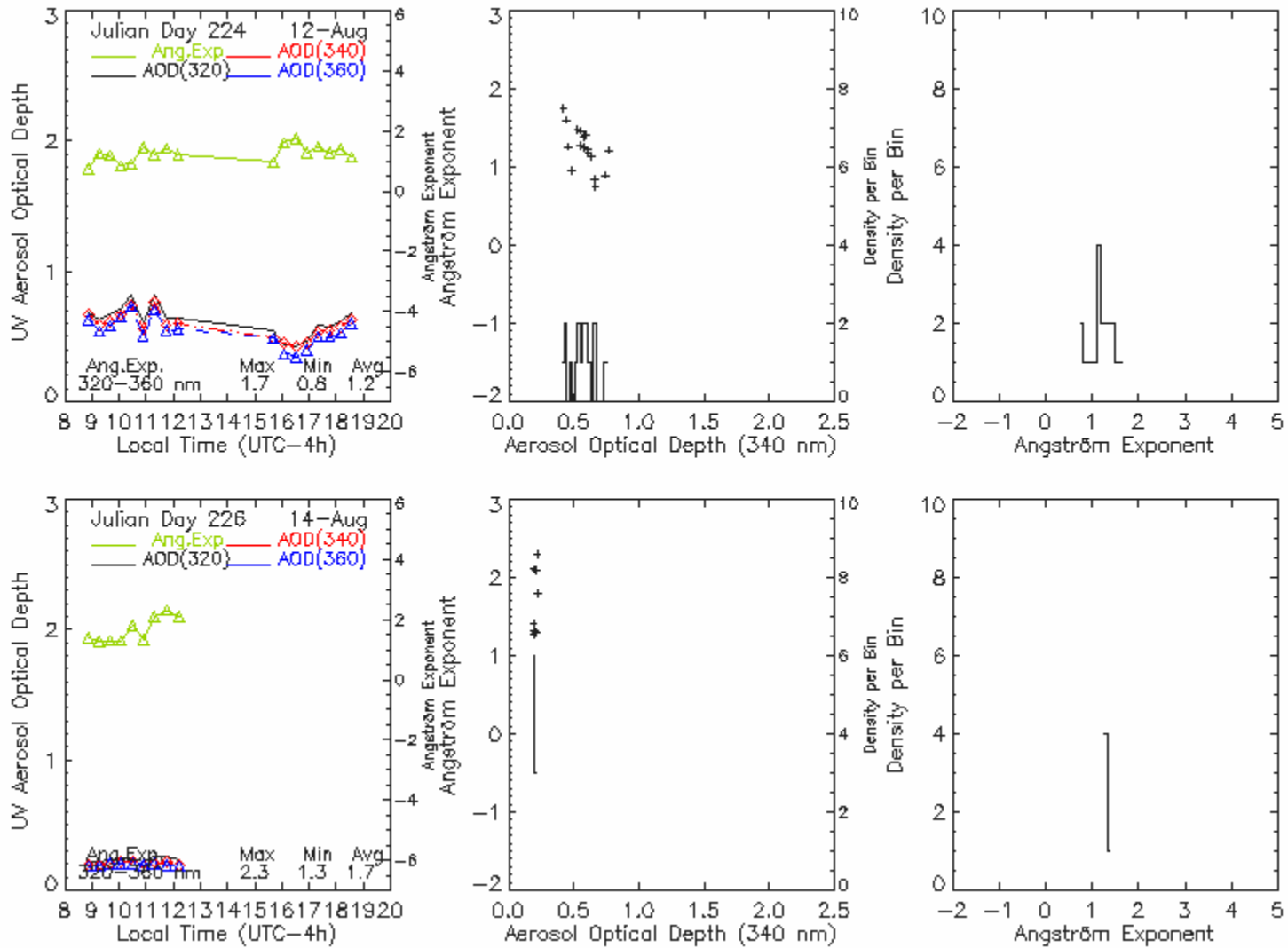
This appendix presents detailed graphs for each of the 16 measurement days for Atlanta and Griffin. Each row of graphs corresponds to a given day (e.g. Aug. 2, Aug 4, etc). The Atlanta measurements start on page 142 and the Griffin measurements on page 150.

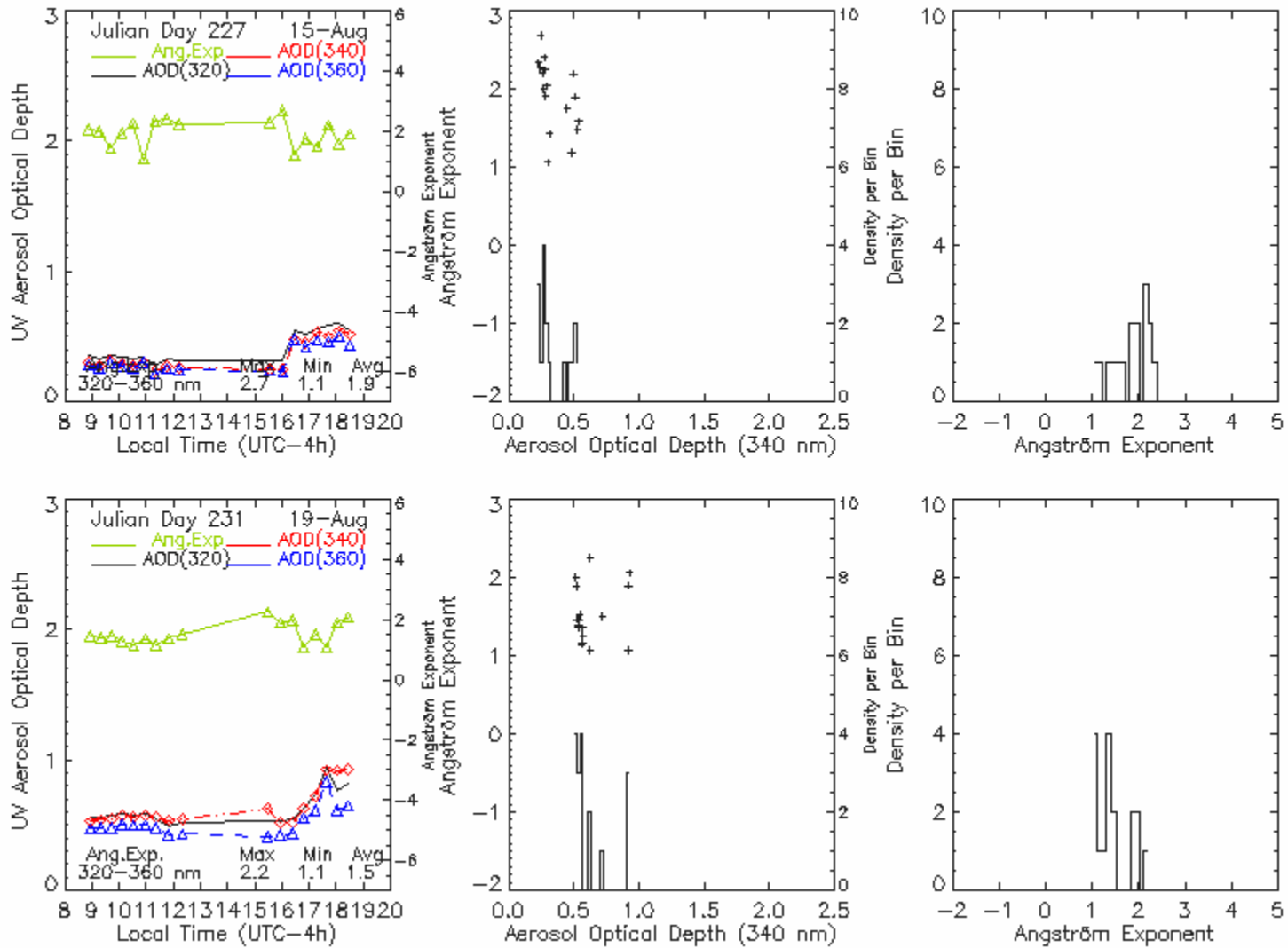
ATLANTA, GA

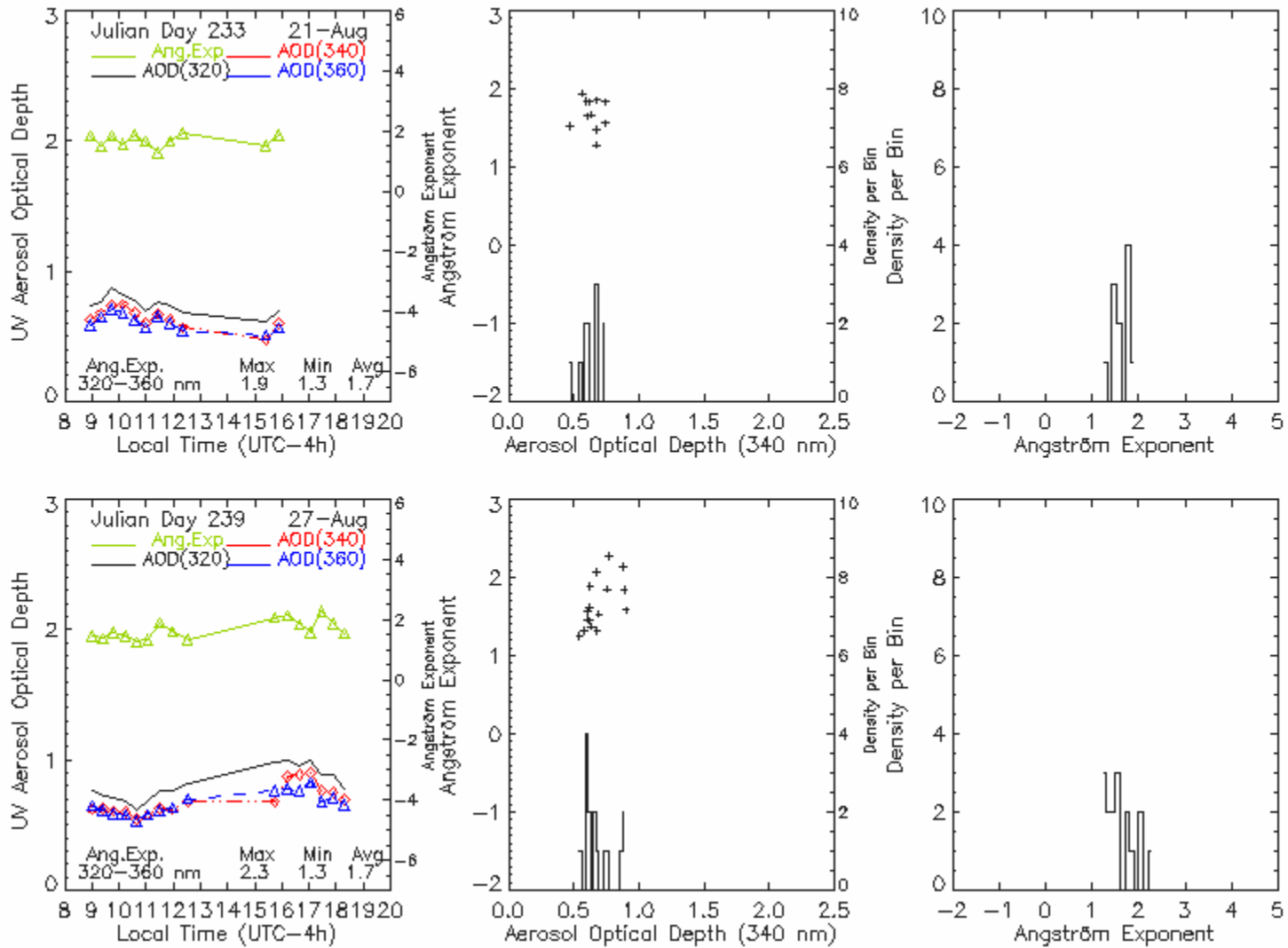


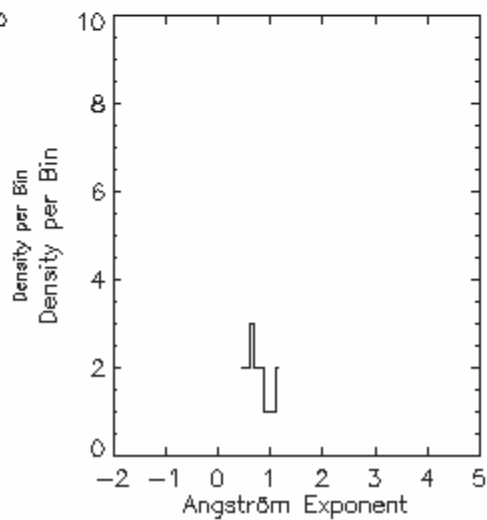
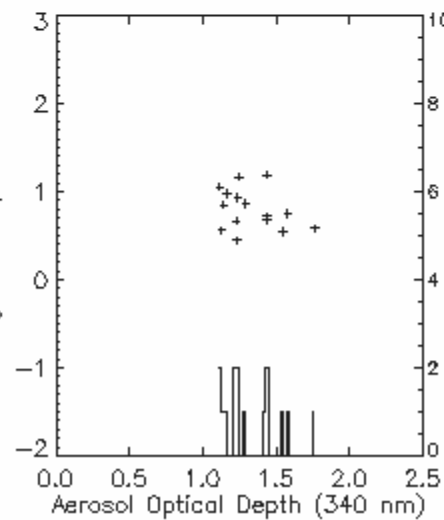
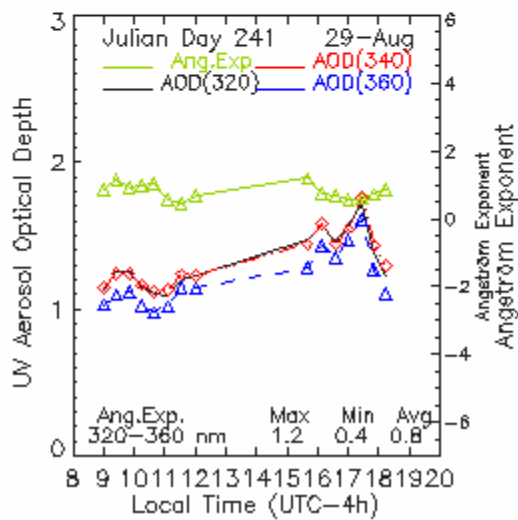
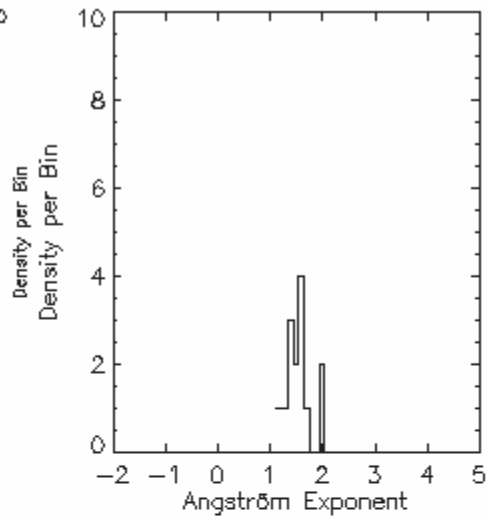
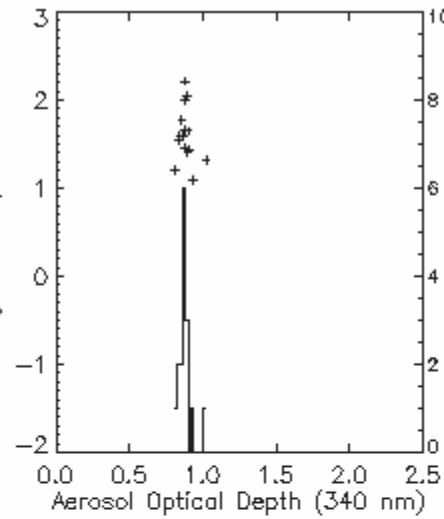
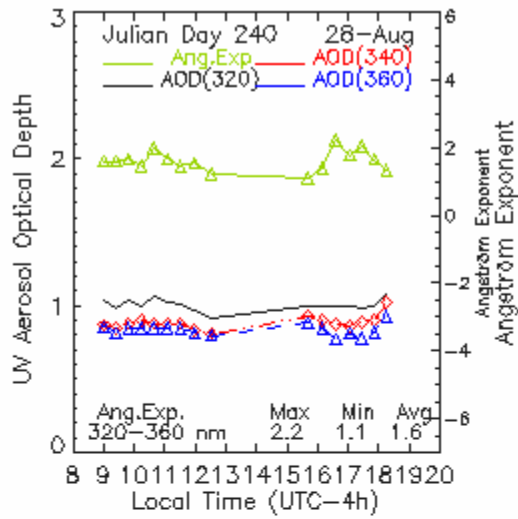


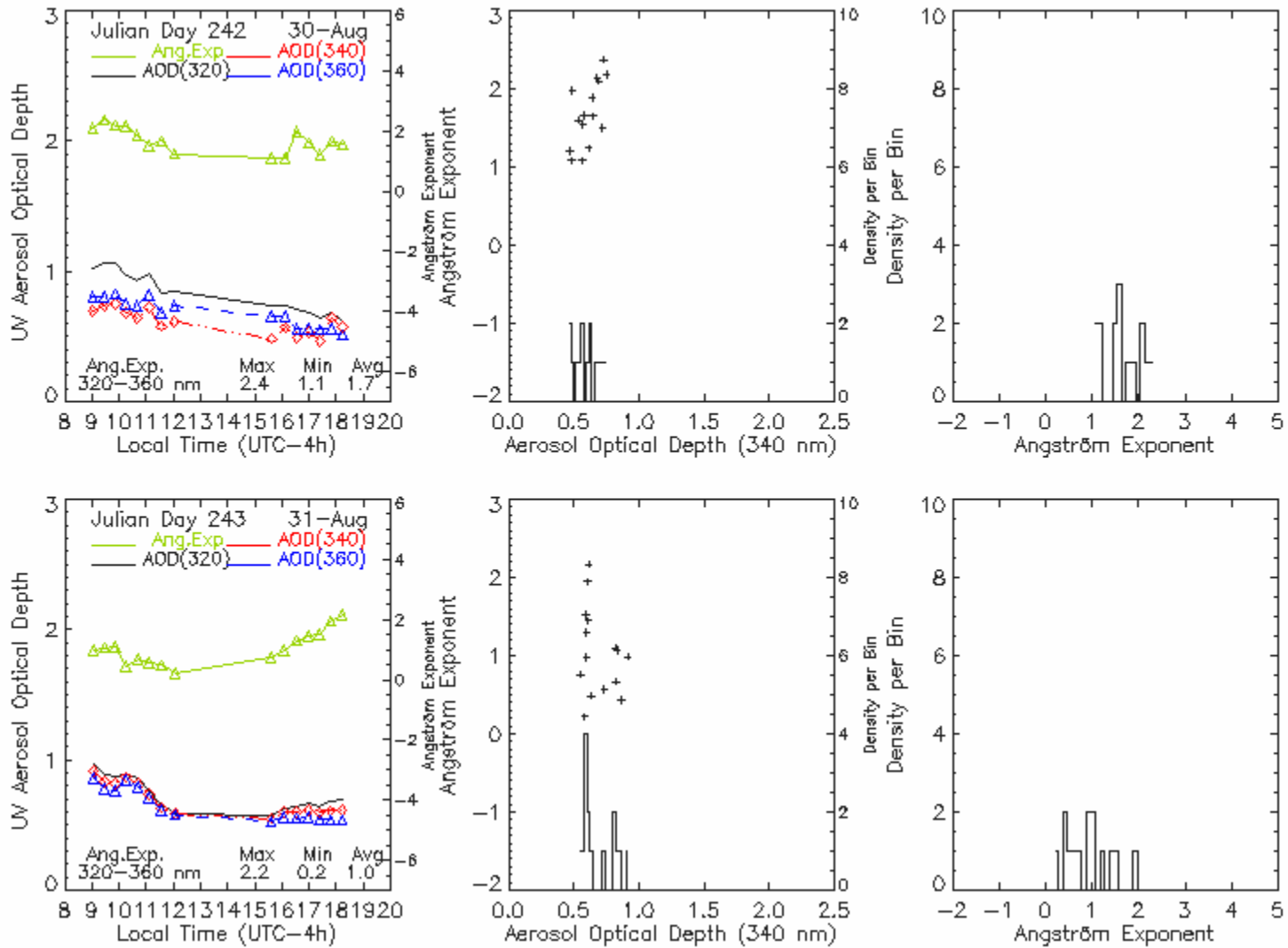




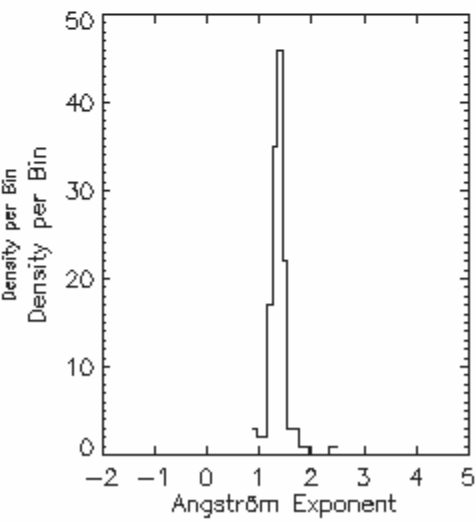
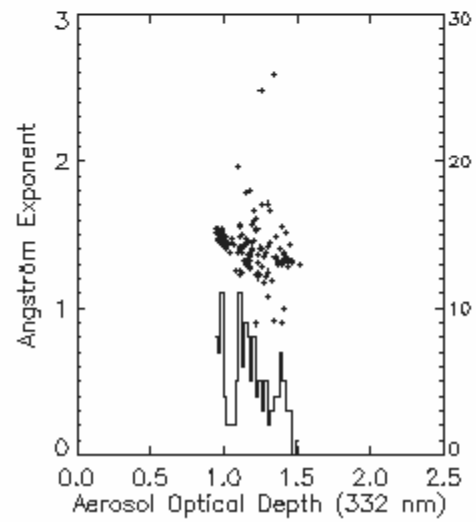
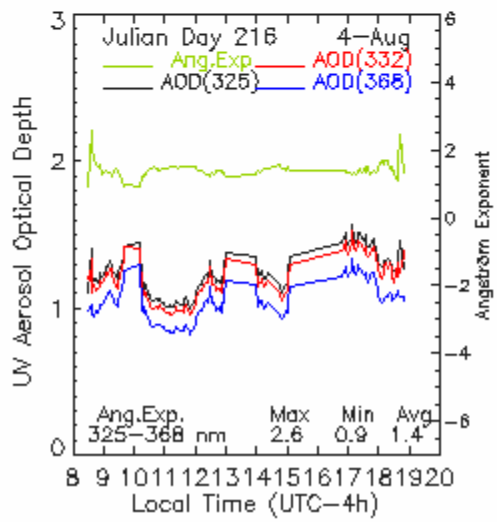
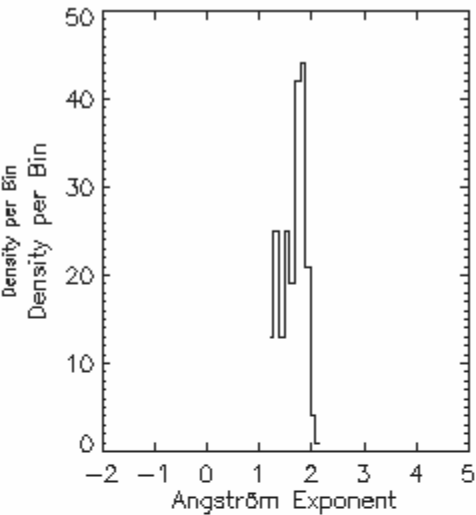
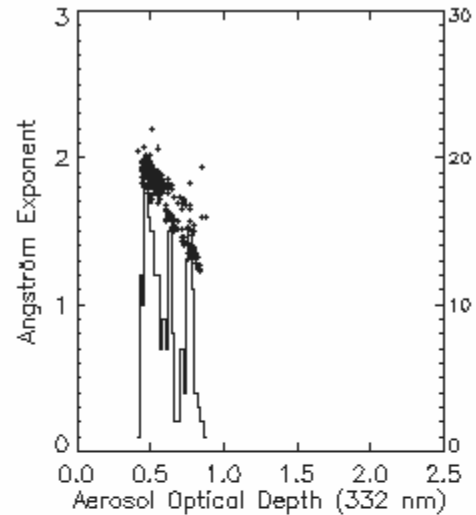
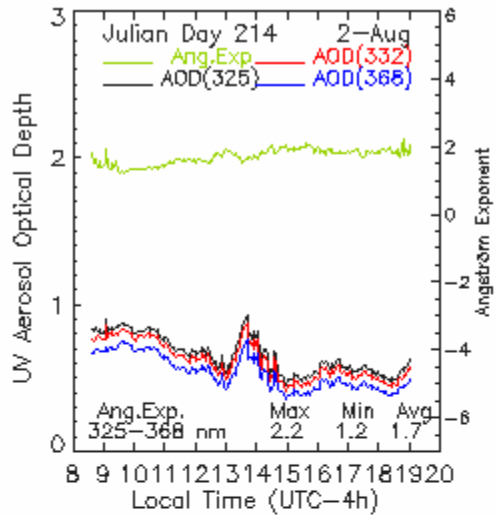


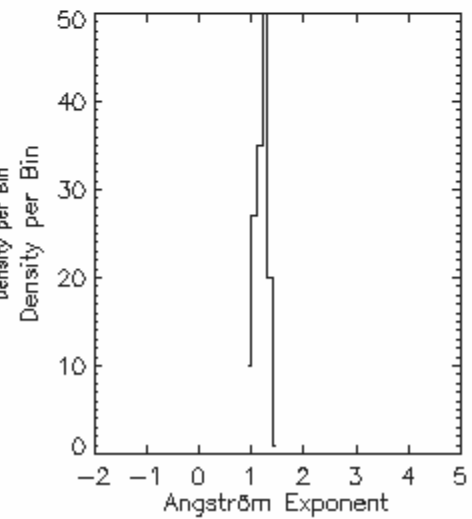
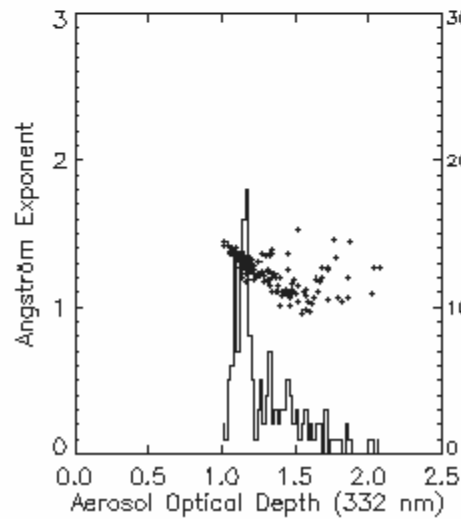
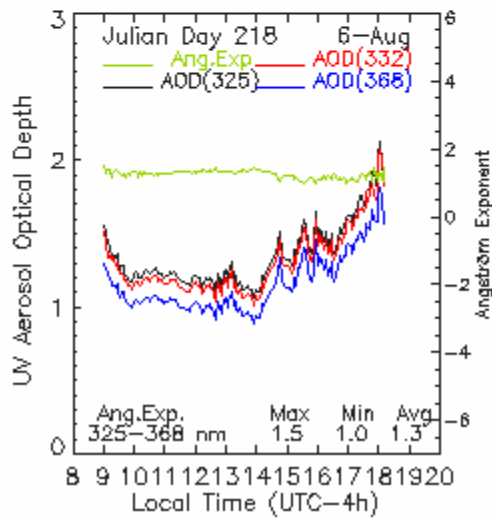
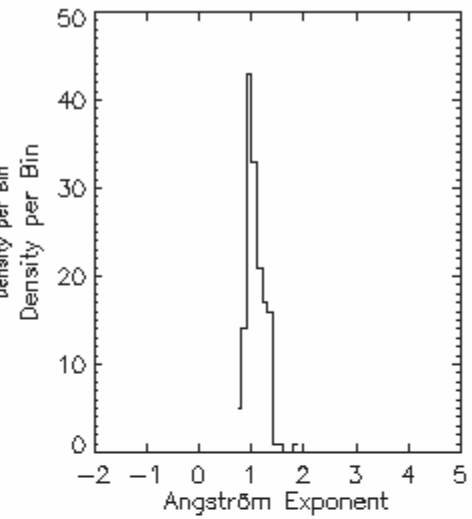
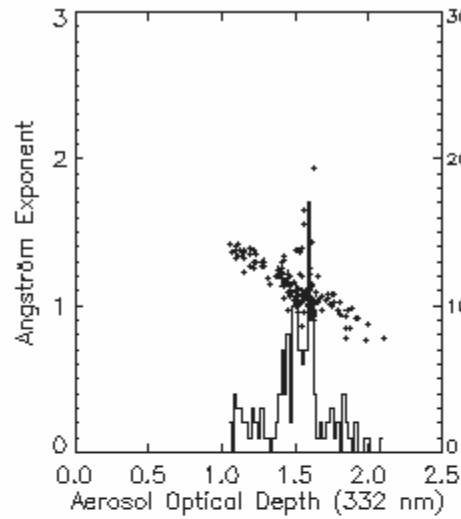
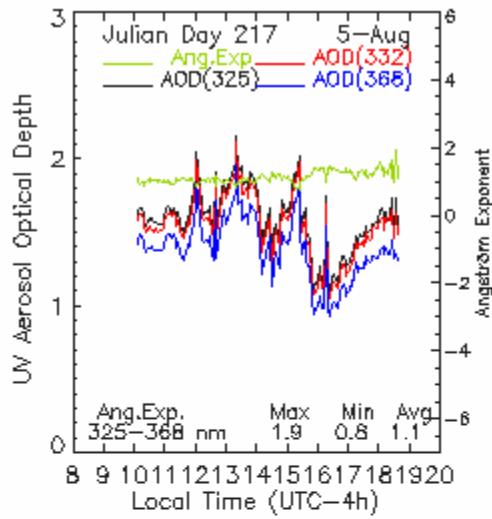


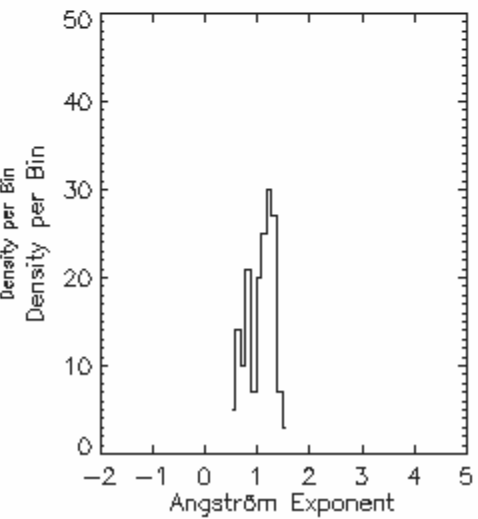
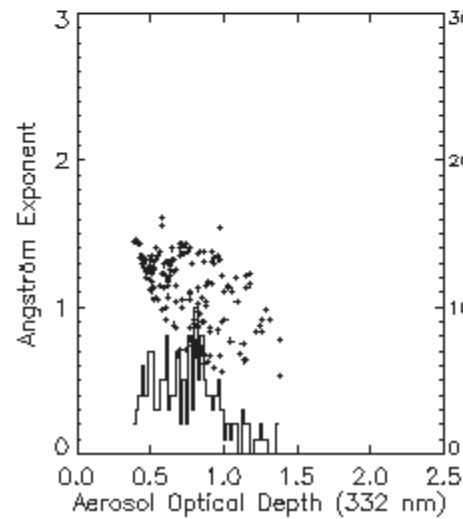
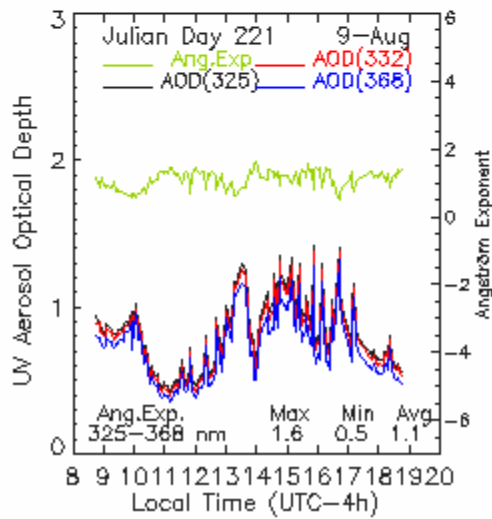
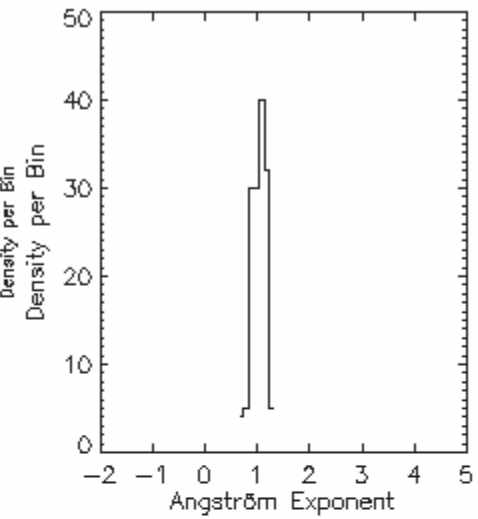
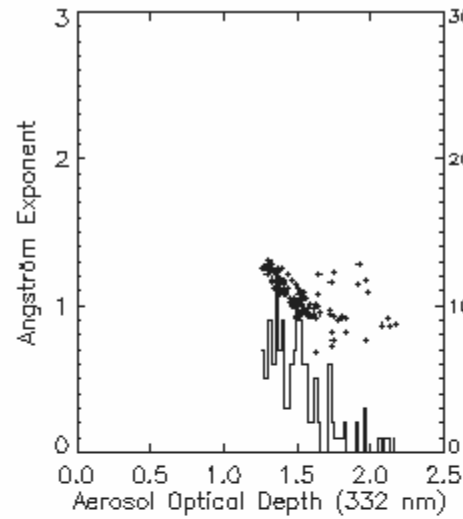
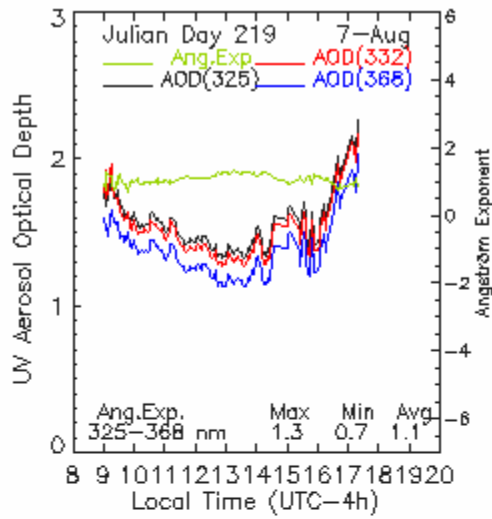


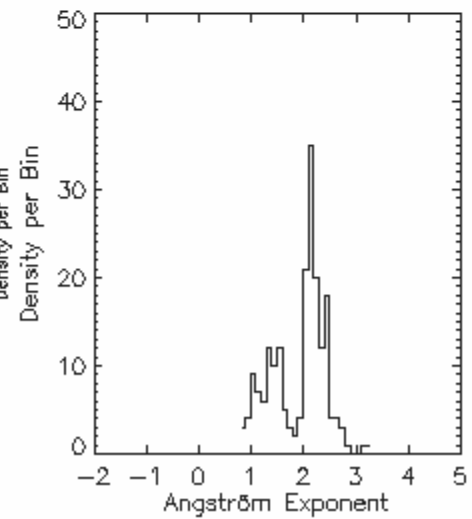
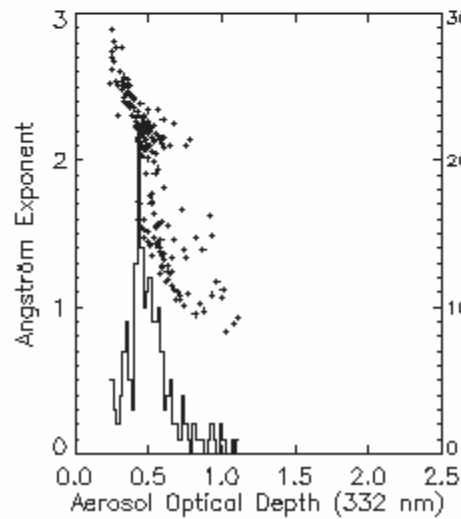
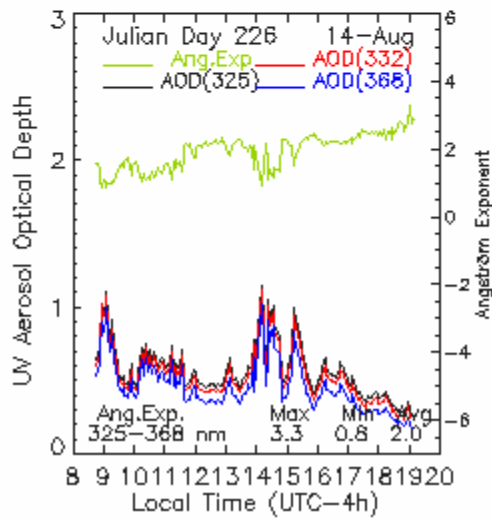
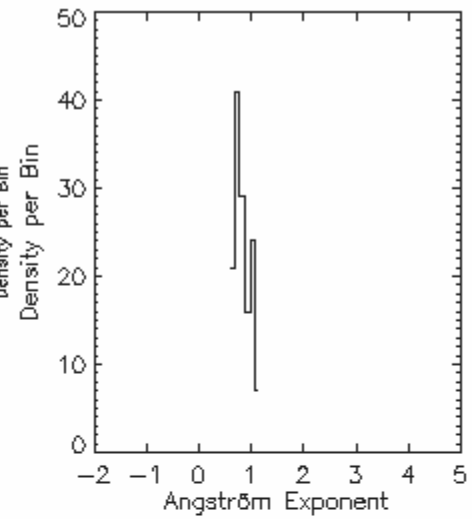
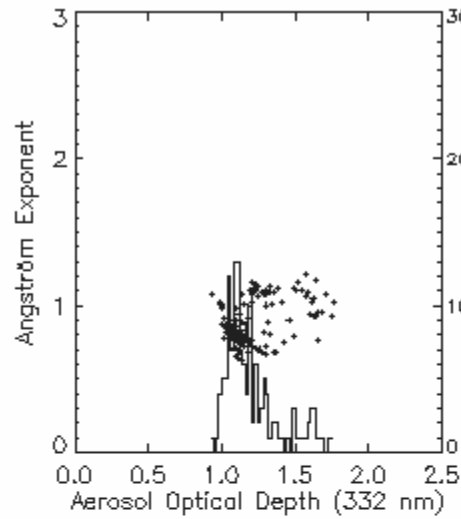
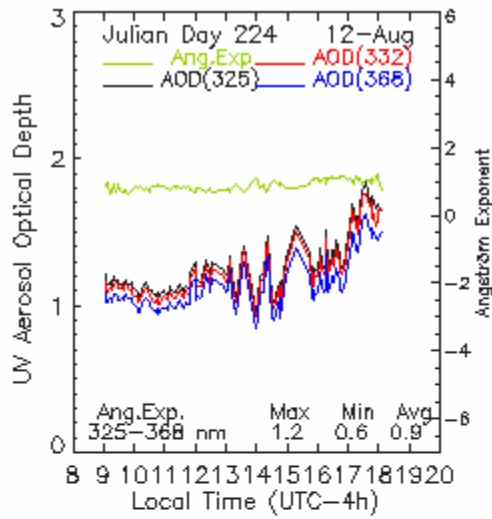


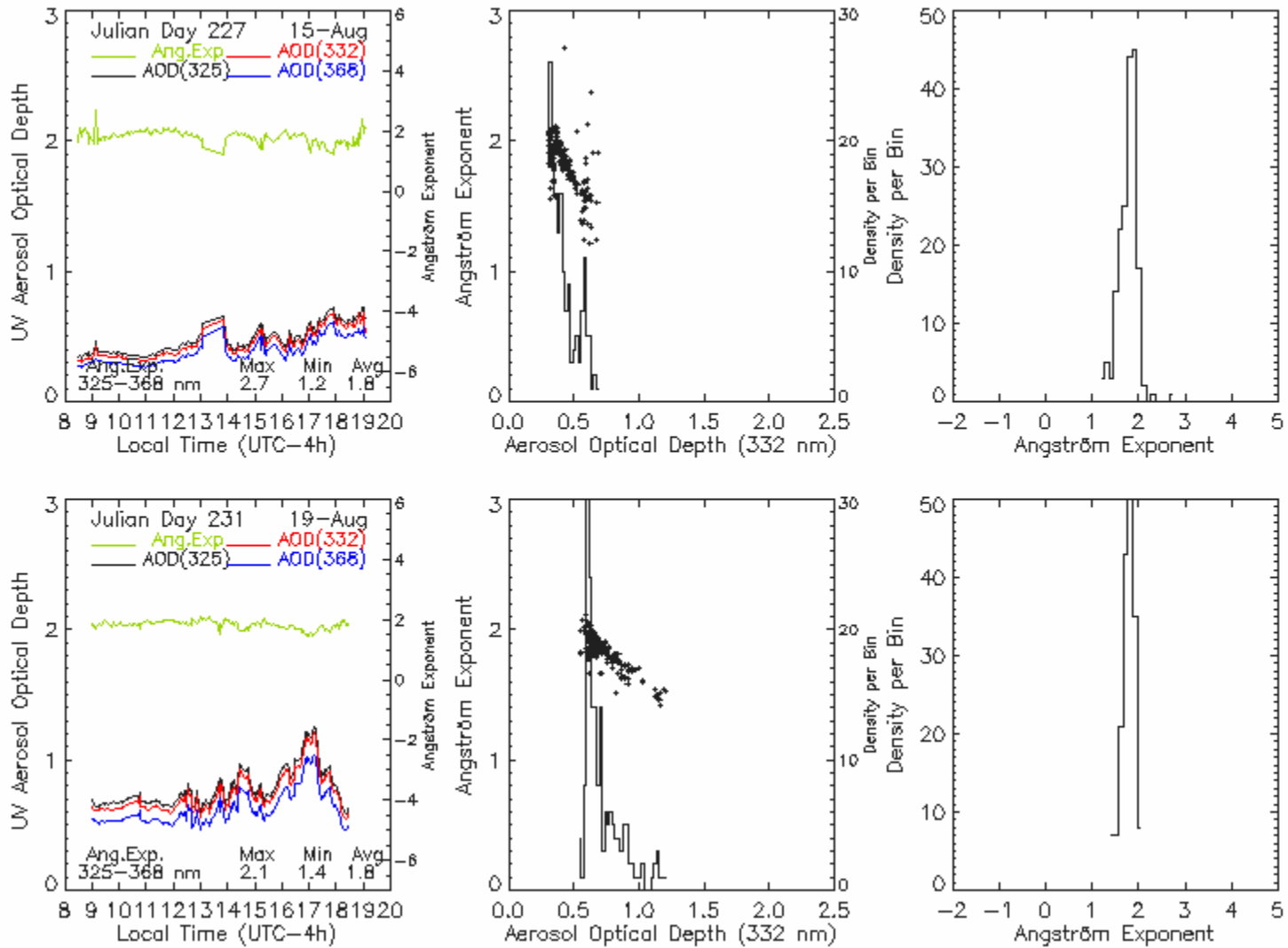
GRIFFIN, GA

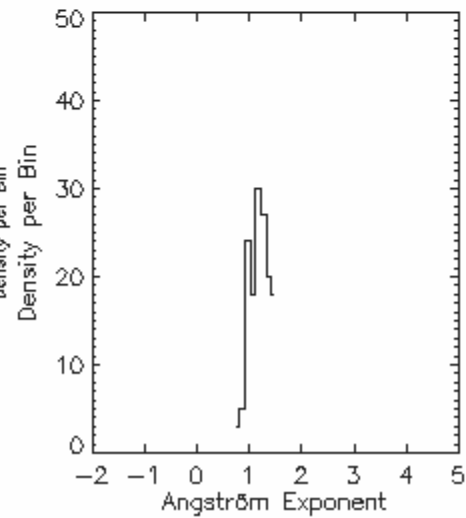
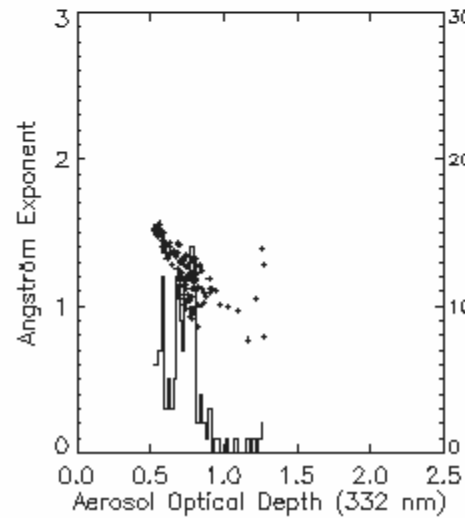
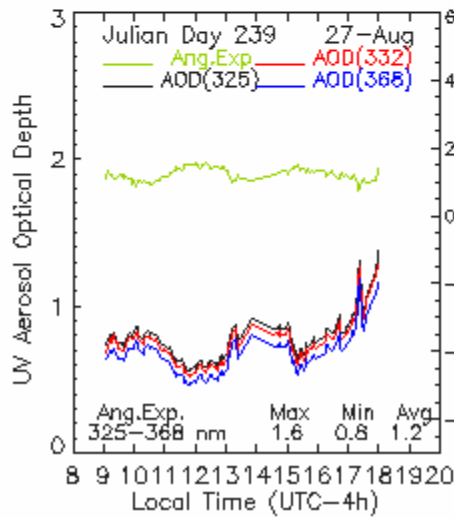
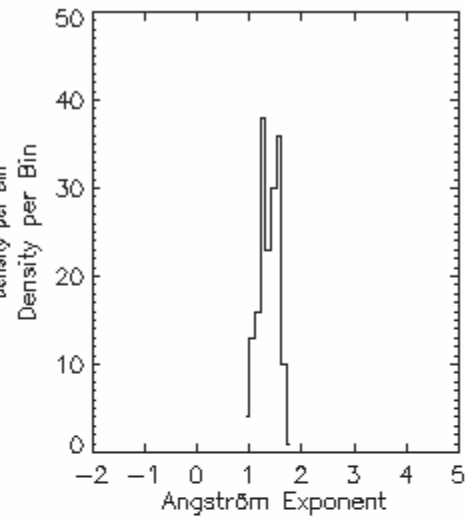
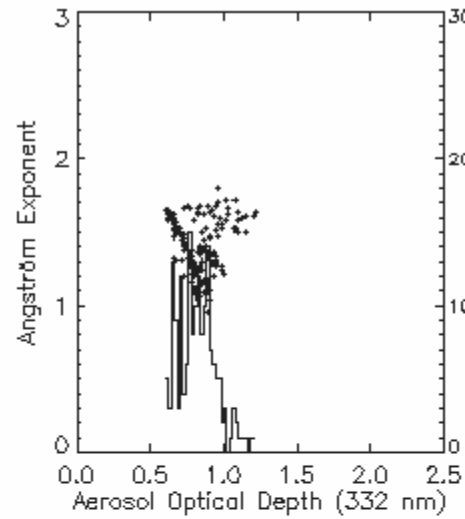
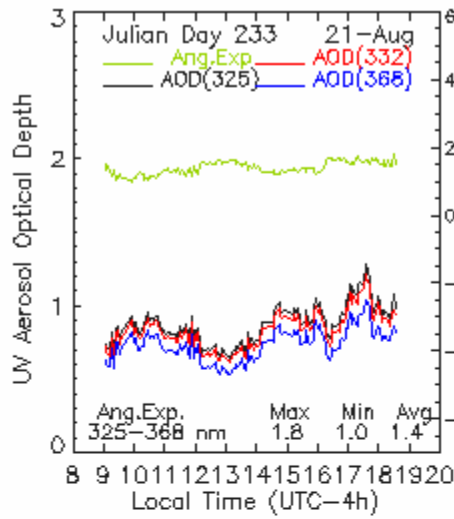


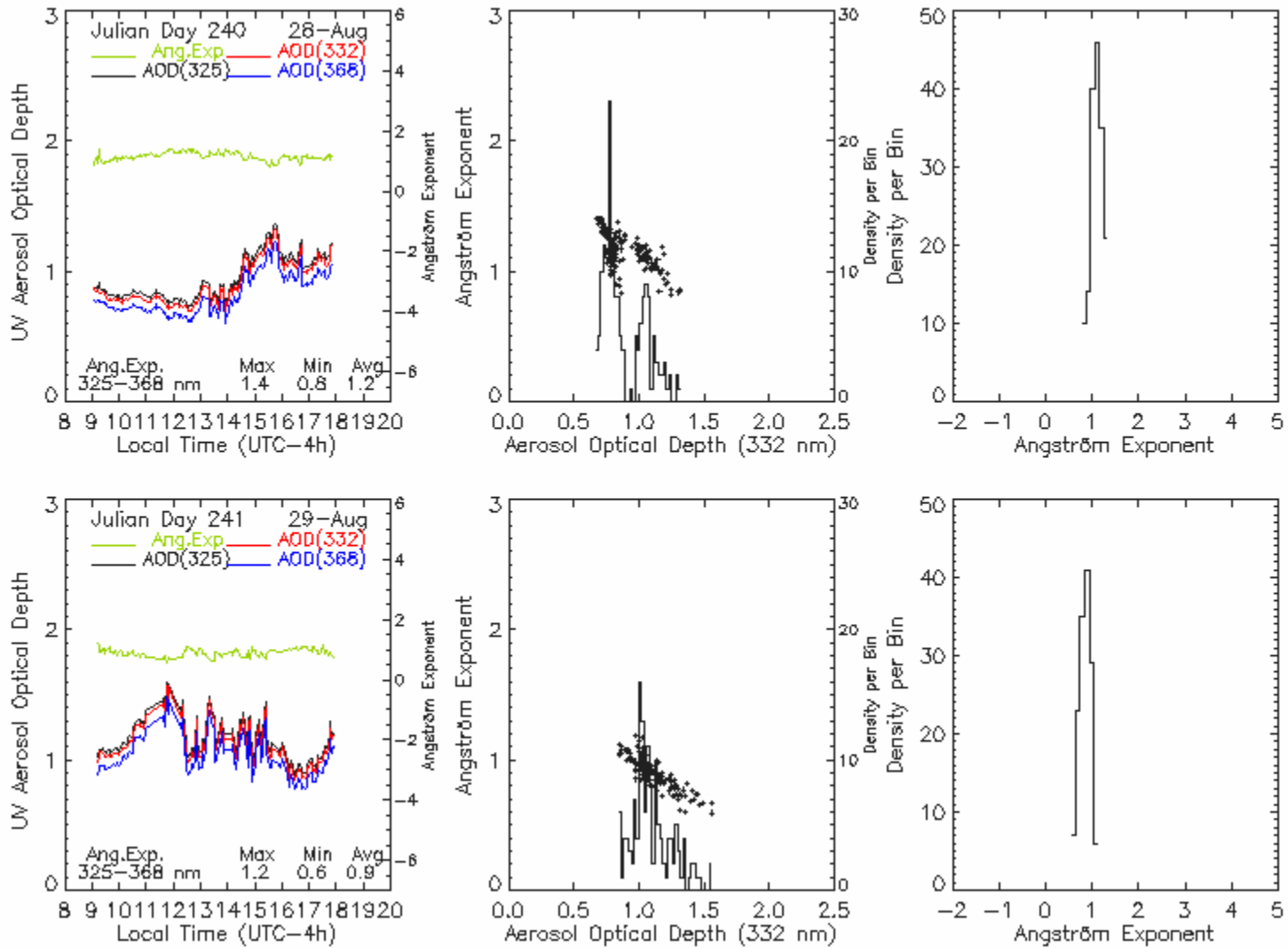


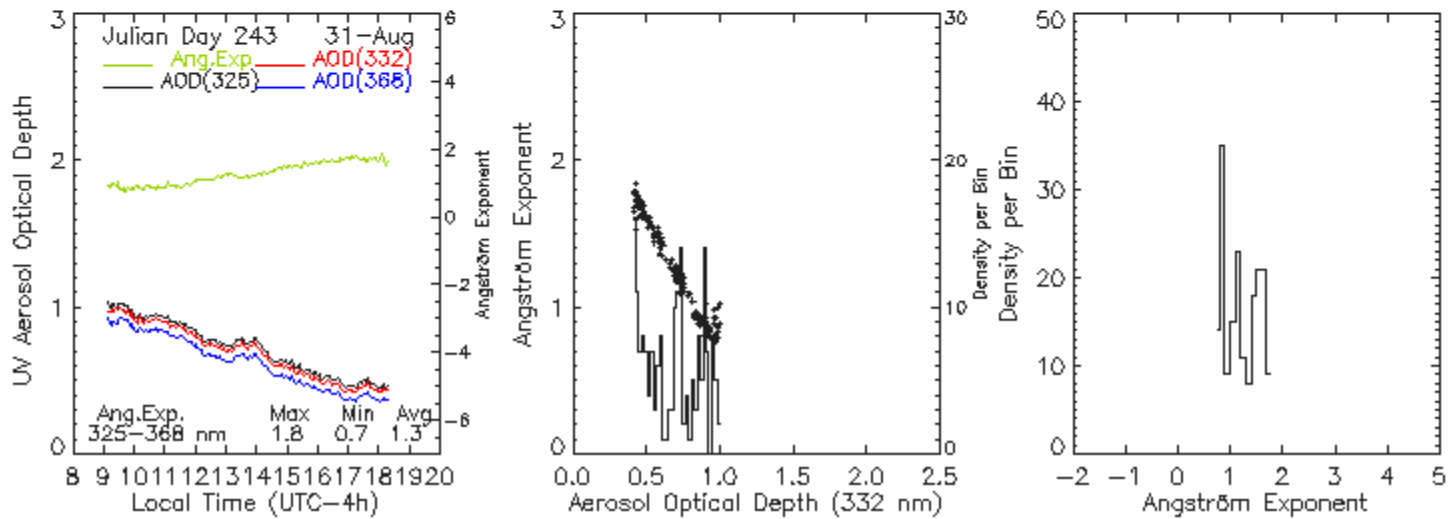
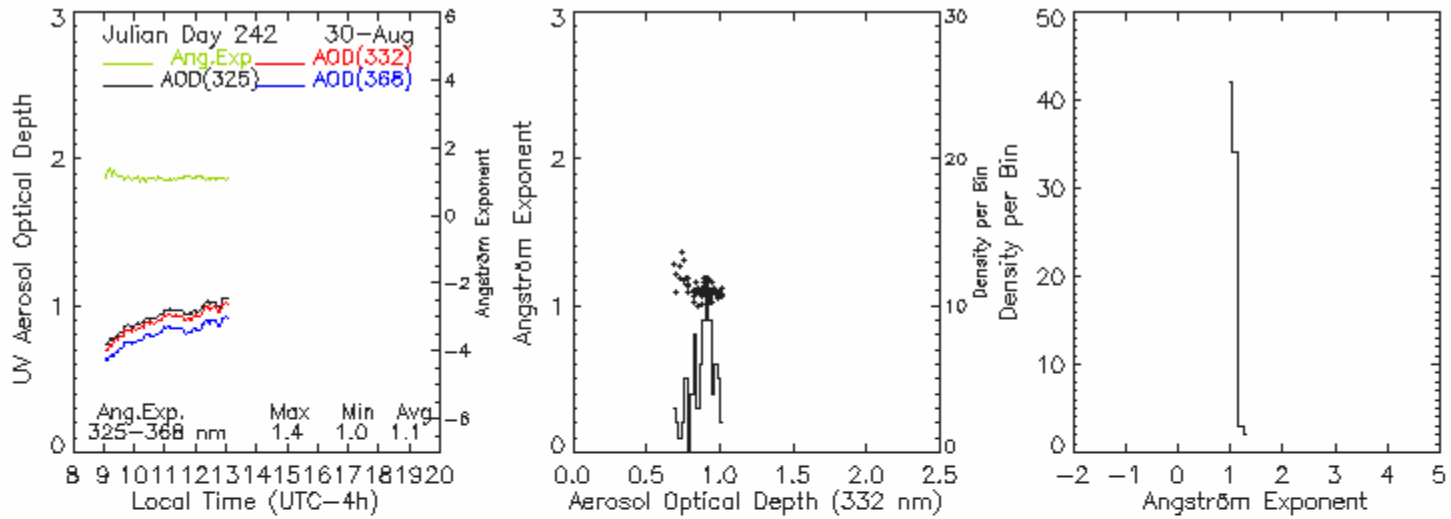












REFERENCES

- Adeyefa, Z. D., and B. Holmgren, 1996: Spectral solar irradiance before and during a Harmattan dust spell, *Solar Energy*, **57**, 195-203.
- Andreae, M. O., 1995: A World Survey of Climatology. *Future Climates of the World* (ed. Henderson-Sellers, A.), Elsevier, New York, **16**, 341-392.
- Bais, A. F., 1997: Absolute spectral measurements of direct solar ultraviolet irradiance with a Brewer spectrophotometer, *Appl. Opt.*, **36**, 5199-5204.
- Bais, A. F., C. S. Zerefos, C. Meleti, I. C. Ziomas, and C. Tourpali, 1983: Spectral measurements of solar UVB radiation and its relations to total ozone, SO₂, and clouds. *J. Geophys. Res.*, **98**, 5199-5208.
- Bais, A.F., A. Kazantzidis, S. Kazadzis, D.S. Balis, C.S. Zerefos, and C. Meleti, 2005: Deriving an effective aerosol single scattering albedo from spectral surface UV irradiance measurements, *Atmospheric Environment*, **39**, 1093-1102.
- Bergin, M.H., Schwartz, S.E., Ogren, J.A, McInnes, L.M., 1997: Evaporation of Ammonium Nitrate Aerosol in a Heated Nephelometer: Implications for Field Measurements, *Environ. Sci. Technol.*, **31**, 2878-2883.
- Bigelow, D. S., J. R. Slusser, A. F., Beaubien, and J. H. Gibson, 1998: The USDA Ultraviolet Radiation Monitoring Program. *Bull. Am. Meteorol. Soc.*, **79**, 601-615.
- Bohren, C.F., and D.R. Huffman, 1983: *Absorption and Scattering of Light by Small Particles*, John Wiley, New York.
- Bokoye, A. I., A. de La Casinière, and T. Cabot, 1997: Ångström turbidity parameters and aerosol optical thickness: A study over 500 solar beam spectra, *J. Geophys. Res.*, **102**, 21,905-21, 914.
- Borghesi, A., E. Bussolletti, G. Falcicchia, and A. Minafra, 1982: Determination of atmospheric water vapor and turbidity parameters from diurnal infrared hygrometer and turbidimeter data", *Infrared Phys.*, **22**, 149-155.
- Brash DE, J.A. Rudolph, J.A. Simon, A. Lin, G.J., McKenna, H.P. Baden, 1991: A role for sunlight in skin cancer: UV-induced mutations in squamous cell carcinoma. *Proc Natl Acad Sci U S A*; **88**, 10124-8.
- Carrico, M. Christian, M. H. Bergin, and Jin Xu, 2003: Urban aerosol radiative properties: Measurements during the 1999 Atlanta Supersite Experiment, *J. Geophys. Res.*, **108**, 8422.

- Cede, A., S. Kazadzis, M. Kowalewski, A. Bais, N. Kouremeti, M. Blumthaler, and Jay Herman, 2006: Correction of direct irradiance measurements of Brewer spectrophotometers due to the effect of internal polarization, *J. Geophys. Res.*, **33**, L0286.
- Charlson, R.J. S.E., Schwartz, J.M. Hales, R.D., Cess, J.A. Coakley, J.E. Hansen, and D.J., Hoffmann, 1992: *Science*, **255**, 423-430.
- Cutchis, P., 1980: A formula for comparing annual damaging ultraviolet (DUV) radiation doses at tropical and midlatitude sites, *Federal Aviation Administration Report FAA-EE 80-81*, U. S. Department of Transportation, Washington, D.C..
- d'Almeida, G.A., P. Kopke, E.P., Shettle, 1991: *Atmospheric aerosols: global climatology and radiative characteristics*, A. Deepak Publishing, Hampton, VA, USA pp. 73-74.
- de Gruijl FR, 1997: Health effects from solar UV radiation, *Radiat. Protect. Dosim.*, **46**, 20-30.
- Deirmendjian, D., 1969: *Electromagnetic scattering on spherical polydispersions*, Elsevier, New York.
- Dickerson, R.R., S. Kondragunta, G. Stenchikov, K.L. Civerolo, B.G. Doddridge, B.N. Holben, 1997: The impacts of aerosols on solar ultraviolet radiation and photochemical smog, *Science*, **278**, 827-830.
- Duthie, M.S., I. Kimber, M. Norval, 1999: The effects of ultraviolet radiation on the human immune system, *British Journal of Dermatology*, **140**, 995-1009.
- Dutton, E. G., P. Reddy, S. Ryan, and J. J. DeLuisi, 1994: Features and effects of AOD observed at Mauna Loa, Hawaii: 1982-1992, *J. Geophys. Res.*, **99**, 8295-8306.
- Eck, T.F., B.N. Holben, D.E. Ward, M.M. Mukelabai, O. Dubovik, A. Smirnov, J.S. Schafer, N.C. Hsu, S.J. Piketh, A. Queface, J. Le Roux, R.J. Swap, and I. Slutsker, 2003: Variability of biomass burning aerosol characteristics in southern Africa during the SAFARI 2000 dry season campaign and a comparison of single scattering albedo estimates from radiometric measurements, *J. Geophys. Res.*, **108**, 13-1 to 12-21..
- Elterman, L., 1968: *UV, Visible, and IR attenuation for altitudes to 50 km*, Rep AFCRL-68-0153, Environ. Res. Pap. No. 285, Air Force Cambridge Research Laboratories, pp. 49.
- Elwood, J. M., 1992: Melanoma and sun exposure: contrasts between intermittent and chronic exposure, *World J. Surg.*, **16**, 157-165.
- Estupiñán, J. G., S. Raman, G. H. Crescenti, J. J. Streicher, and W. F. Barnard, 1996: The effects of clouds and haze on UV-B radiation, *J. Geophys. Res.*, **101**, 16,807-16,816.

- Fioletov, V.E., J.B. Kerr, D.I., Wardle, N. Krotkov, and J.R. Herman, 2002: Comparison of Brewer ultraviolet irradiance measurements with Total Ozone Mapping Spectrometer satellite retrievals, *Opt. Eng.*, **41**, 3051-3061.
- Flowers, E. C., R. A. McCormick, and K. R. Kurfis, 1969: Atmospheric turbidity over the United States, 1961-1966, *J. Appl. Meteorol.*, **8**, 955-962.
- Gilmour, J. W., J. P. Vestey and M. Norval, 1993: The effect of UV therapy on immune function in patients with psoriasis, *British Journal of Dermatology*, **129**, 28-38.
- Gröbner, J., R. Verfaz, V.E.Cachorro, D.V. Henriques, K. Lamb, A. Redondas, J.M. Vilaplana, and D. Rembges, 2001: Intercomparison of aerosol optical depth measurements in the UVB using Brewer spectrophotometers and Li-Cor spectrophotometer, *Geophys. Res. Lett.*, **28**, 1691-1694.
- Hansen, J. E., and L. D. Travis, 1974: Light scattering in planetary atmospheres, *Space Sci. Rev.*, **16**, 527.
- Harrison, L., and J. Michalsky, 1994: Objective algorithms for the retrieval of optical depths from ground-based measurements, *Appl. Opt.*, **33**, 5126-5132.
- Hastenrath, S., 1997: Measurements of solar radiation and estimation of optical depth in the High Andes of Peru, *Meteorol. Atmos. Phys.*, **64**, 51-59.
- Holben, B., Tanre, D., Smirnov, A., Eck, T., Slutsker, I., Abuhassan, N., Newcomb, W.W., Schafer, J., Chatenet, B., Lavenue, F., Kaufman, Y., Van de Castle, J., Setzer, A., Markham, B., Clark, D., Frouin, R., Halethore, R., Karnieli, A., O'Neill, N.T., 2001b: An emerging ground based aerosol climatology: Aerosol optical depth from Aeronet. *Journal of Geophysical Research*, **106**, 12067-12097.
- Holben, B.N. et al., 1998: AERONET-A federal instrument network and data archive for aerosol characterization, *Remote Sens. Environ.*, **66**, 1-16.
- Holben, B.N., T.F Eck, and R.S. Fraser, 1991a: Temporal and spatial variability of aerosol optical depths in the Sahel region in relation to vegetation remote sensing, *International Journal of Remote Sensing*, **12**, 1147-1163.
- Ilyas, M., 1987: Effect of cloudiness on solar ultraviolet radiation reaching the surface. *Atmos. Environ.*, **21**, 1483-1484.
- Jacobson, M.Z., 1999: Isolating nitrated and aromatic aerosols and nitrated aromatic gases as sources of ultraviolet light absorption, *J. Geophys. Res.*, **104**, 3527-3542.
- Jaroslawski, J. and J.W. Krzyscin, 2000: AOD in the UV range derived from direct sun ozone observations performed by the Brewer Spectrophotometer Mark II No. 064 at Belsk, Poland, Quadrennial Ozone Symposium, Hokkaido University, Sapporo, 3-8 July, Japan, 449-450.

- Josefsson, W. 1986: Solar ultraviolet radiation in Sweden, *SMHI Report 53*, National Institute of Radiation Protection in Stockholm, Norrköping, Sweden.
- Jun, C., W. Zhen, Han Jiecai, Hu Huanling, 1996: Variability of aerosol optical properties over Hefei during September 1993 to September 1994, *Acta Meteorologica Sinica*, **10**, 82-95.
- Kazadzis, S., A. Bais, N. Kouremeti, E. Gerasopoulos, K. Garane, M. Blumthaler, B. Schallhart, and A. Cede, 2005: Direct spectral measurements with a Brewer spectroradiometer: absolute calibration and aerosol optical depth retrieval, *Appl. Opt.*, **44**, 1681-1690.
- Kerr, J. B., 1997: Observed dependencies of atmospheric UV radiation and trends, in *Nato ASI Series*, Vol. I 52, Edited by Christos S. Zerefos and Alkiviadis F. Bais, pp. 259-266, Springer-Verlag Berlin Heidelberg.
- Kerr, J. B., and C. T. McElroy, 1995: Total ozone measurements, made with the Brewer ozone spectrophotometer during STOIC 1989, *J. Geophys. Res.*, **100**, 9225-9230.
- Kouvarakis, G., Y. Doukalis, N. Mihalopoulos, S. Rapsomanikis, J. Sciare, and M. Blumthaler, 2002: Chemical, physical, and optical characterization of aerosols during PAUR II Experiment, *J. Geophys. Res.*, **107**, 8141.
- Koval, J, J. G. Estupiñán and J. Staudinger, 2006: Verification of a Real-Time System to Estimate Weather Conditions at High Resolution in the United States, *Extended Abstracts, 22nd International Conference on Interactive Information Processing Systems for Meteorology, Oceanography, and Hydrology*, Atlanta, GA.
- Kraus, R, M. Buhning, W. Hopfenmuller, M.F. Holick, A.M. Sharma, 1998: Ultraviolet B and blood pressure, *Lancet*, **352**, 709-710.
- Kripke, M., 1992: Health effects of UV-B radiation, paper presented at UV-B Monitoring Workshop: A Review of the Science and Status of Measuring and Monitoring Programs, Sponsored by Alternative Fluorocarbons Environmental Acceptability Study and the U. S. Department of Agriculture, Mar. 10 to 12.
- Krotkov, N., P. K., Bhartia, J. Herman, J. Slusser, G. Labow, G. Scott, G. Janson, T. F. Eck, and B. Holben, 2005: Aerosol ultraviolet absorption experiment (2002 to 2004), part 1: ultraviolet multifilter rotating shadowband radiometer calibration and intercomparison with CIMEL sunphotometers, *Optical Engineering*, **44**, 041004-1-17.
- Krzyścin, J.W. and S. Puchalski, 1998: Aerosol impact on the surface UV radiation from the ground-based measurements taken at Belsk, Poland, 1980-1996, *J. Geophys. Res.*, **103**, 16175-16181.
- Kylling, A., A. F. Bais, M. Blumthaler, J. Schreder, C. S. Zerefos, and E. Kosmidis, 1998: Effects of aerosols on solar UV irradiances during the Photochemical Activity and Solar Ultraviolet Radiation Campaign, *J. Geophys. Res.*, **103**, 26051-26060.

- Lavker, R. M., D. A. Veres, C. J. Irwin, and K. H. Kaidbey, 1995: Quantitative assessment of cumulative damage from repetitive exposures to suberythemogenic doses of UVA in human skin, *Photochem. Photobiol.*, **62**, 348-352.
- Lavker, R., and K. Kaidbey, 1997: The spectral dependence for UVA-induced cumulative damage in human skin, *Journal of Investigative Dermatology*, **108**, 17-21.
- Lemus-Deschamps, L., L. Rikus, and P. Gies, 1999: The operational Australian Ultraviolet index forecast 1997. *Meteorol. Appl.*, **6**, 241-151.
- Long, C. S. , A. J. Miller, H. -T. Lee, J. D. Wild, R. C. Przywarty, and D. Hufford, 1996: Ultraviolet index forecasts issued by the National Weather Service. *Bull. Amer. Meteorol. Soc.*, **77**, 729-748.
- Longstreth, J. D., and J. Wiseman, 1989: The potential impact of climate change on patterns of infectious disease in the United States, in *The potential effects of global climate change on the United States: Appendix G Health*, ed. J. B. Smith and D. A. Tirpak for the Office of Policy, Planning, and Evaluation, U.S. Environmental Protection Agency. Washington, D.C., U.S. Environmental Protection Agency.
- Longstreth, J., de Gruijl, F.R., M.L Kripke, S. Abseck, F. Arnold, H.I. Slaper, G. Velders, Y. Takizawa, J.C. van der Leun, 1998: Health risks, *J. Photochem Photobiol B*, **46**, 20-30.
- Madronich, S. and S. Flocke, 1999: The role of solar radiation in atmospheric chemistry, in *Environmental Photochemistry*, edited by P. Boule, pp. 1-26, Springer-Verlag, New York.
- Madronich, S., UV radiation in the natural and perturbed atmosphere: 1993, in *Environmental Effects of Ultraviolet (UV) Radiation*, pp. 17-69, Lewis, Boca Raton, FL.
- Marenco, F, A.D. Sarra, and J. De Luisi, 2002: Methodology for determining aerosol optical depth from Brewer 300-320-nm ozone measurements, *Appl. Opt.*, **41**, 1805-1814.
- Marenco, F. V., Santacesaria, A. F. Bais, D. Balis, A. disarray, A. Papayannis, and C. Zerefos, 1997: Optical properties of tropospheric aerosols determined by lidar and spectrophotometric measurements (Photochemical Activity and Solar Radiation Campaign), *Appl. Opt.*, **36**, 6875-6886.
- McKenzie, R. L., G. Seckmeyer, A.F. Bais, J.B. Kerr, and S. Madronich, 2001a: Satellite retrievals of erythemal UV dose compared with ground-based measurements at northern and southern midlatitudes, *J. Geophys. Res.*, **106**, 24051-24062.
- Middleton, W.E., 1961: *Pierre Bouguer's Optical Treatise Gradation of Light*, University of Toronto Press, 241 pp.

- National Oceanic and Atmospheric Administration (NOAA), 1976: National Aeronautics and Space Administration (NASA), United States Air Force, *US Standard Atmosphere*, Washington, D.C.
- Neilley, P, and B. Rose, 2006: A real-time system to estimate weather conditions at high-resolution, *Extended Abstracts, 22nd International Conference on Interactive Information Processing Systems for Meteorology, Oceanography, and Hydrology*, Atlanta, GA.
- Ohnaka, T, 1993: Health effects of ultraviolet radiation, *Ann Physiol Anthropol.*, Jan; **12**(1), 1-10.
- Peak, M. J., J. G. Peak, M. P. Mohering, and R. B. Webb, 1984: Ultraviolet action spectra for DNA dimer induction, lethality and mutagenesis in *Escherichia coli* with emphasis on the UV-B region. *Photochem. Photobiol.*, **40**, 613-620.
- Peterson, J. T., E. C. Flowers, G. J. Berri, C. L. Reynolds, and J. H. Rudisill, 1981: Atmospheric Turbidity over central North Carolina, *J. Appl. Meteorol.*, **20**, 229-241.
- Petters, J. L., V.K. Saxena, J.R. Slusser, B.N. Wenny, and S. Madronich, 2003: Aerosol single scattering albedo retrieved from measurements of surface UV irradiance and a radiative transfer model, *J. Geophys. Res.*, **108**(D9), 4288.
- Sabburg, J., J. E. Rives, R.S. Meltzer, T. Taylor, Zheng Schmalzle, N. Huang, A. Wilson, P.M. Udelhofen, 2002: Comparisons of corrected daily-integrated erythemal UVR data from the U.S. EPA/UGA network of Brewer spectroradiometers with model and TOMS-inferred data. *J. Geophys. Res.* **107**, 4676-4686.
- Sabziparvar, A.A, P.M. de F. Forster, and K.P. Shine, 1998: Changes in ultraviolet radiation due to stratospheric and tropospheric ozone changes since preindustrial times, *J. Geophys. Res.* **103**, 26107-26113.
- Schnaiter, M., O. Möhler, K.-H. Naumann, A. Nink, H. Saathoff, W. Schöck, and U. Schurath, 2000: UV-Vis-NIR extinction spectroscopy of aerosols relevant for the atmosphere, 5th Conference on Electromagnetic and Light Scattering by Nonspherical Particles: Theory, Measurements, and Applications, 28 Aug – 1 Sep 2000, Dalhousie Univ., Halifax, Canada.
- Schreiner, A.J., 2001: Derived cloud products from the GOES-M Imager, *Extended Abstracts, 11th Conference on Satellite Meteorology and Oceanography*, Madison, Wisconsin.
- Schwander, H, P. Koepke, and A. Ruggaber, 1997: Uncertainties in modeled UV irradiances due to limited accuracy and availability of input data, *J. Geophys. Res.*, **102**, 9419-9429.
- Setlow, R. B., 1974: The wavelengths in sunlight effective in producing skin cancer: a theoretical analysis. *Proc. Nat. Academ. Sci.*, **71**, 3363-3366.

Stamnes, K., S.-C. Tsay, and K. Jayaweera, 1988: Numerically stable algorithm for discrete ordinate method radiative transfer in multiple scattering and emitting layered media, *Appl. Opt.*, **27**, 2502-2509.

Sullivan, J., 1992: Effects of UV-B radiation on crops and terrestrial ecosystems, paper presented at UV-B Monitoring Workshop: A Review of the Science and Status of Measuring and Monitoring Programs, Sponsored by Alternative Fluorocarbons Environmental Acceptability Study and the U. S. Department of Agriculture, Mar. 10 to 12.

Sung-Nam OH, Byung-Ju Sohn, and Sang-Sam Lee, 2004: Aerosol optical and radiative properties at Anmyeon and Jeju, Korea in the Spring of 2000 and 2001, *Environmental Monitoring and Assessment*, **92**, 95-115.

Taylor, H.R., S.K. West, and F.S. Rosenthal, B. Munoz, H.S. Neland, H. Abbey, E.A. Emmett, 1988: Effect of ultraviolet radiation on cataract formation, *New Engl. J. Med.*, **319**, 1429-1433.

Teillet, P. M., 1990: Rayleigh optical depth comparisons from various sources, *Appl. Opt.*, **29**, 1897-1900.

Vignola, F.: 2001, Variability of Solar Radiation over Short Time Intervals, *Proc. Solar 2001, American Solar Energy Society Conf.*, Washington, D.C.

Wauben, W. M. F, and F. Kuik, 1998: Sensitivity study of the Brewer direct sun ozone retrieval algorithm using numerical simulations, in *Proc. XVIII Quadr. Ozone Symp., Aquila, 1996*, edited by R. D. Bojkov and G. Visconti, 85-88.

Wenny, B. N., J. S. Schafer, J. J. DeLuisi, V. K. Saxena, W. F. Barnard, I. V. Petropavlovskikh, and A. J. Vergamini, 1998: A study of regional aerosol radiative properties and effects on ultraviolet-B radiation, *J. Geophys. Res.*, **103**, 17083-17097.

Wenny, B. N., V.K. Saxena, and J.E. Frederick, 2001: Aerosol optical depth measurements and their impact on surface levels of ultraviolet-B radiation, *J. Geophys. Res.*, **106**, 17311-17319.

Wilson, L. J.: 1993. Canada's UV Index-How It Is Computed and Disseminated, Environment Canada, Atmospheric Environment Service, 3 pp.

WMO (World Meteorological Organization), 1995: Report of the WMO Meeting of Experts on UV-B Measurements, Data Quality, and Standardization of UV Indices (Les Diablerets, Switzerland, 25-28 July 1994), Global Atmospheric Watch, Report No. 95, World Meteorological Organization), Scientific Assessment of Ozone Depletion: 1994, Global Ozone Research and Monitoring Project – Report No. 37, World Meteorological Organization, Geneva.

Zerefos, C., C. Meleti, D. Balis, K. Tourpali, and A.F. Bais, 1998: Quasi-biennial and longer-term changes in clear sky UV-B solar irradiance, *Geophys. Res. Lett.*, **25**, 4345-4348.

VITA

Jeral G. Estupiñán was born on March 5th, 1969 in Caracas, Venezuela. Before he was one year old his parents relocated to their home country (Spain – The Canary Islands) where he grew up and completed all his elementary, primary and secondary education at Colegio Hispano-Inglés in the Island of Tenerife. Jeral developed a strong interest in meteorology since an early age, and since he was in the 6th grade, he operated a meteorological station in the southeastern part of the Island of Tenerife. At the time there were no Universities in the Canary Islands that offered a degree in applied science, which forced him to look outside of the Canary Islands to be able to pursue his college education. He selected the United States as the country where he wanted to study atmospheric sciences. In the fall of 1986 Jeral enrolled in the 12th grade at Susquehanna Community High School in northeastern Pennsylvania in order to familiarize with the US educational system before starting his college education. In spring of 1987 he completed his 12th grade with the honor of salutatorian. He completed his Bachelor's degree in Meteorology from North Carolina State University in December of 1992. In May, 1991 he also completed a B.A. in French from Ferrum College in Virginia where he was awarded a Salutatorian scholarship. During the summer of 1992 Jeral worked at the National Center for Atmospheric Research (NCAR) in Boulder, Colorado investigating sea breeze front and convection initialization as part of a project sponsored by NCAR in Florida during the summer of 1991. Jeral continued his studies in North Carolina State University and in spring of 1995 he completed his Master of Science from the Department of Marine, Earth, and Atmospheric Sciences. During the program he conducted all his research at the US Environmental Protection Agency (EPA), which is conveniently located at Research

Triangle Park near North Carolina State University. At EPA, Jeral investigated the effects of clouds and haze on the solar ultraviolet radiation as part of a project funded by the US Government intended to do research toward the development of the National Weather Service ultraviolet forecasts. In the summer of 1995, Jeral was accepted at the University of Colorado at Boulder to start his Ph.D. in atmospheric sciences. However, he only stayed at CU Boulder for one year and transferred to Georgia Tech to continue his Ph.D. closer to his family who lived in Atlanta at the time. At CU Boulder Jeral took many classes in Physical Geography which he transferred to Georgia Tech as his Doctoral minor. After Jeral completed all his course work and comprehensive exam at Georgia Tech he took his first full-time research job at the National UV Monitoring Program at the University of Georgia in Athens. In this position Jeral conducted UV research with the US EPA Brewer spectrophotometers and also performed day-to-day operational activities to support the quality assurance of the US EPA Brewer network. In June of 1999 Jeral started working at the Weather Channel located in Atlanta, GA. Jeral started at the Weather Channel as an international product coordinator creating meteorological products for the Weather Channel international web sites. In June 2000 Jeral was promoted to Senior Weather Developer and in May 2001 Jeral was promoted to Manager of the International Product Development team. In this position Jeral managed the creation of all meteorological products (maps and content) for all weather.com international web sites. He supervised a team of two full time meteorologists and three additional summer students who now work full time at the Weather Channel. In June, 2002 Jeral transferred to the department of Weather Systems. Since then, his title has been Manager – Forecast Systems where he is responsible for the to evaluation and

improvement of The Weather Channel model performances through the investigation of ensemble approaches, analysis of verification results, and creation of new operational tools needed to support a team of twelve forecasters. Jeral is author of an operational verification system as a way to improve weather forecasts and maximize effectiveness at the Weather Channel. The system, Advanced Verification Information for Advanced Operational Results (ADVISOR), utilizes real time maps and graphical tools to support the operations of the Weather Channel forecasters. ADVISOR is a performance support system for the Weather Channel forecasters, which delivers real-time feedback about previous forecast performance. The goal of ADVISOR is to optimize the human forecaster's effectiveness. The increase in computing power and new automated forecasting systems challenges the role of human forecasters, increasing the need for monitoring and verification tools to direct forecasters to situations where they can make a real contribution.